Sensory processing and decision making in a social context: From odors to swarm motion in insects

Doctoral thesis for obtaining the

academic degree

Doctor of Natural Sciences

Dr. rer. nat.

submitted by

Petelski, Inga

at the

Faculty of Sciences

Department of Biology

Konstanz, 2025

Date of the oral examination: 16.07.2025

1. Reviewer: Dr. Einat Couzin Fuchs

2. Reviewer: Prof. Dr. Giovanni Galizia

1. Reviewer	Dr. Einat Couzin Fuchs
2. Reviewer	Prof. Dr. Giovanni Galizia
Head of commission	PD Dr. Dina Dechmann
Submission date	Konstanz, 29.05.2025

CONTENTS

GENERAL SUMMARY

'They covered the ground until it was black. They consumed everything left after the hail - every plant in the fields and all the fruit on the trees...' (Exodus 10).

The plague of locusts was the eighth disaster God sent to punish the Pharaoh. Nevertheless, despite millennia of progress, in the age of genetic engineering and space exploration, humanity still struggles to control the recurring devastation by locust swarms, which keep on threatening nearly 10% of the global human population during outbreaks. Another creature thriving between us and resisting humanity's best efforts to eradicate it is the cockroach - an evolutionary survivor that has outlasted most species for over 300 million years. Locusts and cockroaches exemplify how simple individual actions can scale into detrimental, yet extremely fascinating complex collective dynamics, which enable the survival of the two species in ever fluctuating environments.

The neurophysiological processing of external stimuli through sensory pathways allows those two non-model organisms to successfully navigate their surroundings, which, most often, include conspecifics. Social cues have the capability of triggering drastic changes in behavior and of influencing the perception of other non-social cues. Thus far, neuroscience has paid little attention to the neuronal mechanisms underlying natural social influences on behavior, traditionally focusing on preparations of tethered, isolated individuals under controlled laboratory conditions.

During my PhD research, I explored how key ecological behaviors during decision-making are adapted and modulated under varying social contexts and how this is reflected in the sensory perception and information processing along specific neuronal pathways. The present cumulative dissertation aims to better understand the neuroethological foundations underlying social-enhancement or modification of an individual's sensory perception. It comprises a general introduction and discussion, framing three consecutive publications, each presented as a separate chapter and introduced with a chapter summary.

In *Chapter 1*, we investigated the modulatory impact of social cues during shelter selection in American cockroaches. Combining binary choice experiments and in-vivo calcium imaging, we found a socially induced preference shift, corresponding to an altered, early-stage neuronal coding. This neuronal modification and induced behavioral switch could help regulate resource

use by reducing attraction to previously exploited sites, potentially promoting the exploration of new resources.

Building on the understanding of how social cues can reshape individual biases, and inspired by field work on locusts in Africa, *Chapter 2* moves on to the foraging decisions of locusts, which demonstrate a remarkable and fascinating form of social plasticity. We studied how sensory integration, with and without a social context, influences foraging decisions by combining behavioral assays, Bayesian modeling, and neural imaging. By means of the first applications of *in-vivo* calcium imaging in a large proportion of projection neurons in desert locusts, the neuronal analysis revealed that gregarious locusts, unlike solitarious individuals, exhibit modulations originating in the first olfactory processing center. We assume that this effect enhances food detection in the distractive swarm environment. In accordance with our findings in *Chapter 1*, this study corroborates the result that the social context can reshape or override individual preferences, emphasizing the neuronal influence of groups on decision-making.

Driven by the spectacular swarming behavior of locusts, which we witnessed during a major outbreak in Africa, *Chapter 3* shifts the focus from how the social context influences individual choices and neural firing, to how socially induced individuals coordinate their coherent movement so as to form the foundation of collective swarm behavior. Through field experiments, virtual reality, quantitative behavioral analyses, and modeling approaches, we scrutinized the rules governing synchronized motion within large juvenile locust groups. Our findings reveal a sophisticated, self-reflective and vision-based mechanism underlying swarm alignment during motion.

Together, the three studies provide new insights into the dynamic interplay between neural mechanisms, social influence, and swarm coordination, with broader implications for fundamental neuroscience and behavioral biology. I hope that our work, including the development of technical methods, can contribute to elaborating targeted pest management strategies in the future - a crucial step for combatting human starvation while also protecting countless ecologically relevant and threatened insect species from broad-spectrum insecticides.

ZUSAMMENFASSUNG

"Denn sie bedeckten das Land und verfinsterten es. Und sie fraßen alles Kraut im Lande auf und alle Früchte auf den Bäumen, die der Hagel übriggelassen hatte…"(2. Mose 10).

Heuschreckenschwärme waren die achte Plage, die Gott zur Strafe des Pharaos auf die Erde schickte. Doch trotz Jahrtausenden menschlichen Fortschritts, in Zeiten von Gentechnik und der Entdeckung ferner Galaxien, gelingt es der Menschheit noch immer nicht, die wiederkehrenden Heuschreckenschwärme zu kontrollieren, welche bei Ausbrüchen die Ernährung von knapp 10 % der Weltbevölkerung bedrohen. Eine weitere Kreatur, die unter uns gedeiht und sich hartnäckig allen Ausrottungsversuchen widersetzt, ist die Kakerlake - ein evolutionärer Überlebenskünstler, der seit über 300 Millionen Jahren existiert. Heuschrecken und Kakerlaken veranschaulichen, wie einfache individuelle Handlungen in komplexen, kollektiven, schädlichen und doch faszinierenden Dynamiken münden können, die das Überleben dieser Arten in variablen Umgebungen ermöglichen.

Die neurophysiologische Verarbeitung unterschiedlichster sensorischer Reize ermöglicht es diesen Organismen, sich in ihrer Umwelt, welche meist auch Artgenossen beinhaltet, erfolgreich zu bewegen. Soziale Reize haben das Potenzial, drastische Verhaltensänderungen auszulösen und die Wahrnehmung anderer Reize zu beeinflussen. Dennoch beschäftigte sich die Neurowissenschaft bisher wenig mit den neuronalen Mechanismen, die dem sozial beeinflussten Verhalten unter natürlichen Bedingungen zugrunde liegen. Die Forschung konzentrierte sich meist auf isolierte Individuen unter kontrollierten Laborbedingungen.

Während meiner Doktorarbeit untersuchte ich, wie zentrale ökologische Verhaltensweisen bei Entscheidungsfindungen unter variierenden sozialen Einflüssen angepasst und moduliert werden, und wie sich dies in der sensorischen Wahrnehmung und Informationsverarbeitung entlang spezifischer Nervenbahnen widerspiegelt. Die vorliegende kumulative Dissertation zielt darauf ab, die neuroethologischen Grundlagen zu verstehen, die dem sozialen Einfluss der individuellen Wahrnehmung zugrunde liegen. Die Dissertation besteht aus einer allgemeinen Einleitung und Diskussion, welche drei aufeinanderfolgende Publikationen umrahmen, die jeweils als separates Kapitel mit einer Zusammenfassung eingeführt werden.

In *Kapitel 1* untersuchten wir den modulierenden Einfluss sozialer Reize während der Unterschlupfwahl bei amerikanischen Kakerlaken. Durch die Kombination von Verhaltenstests und in-vivo-Calcium-Imaging fanden wir eine sozial bedingte

Präferenzverschiebung, die mit einer veränderten neuronalen Kodierung in frühen Verarbeitungsstadien einherging. Diese neuronale Modifikation und das daraus resultierende Verhalten können helfen, die effiziente Nutzung von Futterstellen zu regulieren, indem ausgebeutete Ressourcen vermieden und neue Nahrungsquellen erkundet werden.

Aufbauend auf dem Verständnis, wie soziale Reize individuelle Präferenzen umformen können und inspiriert durch Feldforschung in Afrika, widmet sich *Kapitel 2* der Futtersuche von Heuschrecken, welche eine faszinierende Form sozialer Plastizität zeigen. Wir untersuchten, wie sensorische Verarbeitung, mit und ohne sozialen Kontext, das Nahrungssuchverhalten beeinflusst, indem wir Verhaltensanalysen, Bayes'sche Modellierung und neuronale Bildgebung kombinierten. Mithilfe der erstmaligen Anwendung von in-vivo-Calcium-Imaging von Projektionsneuronen der Wüstenheuschrecke zeigte unsere Analyse, dass gregäre Tiere, im Gegensatz zu solitären Individuen, Neuromodulation im ersten olfaktorischen Verarbeitungszentrum aufweisen. Wir vermuten, dass dieser Effekt die Futtererkennung in der ablenkungsreichen Schwarmumgebung verbessert. Im Einklang mit unseren Ergebnissen aus *Kapitel 1* bestätigt diese Studie, dass der soziale Kontext individuelle Präferenzen verändern oder sogar überlagern kann und unterstreicht somit den neuronalen Einfluss sozialer Gruppen auf Entscheidungsprozesse.

Angesichts des eindrucksvollen Schwarmverhaltens, welches wir während einer riesigen Heuschreckenplage in Afrika beobachteten, verlagert das *Kapitel 3* den Fokus von der Beeinflussung individueller Entscheidungen und neuronaler Aktivität hin zu der Frage, wie sozial geprägte Tiere ihre Bewegung koordinieren und somit die Basis des kollektiven Schwarmverhaltens bilden. Mittels Feldversuchen, virtuellen Realitätsversuchen, quantitativen Verhaltensanalysen und Modellierungsansätzen untersuchten wir die Regeln, die synchronisierte Bewegungsmuster in großen Gruppen junger Heuschrecken steuern. Unsere Ergebnisse offenbaren einen ausgeklügelten, selbstreflektierenden und visuell gesteuerten Mechanismus, der der Orientierung im bewegten Schwarm zugrunde liegt.

Zusammen liefern die drei Studien Einblicke in das dynamische Zusammenspiel neuronaler Mechanismen, sozialer Einflüsse und Schwarmkoordination, mit weiterreichenden Implikationen für neurowissenschaftliche und verhaltensbiologische Grundlagenforschung. Ich hoffe, dass unsere Arbeit, einschließlich der entwickelten technischen Methoden, zu gezielten Strategien im Schädlingsmanagement beitragen kann, um menschliche Hungersnöte zu bekämpfen und gleichzeitig ökologisch wertvolle oder bedrohte Insekten vor Breitband-Insektiziden zu schützen.

GENERAL INTRODUCTION

Imagine yourself strolling through Konstanz city on a hot summer Sunday afternoon. You crave a refreshing ice cream to cool down, finally spot two ice cream parlors, and are immediately faced with a dilemma: Which one should you choose? On the one hand, there is a vendor just around the corner. A massive queue stretching out of the door suggests that this parlor is extremely popular. Perhaps those lining up are locals who have discovered that this is the best ice cream in town, well worth the wait! On the other hand, another small vendor offers sweet-smelling cones from a nondescript window on the side of the marketplace. The line is short, meaning you will likely enjoy your treat in just a few minutes. Also, due to the simple appearance of that vendor, there is the chance that you found a hidden gem overlooked by all those naive tourists. However, that ice cream might be unpopular because of its poor quality.
As you stand there, contemplating your two options, you find yourself torn. Should you trust the long line of the popular vendor as a sign of quality, hoping that you reach the counter before the ice cream is sold out? Or should you go for the quick, less crowded option and rely on your own sense of smell? You are not alone in your indecision. Observing the choices and behaviors of others often steers our personal tendencies. Most humans interpret a longer line as an indicator of a superior option, which leads individuals to assign greater value to it and nudges them towards choosing it (Munichor & Cooke, 2022). Subsequent customers have even been shown to unintentionally eat larger ice cream quantities in the presence of others (Berry et al., 1985) and clients in a queue adjust the number of scoops to match the ones of the persons in front (McFerran et al., 2010).

UBIQUITY OF GROUP INFLUENCE

Even though we might not consciously recognize it, we humans are inherently social, and our reliance on public cues, including the selfish exploitation of herd benefits, regularly guides our decisions, especially in uncertain situations. Interestingly, this influence of the group is not confined to human behavior alone. Individuals of species across the animal kingdom also make decisions that influence their conspecifics, and, at the same time, are influenced by their peers' actions, often in a way that mirrors our human social tendencies. Just as we humans might rely on the crowd conformity to choose an ice cream parlor, birds effectively navigate to their wintering grounds in large flocks, with increasing group formation upon increasing travel

distance (Beauchamp, 2011), fish successfully evade predators by forming coordinated schools (Parrish, 1989), with decreased risk of predation with larger group size (Polyakov et al., 2022), and even bacteria display cohesive mass migration to reach a common goal (Harshey, 2003). It is no surprise that insects, too, navigate their world as part of a complex social network that shapes the course of action when selecting a foraging ground, choosing a new nest site, or deciding on a mate.

The structures within 'social networks' play a role in information spread and decision making and can vary greatly, spanning from open, loose associations to tightly, hierarchically organized associations (Wey et al., 2008). Furthermore, the mechanisms enabling most collective phenomena within a group are known to be self-organizing and decentralized, without a dominant, leading authority (Camazine et al., 2020). They rely on processes such as information flow, local interactions, or positive and negative feedback (Conradt & Roper, 2005; Couzin et al., 2005; Sumpter, 2005). For example, hundreds of honeybee scouts of a colony individually explore potential nesting sites, once their hive has grown too large, advertising the most promising places via waggle dance. The strength and duration of each dance reflects the quality of a location, recruiting more and more scouts to explore that specific place. If convinced, those scouts actively join in the dance and amplify the choice. At the same time, bees are discouraged when dancing for inferior alternatives (Seeley et al., 2006; Visscher, 2007). Once a quorum advertises a certain site, the whole swarm takes off for relocation. This seemingly democratic process enables a colony, which lacks knowledge about the global structure, to reliably select high-quality nesting sites and to master a highly complex decision task without any kind of hierarchical or centralized control.

EUSOCIALITY

The most extreme and fascinating form of social living in the animal kingdom can be observed in eusocial species. Eusociality is the highest level of perfectly coordinated social organization, characterized by strong altruism, cooperative brood care, overlapping generations, and a complex division of labor, including reproductive roles (Wilson & Hölldobler, 2005). With rare exceptions among mammals and crustaceans, eusociality is confined to a few insects, with ants, bees, and termites as popular representatives (Queller & Strassmann, 2003). For example, the leaf-cutter ant species Atta and Acromyrmex form the most advanced, complex eusocial structure on earth, where millions of miniature individuals are divided into specialized casts that work together in perfect harmony, resembling one single organism. Those ants have even

developed insect agriculture by growing and harvesting a certain fungus, providing food and antimicrobial defense (Nowak et al., 2010). While eusociality represents the pinnacle of cooperative living, a broad spectrum of sophisticated social behaviors is exhibited by non-eusocial insect species.

SOCIAL IMPACT IN INSECTS

Despite drawbacks such as increased resource competition and aggression (Strohm & Bordon-Hauser, 2003), cannibalism (Bazazi et al., 2008), or higher pathogen transmission (Meunier, 2015; Strohm & Bordon-Hauser, 2003), the evolutionary advantages of group cohesion have driven its widespread success. Intraspecies aggregation up to a specific, self-regulated group size (Estevez et al., 2007) improves predator avoidance (Polyakov et al., 2022) and allows defensive strategies through collective resistance and confusion (Milinski, 1984). It further facilitates social learning (Leadbeater & Dawson, 2017) and enhances communication (Bortolotti & Costa, 2014; Dussutour et al., 2005; Uzsák et al., 2014). Additionally, group living enables faster predator detection (Foster & Treherne, 1981) and improves foraging efficiency and resource exploitation (Krause & Ruxton, 2002; Lihoreau et al., 2016; Polyakov et al., 2022), while ensuring constant mate availability.

The social environment has key impacts on the lifespan and ageing across a huge range of invertebrate taxa (Harrison et al., 2024) and the cohesiveness of various species is so strong that individuals even suffer under ‘isolation syndromes’ when kept in solitude. Young worker ants, for example, lose up to 15% of their body weight after just 72 h of isolation and often die shortly after that, whereas this effect could not be observed in individuals kept within a small group (Godziiiska & Lenoir, 2006; Koto et al., 2015). Similarly, cockroaches in isolation show reduced essential engagement in exploration, foraging activity, or mating partner assessment (Lihoreau et al., 2009), while fruit flies under chronic separation suffer from reduced sleep (Donlea & Shaw, 2009), increased hunger, overheating (Li et al., 2021), and rapid cancer progression (Dawson et al., 2018).

To maintain group cohesion, gregarious species thus closely monitor the actions or cues of their peers and tend to join certain feeding or sheltering sites, even when equally suitable alternatives are available. In this context, the larger the group, the more convinced individuals become, and the more likely they are to join (Lihoreau et al., 2016). Trusting the majority, or a well-informed minority (Couzin et al., 2011; Dyer et al., 2008), often proves advantageous, especially in certain life cycle stages (Krafft et al., 1986) or in environments where

unpredictable or unfavorable fluctuations limit an individual's ability to gather easily available, reliable information (Hall & Kramer, 2008; Lihoreau et al., 2017; Smolla et al., 2016). Thus, the greater the uncertainty of personal information and the larger the group of conspecifics, the more the decision-making process is aligned with the predominant group choice (King & Cowlishaw, 2007).

PERSONAL VS SOCIAL INFORMATION

However, conforming to social consensus and relying on intentionally - or even unintentionally - dropped cues of conspecifics is not always straightforward, nor is it necessarily the most beneficial choice. In some cases, the costs of group living might outweigh its benefits. In fact, individual guppies may sometimes conform to social information even when they conflict with their own experience, leading to suboptimal foraging decisions (Kendal et al., 2004). To maintain group cohesion and avoid isolation, both of which can reduce individual fitness, it is important that gregarious animals continuously weigh asocial cues against potentially conflicting social information derived from their peers, depending on the ecological conditions (Miller et al., 2013; Van Bergen et al., 2004) and the animal's internal state (Plenzich & Despland, 2018). For instance, some 'socially plastic', facultatively eusocial bee species can swap between a fully eusocial and a solitary life cycle (Séguret et al., 2016), and bumblebees (*Bombus impatiens*) can assess the reliability of social and personal cues, preferring social cues only when they are equally or more reliable than personal ones (Dunlap et al., 2016). Notably, the ability to evaluate and integrate asocial information is further enhanced when individuals rely on multimodal signals. The same species of bumblebee makes more effective foraging decisions when combining multiple sensory modalities during flower selection (Kulahci et al., 2008), and mosquitoes only find their host through the elaborate, hierarchical integration of multiple sensory cues (Vinauger et al., 2019).

DECISION MAKING IN COCKROACHES

Another excellent example of the trade-off between personal and public information is the domiciliary cockroach (typically referring to species like *Blattella germanica* or *Periplaneta americana*) (Lihoreau et al., 2012). Cockroaches integrate private and social cues when navigating the environment and responding to biotic (food, mates) and abiotic (temperature, humidity) cues, with olfaction being their primary sensory modality (Durier & Rivault, 2000; Rivault & Cloarec, 1998). Those insects usually rest in communal shelters, where they actively

aggregate to form cohesive groups, which they leave for solitary foraging trips (Lihoreau & Rivault, 2011). During those trips, cockroaches primarily rely on personal information to locate food sources, using olfactory and gustatory cues to assess quality (Durier & Rivault, 2000). At the same time, however, they are highly social and depend on cuticular hydrocarbon profiles and pheromone-based communication for aggregation (Saïd et al., 2005; Wada-Katsumata et al., 2015), predator warnings (Lihoreau et al., 2012) and mate attraction (Sass, 1983; Zhukovskaya, 1995). They also use visual and tactile signals to coordinate movement (Wendler & Vlatten, 1993) and assess conspecifics (Lihoreau & Rivault, 2008). Cockroaches in groups benefit from increased growth rate or reduced water loss (Dambach & Goehlen, 1999; Prokopy & Roitberg, 2001). Even in their larval stage, young cockroaches show strong aggregation tendencies in an empty arena, which are amplified by the sheer increase in the number of conspecifics (Jeanson et al., 2005).

When a cockroach encounters a food source or shelter during solitary foraging but finds no sign of conspecifics, it faces a dilemma: trust its own assessment and remain in isolation, or follow social cues and exploit a potentially inferior, overexploited and overcrowded resource that is socially validated (Canonge et al., 2011; Doi & Toh, 1992; Durier & Rivault, 2000). Once conspecifics aggregate, social information becomes increasingly influential, with the presence of other cockroaches indicating resource reliability. Public group members reinforce the collective exploitation of specific patches (Lihoreau & Rivault, 2011) and even increase the efficiency of problem-solving abilities (Canonge et al., 2011). Several studies have already highlighted that cockroaches stay longer (retention effect) in shelters or at food sources previously or currently occupied by conspecifics due to social amplification, even when alternatives are available or when it conflicts with individual information (Ame et al., 2004; Calvo Martín et al., 2021; Canonge et al., 2009; Imen et al., 2015; Lihoreau et al., 2010; Saïd et al., 2005). In this context, the larger the group of conspecifics, the lower the probability of leaving the shelter (Amé et al., 2006). Interestingly, when cockroaches are confronted in a Y-olfactometer with the binary choice between feeding conspecifics and a combination of food odor plus non-feeding conspecifics, they rely on inadvertently dropped cues through local enhancement, preferentially joining feeding conspecifics (Lihoreau & Rivault, 2011). Remarkably, individuals of *Periplaneta americana* display individual variation in the robustness and degree of their behavioral choice, even though they lack a formal social hierarchy (Planas-Sitja & Deneubourg, 2018).

CONFLICTING INTERESTS IN COCKROACHES

The complexity of the balance between group dynamics and independent decision-making to avoid negative consequences becomes evident when cockroaches are exposed to environmental factors such as humidity, brightness level, overcrowding, or specific scents. In some of those cases, the commonly reported self-amplification of group attraction does not hold (Calvo Martín et al., 2019; Canonge et al., 2009; Doi & Toh, 1992; Durier & Rivault, 2000; Dussutour et al., 2005). For example, when the carrying capacity of a shelter is reached, cockroaches shift their preference towards an unoccupied shelter. This behavior reflects an adaptive trade-off, where avoiding group members, and with that minimizing exposure to risky edges, becomes more beneficial than aggregation (Amé et al., 2006). Another research group investigated the role of humidity in shelter selection. They found that, while individual American cockroaches *Periplaneta americana* seek out high-humidity environments, social cues of a group suddenly drive them away toward drier shelters. The internal state of cockroaches further shapes the shelter affinity, with increasing dehydration causing the preference for more humid shelters (Doi & Toh, 1992). Especially in densely occupied spaces, this behavioral change may serve as an adaptive strategy to mitigate the risk of pathogen and fungal transmission (Calvo Martín et al., 2019). Similarly, Salazar et al. found that isolated cockroaches favor vanillin-scented shelters over an empty control shelter. However, their mathematical model and behavioral trials revealed that the preference quickly diminished in groups, in which the cockroaches preferred the unscented control. The authors proposed that vanillin's negative effect on intraspecific attraction causes the occurrence of this shift (Laurent Salazar et al., 2017).

Expanding on this study, our research, described in *Chapter 1* of the current dissertation, discovered that the social context in a setup, similar to the one of Laurent Salazar et al., could even be mimicked by social odors (colony feces extract). We found that the preference inversion described by Laurent Salazar et al. occurred not only in the presence of live conspecifics, but could be induced by the social odor alone, emphasizing the critical role of olfactory cues in driving the shift. We tested a range of social odor and vanillin concentrations, with a preference change observed up from a certain threshold. Notably, higher concentrations of social odor significantly reduced cockroaches' attraction to vanillin-scented shelters, contradicting the hypothesis that vanillin negatively affects aggregation. Our calcium imaging trials in the first olfactory processing center matched the behavioral observations. Analysis revealed decreased activity in vanillin-responsive brain regions when cockroaches are exposed to the combination of social odor and vanillin. Interestingly, activation in social odor-

responsive regions remained unchanged, maintaining a steady level of neuronal activity, possibly negatively intervening with vanillin-responsive regions and not vice versa (Günzel et al., 2021). The findings suggest that social dynamics, even at an early neuronal processing level, can override innate preferences, resulting in group choices that contradict solitary inclinations (Figure 1).

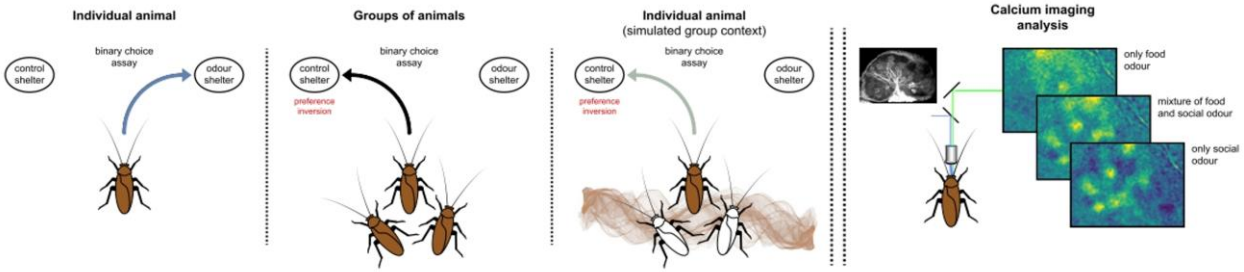

Figure 1: Graphical abstract of the socially-induced shift of behavior and neuronal activity during shelter selection in cockroaches, as described in *Chapter 1* of this thesis ('Social Modulation of Individual Preferences in Cockroaches'). The initial attraction of individuals towards the vanillin-scented shelter diminishes in a social context. This context can be mimicked by the social odor alone. Exposing cockroaches to the combination of vanillin scent and the social odor reduces activity in vanillin-responsive regions in the antennal lobe. (Drawing by Yannick Günzel; microscopy images by author)

Further adding complexity to the topic, another publication found that the collective decision-making process in heterogenous cockroach groups could effectively be steered by a minority, adding another layer to our understanding of how social cues can outweigh individual preferences, with minority groups driving consensus (Calvo Martín et al., 2021).

LOCUST ECOLOGY

A hemimetabolous species that exemplifies the most extreme contrast between individualism and group behavior is also one of the most destructive pests on the planet, threatening the livelihoods of approximately 10% of the world's human population during outbreaks - the locust (FAO; Sword et al., 2010). Witnessing the disastrous scale, and yet unimaginable, breathtaking phenomena of gigantic locust swarms in the wild during the major plague in Kenya in 2019 profoundly influenced my own scientific perspective on my PhD journey and deepened my commitment to understanding the mechanisms underlying locust behavior.

Unlike cockroaches, whose social tendencies remain relatively stable, locusts, such as the two most extensively studied - though phylogenetically distant – species, the migratory locust *Locusta migratoria* and desert locust *Schistocerca gregaria*, undergo a remarkable transformation in response to environmental conditions (Cisse et al., 2013) and population

density (Song, 2005). After heavy rainfall and good breeding conditions in their recession area, food limitations urge solitarious locusts to congregate and interact on limited, highly clumped (Despland & Simpson, 2000) food sources (Cisse et al., 2013; Simpson et al., 1999).

LOCUST PHASE POLYPHENISM

Once a critical threshold of animals is reached, the polyphenic individuals shift within a single generation from the cryptic, solitary phase, where they actively avoid each other, to a highly cohesive, gregarious phase. In the latter, billions of animals, influenced by mechanosensory feedback (Miller et al., 2013), actively seek out conspecifics, aggregating and aligning into massive, synchronized marching hopper bands, which transition into flying swarms once the animals reach adulthood (Roessingh et al., 1993; Sword et al., 2010). While locust plagues were already documented over 3000 years ago, climate change and the resulting extreme weather events with heavy localized rainfall are expected to trigger increasingly frequent locust plague upsurges in the near future (Tucker et al., 1985). According to the Food and Agriculture Organization (FAO), during plagues, locust swarms can spread across 60 countries of northern Africa and the Middle East towards southeast Asia, covering an area of approximately 29 million km², which is equivalent to 20% of the world's land surface (Cullen et al., 2017). Given that each locust consumes its body weight of around 2g of vegetation per day, a single swarm, consisting of approximately 35 million locusts, can consume an amount of crops that could feed around 35,000 people daily (FAO).

With olfactory and visual cues of conspecifics contributing to a partial gregarization, tactile stimulation from conspecifics on the hind femur is the main trigger for the dramatic change from the solitary to the gregarious phase in the desert locust *Schistocerca gregaria* (Forskål, 1775) (Dillon et al., 2001; Roessingh et al., 1998; Simpson et al., 2001). Notably, the olfactory ability to perceive the aggregation pheromone 4-vinylanisole, produced by gregarious animals, plays a significant role in maintaining gregarious cohesion and attraction. Besides tactile stimuli, the pheromone contributes to the changing sensory responses to conspecifics and the engagement in social interactions in migratory solitary locusts (Guo et al., 2020).

The differences between the solitary and gregarious phase are so pronounced that they were believed to represent two distinct species. However, in 1921, Boris Uvarov debunked this error, discovering that the solitary and gregarious forms belong to the same species (Burtt & Uvarov, 1967).

The phase transformation in locusts is coordinated by a complex interplay of hormones, neuropeptides, epigenetic mechanisms, and neurotransmitters (Ernst et al., 2015; Rogers et al., 2004). Among these, rising serotonin in the thoracic ganglia, but not the brain, induced by mechanosensory stimulation upon crowding, appears to play a prominent and crucial role in the initiation of desert locusts' gregariousness, as the levels positively correlate with the degree of gregarization (Anstey et al., 2009; Burrows et al., 2011). Notably, gregarious behavior could even be initialized by the sole injection of the biogenic amine serotonin or serotonin receptor agonists (Anstey et al., 2009). In contrast, a more recent study recorded that serotonin injection could not elevate attraction behavior in solitary *Schistocerca gregaria* (Tanaka & Nishide, 2013), while a second publication stated that the injection into the brain accelerates solitarization, and that serotonin antagonists could block the transition from the solitary to the gregarious phase (Guo et al., 2013). However, those findings were later re-evaluated in a meta meta-analysis by Rogers et al., who questioned the methodologies and interpretations of the conflicting studies. In their carefully controlled replication, they demonstrated that serotonin application to the thoracic ganglia, when administered at the correct developmental stage and time point, robustly caused gregarious behavior (Rogers et al., 2014).

In contrast to the findings in desert locusts, serotonin was reported to enhance solitariness in gregarious individuals of *Locusta migratoria* (Guo et al., 2013), or induce only partial, short-term initiation of gregarious behavior, whereas dopamine, which is regulated by epigenetic miRNAs (Guo et al., 2018), appeared to play a more important role in promoting the gregarious phase of this species (Ma et al., 2011). Elevated dopamine levels in *Schistocerca gregaria* have been associated with maintenance or induction of solitarization (Alessi et al., 2014), which points out the species-specific neurochemical (and genetic) pathways that are underlying the phase change.

The juvenile hormone (JH) titers have also been shown to modulate the peripheral olfactory system in locusts by affecting the responsiveness of antennal lobe local interneurons to aggregation pheromones. Specifically, increased JH levels reduce olfactory attraction and aggregation behavior in gregarious animals (Guo et al., 2020; Ignell et al., 2001; Wiesel et al., 1996).

While initial behavioral modifications occur within hours, the entire phase transformation unfolds over generations, involving profound morphological, physiological, and neurological modifications (Simpson et al., 2001). The solitary and gregarious phases differ substantially across multiple dimensions with exceptionally well-adapted traits for the specific demands of

their respective lifestyle. Solitary locusts are inconspicuous, camouflaged in green (Figure 2) that turns brown in the adult stage, avoid conspecifics, and display limited movement (Rogers et al., 2014). They invest more in low-level sensory processing and, thus, possess disproportionally larger primary visual and olfactory neuropiles, possibly to enhance sensitivity (Ott & Rogers, 2010), which fits their solitary lifestyle.

While solitary *Schistocerca gregaria* quickly develop a conditioned aversion to odors associated with toxic substances, they undergo a drastic behavioral reversal upon crowding. During the transition into the gregarious phase, locusts effectively 'unlearn' their conditioned aversion and lose their innate avoidance behavior, actively incorporating toxic plants into their diet (Despland & Simpson, 2005; Simões et al., 2013; Sword et al., 2000). Ingested phytotoxins serve as an antipredator defense (Despland & Simpson, 2005). Dietary choices are further one of the causes for the conspicuous black and yellow coloration of gregarious *Schistocerca gregaria* nymphs (Figure 2), which, in the adult stage, transition into pink (Despland & Simpson, 2005; Sword et al., 2000). In contrast to the solitary phase, gregarious locusts show a lower threshold for wind-induced flight initiation (Fuchs et al., 2003), increased activity levels, strong aggregation tendencies, and the ability to migrate over vast distances in a collective manner (Rogers et al., 2014). These behavioral modifications are accompanied by physiological changes that enable rapid, exponential population expansion, with approximately 8000-fold increase in number over just three generations (Cai et al., 2009). Changes include elevated metabolic rates, enhanced endurance, and increased and faster reproductive capacity (Pener & Simpson, 2009; Pflüger & Bräunig, 2021). On a neuronal level, the gregarious phase is characterized by increased brain size, emphasizing higher-order processing brain regions such as the mushroom bodies and the central complex. This alteration prioritizes greater neural integration, which supports the behavioral demands of living in dense swarms that migrate through complex environments (Ott & Rogers, 2010).

Figure 2: Juvenile desert locusts *Schistocerca gregaria*. Both nymphs originate from the same parental generation. The left, solitary individual was raised in isolation, while the right, gregarious one was kept in a crowded condition. (Photo by author)

LOCUST MARCHING AND SWARMING BEHAVIOR

Despite their remarkable adaptability to environmental conditions, gregarious locusts face diverse challenges, which go hand in hand with the mass aggregation. As previously described, high densities of individual insects amplify intraspecific resource rivalry. Bazazi et al. suggested that the cannibalistic appetite of hungry locusts from the rear might be among the causes of mass migration (Bazazi et al., 2008), particularly when crossing harsh, arid landscapes. In this context, recent research by Chang et al. uncovered a chemical defense mechanism in juvenile migratory locusts *Locusta migratoria*. They found that, in response to crowding, locusts synthesize phenylacetonitrile, the precursor of the toxin hydrogen cyanide, whose concentration increases with rising locust densities. This mechanism most probably evolved as a warning signal against cannibalistic conspecifics, which detect phenylacetonitrile through a specific olfactory receptor. Locusts with a knockout of the gene responsible for phenylacetonitrile production are attacked more frequently, highlighting the role of this molecule in deterring intraspecies aggressors (Chang et al., 2023). In contrast, adult gregarious male *Schistocerca gregaria* only produces this compound to deter rival males during courtship. As mentioned in the section above, juvenile desert locusts may gain protection from ingesting toxic plants during mass migration (Couzin & Couzin-Fuchs, 2023; Despland & Simpson, 2005). During their solitary phase, neither of the two species invests in the production of phenylacetonitrile.

Despite the intense competition within dense swarms, migratory locust groups exhibit remarkable coordination, maintaining ordered movement over vast distances. Understanding the mechanisms behind collective motion in animal groups has long been focus of both physics and biology. Over the years, researchers have proposed several hypotheses to explain this phenomenon (Ariel & Ayali, 2015; Bazazi et al., 2008; Couzin et al., 2005; Katz et al., 2011; Sumpter, 2005). Among those, some models elaborated on the role of local attraction, alignment, and repulsion forces between individuals in different zones (Couzin et al., 2002, 2005, 2011), while others suggest the innate optomotor response – a visually guided behavioral trait, which is driven by optic flow and caused by neighboring individuals. In this regard, experiments have been conducted on several animal species, in which neighboring individuals were simulated using moving dot stimuli (Castro et al., 2024). Furthermore, the coherent motion observed in swarms has been abstracted using self-propelled particle models, which simulate collective behavior based on local alignment rules. These models show that direct interactions reduce noise and lead to spontaneous alignment once a critical, minimum density

of individuals is reached (Buhl et al., 2006, 2012). Similar principles have also been applied to describe the abiotic particle flow of, for example, fluids (Vicsek et al., 1995).

Our recent research (Sayin et al., 2025), described in *Chapter 3* of this thesis, challenges the prevailing, classical views and highlights that locust alignment is independent of a critical density and cannot be explained through fixed, physical rules that are based on tactile, local interactions or optomotor response to moving dot patterns. The study combines field, laboratory, and virtual reality experiments to uncover that marching locusts use optical information to navigate in the group and dynamically adjust their own bearings to a vectorial representation of their peers to regulate movement. Instead of reacting to directly neighboring animals, individuals most possibly integrate visual input using a neural ring attractor network, which is known for navigational tasks. This neural structure encodes the relative positions of multiple objects as 'activity bumps' in a circular representation of space. This mechanism might enhance sensitivity to ordered, high-quality motion, allowing locusts to prioritize and follow coherent cues from structured swarm motion while filtering out noisy, disorganized or erratic signals. As a result, the emergence and maintenance of swarm cohesion is not simply an outcome of local alignment but an emergent property of cognitive decision-making, where locusts adaptably integrate visual cues to optimize their activity (Sayin et al., 2025).

LOCUST OLFACTION IN A SOCIAL CONTEXT

The ability to switch between the two strongly contrasting lifestyles places unique demands on the locust's olfactory system, which has consequently evolved an exceptional, phase-dependent plasticity (Ott & Rogers, 2010). Olfactory processing plays a critical role during foraging processes, where solitary locusts are limited to their private information. In contrast, gregarious individuals, just like cockroaches (as described in *Chapter 1*), must evaluate both social cues from conspecifics and direct sensory input from food sources. Research by Günzel et al. demonstrated that *Schistocerca gregaria* gathers and integrates personal (mainly gustatory and olfactory) and social (primarily visual) information when choosing feeding sites. While social cues, meaning high animal densities around a food patch, initially drive patch selection and aggregation, regardless of the option´s quality, the subsequent accumulation of selfish, individual knowledge advances consideration of the two information sources. With both individual and social information channels aligning, decisions are reinforced, and locusts gather at a high-quality food patch. Conversely, inconsistent input is constantly updated and weighed up and results in more optimal choices. This adaptive behavior promotes dynamic

foraging strategy adjustments and supports the tendency of an even distribution at equal food patches (Günzel et al., 2023). The investigation of phase-specific neuronal responses recently revealed that the olfactory system of gregarious desert locusts is specially tuned to support their feeding strategies in a socially complex environment. By performing calcium imaging in the locusts' primary olfactory processing center, our team discovered that gregarious locusts exhibit heightened, synergistic neuronal responses when food-related odors are combined with the scent of conspecifics. We expect this synergy, which is absent in the solitarious type, to enhance food localization and evaluation in a group and, at the same time, to reinforce social cohesion. Behaviorally, this manifests in the foraging choices of gregarious locusts, which actively approach the combined scent of conspecifics and food, whereas solitarious locusts are attracted by the food odor alone (Petelski et al., 2024). This study is detailed in *Chapter 2* of the present dissertation.

CHEMOSENSORY RECEPTION IN INSECTS

For a better understanding of the function and exceptional anatomy of the olfactory system in locusts, it is helpful to take a step back and to examine the general odor perception and processing in insects (Figure 3). In most insects, olfaction is the primary sensory modality when navigating their environment. The sense of smell is essential for locating appropriate food sources, identifying suitable habitats, recognizing mates, avoiding predators, or coordinating social behaviors (Szyszka & Galizia, 2015). Despite the vast diversity of insect species, the overall architecture of their olfactory system varies little. They even share the same fundamental principles, with a conserved organizational pattern across most species in most phyla, including mammals, from peripheral odor detection to central processing in dedicated brain centers (Ache & Young, 2005; Hansson & Stensmyr, 2011; Hildebrand & Shepherd, 1997).

In insects, odor molecules are detected by olfactory receptor neurons (ORNs) that are housed within hair-like sensilla of different types and morphology on the antennae, and, in some species, on the maxillary palps or other appendages (Shanbhag et al., 1999). When odor molecules enter the sensilla through minute pores, they are guided by olfactory binding proteins and finally bind to receptor sites on the dendrites of ORNs, which differ in their odor affinity (Galizia & Sachse, 2010). Most vertebrate and invertebrate ORNs are broadly tuned, with decreasing specificity upon increasing odor concentration (Sachse & Galizia, 2003; Sato et al., 1994; Wang et al., 2003).

ORNs usually express a single seven-transmembrane odorant receptor (OR) gene, which is closely related to the family of seven transmembrane G-protein-coupled receptors of mammals (Vosshall & Laissue, 2008), or to an ionotropic receptor (IR) gene, which is part of the ionotropic glutamate receptor family (Benton et al., 2009; Missbach et al., 2014; Wicher et al., 2008). In rare cases, a single ORN co-expresses up to three ORs (Galizia & Sachse, 2010). ORs are heteromeric complexes, comprising a highly conserved co-receptor, Orco (odorant receptor co-receptor), and a ligand-specific OR subunit (Sato et al., 2008). Some of those receptors are broadly tuned to their ligands, while others are narrowly selective (Andersson et al., 2015). Locust olfactory receptor affinity differs strongly from the norm, exhibiting unusually low redundancy and narrow tuning to specific ligands (Chang et al., 2023).

The interaction with an odor molecule triggers signal transduction, which induces action potentials that encode the odor identity and concentration (Wilson, 2013). The signal is transduced via ORN axons to the bilaterally symmetrical antennal lobe (AL), a neuropil clearly separated by a surrounding glia sheath (Edwards & Meinertzhagen, 2010). The AL is the first olfactory processing center in the insect brain and the functional analog to the vertebrate olfactory bulb (Hansson & Anton, 2000).

ODOR CODING IN INSECTS

Odorants vary drastically in quality and quantity as well as in temporal and spatial distribution (Laurent, 2002). A highly sophisticated coding mechanism is required to receive and process the vast amount of sensory information. Within the AL, incoming electrical signals are organized into distinct units called glomeruli, where projection neurons (PNs) and local interneurons (LNs) receive synaptic excitatory input from the ORNs (Galizia, 2020). These glomeruli serve as specialized processing centers for different odorants, facilitating the representation of odor information (Galizia & Sachse, 2010). As the countless number of odor molecules exceeds the number of ORs, odors typically activate a specific, reproducible set of glomeruli. This results in spatial, combinatorial canonical coding, where odors evoke distinct patterns of glomerular activation, which is similar across individuals of the same species (Galizia & Menzel, 2001; Galizia & Szyszka, 2008; Wang et al., 2003). Within the AL, odorants of similar chemical properties, such as carbon chain length or functional group, were found to elicit activity in spatially organized, adjacent clusters of glomeruli. This so called ‘chemotopic map’ can be found, for instance, in flies (Couto et al., 2005), moths (Bisch-Knaden et al., 2018), or bees (Mertes et al., 2021).

Remarkably, the representation of odor blends is not merely the simple sum of all odorant response patterns in the mixture. Instead, synapses from ORNs to PNs integrate odor mixture input in a non-linear, synergistic or antagonistic manner. Those interactions may enhance or suppress recruitment of glomeruli, even reshaping the whole network response (Nawrot, 2012; Riffell et al., 2014). While the coding pattern for a given odor is relatively stereotyped within species of the same developmental stage and sex, it varies with odor dilution - higher concentrations attenuate receptor specificity, leading to the recruitment of additional glomeruli (De Bruyne et al., 2001; Sachse & Galizia, 2003; Silbering et al., 2008).

Environmental factors or experiences further modulate olfactory processing. For example, non-associative learning in honeybees (S. Das et al., 2011; Locatelli et al., 2013) or prolonged odor exposure in fruit flies can alter odor-induced brain activity (S. Das et al., 2011). In contrast to the multiglomerular innervation, labeled line coding implies that individual odorants, primarily those of critical ecological importance, such as sex pheromones or CO2, are processed through particular, dedicated pathways (Galizia, 2014). As prominent examples, the pheromone cis-vaccenyl acetate evokes activity, restricted to the DA1 glomerulus in *Drosophila*, while geosmin detection, which alerts flies to the presence of toxic microbes, innervates only one type of ORN, that target the DA2 glomerulus (Datta et al., 2008). Similarly, clonal raider ants possess a labeled line leading to the ‘panic glomerulus’ (Hart et al., 2024) and the cockroach AL contains, besides ordinary glomeruli, a separated macroglomerular complex, specialized in processing pheromone signals (Periplanone-a and b) (Linster et al., 1993; Nishino et al., 2009). Calcium imaging studies in cockroaches, pioneered by Paoli et al., demonstrated that the olfactory coding scheme in this hemimetabolous insect shares key similarities with holometabolous insects. Despite the absence of complete brain reorganization during development, cockroaches exhibit a glomerulus-based activation pattern characterized by stimulus specificity, concentration dependency, and topological mapping of chemical structures (Paoli et al., 2020).

Unlike cockroaches, hemimetabolous locust odor coding derives strongly from holometabolous insects. Recent research by Jiang et al. discovered that odors activate a ring-shaped activity pattern around the PN nerve fiber, rather than an isolated glomerulus innervation. This combinatorial pattern encodes ecological importance and chemical identity (Jiang et al., 2024). In the context of pheromone recognition, as observed in holometabolous insects, sensory neuron membrane protein 1 (SNMP1) has been reported to be co-expressed with several OR types and to play a crucial role in pheromone detection (Lehmann et al., 2024).

Typically, the number of ORs and glomeruli in insects is equal, supporting the validity of the one glomerulus - one receptor principle, which means that ORNs expressing a specific OR converge onto the same, topographically fixed glomerulus (Couto et al., 2005; Gao et al., 2000; Vosshall et al., 2000). However, exceptions to this mapping rule were found to exist (Fishilevich & Vosshall, 2005); for example, in fruit flies (Task et al., 2022) and mosquitoes (Herre et al., 2022), where some ORs are linked to multiple glomeruli through the co-expression of multiple receptors in one ORN.

One of the most substantial outliers is, the locust, which possesses more than ten times fewer OR types than glomeruli (Pregitzer et al., 2017; Wang et al., 2015), with ORNs innervating far more than one single glomerulus (Ernst et al., 1977). This unique sensory perception is thought to be reflected in their complex glomerular organization (Wang et al., 2015) (Figure 4).

In some species, such as holometabolous butterflies (Wang et al., 2024) or ants, the number of glomeruli varies between developmental stages or sexes. In the ant species *Camponotus floridanus*, males have approximately 45% fewer glomeruli than females (Zube & Rössler, 2008). The number, shape, and arrangement of glomeruli in the ALs, most likely reflect a divergent evolution (Engel & Grimaldi, 2004). Possibly, differences in olfactory processing capabilities vary clearly across species but are conserved within.

For example, *Drosophila melanogaster* possesses around 50 (Gruber et al., 2023), *Periplaneta americana* about 205 (Watanabe et al., 2010), and *Apis mellifera* approximately 160 glomeruli (Galizia et al., 1999). In striking contrast, adult *Locusta migratoria* and *Schistocerca gregaria*, where glomeruli are arranged in a donut shape around the PN axonal string (Figure 4), have been found to possess an astounding number of up to 2000, and over 1000, microglomeruli, respectively, far surpassing the counts of other insects (Hansson et al., 1996; Jiang et al., 2024). Those high glomeruli counts are close to those of some vertebrates, with, for example, mice housing around 1800 glomeruli (Royet et al., 1988).

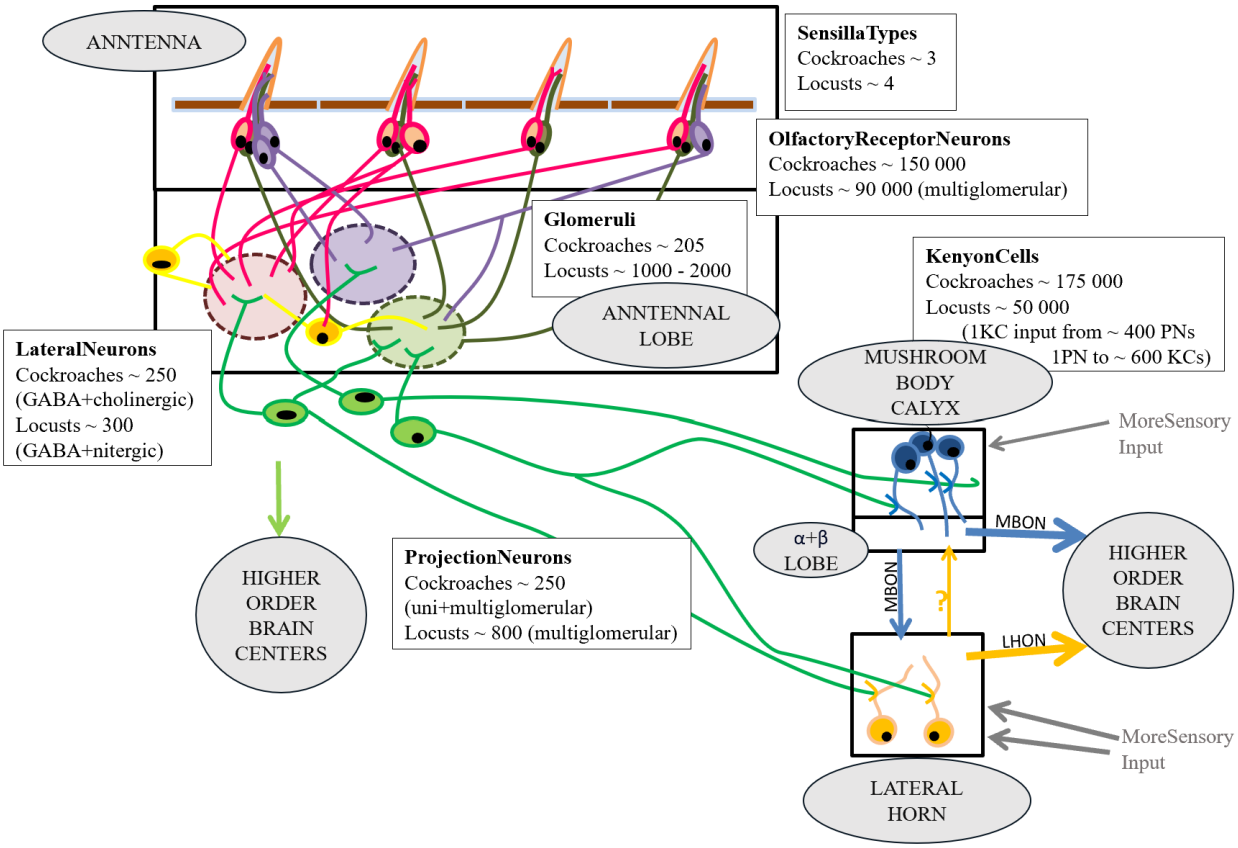

Figure 3: Schematic of the olfactory system in insects, with numbers representing approximations of current literature for cockroaches and locusts. Odorants are detected by olfactory receptor neurons (ORNs) housed in sensilla on the antennae (~3 types in cockroaches, ~4 in locusts). ORNs project to glomeruli in the antennal lobe (AL) (~205 in cockroaches; 1000–2000 in locusts), where olfactory input is organized and shaped by local interneurons (~250 in cockroaches, both GABAergic and cholinergic; ~300 in locusts, GABAergic and nitergic). Projection neurons (PNs; ~250 in cockroaches, ~800 in locusts) transmit processed signals from the AL to higher-order brain centers (PN tracts; ~3 main ones in cockroaches, ~1 main one in locusts), primarily the ipsilateral mushroom body (MB) and lateral horn (LH). In the MB calyx, Kenyon cells (KCs; ~175,000 in cockroaches, ~50,000 in locusts) receive sparse, combinatorial input from PNs. MB output neurons (MBONs) relay information to downstream regions, including the LH and other protocerebral centers. The LH also receives direct PN input and further integrates olfactory and additional sensory modalities. (Schematic by author) (numbers from: Anton & Hansson, 1996; Distler & Boeckh, 1997; Fuscà & Kloppenburg, 2021; Ignell et al., 2001; Jortner, 2013; Jortner et al., 2007; Leitch & Laurent, 1993; Ochieng et al., 1998; Patel & Rangan, 2021; Watanabe et al., 2010; Watanabe & Tateishi, 2023; Wehr & Laurent, 1996)

SIGNAL MODULATION AND PROCESSING IN INSECTS

Once electrical input is received, the signals within the glomeruli are refined through interactions with mainly GABAergic inhibitory (Wilson & Laurent, 2005) and, in some species, additional cholinergic excitatory LNs (Shang et al., 2007). Within the AL, LNs synapse on ORN terminals, PNs, and other LNs (Galizia & Sachse, 2010). Via gain-control, these inter- and intraglomerular interactions enhance the contrast and specificity and adjust the sensitivity of odor signals (Fusca & Kloppenburg, 2021). The processed information is then relayed by a moderate number of PNs, which, in cockroaches, for instance, split into parallel,

bundled pathways, specialized in CO2, sexual pheromones, temperature, or humidity, respectively (Watanabe & Tateishi, 2023). Dual PN streams related to overlapping odors exist in Hymenoptera (Galizia & Rössler, 2010). Uniglomerular PNs, originating from a single glomerulus, bifurcate into two and three tracts in flies and cockroaches, respectively. They transfer their odor information towards higher-order protocerebrum centers, such as the mushroom bodies (MBs) and lateral horn (LH) (Galizia & Rössler, 2010; Martin et al., 2011; Watanabe & Tateishi, 2023). Multiglomerular PNs lead to other forebrain areas through several tracts (Galizia & Sachse, 2010).

Then, once again, the olfactory coding in locusts differs from other insects, with only multiglomerular PNs, each originating from 10 to 25 glomeruli (Anton & Hansson, 1996), which are not innervated by the same ORNs (Anton et al., 2002). PNs transfer the signals in few small tracts elevating to higher order areas (Anton et al., 2002; Ignell et al., 2001) and in a prominent medial tract to the ipsilateral MB calyx (Leitch & Laurent, 1996; Moreaux & Laurent, 2007), with a subset passing the MB to innervate the LH.

Generally, Kenyon cells (KCs) of the MB calyces play a crucial role in odor identification, enabling insects to differentiate and recognize odors, critical for plastic processes such as associative learning, memory storage and retrieval, and behavioral responses (Heisenberg, 1998). In their role as integration centers, they might also contribute to multisensory integration and decision making (Bräcker et al., 2013; Strube-Bloss & Rössler, 2018). In *Drosophila*, each PN forms synapses with approximately 100–200 KCs, while each KC receives convergent input from only about 10 PNs, resulting in sparse and highly selective odor responses (Caron et al., 2013; Turner et al., 2008). KCs project mainly to the alpha and beta MB lobes to synapse onto a small number of extrinsic MB output neurons, of which a few target the LH (Das Chakraborty & Sachse, 2021; Mucignat-Caretta, 2014).

Meanwhile, the LH modulates other brain regions and is associated with naïve odor recognition, valence and evaluation, integrating both innate and learned aspects of olfactory, gustatory, mechanosensory, thermal and visual processing to guide rapid adaptive behaviors, such as attraction and avoidance. The connectivity from PNs to LH neurons is less sparse and more stereotyped (Fişek & Wilson, 2013; Galizia & Szyszka, 2008; Jeanne et al., 2018; Schultzhaus et al., 2017; Seki et al., 2017). LH local neurons and output neurons connect to third-order olfactory centers. Importantly, the long hold believes about a ‘memory versus innate processing pathway’ to the MBs and LHs respectively is currently under debate, as

context-dependent memory was found to be mediated by neurons in the LH (Zhao et al., 2019). At last, the lateral horn most probably sends feedback to the MBs (Schultzhaus et al., 2017).

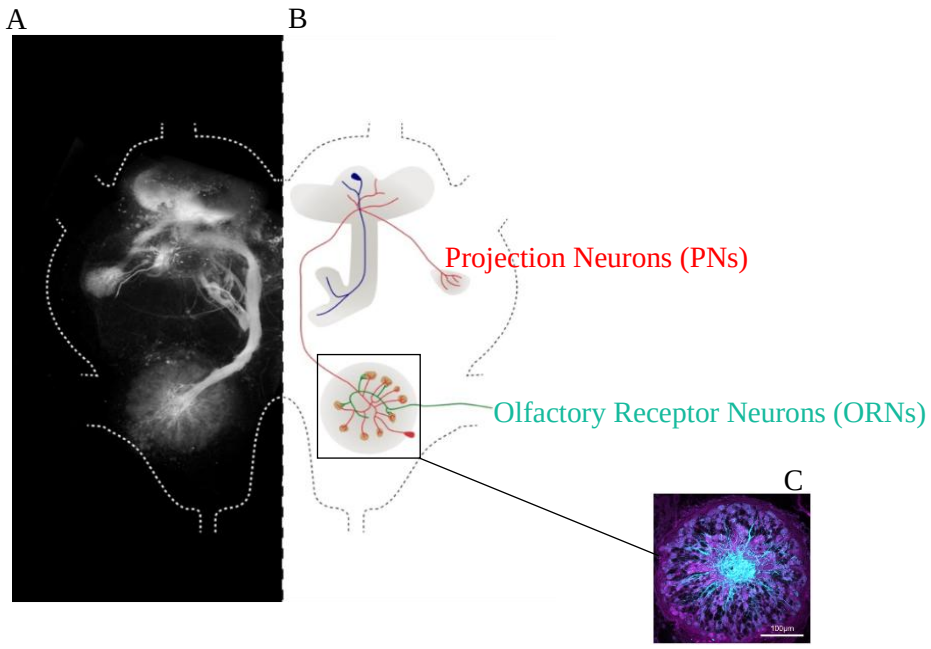

Figure 4: Composite illustration of the olfactory system in locusts. (A) Confocal laser scanning microscope image of the central brain in locusts, visualizing the antennal lobe AL) and its projections after Alexa 488 injection into the mushroom body (MB) calyx. Major tract pathways of the AL are visible. (B) Schematic representation of major olfactory pathways overlaid over the brain outline. Olfactory Receptor Neurons (ORNs, green) project to the AL, where they synapse onto Projection Neurons (PNs, red). PNs relay processed signals to higher order brain centers such as the MB Kenyon Cells (KCs, blue) in the calyx and the lateral horn. (C) Compiled z-stack image of a double-backfilled staining of the locust AL, illustrating its organization into over 1000 microglomeruli. PNs (blue) and ORNs (magenta) are labeled with Alexa 488 and Alexa 568 respectively to highlight their respective distribution. (Graphic and microscopy scans by author)

CALCIUM IMAGING

In the past, the study of the structural complexity of the olfactory system in insects raised important questions about how odor information is perceived and processed dynamically. While anatomical studies could reveal the intricate organization of glomeruli in the AL and its connection to higher brain centers in cockroaches (Watanabe et al., 2010) or bees (Galizia et al., 1999), investigating neural activity was essential to uncover olfactory coding. In this regard, physiological approaches enabled researchers to observe how neurons dynamically respond to sensory stimuli *in vitro* and *in vivo*. For example, electrophysiological single-cell recordings and patch-clamp techniques could provide insights into the electrical properties of individual neurons, their spontaneous activity (Meyer et al., 2013), and their general role in olfactory signaling (Shang et al., 2007). In addition to single-cell methods, multi-electrode arrays made it possible to simultaneously record the activity from multiple neurons (Krüger & Bach, 1981),

facilitating the study of the coordinated activity of large populations of neurons in areas such as the AL (Christensen et al., 2000). Still, the monitoring of large-scale neuronal activity across the entire network is limited when using electrophysiological methods. Thence, optogenetics overcame some of these challenges. Here, light-controlled proteins (opsins) can activate or inhibit neuronal activity (Gholami Pourbadie & Sayyah, 2018). This method can even be combined with electrophysiological recordings to selectively control specific neurons in real-time (Berg et al., 2020). However, all these methods dealt with relatively small populations of neurons.

The technique of calcium imaging revolutionized the spatiotemporal research on large neuronal networks in live animals (Russell, 2011). It offers the advantage of enabling simultaneous visualization of the encoding of different sensory information or behavioral traits in the brain (Aimon et al., 2019). The calcium imaging technique employs calcium-sensitive fluorescent indicators to monitor fluctuations in intracellular calcium levels, which are closely correlated with neuronal activity (Ingram et al., 2024). In signaling events across various organisms, calcium serves as a second messenger (Galizia & Lledo, 2014). The initial depolarization of an action potential involves an influx of positive sodium ions (Na^+) into the neuron, making the interior of the cell more positive than the extracellular space. This phase is followed by an efflux of potassium ions (K^+) during repolarization, which is fading out during hyperpolarization (Grider et al., 2023). In neurons, receptor activation and depolarization by passing action potentials cause a significant calcium concentration shift, meaning that a sudden and rapid increase in intracellular calcium levels accompanies high action potential firing rates. The calcium influx occurs primarily through voltage-gated calcium channels at presynaptic terminals and dendritic spines (Catterall, 2011). Furthermore, in several insects, such as mosquitoes, silk moths, or fruit flies, ligand-gated channels of ORNs cause an influx of extracellular calcium upon odor stimulation (Sato et al., 2008). Also, calcium can be released from intracellular stores - mainly the endoplasmatic reticulum - further amplifying the signal (Grienberger & Konnerth, 2012; Verkhratsky, 2005). Due to this correlation between action potential firing rates and intracellular calcium levels, calcium does serve as a proxy for the neuronal activity (Charpak, 2001). Accordingly, calcium indicators are a perfect tool to monitor neuronal excitation patterns and the synaptic input.

The most popular and widely used genetically encoded calcium indicator is GCaMP (Nakai et al., 2001). It derives from the green fluorescent protein (GFP), which was initially discovered in a jellyfish species by Osamu Shimomura (Shimomura, 2005). GCaMP consists of a

circularly permuted GFP molecule that is fused to a calmodulin calcium-binding domain and a calcium-binding peptide (M13) (Akerboom et al., 2012). The binding of calcium induces a conformational change in calmodulin, which subsequently interacts with the M13 peptide. This interaction alters and stabilizes the structure of GFP, leading to an increase in fluorescence intensity and enabling a direct readout of neuronal activity (Akerboom et al., 2012; Chen et al., 2013). GCaMP can be introduced into the cells of invertebrates and vertebrates through transfection, or integrated into the genome over transgenic approaches (Tian et al., 2009). Transgenic laboratory insect species which genetically encode GCaMP now range from *Drosophila* (Tian et al., 2009), to ants (Hart et al., 2023), and mosquitos (Bui et al., 2019).

In locusts, an effortful application of the CRISPR-Cas9 system by Jiang et al. successfully generated transgenic migratory locusts, which express GCaMP in olfactory sensory neurons. This facilitated two-photon functional imaging of odor-evoked neuronal responses in the entire AL of *locusta Migratoria* (Jiang et al., 2024). In species where genetically encoded calcium indicators are unavailable, or have not been established yet, calcium-sensitive dyes provide an alternative, affordable approach to genetically encoded calcium indicators. These dyes can be introduced into specific neuron populations via direct loading, bath application, electroporation, or retrograde labeling.

Due to the lack of stable genetic GCaMP lines, method of retrograde PN labeling with fluorescent indicator dyes has thus been applied in the research on cockroaches and locusts for the current dissertation. In this context, dyes were injected at axonal PN sites, where they are transported retrogradely to neuronal cell bodies and dendrites. Dye loading permitted quantitative calcium imaging of glomerular activity in the AL. Fura 2 is one of the most popular radiometric calcium-sensitive dyes, which shifts its fluorescence excitation spectrum upon calcium binding (Grynkiewicz et al., 1985). Fura 2 can be coupled to a dextran to prevent dye leakage and improve neuronal transport and stability. Photobleaching of this dye is minimized due to its excitation at two distinct wavelengths in the ultraviolet spectrum, allowing for ratio-based measurements that compensate for signal loss. Another widely used synthetic dye, Cal-520, provides a high signal-to-noise ratio and is well-suited to detect fast neuronal calcium transients (Tada et al., 2014).

In a final step, the visualization of calcium imaging applications has been enhanced through ultra-high-resolution microscopy techniques, which permit intrusion into deep cell layers. Especially two- and three-photon microscopy with high excitation wavelengths (Lin et al., 2019) can reduce light scattering and phototoxic effects while reaching deep cell layers.

CHAPTER OUTLOOK

The study of insects points out just how fluid the boundaries can be between personal choices and group behavior. Fortunately, modern techniques allow us to explore how insect brains weigh and integrate the intertwined multisensory personal and social information they receive in order to adapt to their complex surroundings. To comprehend how such multifaceted behaviors emerge and how they can scale up to produce some of the most breathtaking collective phenomena, it is crucial to unravel if and how sensory processing can be reshaped at the level of the individual.

Over the next three chapters, we will gain knowledge about sensory processing and decision making in a social context, tracing the path from odor molecules reaching the antennae to massive swarm motion in insects. We will explore how cockroaches adjust the early olfactory coding, how the internal physiological state and the social context can interact and reconfigure the behavior and early sensory perception in locusts, and finally, how this extends to a swarm-wide range.

In *Chapter 1*, we encounter cockroaches whose preferences shift under the invisible influence of conspecifics, and find out how sensory processing in the first olfactory neuropil encodes social presence. In *Chapter 2*, we move into the phase-dependent sensory world of locusts, to uncover how food and social signals interact non-linearly in the brain to guide gregarious animals during group foraging. To this end, *Chapter 3* follows the momentum of gregarious hoppers and explores how visually guided alignment can create coherent movement patterns.

CHAPTER 1

SOCIAL MODULATION OF INDIVIDUAL PREFERENCES IN COCKROACHES

Yannick Günzel, Jaclyn McCollum, Marco Paoli, Giovanni Galizia, Inga Petelski, Einat Couzin-Fuchs

iScience 2021

CHAPTER SUMMARY

This study was inspired by the work of Salazar et al. 2017, who discovered a striking collective inversion of shelter selection in socially influenced cockroaches. Their findings attracted our attention, as they contradicted much of the literature about social amplification, consensual decisions or group mediated choices. The authors conducted behavioral experiments, which they modelled mathematically, and revealed that under given circumstances, social interactions can override rather than amplify individual choices, as observed in other contexts. In their experiments and models, cockroaches, despite their highly social nature, abandoned their innate preference for a food-scented shelter in favor of an empty control shelter, when in a group.

Building on these results, we successfully managed to replicate this phenomenon. Furthermore, we uncovered that this collective preference shift can be driven by olfactory social cues alone - without any visual, tactile or auditory indication of the physical presence of conspecifics. While both vanillin extract and the social odor, a fecal odor blend, were individually attractive, their combination reduced the tendency for vanillin-scented shelters.

The development of a technique to label the entire population of projection neurons (PNs) in cockroaches with Fura 2, pioneered by our colleague and co-author Paoli et al. (Paoli et al., 2020), allowed us to directly link behavioral results with distinct neural stimulus representations in the antennal lobe (AL). We exposed stained individuals during calcium imaging to appetitive vanillin, the social odor, and their combination, at varying concentrations and analyzed how these odors are encoded in AL glomeruli. Interestingly, when cockroaches are confronted with both stimuli simultaneously, an altered response pattern is displayed, which

is characterized by a decreased activity in vanillin-responsive regions. In contrast, neuronal activity remains stable or slightly increases in areas responsible for the social odor.

Our results suggest that the sensory integration and valence of a food odor is already modified by social dynamics at an early neuronal processing level. This negative feedback, caused by conspecifics, is capable of ultimately overriding individual preferences and guiding collective decision-making. In this context, the reversed evaluation of the initially attractive odor might be a crucial factor in encouraging cockroaches to explore new feeding sites and in hindering them from wasting energy on overexploited resources.

Our study raises numerous follow-up questions for future research, such as the transferability of our findings to varying internal states, odors, sensory modalities and to other species. Additionally, a detailed exploration of the modulated neuronal mechanisms within the whole, three-dimensional AL during odor mixture exposure may provide insights into the glomerular crosstalk via local interneurons (LNs). Tracing sensory signals from sensory input in the antennae, through processing in the ALs, mushroom bodies and lateral horn, towards motor output, would yield extremely interesting insights into the sensory impact of social structures. In this regard, *Chapter 2* of this thesis will pursue the direction of social modulation of appetitive odor perception at the level of the antennae and ALs in another insect species, renowned for a remarkable social plasticity.

› iScience. 2020 Dec 19;24(1):101964. doi: 10.1016/j.isci.2020.101964. eCollection 2021 Jan 22.

Social modulation of individual preferences in cockroaches

Yannick Günzel [1 2 3], Jaclyn McCollum [1], Marco Paoli [1 4], C Giovanni Galizia [1 2], Inga Petelski [1 3] Einat Couzin-Fuchs [1 2 3]

Affiliations + expand

PMID: 33437942 PMCID: PMC7788088 DOI: 10.1016/j.isci.2020.101964

ABSTRACT

In social species, decision-making is both influenced by, and in turn influences, the social context. This reciprocal feedback introduces coupling across scales, from the neural basis of sensing, to individual and collective decision-making. Here, we adopt an integrative approach investigating decision-making in dynamical social contexts. When choosing shelters, isolated cockroaches prefer vanillin-scented (food-associated) shelters over unscented ones, yet in groups, this preference is inverted. We demonstrate that this inversion can be replicated by replacing the full social context with social odors: presented alone food and social odors are attractive, yet when presented as a mixture they are avoided. Via antennal lobe calcium imaging, we show that neural activity in vanillin-responsive regions reduces as social odor concentration increases. Thus, we suggest that the mixture is evaluated as a distinct olfactory object with opposite valence, providing a mechanism that would naturally result in individuals avoiding what they perceive as recently exploited resources.

INTRODUCTION

Dissecting social feedbacks in collective behavior is notoriously difficult. While modeling has proven to be extremely valuable in constructing plausible hypotheses for how individual behavior scales to collective phenomena, alternative individual-level mechanisms may produce similar higher-order (*e.g.* group-level and population-level) patterns. In order to discriminate among alternative hypotheses - and also to allow the generation of new hypotheses - approaches that allow the tracking of individuals as they make decisions within their social context, as well as investigating the neural activity during decision-making, may prove to be invaluable. A common feature of decision-making in social species is that relevant information may be individually acquired or socially derived, and the key to achieve effective foraging is a context-dependent balance of both (Dunlap et al., 2016; Kendal et al., 2009; King & Cowlishaw, 2007; Miller et al., 2013; Rieucau & Giraldeau, 2011). Furthermore, the question whether to use social information, and to what degree, will often depend on the context (Dunlap et al., 2016; Kendal et al., 2009); for example, the presence of conspecifics on a resource patch may imply high food quality but also strong competition. In general, social information becomes more valuable when environmental cues are weak, unreliable, or costly to acquire (Ame et al., 2004; Dunlap et al., 2016; Kendal et al., 2004; Miller et al., 2013). Without an explicit calculation of reliability (Torney et al., 2009), inferring the preferences of conspecifics can provide a valuable indication of resource quality. At the same time, this information means that the resource has already been, at least partially, exploited (Canonge et al., 2011; Hall & Kramer, 2008).

How do animals balance individual and social information? The tractability of cockroaches for the study of collective behavior, and their easily accessible nervous system offer new opportunities to tackle this question (Amé et al., 2006; Lihoreau et al., 2012; Lihoreau & Rivault, 2011). Cockroaches reside in large and cohesive aggregates in dark shelters during their resting phase, which they leave mainly solitarily to locate resources in their home range (Durier & Rivault, 2000; Lihoreau et al., 2012). Different physical properties influence the decisions to settle in or to leave a shelter, including illumination level, humidity, and cues for food presence (Calvo Martín et al., 2019; Canonge et al., 2009; Doi & Toh, 1992). In addition, past visits, as well as presence of conspecifics, increase the probability of individuals to utilize a shelter, as long as it is not overcrowded (Ame et al., 2004; Canonge et al., 2009, 2011; Jeanson et al., 2005; Planas-Sitjà et al., 2015). Taken together, these findings suggest that cockroach's shelter-selection behavior results from the interplay between the tendency to aggregate and

competition for resources, offering a model system to study the mechanisms underlying collective decision-making (Amé et al., 2006; Canonge et al., 2011).

Recently, it has been reported that individual cockroaches Periplaneta americana prefer vanillin-scented shelters over unscented controls in a binary choice assay (Laurent Salazar et al., 2017). Vanillin is known to be an attractant to cockroaches, most likely indicating a potential food source, as it can be found in various plants and decaying wood (Meyer & Norris, 1967). The preference for vanillin is reversed, however, when individuals are tested in a group (Laurent Salazar et al., 2017). Supported by a computational model, it has been suggested that this preference inversion can be accounted for if individuals exhibit a weaker social interaction in the presence of vanillin (Calvo Martín et al., 2019; Laurent Salazar et al., 2017). As a result, a stronger social amplification would occur in the absence of vanillin such that groups form more easily in the unscented shelter. A similar inversion phenomenon has also been observed when cockroaches were faced with shelters of different humidity levels: individuals showed the tendency to prefer humid shelters, while groups aggregate more in a drier alternative (Calvo Martín et al., 2019).

A complementary approach to behavioral experimentation, and one that may reveal new insights into underlying mechanisms, is to investigate how sensory information is integrated by individuals (i.e. via neural imaging). Since cockroaches are nocturnal animals, they rely heavily on their sense of smell to gain information about their surroundings—*e.g.*to locate food sources, sense conspecifics, potential danger, and to find mates (Bell et al., 2007). Olfactory cues are received by approx. 230,000 olfactory sensory neurons (OSNs) located on their antennae, and relayed to the antennal lobe (AL), the first odor processing center in the insect brain, analogous to the vertebrate olfactory bulb (Sass, 1983; Schafer & Sanchez, 1973). The cockroach AL comprises 200 anatomical and functional units, the glomeruli (Watanabe et al., 2010), which collect the input from the OSNs and forward it to higher-order brain centers by means of uniglomerular and multiglomerular projection neurons (PNs) (Malun et al., 1993; Watanabe et al., 2017). All sensory neurons bearing the same olfactory receptor project to a single glomerulus, converging onto the same uniglomerular PN. This parallel flow of information from cognate OSNs to uniglomerular PNs is cross-linked by a network of inhibitory local interneurons (LNs) (Distler, 1989), which interconnects multiple glomeruli and contributes to shaping the neural representation of an olfactory cue (Fusca et al., 2013; Husch et al., 2009; Olsen & Wilson, 2008; Silbering et al., 2012).

Here, we employed shelter selection as an assay to investigate the sensory basis of individual and collective decision-making in cockroaches (*Periplaneta americana*). We discover that the presence of a social odor influences individual shelter selection and monitor how food- and social-related olfactory information shape individual preference. To test how behavioral choices relate to the neural representation of the stimuli, we adopted a recently established method for selectively labeling the uniglomerular PNs population with a calcium sensitive dye for AL functional imaging (Paoli et al., 2020). Thus, combining neuroimaging with behavioral assays, we studied how food and colony odor cues, alone or combined, are encoded by the cockroach brain and how their perception guides behavioral choices.

RESULTS

Inversion of shelter preference when in groups

Shelter preference was assessed from the behavior of individuals and groups of cockroaches in a circular arena with two opaque shelter options: one containing an olfactory cue and one unscented as a control (Figure 1A). Animals were tracked for 30 min to characterize individuals' behavior both outside and within the shelters (Figure 1B). During this time, cockroaches typically explored the arena and intermittently visited both shelters.

As previously documented (Laurent Salazar et al., 2017; Sakura & Mizunami, 2001), individual cockroaches show innate attraction to vanillin, and spent more time in close proximity to the vanillin shelter than to the unscented one (Figure 2A$_{ii}$). A similar trend, although weaker, could be observed also when the scented shelter contained lower vanillin concentration (Figure 2B and Supplemental information Appendix, Figure S1A$_{ii}$ n = 15 for each). However, when groups of cockroaches were tested together, the behavioral outcome was reversed, in agreement with the observation of (Laurent Salazar et al., 2017). In groups, individuals spent more time in and around the unscented control shelter compared to those that were tested individually (Figures 2A$_{i}$ and 2B; n = 10 groups, 20 individuals each).

Density maps of the different tested conditions show the spatial distribution of individuals throughout trials, with the overall density along the two dimensions of the arena plotted in a solid line above and beside the heatmaps (Figure 2A and Supplemental information Appendix, Figure S1A for all other tested conditions). Note that while randomized in the experiments, all data presented are oriented to present the odor side on the right. Cockroaches were attracted to the shelters in all tested conditions and the direction of preference was quantified by the proportion of time (Figure 2B) and number of entries

(Figure 2C) to the odor versus the control shelter. In particular, when facing the choice between vanillin and the unscented control in the individual assay, cockroaches clearly shifted their preference toward the vanillin shelter (individuals overall displayed significantly increased shelter (Figure 2B, $p = 0.004$) and entry (Figure 2C, $p = 0.009$) preference indices in comparison the the mean group level, one-sample two-tailed randomization tests).

When 20 individuals are tested together, despite the fact that cockroaches exhibit a higher propensity to aggregate in the control shelter (the likelihood of the vanillin shelter being empty ($n = 0$) is double than that of the unscented one [Figure 2D, blue/gray histogram shows the number of individuals at the vanillin/control shelter in all group trials]), we do not find evidence that individuals exhibit a different social tendency. For both shelters, cockroaches tend to remain longer (exhibit longer bouts) in shelters with higher occupancy, as long as they are not overcrowded, but this social relationship does not differ between the two shelters (Figure 2E, if anything overcrowding—or reduction in social feedback above a high occupancy limit—is more apparent in the control). This suggests that the increased group sizes found in the control shelter may not result solely from a decreased social attractivity in the presence of vanillin. A mutually not exclusive alternative possibility is that individuals exhibit an innate change in their shelter preference in the presence of social cues.

How social cues impact individual shelter preference

In order to better understand the basis of the preference inversion, we investigated how individual preference is influenced by social cues. We hypothesized that the presence of an odor of conspecifics would influence decisions of individuals and thus tested whether a similar inversion of preference is also observed when the only indication for conspecifics presence is a group-related smell. For this an extract of the colony feces was used as a social-related odor (Wada-Katsumata et al., 2015; Zhang et al., 2019) and added to the vanillin shelter at varying concentrations (fe2(3),van2+fe3, van2+fe2, van3+fe2; van2(3), vanillin dilution of $10^{-2(3)}$; fe2(3), feces extract dilution of $10^{-2(3)}$).

We analyzed individuals' preferences for both for the shelters (Figure 3A) and also the area in close proximity of the shelters (splitting the arena into quarters, as shown in Figure 3B). The latter analysis was conducted because we observed that the shelter influences cockroach behavior when they are in its vicinity as well as within it. Both vanillin and social odor, when presented alone, are attractive. However, when presented together at one shelter, if the concentration of social odor is sufficiently high, individuals invert their preference, as seen in

the group experiments (see Figure Figures 3A$_{ii}$and 3B$_{ii}$for the proportion of time spent in the odor (colored bar) and control (empty bar) shelter/quarter, respectively, and Supplemental information Appendix, Figure S1 for density maps across the arena in all tested conditions). For the duration of our experiments, we found that, over time, individuals exhibited intermittent visits to both shelters and their respective quarters, while their preferences remained consistent (Figures 3A$_{iii}$and 3B$_{iii}$). This allowed us to determine a single preference index (the relative time in the odor vs. control shelter/quarter) for each condition (Figures 3A$_{iv}$ and 3B$_{iv}$).

Tracking of individual cockroaches allowed us to evaluate the relative proportion of entries into the odor and the control shelter for each condition. For each condition, individuals were found to enter more frequently their shelter of preference (Figures 4A$_{ii}$ and 4A$_{iii}$). In addition, the time spent in the shelter for each visit (bout duration) was longer in the preferred shelter (Figures 4B$_{ii}$and 4$_{iii}$). This demonstrates that both the probability of visiting a shelter, as well as the duration of stay during each visit, contribute to the overall time spent by individuals in each shelter, and thus to the observed differences in shelter preference.

Taking into account the different behavioral features shown in Figures 3 and 4, behavioral similarity across all tested conditions was evaluated using a hierarchical clustering algorithm, indicating that the behavior of individuals in the group context are overall similar to isolated individuals, when vanillin is combined with a social odor component (Figure 4C, red boxes).

Colony odor modulates vanillin-induced response in the AL

To investigate how the observed preferences relate to the neural representation of the stimuli, we employed calcium imaging to determine how vanillin, feces extract, and mixtures of the two, are mapped in the primary olfactory center of the cockroach, the AL. Following a recently developed protocol (Paoli et al., 2020) uniglomerular PNs were selectively labeled with the calcium sensor Fura-2 for functional imaging analysis. Successful labeling resulted in bright fluorescence of the PNs somata clusters as well as their uniglomerular dendritic arborizations, allowing several hours of calcium imaging analysis per individual (n = 10) with multiple olfactory stimulation sessions (Figure 5A; (Paoli et al., 2020)). Hence, we tested the same odor combinations employed in the behavioral assays and analyzed their neural representations.

During odor presentation, changes in intracellular calcium levels could be observed in discrete areas comparable in size and shape to individual glomeruli (Figures 5A and 5B). Individuals exhibited stimulus-dependent glomerular response maps that were consistent across repetitions (Figure 5C, see also Supplemental information Appendix, Figures S2 and S3). As no

difference in response latency was observed across the different stimuli (Supplemental information Appendix, Figures S2B and S3B), all analyses were based on the average odor response maps between 0.6 and 1 s after stimulus onset (when the calcium-induced responses were strongest) across three-to-four non-consecutive repetitions of the same stimulus after subtracting the response to the solvent, *i.e.*mineral oil. For further details on calcium signal analysis, see Transparent methods section.

Response intensity increased with increasing stimulus concentrations. At a higher concentration (10^{-2} dilution), both vanillin and feces extract induce calcium responses in multiple areas of the AL with stimulus-specific activity maps (responses to 10^{-3} dilutions were weak across all regions and therefore not included in the analysis). The presentation of both feces extract and vanillin together resulted in response maps similar to those elicited by the single components, depending on their relative concentration. The van10^{-2} + fe10^{-3} mixture produced a glomerular activation pattern similar to the one elicited by vanillin alone, while the balanced and the low-vanillin mixtures (van10^{-2} + fe10^{-2}, and van10^{-3} + fe10^{-2}) showed response profiles comparable to the one of feces extract alone. To quantitatively assess the physiological similarity among stimulus-induced responses, we calculated the correlation coefficients among odor response maps (Guerrieri et al., 2005; Paoli et al., 2020). For each animal and stimulus condition, we constructed a response vector considering all functional units activated by any of the odor conditions, segmented into 25 regions of interests (ROIs) using a *k*-medoids functional clustering algorithm (see Transparent methods section, examples for the first two animals in Figures 5B–5D, and more in details in Supplemental information Appendix, Figures S2–S4). Response vectors were used to calculate the correlation matrix across conditions and quantify odor response similarity (Figure 5E and Supplemental information Appendix, Figure S4 for correlation matrices of individual animals, and Figure 5G for the same analysis considering all ROIs for all individuals).

As can be seen in the dendrogram, which considers all individuals, the neural representation of vanillin in the glomerular space shifts closer to that one of feces extract as the proportion of the latter in the mixture increases (Figure 5G). When concentration of both vanillin and social odor are high, we find that the latter is dominant (but not exclusive), with only weak activity being observed in the vanillin-sensitive regions (Figure 5G, Supplemental information Appendix, Figure S4). This finding suggests that the way in which vanillin is perceived is different in a social context, and that this perceptual difference could contribute to the observed preference inversion in the behavioral experiments.

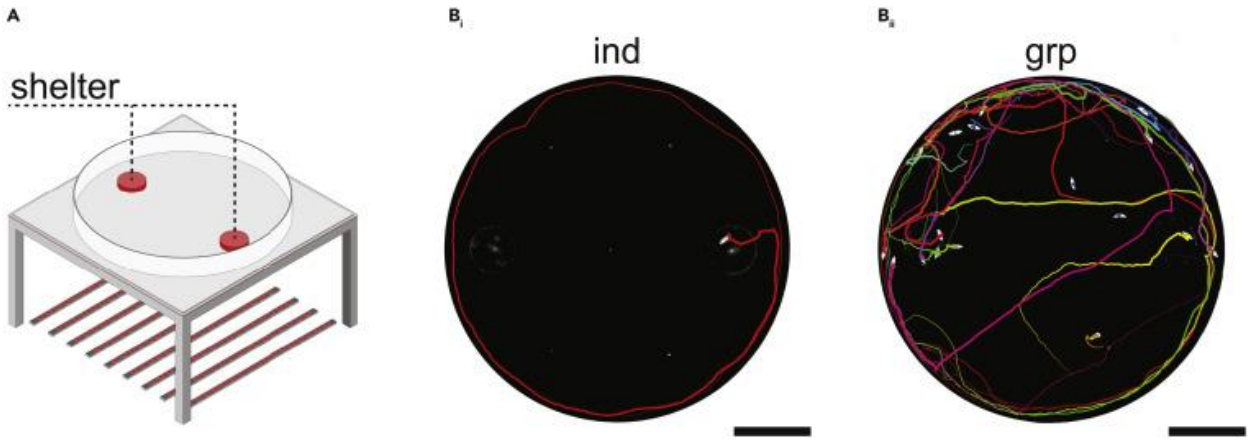

Figure 1. Experimental setup to record shelter selection of individuals or groups. (A) Schematic of the arena. Two shelters (d = 12 cm; h = 2 cm) were placed in randomly selected positions out of six possible locations for odor insertion. Shelters were always opposing each other. The arena (d = 90 cm) was illuminated using arrays of IR LEDs placed below and filmed from above with a Basler camera (not shown). (B) A tracking software (modified from [(Sridhar et al., 2019)] to keep animal identities) was used to record animal trajectories in individual (B_i) and group trials (B_{ii}). Images were cropped and colors inverted to highlight the exemplary trajectories during a period of 60 s. Thickness of strokes codes time. Scale bars: 20 cm.

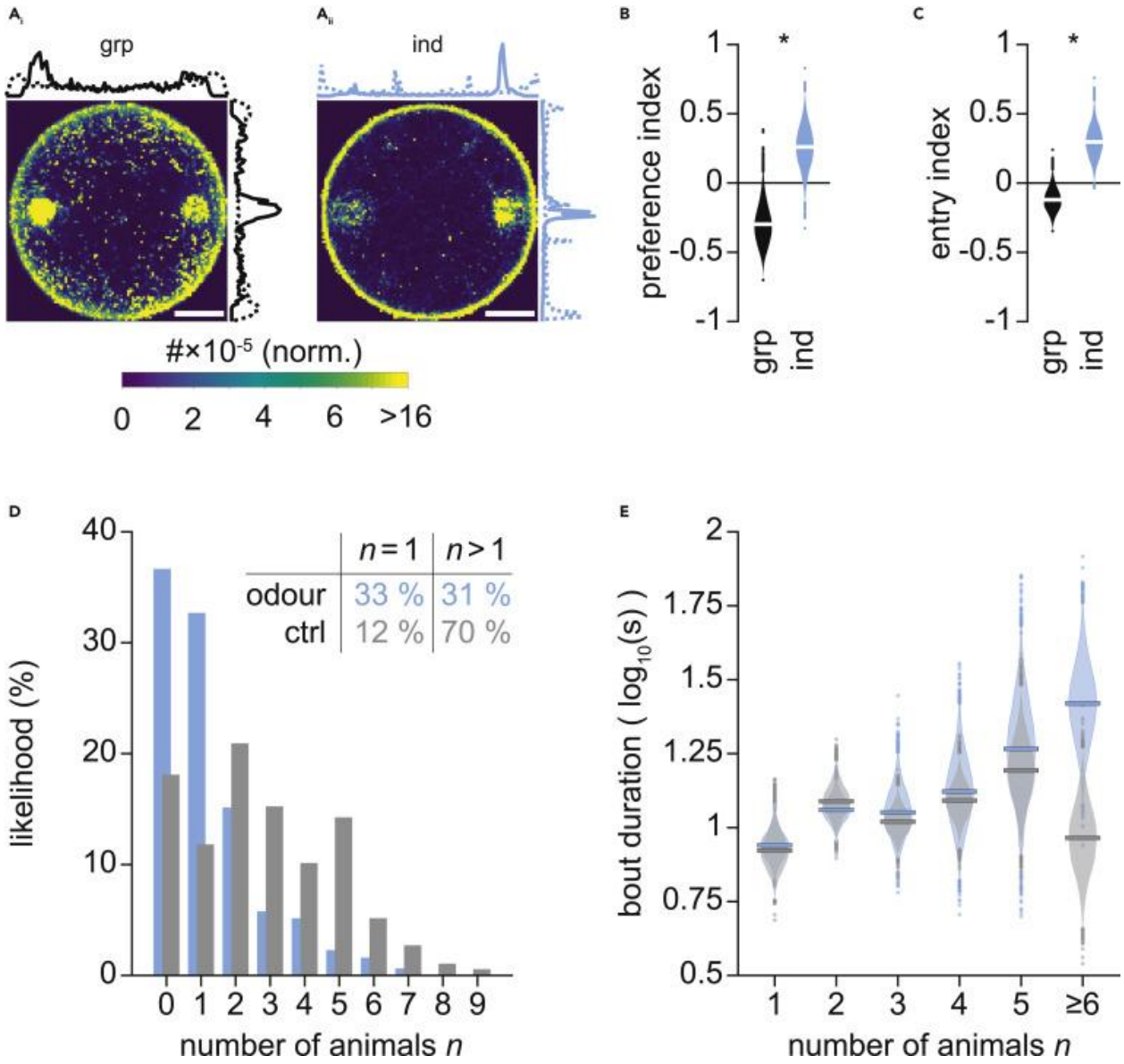

Figure 2. Shelter preference in individual and group trials. In all panels, vanillin diluted to 10−2 was administered to the odor shelter, while pure mineral oil was administered to the control shelter. (A) Density maps of animal positions over all group (Ai) and individual (Aii) trials. Heatmaps show counts per pixel, normalized to 1 and averaged for the number of tested animals. Presence densities across and along the arena are indicated above and beside the heatmaps. As wall-following bouts were highly prevalent in all tested conditions, especially during the beginning of each trial, presence density was separated for the outer (wall-following bouts, dotted lines) and inner (solid lines) part of the arena. The sum of both yields the presence density for the whole arena. Scale bars: 20 cm. (B) Shelter preference index based on the proportion of time individuals spend in the odor versus control (unscented) shelter, for group (black) and individual (blue) trials.
(C) Preference index based on entries to the odor vs. control shelter for groups and individuals. For both preference indices, a value of positive one indicates a complete preference for the odor shelter/quarter, while and a value of negative one a complete preference for the control shelter/quarter (for details see subsection Tracking and data analysis of the Transparent methods section). Asterisks indicate significant differences between distributions of individual trials and the mean group level($p < 0.05$), using a one-sample two-tailed randomization test. (D) Probability histograms for the number of sheltered individuals in the odor (blue) and control (gray) shelters during group trials. The likelihood of observing a single animal, or a group of animals is not independent of the shelter (chi-squared test, $\chi2 = 69.37$, $df = 1$, $p < 0.001$). (E) Bout duration as a function of the average number of animals (rounded) sheltered during each stay, depicted as violin plots (as in D, blue and gray represent the odor and control shelters, respectively). Horizontal lines show distribution means. Values of six or more sheltered individuals are rare, especially for the odor shelter (see D), and grouped together. Abbreviations: grp, group; ind, individual; ctrl, control

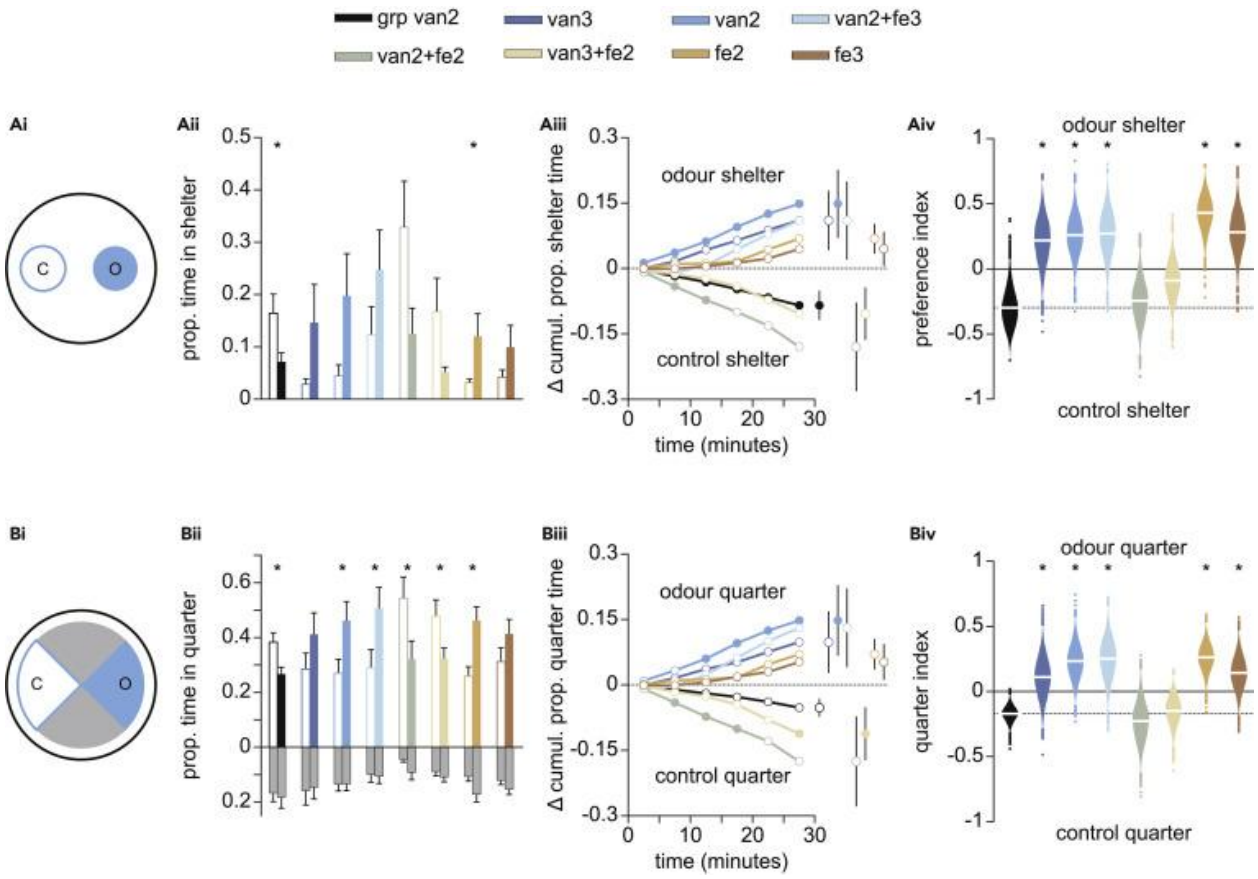

Figure 3. Individual preference is inverted in an olfactory simulated group context. Proportion of time in the shelters (A) and in the four different quarters (B) of the arena. (A_{ii}) and (B_{ii}) show the proportion of time in the odor (full bars) and control (empty bars) shelter/quarter. Error bars denote standard deviations and asterisks statistically significant differences ($p < 0.05$) between proportion of time in the odor vs. control shelter/quarter, using a two-sample two-tailed randomization test. In (B) upright bars above the x axis represent the odor and control quarters and the inverted correspond to the empty quarters. (A_{iii}) and (B_{iii}) The difference in the cumulative proportion of time in the odor vs. the control shelter/quarter for each tested condition. The differences in cumulative time were calculated in six bins of five minutes each. Standard deviation around the means of the last time bins are shown on the right of the line plots. Filled circles in (A_{iii}) and (B_{iii}) indicate a statistically significant difference between odor and control shelter/quarter ($p < 0.05$) using a two-sample two-tailed randomization test. (A_{iv}) and (B_{iv}) Preference index calculated based on the total time in the odor vs. control shelter/quarter for all eight conditions, based on the proportions shown in (A_{ii}) and (B_{ii}). A value of +1 indicates a complete preference for the odor shelter/quarter, while and a value of −1 a complete preference for the control shelter/quarter (for details see subsection Tracking and data analysis of the Transparent methods section). White horizontal lines show distribution means. Asterisks indicate statistically significant differences ($p < 0.05$) testing the distributions of the seven individual conditions against the mean level of the group condition (dotted line, obtained from the group experiments shown in Figure 2), using a one-sample two-tailed randomization test. Abbreviations: grp, group; van2(3), vanillin dilution of $10^{-2(3)}$; fe2(3), feces extract dilution of $10^{-2(3)}$.

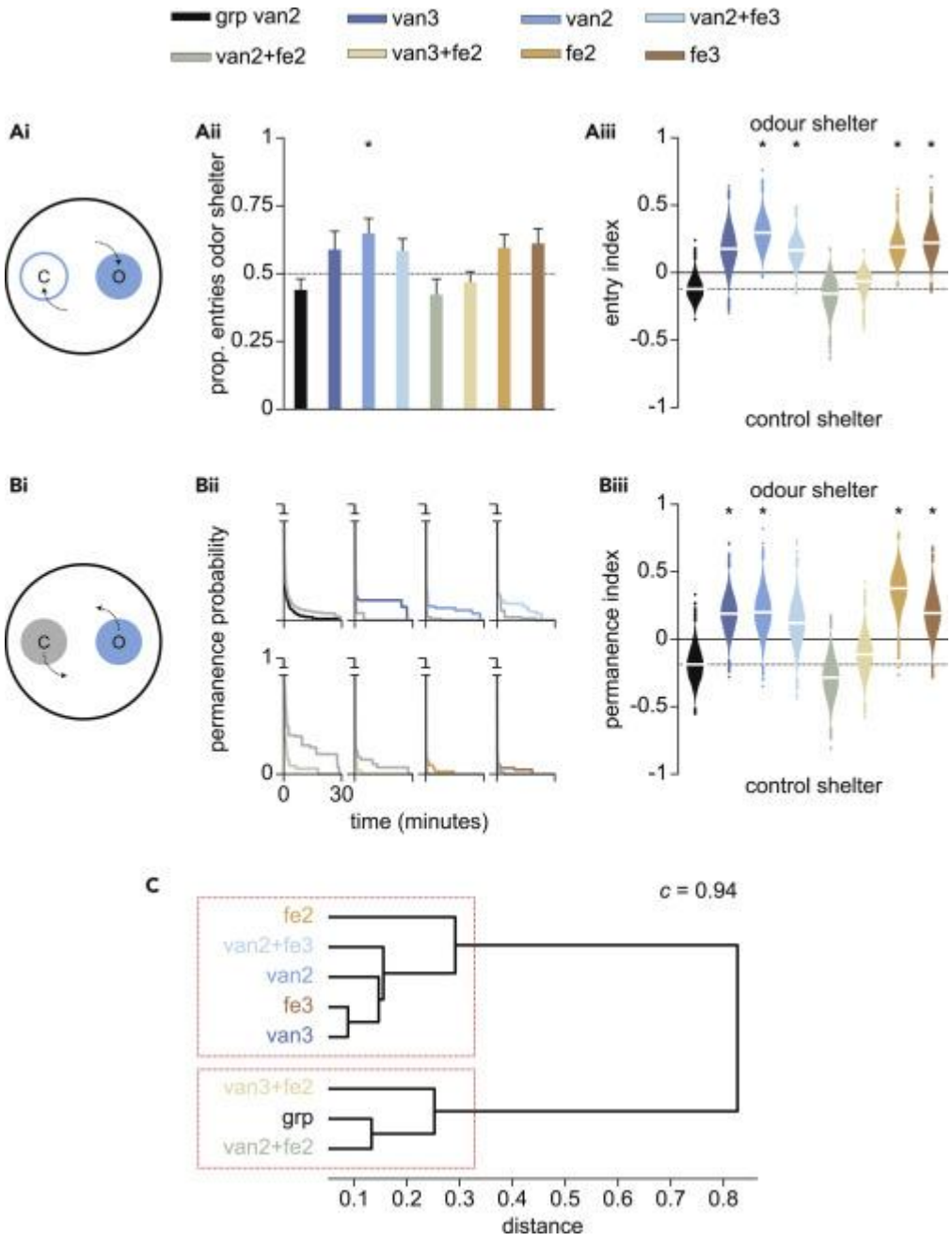

Figure 4. Shelter selection behavior is odor-dependent. (A) The proportion of entries (A_{ii}) for the odor vs. control shelter and resultant entry index (A_{iii}) for the eight tested conditions. (B) Permanence probability (based on bout duration per visit) for each tested condition in the odor (color) and control (gray) shelters. Integrals of permanence probability curves were used to calculate the permanence index in B_{iii} (see Transparent methods section for details). In both A_{iii} and B_{iii} a value of positive one indicates a complete preference for the odor shelter, while and a value of negative one a complete preference for the control shelter (for details see subsection Tracking and data analysis of the Transparent methods section). White horizontal lines show distribution means. Asterisks indicate statistically significant differences ($p < 0.05$) of testing the distributions against chance level (0.5) in $A_{ii}$and comparing distributions of individual trials with the mean level of the group in A_{iii} and B_{iii} (dotted lines), using one-sample two-tailed tests. (C) Similarity among conditions is depicted as a dendrogram of the hierarchical binary cluster tree, resulting from the Euclidean distances between groups. Data used are (I) shelter and (ii) quarter preference index, (iii) entry index and (iv) permanence index. The cophenetic correlation coefficient ($c = 0.94$) was used to evaluate the clustering. Abbreviations: grp, group; van2(3), vanillin dilution of $10^{-2(3)}$; fe2(3), feces extract dilution of $10^{-2(3)}$.

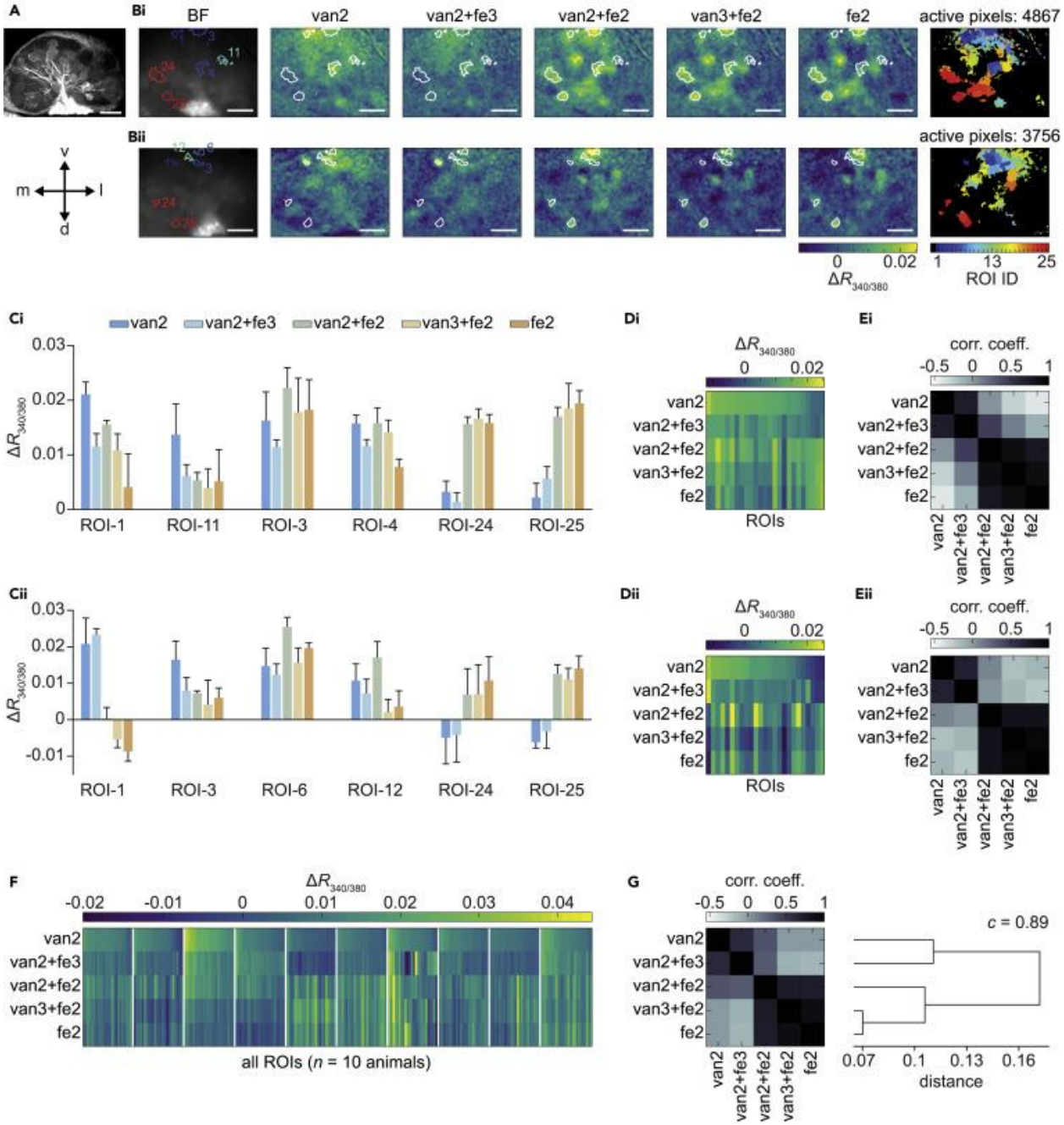

Figure 5. Calcium imaging analysis of antennal lobe representations of tested odorants. (A) A confocal image of the right AL with labeled uniglomerular PNs. (B) Antennal lobe bright field microscopy image (greyscale), false color-coded images of the AL after olfactory stimulation, and distribution of ROIs resulting from *k*-medoids clustering on active pixels (¿0.01 $\Delta R_{340/380}$ for at least one of the five odors) for two representative individuals. ROI identities were sorted by vanillin (van2)-responsiveness. Numbers within the bright field image indicate selected exemplary ROIs displayed in panels (C) and (D). Each response intensity map is the average response pattern of 4 repetitions of the same stimulus. Scale bars in (A) and (B), 100 µm. (C) For the six representative ROIs, the mean response intensity ±SEM (n = 4 repetitions) to the five olfactory stimuli is shown. (D) Mean response intensities (n = 4 repetitions) of all ROIs activated by any of the five olfactory stimuli are plotted as odor response vectors. (E) Similarity matrix based on the Pearson's correlation coefficient among response vectors from (D). (F) Glomerular response vectors from ten cockroaches were combined into a meta-response matrix (n = 10 animals, 250 ROIs, 25 ROIs per animal). (G) Pearson's correlation coefficient matrix and hierarchical dendrogram calculated for response vectors plotted in (F). The cophenetic correlation coefficient (c = 0.89) was used to evaluate the clustering. Abbreviations: BF, bright field; v, ventral; l, lateral; d, dorsal; m, medial; grp, group; van2(3), vanillin $10^{-2}(10^{-3})$; fe2(3), feces extract 10^{-2} (10^{-3}); ROIs, regions of interest.

DISCUSSION

Isolated cockroaches show an innate preference for vanillin-scented versus unscented shelters, a preference that is reversed in the presence of conspecifics (Figures 2, 3, and 4, (Calvo Martín et al., 2019; Laurent Salazar et al., 2017). Previously, it was proposed that this type of inversion results from a weakening of the social attraction in the individually preferred shelter (in this case vanillin) (Calvo Martín et al., 2019; Laurent Salazar et al., 2017) . In our experiments, we found that the propensity to stay in a shelter increases with the number of conspecifics present (a proxy of social attractivity), but this relationship does not differ in the presence of vanillin. Subsequently we show that this preference switch also occurs when the social context is replaced by social odor (colony feces extract) alone, demonstrating that olfaction is a key (and sufficient) modality for inducing the preference inversion.

The balanced mixture has an intermediate neural representation with respect to its two components, although closer to the social odor representation. Still, the observation of a preference inversion for the food-social odor mixture—with respect to both components—suggests that it is evaluated synthetically, *i.e*. as a different olfactory object, with a valence that is different from the one of its elemental components. In the context of foraging, which may also be relevant for shelter selection given that food presence increases shelter attractivity, social feedback can act both as a negative or a positive reinforcer, balancing foraging efficiency, and flexibility in mass-recruiting insect colonies (Grüter et al., 2012). Alone, both the vanillin and the social odor increase shelter attractivity, but together they provide negative feedback. Ecologically, these observations are consistent with the possibility that individuals utilize social cues to avoid what they perceive as recently depleted resources (since the presence of social odor will likely be correlated with the current, or relatively recent, presence of conspecifics).

AL calcium imaging (Figure 5) shows that vanillin and social odor elicit activation in distinct but partially overlapping regions. When presented together, their relative concentrations influence the neural representation of the mixture, shifting it closer to the activity map elicited by the dominant component. In those conditions that promoted reduced preference for the odor shelter, vanillin-specific glomeruli were less responsive, while social odor regions showed stronger activation—in some cases even higher than for the pure component alone (*i.e*. ROI-6 and ROI-12 in Figure 5C_{ii}, and examples 3, 4, and 7 in the Supplemental information Appendix, Figure S3). It is still to be determined if this effect (and the resulting behavior) depends on a glomerular cross-talk within the AL, or if the glomerular representation

of the mixture is further processed in higher-order brain areas (*e.g.* the lateral horn [LH]) and evaluated as an olfactory object different from its two elemental components.

While odor valence evaluation in cockroaches is still understudied, research on other insects—and notably in *Drosophila* - has found that valence can be encoded already at the level of the AL. A study of AL olfactory coding in the fruit fly showed that even if an ensemble of OSNs has no detectable valence specificity, analysis of the elicited glomerular response maps allows valence-based odor classification (Knaden et al., 2012; Knaden & Hansson, 2014). This suggests that, at least in the fruit fly, the AL may dedicate different glomerular populations for attractive and aversive odorants, and that the network of LNs may process OSNs input to enhance valence classification already at the periphery of the olfactory circuit (Knaden et al., 2012; Knaden & Hansson, 2014; Niewalda et al., 2011). AL output neurons relay olfactory information to the mushroom body and LH. The former has a neuronal layout that favors a sparse odor coding, meaning that two odors are encoded by different subsets of intrinsic neurons with little overlapping. This is a very different coding strategy with respect to the AL (where many glomeruli respond to many odorants with a high overlap among the response maps elicited by two stimuli) and provides an efficient neuronal substrate for odor recognition, discrimination, and learning. On the other hand, the LH is innervated without reshaping olfactory information, meaning that distances among PN pre-synaptic response maps elicited in the LH by different odorants are comparable to the distances among the odor response maps induced by the same stimuli in the AL glomerular space (Frechter et al., 2019; Roussel et al., 2014). Moreover, recent neuroanatomical observations have shown that PNs from the same or similarly tuned glomeruli, tend to converge on the same LH output neuron (Frechter et al., 2019; Jeanne et al., 2018). Hence, PN-LH connectivity partially collapses the olfactory space clustering odors by structural and, to some extent, perceptual similarity (Guerrieri et al., 2005; Sachse et al., 1999), providing a good substrate for innate odorant classification. This arrangement suggests that even though overall LH neurons show higher specificity in olfactory stimuli classification and higher capacity to encode complex odor features than AL neurons (Frechter et al., 2019), it cannot be excluded that initial valence evaluation could occur already within the AL. Recent investigation of the cockroaches olfactory coding principles have shown that chemical features of single molecules, such as carbon chain length, maintain a topological mapping within the AL (Paoli et al., 2020), suggesting that coding rules may be similar to other insects (Couto et al., 2005; Sachse et al., 1999) and vertebrates (Uchida et al., 2000). Hence, it is possible that the valence of food, colony, and their mixtures undergoes a first evaluation in

the AL and that an activity change in vanillin-responsive glomeruli when presented together with the colony odor may result in a behavioral preference inversion.

In nature, insects rarely encounter monomolecular odorants, and the AL representations of odorant mixtures can be dominated by either a salient component, or can acquire a new quality and become an olfactory object cognitively different from its constituent components (Renou, 2014; Silbering & Galizia, 2007; Thoma et al., 2014). In general, valences of binary mixtures reflect the combined valence of the components. Two attractants (or repellents) combined are often more attractive (or repulsive) than the individual mixture constituents. In the fruit fly, for example, the presence of vinegar scent together with the male sexual pheromone modulates the AL representation of the latter, making a virgin female more sensitive to the pheromone, thus enhancing her receptivity during courtship (S. Das et al., 2017). Blends of odors with opposing valences, instead, often elicit concentration-dependent intermediate responses, which are mediated by crosstalk interactions between glomeruli responding to the individual components (Mohamed et al., 2019; Thoma et al., 2014). In these cases, glomeruli that strongly responded to the attractive component were shown to be inhibited by the aversive one, thus providing an instance where the processing of conflicting inputs occurs already within the AL, with a direct influence on the behavioral output; whereas those two cases reported the enhancement of a positive stimulus within a mixture of two attractants (S. Das et al., 2017) or the weakening of an attractant in presence of a repellent (Mohamed et al., 2019), here, we observed that a mixture is evaluated with the opposite valence with respect to its elemental components.

Modulation of the neural representation of olfactory stimuli in the AL plays an important role in mediating fundamental behaviors. The above-mentioned example of synergistic interactions between pheromone sensitive PNs and food-responsive glomeruli to increase mating receptivity in presence of food were reported both in flies (S. Das et al., 2017) and moths (Light et al., 1993; Namiki et al., 2008). During starvation, AL modulation has been shown to result in an increase in sensitivity to attractive odors and a decrease response to aversive ones, thus increasing nutrient detection capability at the risk of ignoring potentially toxic resources (Ko et al., 2015). Aligned with these studies, the observed reduction in vanillin-shelter preference induced by the social cue, is paralleled with an altered neural representation of vanillin in the AL, the first relay of odor processing, which may advocate for its ecological prominence.

The possibility of replicating social behavior by utilizing social odor alone can facilitate a systematic study of how food and social cues jointly influence individual decision-making. Further studies are necessary to elucidate the cellular mechanisms involved. In addition, it will

be important to evaluate both the ubiquity, and the ecological value, of preference inversion, which may be an important strategy to exploit resources in unpredictable and patchy environments.

Limitations of the study

Our study investigates the influence of a social environment on individual decisions. It shows that an increasing concentration of a social odor—an otherwise attractive stimulus—resulted in a reduced preference for a vanillin-associated shelter, supported by a change in the neural representation of the different stimuli. Therefore, we suggest that a synthetic perception of the intermediate mixture—perceived as a third object with respect to its elemental components—provides the basis for a different evaluation of odor valence, which mediates the observed behavioral inversion. At this stage, however, it cannot prove causality. In addition, an intrinsic limitation of our imaging procedure is that it allows access only to the superficial glomeruli of the AL. A full decryption of the AL representation of the odor mixture would require the use of 2-photon microscopy to image deeper layers. Further experiments to test behavioral choices and related AL activity will be needed to determine if the observed phenomenon is general to other important food odors in combination with a social odor. Computational modeling of this behavior would also be valuable to create testable predictions regarding the consequences of the observed inversion across spatial and temporal scales. It could be addressed whether this is a strategy for competition avoidance, whether it is a general strategy for social organisms that live in patchy environments, and whether it has adaptive implications.

ACKNOWLEDGMENTS

The authors thank Prof. Hiroshi Nishino for providing the feces extract as well as a general advice along the way; Iain Couzin for his valuable feedback on the manuscript; Antoine Hoffmann for helpful comments on data analysis; Margarete Ehrenfried for rearing *P. americana*. We also thank Alina Hebling, Hannah Honner and Jahn Nitschke for help with experiments and analysis. The authors thank the 4 anonymous reviewers for their insightful suggestions. This work was completed with the support of the Deutsche Forschungsgemeinschaft (DFG, German Research Foundation) under Germany's Excellence Strategy – EXC 2117–422037984.

DECLARATION OF INTERESTS

The authors declare no competing interests.

DATA AND CODE AVAILABILITY

Code used for data analysis and Figure creation is available at:
https://github.com/Couzin-Fuchs-Lab/Guenzel-McCollum-et-al

SUPPLEMENTARY INFORMATION

Figures

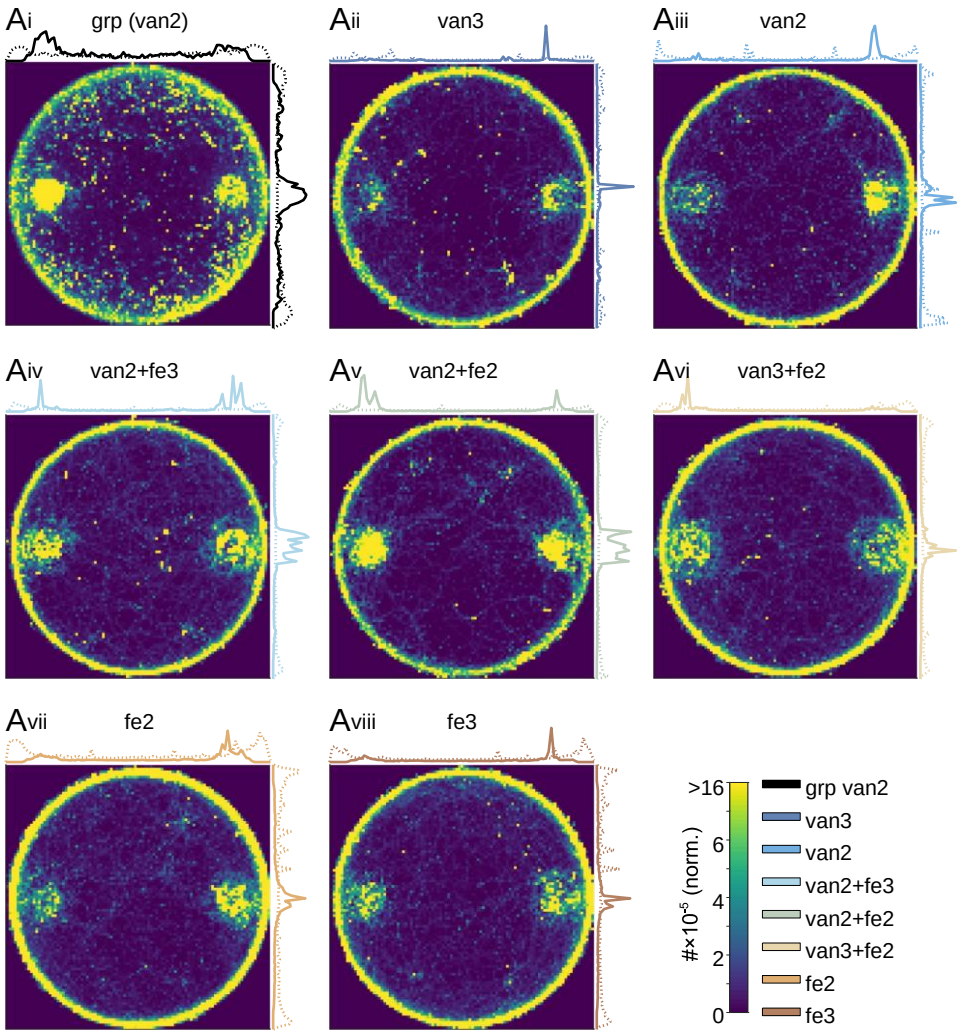

Fig. S1 Density maps for each condition. Extension for Figure 2: Density maps of animal positions over all trials for the group condition (A_i) and single animals ($A_{ii–viii}$). As in Figure 2, coordinate maps were rotated such that the odour shelter is center-right and control is center-left. Heatmaps were normalized to 1 and averaged across animals. Presence densities across and along the arena are indicated above and beside the heat maps, separated for the outer (wall-following bouts, dotted lines) and inner (solid lines) part of the arena. Scale bars: 20 cm. Abbreviations: grp, group; van2(3), vanillin $10^{-2(3)}$; fe2(3), feces extract $10^{-2(3)}$.

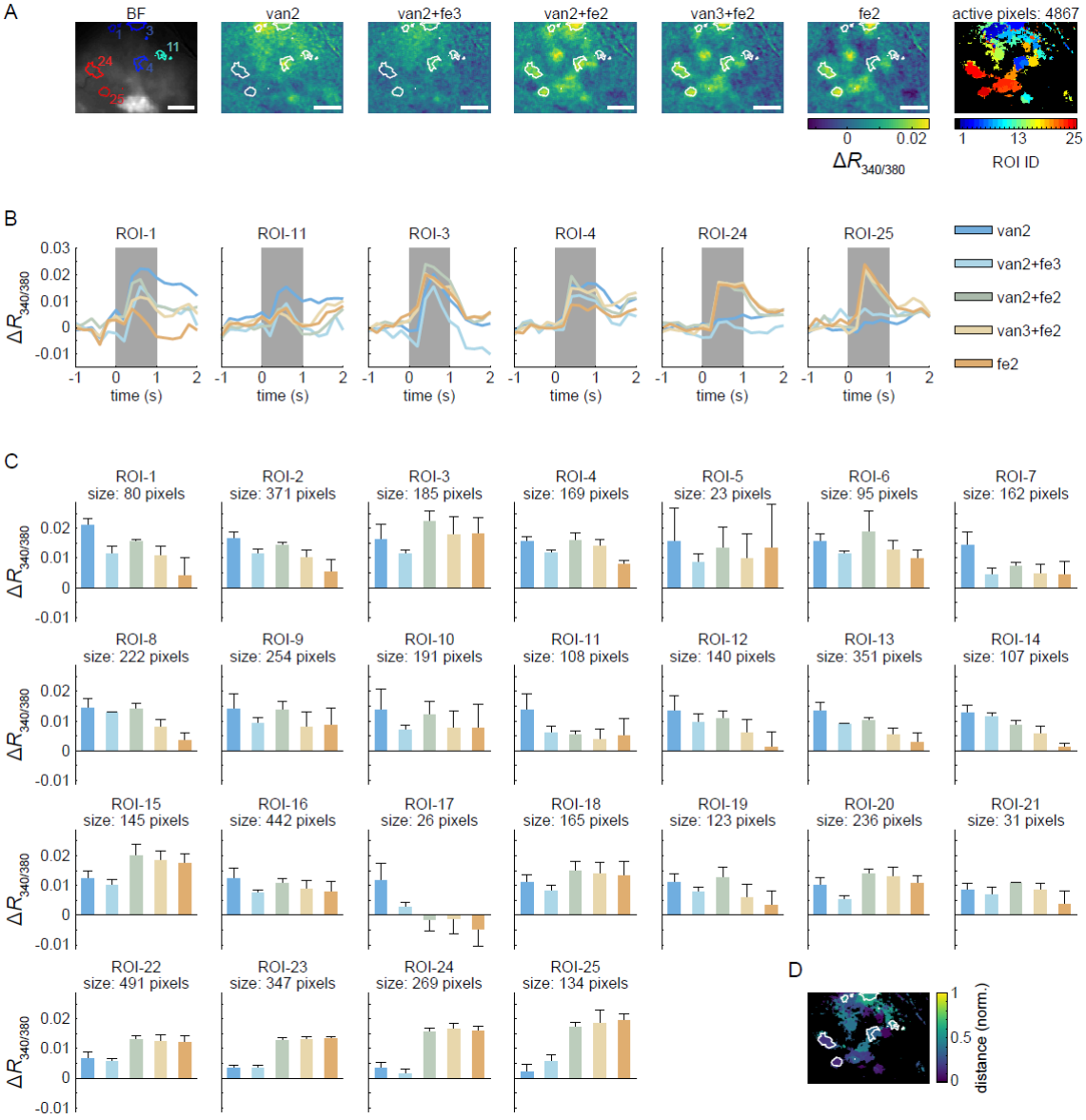

Fig. S2 Spatial and temporal response maps - Example animal mp03, Figure 5Bi. (A) As in figure 5Bi, antennal lobe (AL) bright field microscopy image (greyscale), false colour-coded images of the AL after olfactory stimulation, and distribution of regions of interests (ROIs) resulting from k-medoids clustering on active pixels (>0.01 ΔR340/380 for at least one of the five odours) for two representative individuals. ROI identities were sorted by the corresponding average vanillin-responsiveness (response to van2). Numbers within the bright field image indicate selected exemplary ROIs analysed in the corresponding panels in (B). Each response intensity map is the average response pattern of different repetitions of the same stimulus. Scale bars: 100 µm. (Same as Fig.5Bi) (B) Average temporal responses of six example ROIs to the five different odour stimuli. (C) For all 25 ROIs, the mean response intensity ± SEM (n = 3-4 repetitions) to the five olfactory stimuli is shown. (D) Medoid variability resulting from different runs. Cluster procedure has been repeated 25 times and for each pixel, the average Euclidean distances, is used as proxi for variability. Abbreviations: van2(3), vanillin 10−2(3); fe2(3), feces extract 10−2(3).

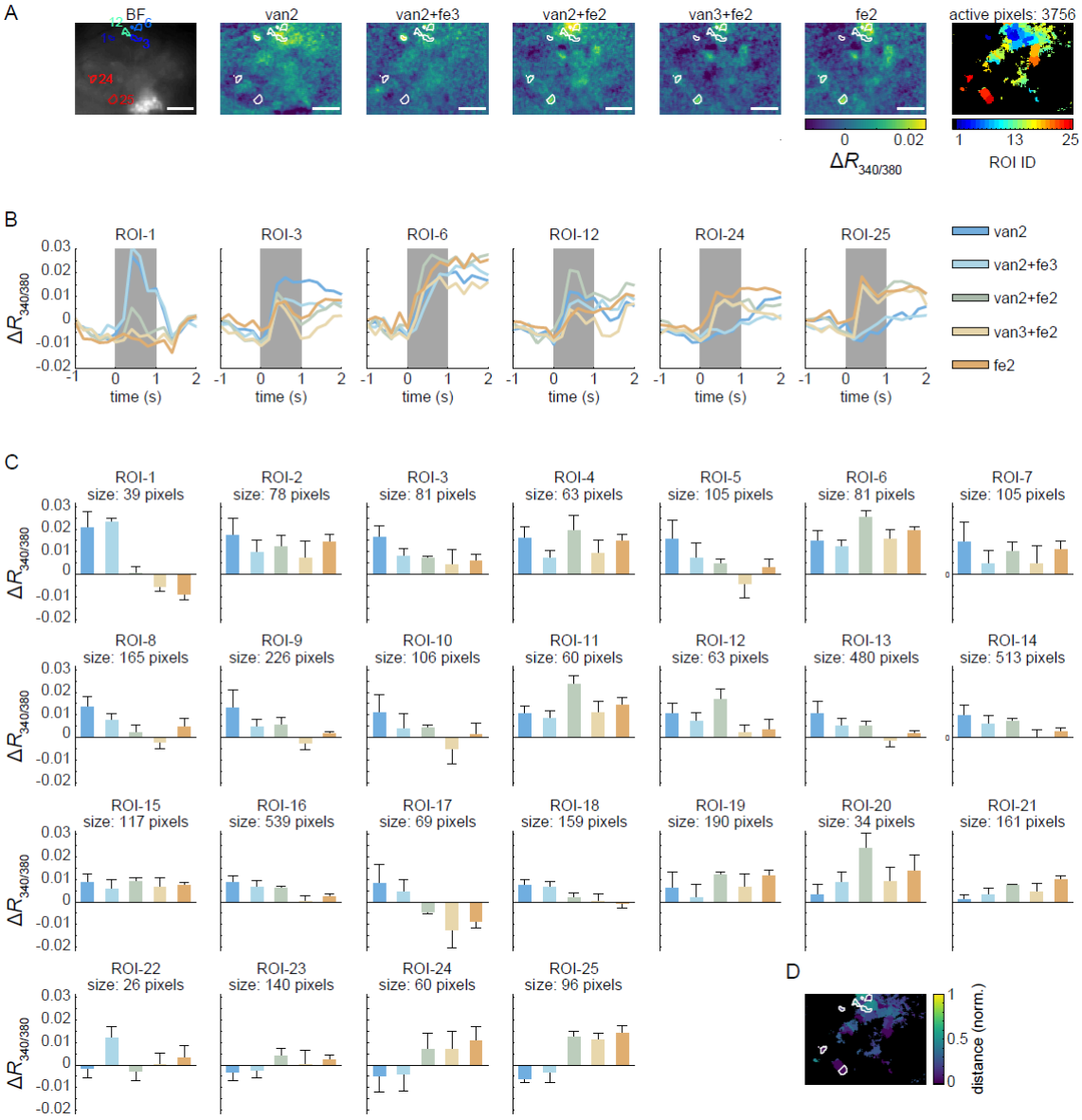

Fig. S3 Spatial and temporal response maps - Example animal mp04, Figure 5Bii. (A) As in Fig.5Bii, antennal lobe bright field microscopy image (greyscale), false colour-coded images of the AL after olfactory stimulation, and distribution of regions of interests (ROIs) resulting from *k*-medoids clustering on active pixels (>0.01 _*R*340/380 for at least one of the five odours) for two representative individuals. ROI identities were sorted by the corresponding average vanillin-responsiveness (response to van2). Numbers within the bright field image indicate selected exemplary ROIs analysed in the corresponding panels in (B). Each response intensity map is the average response pattern of different repetitions of the same stimulus. Scale bars: 100 μm. (B) Average temporal responses of six example ROIs to the five different odour stimuli. (C) For all 25 ROIs, the mean response intensity ± SEM (n = 3-4 repetitions) to the five olfactory stimuli is shown. (D) Medoid variability resulting from different runs. Cluster procedure has been repeated 25 times and for each pixel, the average Euclidean within-pixel distance between the 25 assigned medoids, scaled by the grand mean of between-cluster Euclidean distances, is used as proxi for variability. Abbreviations: van2(3), vanillin $10^{-2(3)}$; fe2(3), feces extract $10^{-2(3)}$.

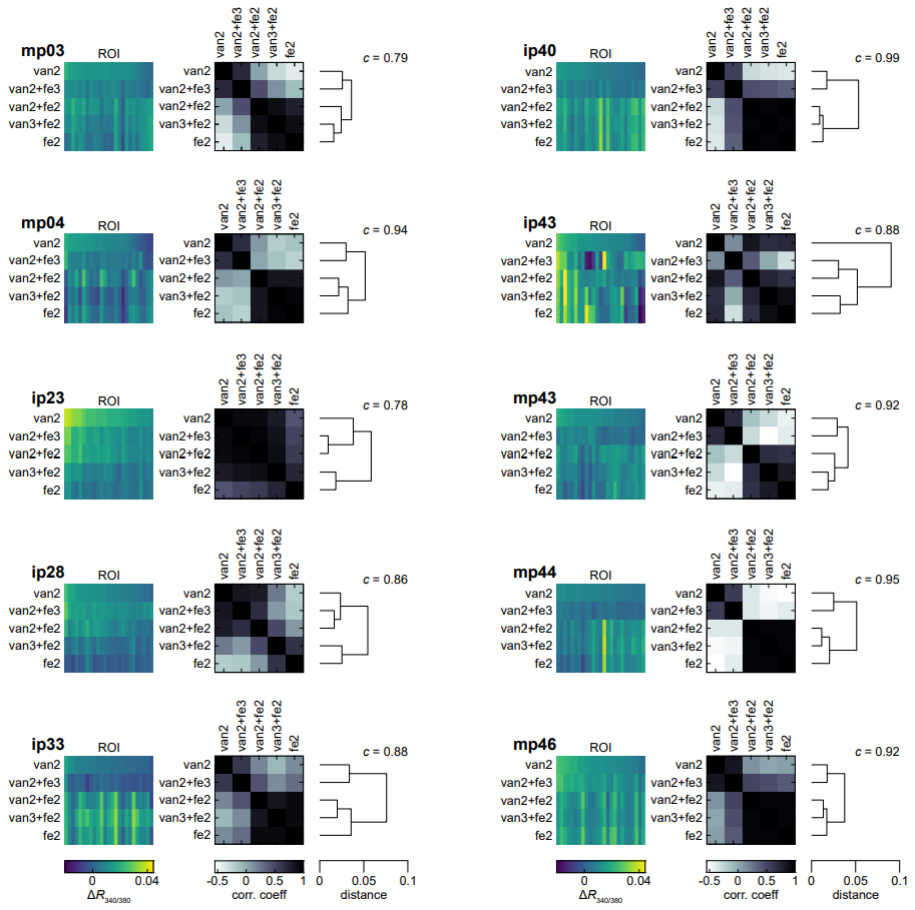

Fig. S4 Analysis of evoked response of ten cockroaches, whose response vectors are shown in Figure 5G. For each animal, response vector maps over all 25 ROIs for the five olfactory stimuli (sorted according to van2 response intensity), together with corresponding Pearson correlation analysis and resulting linkage tree based on agglomerative hierarchical clustering. Cophenetic correlation coefficients c, were used as indication on clustering accuracy. Abbreviations: van2(3), vanillin $10^{-2(3)}$; fe2(3), feces extract $10^{-2(3)}$.

TRANSPARENT METHODS

Animals

Experiments were performed using adult male *Periplaneta americana* from the animal facility of the University of Konstanz (Germany). Animals were reared under constant conditions and kept on a 12/12 h light/dark cycle with 24 °C and 65 % humidity.

Behavioural experiments

The experimental setup (figure 1A) was inspired by [Salazar et al., 2017]. Subjects were tested in a circular arena of 90 cm in diameter made of PVC. Petroleum jelly (Balea Vaseline, dm-drogerie markt GmbH + Co. KG, Karlsruhe, Germany) was applied to the arena wall to prevent

animals from climbing. A transparent Plexiglas plate covered the top of the arena, while the base contained six small, equally spaced holes, in which odours were inserted and administered from below. Two shelters (diameter: 12 cm; height: 2 cm) covered in a transparent red filter paper (LEE filter film No. 106; Primary Red) were placed above two opposing holes, selected randomly from the different odour outlets to form the odour and control shelters. The arena base and shelters were cleaned after each trial in order to remove any remaining chemical traces. All experiments were recorded at 25 fps with a single Basler camera (acA2040 - 90 μm; Basler AG, Germany) with IR long pass filter, located above the arena. A grid array of IR 850 nm wavelength with a diffuser plate was placed below the arena for uniform light conditions in the video recordings. Additional ceiling light provided an ambient illumination. Temperature was kept between 24 °C and 26 °C during experiments. All trials started five minutes after odour administration and lasted 30 minutes. In total, 105 animals were used for individual trials (15 animals per odour condition) and 201 animals for the 10 group trials (in one case, 21 individuals were used).

Odour preparation

Periplaneta americana faeces extract was provided by H. Nishino (Hokkaido University, Japan). Faeces was collected from a colony of cockroaches fed exclusively on agarose, to reduce the presence of secondary metabolites originating from food. Both butter vanillin (Dr. Oetker, Bielefeld, Germany) and the faeces extract were diluted to 10^{-2} and 10^{-3} in 1 mL of mineral oil (CAS 8042-47-5, cat.num. 124020010, Acros Organics, Thermo) in 1.5 mL glass vials for behavioural experiments. For a control, 1 mL of pure mineral oil was placed under the control shelter, opposite to the odour vial in each trial. odours were prepared fresh at the beginning of each day of experiments. For calcium imaging the same dilutions were prepared in 1 mL mineral oil and placed in 20 mL glass vials, covered with nitrogen (Sauerstoffwerk Friedrichshafen GmbH, Friedrichshafen, Germany) and sealed with Teflon septum (Axel Semrau GmbH, Sprockhövel, Germany).

Tracking and data analysis

Behavioural videos were processed in FFmpeg (http://ffmpeg.org/). Tracking of all animals were obtained using a version of the Python-based program Tracktor [Sridhar et al., 2019], modified to better keep individual identities after crossing events. Animals were considered ’sheltered’ when their body centroid had stayed for at least 0.5 s within a radius of 7 cm around

the shelter's centre. Special care was taken that identities of sheltered animals during group trials were not switched. For this, tracking of each sheltered animal for each video was manually corrected using a custom-written GUI in MATLAB (R2020a, The MathWorks Inc, Natick, MA, USA). Since shelter locations in different trials were randomly selected out of six possible positions, animal trajectories were rotated to set the odour outlet as a single position in all trials. Hence, in all figures, the odour shelter is presented on the right and the control on the left.

Data was analysed and plotted using custom-written MATLAB scripts. Density maps represent 2D histograms (100x100 equally-spaced pixel bins) of animal presence, normalized by duration and number of tested animals. They were generated using the entire data set of one condition. To separate wall-following behaviour, tracked locations were divided into an inner (distance to the centre of the arena smaller than 0.85 times arena radius) and an outer subset, as indicated in figure 2A). In order to get a good estimate for estimator properties, *e.g.* spread of the data, trial averages of behavioural data were re-sampled (B = 10'000 bootstrapped means of random samples).

Shelter/quarter preference indices (figure 2B and figure 3A*iv* and 3B*iv*) were calculated as the proportion of time spent in the odour shelter/quarter minus the proportion of time in the control shelter/quarter, divided by the sum of both. Similarly, entry index (figure 2C and 4A*iii*), and permanence index (figure 4B*iii*) were calculated based on the proportion of entries and the integral under the permanence probability curves (showing for each time point the probability of staying in a shelter for at least that time) in the odour shelter, minus those in the control shelter, divided by the sum of both. Therefore, for each preference index a value of -1 indicates a complete preference for the control, and a value of +1 a complete preference for the odour.

Behavioural similarities across the different tested conditions were evaluated using agglomerative hierarchical clustering of the data. Similarities were based on the Euclidean distance among conditions each described by four different preference indices (shelter, quarter, entry, survival). Clustering was based on the unweighted average distances between conditions and evaluated by calculating the cophenetic correlation coefficient, which provides an indication on how accurately the clustering reflects the data (values close to one indicating an accurate cluster solution).

Neurophysiology - Calcium imaging

Calcium Imaging was performed in the right antennal lobe of adult male cockroaches, with the dye application method to stain projection neurons following Paoli et al. (Paoli et al., 2020), adapted from Paoli et al. (Paoli et al., 2017) and Sachse and Galizia (Sachse & Galizia, 2002). On the first day, animals were anesthetized with CO2 to facilitate handling. Cockroaches were then placed into a custom-built holder with their heads restrained by soft dental wax. An incision creating a small window was made in the cuticle of the head to expose the injection site. A crystal of calcium sensitive 10 kDa dextran-conjugated Fura-2 (Thermo Fisher Scientific, Waltham, MA, USA) was injected medio-ventrally into the medial calix of the right mushroom body using a glass capillary. After dye injection, the head capsule was sealed to prevent brain desiccation. The following day, the AL was re-exposed to allow optical access, and the brain was covered in transparent two-component silicon (Kwik-Sil, WPI, Sarasota, FL, USA) for imaging experiments.

Calcium imaging analysis was performed at a widefield fluorescence microscope (BX51WI, Olympus, Tokyo, Japan) equipped with a 10x water immersion objective (Olympus UM Plan FI 10x/0.30w). Images were acquired with a SensiCam CCD camera (PCO AG, Kelheim, Germany) using 120x160 pixel frames and a pixel size of 3.75 μm x 3.75 μm. Recordings were acquired at

5 fps using TILLvisION acquisition system (TILL Photonics, Graefelfing, Germany). A LED system equipped with a 340 and a 385 nm LED (Omicron-Laserage Laserprodukte GmbH, Rodgau-Dudenhofen, Germany) was employed as light source, which was directed onto the cockroach brain via a 410 short-pass filter and a 410 dichroic mirror. Emitted light was filtered through a 440 long-pass filter.

Olfactory stimulation

Olfactory stimulation during calcium imaging analysis was performed with an automatic multi-sampler for gas chromatography (Combi PAL, CTC Analytics AG, Zwingen, Switzerland). Two 1 s odour pulses were injected at 4 s and 12 s with an injection speed of 1 mL/s into a continuous flow of 1 mL/s of purified air. The stimulus was directed towards the right antenna via a Teflon tube (inner diameter, 0.87 mm; length, 40 cm), and the antenna was inserted into the terminal portion of the tube to ensure similar stimulation conditions across animals. Ten cockroaches were tested with 9 different stimuli (van10^{-4}; van10^{-3}; van10^{-2}; van10^{-3}+fe10^{-3}; van10^{-2}+fe10^{-3}; van10^{-2}+fe10^{-2}; van10^{-3}+fe10^{-2}; fe10^{-3}; fe10^{-2}) and with pure mineral oil as

control. For each animal, the order of exposure was pseudo-randomized, although keeping the order of increasing concentrations (*i.e.* decreasing dilution) for each pure odorant (*e.g.* van10^{-4}, van10^{-3}, and van10^{-2}). The whole of nine olfactory stimuli was repeated either three or four times (depending on animal responsiveness). An inter-trial interval of two minutes was kept between stimuli, during which the syringe was flushed with clean air. After each set of stimuli, the syringe was washed with *n*-pentane (Merk KgaA, Darmstadt, Germany), heated to 44 °C, and flushed with clean air.

Calcium imaging data analysis

Calcium imaging recordings were exported and processed in MATLAB.We adopted a ratiometric protocol for calcium imaging using Fura-2 excitation wavelengths of 340 and 380 nm. Ratios of 340 to 380 nm signals were calculated ($R_{340/380}$) and the offset was removed by subtracting the mean signal before odour stimulation ($\Delta R_{340/380}$). Response maps for each frame were smoothed with a 4-by-4 window using 2D median filtering. For each repetition, the response to the solvent (mineral oil) was subtracted from all stimulus-induced responses, and the average odour response map was calculated across the 3 (or 4) repetitions of each stimulus conditions. Regions of interest (ROIs) were automatically segmented using *k*-medoids functional clustering on all time traces of all active pixels, *i.e.* regions showing a stimulus-induced increase in fluorescence $\Delta_{340/380}$ >0.01 for at least one of the five odours. For the cluster analysis, we considered each active pixel as object, whose features were the concatenated responses to each stimulus, resulting in 400 features (five stimuli times 80 frames per stimulus). Dimensionality was then reduced by principal component analysis on the input data set. Thus, to group pixels based on their activity, we only considered the principal components that together explain 95 % of the variance. The initial cluster central positions were determined using a preliminary clustering phase on a random subsample of 10 % of the data. The algorithm ran until a maximum number of 10'000 iterations over 100 replicates. We set the number of clusters - thus the number of ROIs - to k = 25, as this reflects the total possible number of response types of five different stimuli ($k = N^s$; for N = 5 odour stimuli and s = 2 ways of responding, *i.e.* 'response' vs. 'no response'), and provides a good approximation of the number of glomeruli that can be detected on a superficial plane of the cockroach antennal lobe. Other parameters, *e.g.* the distance metric, were kept at their default (standardized Euclidean distance in this example; see MATLAB's kmedoids-function for details). Since medoid-initialisation is based on random processes, we repeated the clustering 20 times and evaluated

the resulting variability with the mean within-pixel Eucidean distance between the 20 assigned medoids, scaled by the mean between-ROI Eucidean distance resulting from the 20 runs (figure S3D and S4D). Resulting ROIs were sorted according to their response to vanillin (van10^{-2}). For each individual, stimulus-specific response vectors were obtained as mean responses of each ROI across repetitions. Response similarities were then assessed by calculating the Pearson's correlation coefficients between response vectors of the different odour conditions, which were then used to construct a dendrogram according to an agglomerative hierarchical clustering method (following the same principle as for the behavioural data - see subsection 'Tracking and data analysis' above). For graphical representation, responses' heatmaps (figure 5B and figure S2) present average odour response maps between 0.6 s and 1s after stimulus onset, across repetitions.

Statistical analysis

If not stated otherwise, bar plots with error bars indicate means and standard deviations. Violin plots are used to show the probability density estimate of the bootstrapped data, while values that were either 1.5xIQR above the 0.75 quantile or 1.5xIQR below the 0.25 quantile were excluded from the violins but depicted as points. Horizontal lines within the violins indicate means. We used a bootstrap-based randomization test to evaluate the statistical significance of our data (Eq. 1). For this, we estimated the probability *p* of observing our sample test statistic $t(x)$ or something even more extreme in the bootstrapped test statistic $t(x^{*b})$, given the null hypothesis is true (for two detailed examples on hypothetical data including calculation paths and resulting implications, see data repository: https://bwsyncandshare.kit.edu/s/JHMzqea7B53Kct6).

$$p = \frac{\#[t(x^{*b}) \geq t(x)]}{B} \quad [1]$$

For a one-sample hypothesis test, estimating whether the mean of the population is statistically significantly different from a pre-determined value μ_0, *e.g.* 0.5, we evaluated the test statistic $t_1(\bullet)$ (Eq. 2) on the observed sample x with sample size n, and on each bootstrap sample x^* of the empirical distribution $\bar{x}_i = x_i - \bar{x} + \mu_0, i = 1, \ldots, n$.

$$t_1(x) = \frac{|\bar{x} - \mu_0|}{\sigma_x / n}$$

$$t_1(\tilde{x}^{*b}) = \frac{|\bar{\tilde{x}}^* - \mu_0|}{\sigma_{\tilde{x}^*} / n} \quad [2]$$

For a two-sample hypothesis test of comparing the sample *z* with sample size *n*, and sample *y* with sample size *m* we followed a similar principle. We evaluated the test statistic *t*2(•) (Eq. 3) on the observed samples and on each bootstrap sample coming from a combined sample of *z* and *y*, denoted as *x*. Meaning, we randomly drew with replacement and the size of *n* +*m* from *x* and assigned the first *n* samples to *z** and the remaining *m* samples to *y**. Then, this has been repeated *B* times.

$$t_2(z, y) = \frac{|\bar{z} - \bar{y}|}{\sqrt{\sigma_z / n + \sigma_y / m}}$$

$$t_2(\tilde{z}^{*b}, \tilde{y}^{*b}) = \frac{|\bar{\tilde{z}}^* - \bar{\tilde{y}}^*|}{\sqrt{\sigma_{\tilde{z}^*} / n + \sigma_{\tilde{y}^*} / m}} \quad [3]$$

Note, with the absolute difference in the numerators of Eq. 2 and Eq. 3, respectively, our test statistics yield a two-tailed comparison.

CHAPTER 2

SYNERGISTIC OLFACTORY PROCESSING FOR SOCIAL PLASTICITY IN DESERT LOCUSTS

Inga Petelski, Yannick Günzel, Sercan Sayin, Susanne Kraus, Einat Couzin-Fuchs

Nature Communications 2024

CHAPTER SUMMARY

Guided by the insights in social modulation of cockroaches, as described in *Chapter 1*, our team set out for a field trip to Northern Kenya in 2020, which, by that time, was hit by a devastating locust plague. We were eager to explore how another non-eusocial, hemimetabolous species copes with the presence of conspecifics during foraging. Contrary to our acquired understanding of cockroach shelter selection, we noticed that, in the field, marching juvenile gregarious locusts did not abandon their conspecifics to pursue a remote, deliberately placed appetitive olfactory trace. Instead, they restricted their foraging range to an area in close proximity to their peers. Having mastered *in vivo* calcium imaging in cockroaches, we started the effortful process of pioneering this method in the complex olfactory system of locusts, laying the foundation for a neural investigation into the factors governing socially influenced feeding decisions.

Back in the lab, we combined food patch experiments with Bayesian modeling, which revealed that both vision and olfaction serve as crucial sensory modalities during food seeking in locusts. While gregarious individuals were attracted to a combination of conspecifics and food-related stimuli, ignoring isolated food signals and social signals alone, their solitary-reared counterparts responded positively only to the food source signal in isolation. Illuminating the olfactory neuronal dynamics that trigger these disparate tendencies between gregarious and solitarious animals, we performed electroantennograms and calcium imaging.

We found consistent, reproducible and stable - though mainly overlapping - odor responses in locust projection neuron (PN) dendrite arborization and somata of the antennal lobe (AL). In accordance with the behavioral performance, gregarious animals exhibited a synergistic

increase in PN magnitude upon exposure to a mixture of conspecific signals and diverse leaf volatiles. The number of synergistically responding glomeruli and the overall response strength far exceeded those elicited by the sum of respective odorants. The response was accompanied by phasic, excitatory response motifs in cell bodies. This amplification, exclusive to the combination of social and appetitive odors in gregarious animals, must originate in the ALs, as electroantennogram recordings were lacking any signal distortions. Mechanistically, we expect the effect to be guided by local interneurons (LNs), which could amplify the signals through disinhibition.

To us, it seems as if those striking neuronal modifications, which have been observed from a single generation of unequal social exposure, may act as adhesive force in gregarious animals. Along with several evolutionary advantages of the locust phase shift towards swarm formation, dense cohesions do challenge the ability to localize food, potentially leading to swarm dispersion during foraging. Thus, synergistic neuronal responses during food detection in the crowd could represent a phase-specific adaptation which aids the survival of each individual while ensuring the collective benefit of the group.

Conversely, solitary locusts showed a decreased mixture response, a lower number of mixture-specific glomeruli, and increased representation of food-associated glomeruli. This was coupled with inhibitory and delayed response motifs to the social odor, and sustained or phasic motifs during food odor exposure in the somata. Those responses in solitarious animals perfectly fit their cryptic lifestyle, which is designed for group avoidance and solitary foraging expeditions.

As previously hinted, our analysis suggests that locusts rely not only on olfaction but rather a combination of visual and olfactory cues to successfully select their feeding choices. While the present *Chapter* focuses on the role of olfaction, the following *Chapter 3* elaborates on the sense of vision in gregarious locusts, albeit in the context of collective movement in massive swarms.

Nat Commun. 2024 Jun 28;15(1):5476. doi: 10.1038/s41467-024-49719-7.

Synergistic olfactory processing for social plasticity in desert locusts

Inga Petelski [#] [1] [2] [3], Yannick Günzel [#] [4] [5] [6] [7], Sercan Sayin [2] [8], Susanne Kraus [2], Einat Couzin-Fuchs [9] [10] [11]

Affiliations + expand

PMID: 38942759 PMCID: PMC11213921 DOI: 10.1038/s41467-024-49719-7

ABSTRACT

Desert locust plagues threaten the food security of millions. Central to their formation is crowding-induced plasticity, with social phenotypes changing from cryptic (solitarious) to swarming (gregarious). Here, we elucidate the implications of this transition on foraging decisions and corresponding neural circuits. We use behavioral experiments and Bayesian modeling to decompose the multi-modal facets of foraging, revealing olfactory social cues as critical. To this end, we investigate how corresponding odors are encoded in the locust olfactory system using *in vivo* calcium imaging. We discover crowding-dependent synergistic interactions between food-related and social odors distributed across stable combinatorial response maps. The observed synergy was specific to the gregarious phase and manifested in distinct odor response motifs. Our results suggest a crowding-induced modulation of the locust olfactory system that enhances food detection in swarms. Overall, we demonstrate how linking sensory adaptations to behaviorally relevant tasks can improve our understanding of social modulation in non-model organisms.

INTRODUCTION

The ability to adapt to a changing social environment is a fundamental aspect of life. Locusts exhibit the distinct ability to switch between a solitary and gregarious lifestyle rapidly, rendering them an ideal model for studying social plasticity and the emergence of collective behavior. Furthermore, these transitions are central to the formation of large-scale destructive locust outbreaks, which are precipitated by an autocatalytic process of positive feedback between population density and aggregation behavior (Cullen et al., 2017; Pener & Simpson, 2009; Simpson et al., 2009; Simpson et al., 1999). When population density spontaneously increases, formerly solitarious locusts are forced to conglomerate on limited resources, leading to further increases in local density and subsequent directed aggregation of animals that have become gregarious. These dynamics also trigger changes in other density-dependent traits, including metabolism, developmental, and reproductive physiology, which together foster population growth and swarm formation (cumulatively termed “phase change”, (Pener & Simpson, 2009). As crowding further increases, the demand for nutrients rises, compelling large locust aggregations to leave areas with low food availability and forage despite associated risks of predation and cannibalism (Chang al., 2023; Collett et al., 1998; Guttal et al., 2012; Sword et al., 2000; Wei et al., 2019). These rapid density-dependent adaptations pose questions about the neural processing in changing social environments that allow animals to adjust their decision-making appropriately in a context-dependent manner.

The transition to group living also alters the sensory information available to locusts when searching and selecting feeding sites. Gregarious desert locusts (*Schistocerca gregaria*) effectively utilize both asocial (e.g., sight and/or smell of food) and social (e.g., presence or action of conspecifics) cues for their foraging decisions (Günzel et al., 2023). Specifically, the decision to join a food patch is positively influenced by the number of conspecifics on the patch, as well as by its quality and the locust's prior experience with it. However, our understanding of the sensory processes that mediate these density-dependent decisions remains limited.

Like many animals, locusts use olfactory information to locate food, find mates, and avoid predators or toxins. Invariably, olfactory systems face the challenge of encoding and decoding a vast array of chemical structures across varying odor concentrations and mixtures in turbulent environments. Knowledge gained about olfactory systems across the animal kingdom has demonstrated a largely typical organization of a single neuropile – the antennal lobe (AL) in insects and the olfactory bulb in mammals – located only one synapse away from the peripheral

sensory neurons (Wilson & Mainen, 2006). To meet the challenge of complexity in chemical space, the antennal lobe (like the olfactory bulb) acts as an early processing center in which numerous incoming olfactory receptor neurons (ORNs) converge on fewer output projection neurons (PNs). Non-linear summation in such synapses and gain control mediated by local neurons enables the coding of odors over dynamic ranges (Galizia, 2014).

Invertebrate and vertebrate model systems in olfactory research, including rodents (Stewart et al., 1979) , zebrafish (Korsching et al., 1999), and fruit flies (Hallem & Carlson, 2004), have a typical early olfactory coding architecture. Convergent input and output neurons form a computational unit called the glomerulus. Each glomerulus receives input from all ORNs expressing the same olfactory receptor type, and most output neurons are exclusive to a particular glomerulus (Wilson & Mainen, 2006). Such a glomerular structure effectively organizes olfactory coding in linear and parallel channels. In locusts, however, the AL structure and connectivity deviate from those of many insects (Ignell et al., 2001). In contrast to, for example, 50 individually identified glomeruli in the fruit fly (Hallem & Carlson, 2004), it houses an unusually large number of more than a thousand so-called microglomeruli and more strikingly, all output PNs innervate up to 20 microglomeruli (no uniglomerular PNs have been described to date), and each ORN projects to multiple glomeruli (Anton & Hansson, 1996; Hansson et al., 1996; Hansson & Stensmyr, 2011; Ignell et al., 2001; Ignell et al., 1998). Consequently, it is largely unknown how this structural difference impacts locust olfaction and if it is related to the notable phenotypic plasticity many locust species exhibit.

While the wiring of the locust antennal lobe remains unresolved, research on odor processing in locusts has played a pioneering role in advancing our understanding of combinatorial coding in olfactory systems (Laurent et al., 1996; Laurent & Davidowitz, 1994; Wehr & Laurent, 1996). Using intracellular and extracellular recording techniques and computational models, locust odor representation has been postulated as a dynamic combinatorial code (Anton & Hansson, 1996; Ignell et al., 1998), suitable for rapid discrimination of odor identity and intensity (Mazor & Laurent, 2005; Stopfer et al., 2003) , as well as for contrast enhancement when stimuli overlap or follow distractor odors (Broome et al., 2006; Brown et al., 2005; Nizampatnam et al., 2018). Despite the importance of combinatorial coding and ensemble dynamics, most data sets captured only a fraction of antennal lobe output at a given recording or lacked the cell's identity, which prevented assigning structure to function. Both problems can be addressed with functional imaging techniques that allow monitoring of network-

spanning dynamics, which is particularly important for the highly distributed innervation of the locust AL.

To this end, we have established a functional imaging protocol to investigate the spatial organization of odor-evoked activity in a large subset of PNs of the locust AL. We map the interaction between food and social odors in gregarious and solitarious locusts to examine how odor representation is impacted by crowding. We link our findings to the animals' preferences in a behavioral assay by estimating the contribution of different sensory cues to foraging decisions. Our results reveal a crowding-induced olfactory modulation and advance the accessibility of locusts as a model system for studying collective behavior and the neuronal mechanisms underlying social plasticity.

METHODS

Animals

All experiments were performed on gregarious and solitarious desert locusts *Schistocerca gregaria* (Forskål, 1775) obtained from our breeding colony at the animal facility of the University of Konstanz (Konstanz, Germany). Behavioral experiments were done with the last larval instar and functional imaging with freshly molted (<7 days old) adults. Gregarious locusts were reared in crowded cages (approx. 200 animals per 50-by-50-by-80 cm cage), while solitarious locusts were raised in individual boxes (9-by-9-by-14 cm) with opaque walls in a well-ventilated room with constant air exchange (following Hoste et al., 2002). Except for animal density, all other conditions were kept similar for the two colonies with a 12:12h light:dark cycle, temperature of 27-29°C, relative humidity of 45% and a diet of in-house grown wheat seedlings, and freshly collected blackberry leaves (*Rubus* sect. *Rubus*). For all experiments, locusts of both sexes were used after one night of starvation. All experiments were carried out following the recommendations of the "3Rs" principles as stated in the Directive 2010/63/EU and all procedures were performed according to the guidelines of the German animal welfare law.

Behavioural choice assay

We initiated our study with an analysis of the interactions between social and food cues in a patch selection assay (modified from Günzel et al.) (Günzel et al., 2021) which presented single locusts with four options: food (blackberry leaves, denoted as *Lvs*), a social setting (eight

gregarious locusts, *Lct*), a combination of leaves and locusts (*LvsLct*), and an empty control patch (*Ctr*). Locusts were tested in a 90 cm diameter arena with the four patch choices distributed equally (exchanging positions between trials) in the arena, with a distance of approximately 7 cm from the wall. The four patch choices were made from identical circular plastic containers (Fig. 1a; width: 12 cm; height: 9 cm) and contained either 5 g of ripped blackberry leaves, eight locusts, eight locusts with 5 g of ripped blackberry leaves, or an empty control. In order to allow/prevent access to olfactory and/or visual cues, containers were either transparent with small holes, opaque with holes, or transparent but fully odor-sealed with Parafilm sealing film (Sigma-Aldrich, St. Louis, MO, USA). Each trial lasted 30 minutes and was recorded at 25 fps by a Basler camera (acA2040 – 90µm; Basler AG, Ahrensburg, Germany) with an IR longpass filter at the top of the arena. Uniform illumination was composed of a ceiling LED ring light (Hakutatz LED ring light, 33 cm, 35 W Bi-color 3200-5600 K) and a grid array of IR 850 nm with a diffuser plate below the arena. In order to prevent potential surrounding visual cues from the lab, uniform white walls of 1 m height were placed around the arena. Experiment containers and the arena were cleaned after each trial. The ambient temperature during experiments was kept between 24 and 26°C.

Analysis of behavioral data

We obtained trajectories of individual locusts using a custom-written GUI (*www.github.com/YannickGuenzel/BlobMaster3000*) in MATLAB (R2023a, The MathWorks Inc, Natick, MA, USA) for automated tracking with manual supervision. Obtained trajectories were temporally smoothed by convolution with a Gaussian kernel (half-width = 2 s, σ = 2/3 s). Visit density at each patch option was estimated as previously described (Günzel et al., 2023) by binning *x/y*-coordinates in a 1000x1000 pixel grid, followed by a frame-wise application of a 2-D Gaussian smoothing kernel (s.d. = 78, spatial filter domain, filter size = grid size minus one; matching the density-independent interaction range employed by locusts of approx. 7 cm (Buhl et al., 2006)). The resulting visit density maps were normalized by frame count, divided into four quarters, centered around each patch, and realigned so trials could be pooled across different patch configurations.

To dissect the processes underlying locust patch choice and to evaluate the contributions of the four information classes in the current assay (socio-visual, food-visual, socio-olfactory, and food-olfactory), we extended a Bayesian decision-making rule previously used in patch choice studies (Eqn.

[1; (Arganda et al., 2012; Günzel et al., 2023)). Given the availability of each information class (e.g., $w_{(socio\text{-}olfactory)} = 1$ for options containing locusts in the *Olf*(+) conditions, but 0 for the control option), we fitted the corresponding reliability parameter (C_i) to the experimental visit density data in each patch quarter (P_x).

$$P(\text{x is good}|C_i) = \frac{1}{1 + C_i^{-w_j}}$$

$$P_x = \frac{\prod_{i=1}^{4} P(\text{x is good} \mid C_i)}{\sum_{j=1}^{4} \prod_{i=1}^{4} P(\text{x is good} \mid C_i)} \quad [1]$$

We used Bayesian hyperparameter optimization (MATLAB built-in function *bayesopt*) to fit the parameters in the range of $1e^{-1}$ and $1e^{1}$ (log-transformed). We repeated the fitting process 5000 times, resulting in a predictive distribution based on which we estimated 95% credible intervals. Moreover, the nature of parameter C_i allowed us to estimate an information reliability score ($\log_{10}(C_i)$) that assesses the degree of attraction (values approaching 1) or aversion (values approaching -1) each information class had on the tested locusts.

Preparation of animals for functional fluorescence microscopy

We performed functional fluorescence microscopy in the antennal lobes (ALs) of young adult desert locusts by modifying protocols for backfilling AL projection neurons with dextran-coupled calcium indicator (Paoli et al., 2025; Sachse & Galizia, 2002). For dye application, we anesthetized animals with CO_2 to facilitate handling, removed wings and legs, and restrained the locusts in a custom-made holder using dental wax. On the first day, we opened a small window in the head capsule between the compound eyes, exposing the injection site. Next, using a glass capillary, we injected a crystal of a calcium indicator (Cal-520-Dextran Conjugate MW 10'000, AAT Bioquest | Biomol GmbH, Hamburg, Germany) into the medial calixes of both mushroom bodies for a retrograde backfill of AL projection neurons. Following the injection, the brain was covered with locust saline (Laurent & Davidowitz, 1994), and the head capsule was sealed with a drop of Eicosane (Sigma-Aldrich, St. Louis, MO, USA) to prevent brain desiccation. We allowed the dye to travel overnight with the animal kept in a humid box at 15°C. On the following day, we exposed the brain and especially both antennal lobes. However, as the antennal base is located directly above the antennal lobes and consequently occluding them, we carefully relocated each antenna ventrally toward the ipsilateral compound eye. Special care was taken to prevent damage to the antennal nerves. Following a successful

relocation, we carefully removed the neural sheath covering the AL using fine forceps. For better optical accessibility, we gently elevated the brain with a stainless steel needle. As a last preparation step, we covered the preparation site with a transparent two-component silicon (Kwik-Sil, WPI, Sarasota, FL, USA).

Neuroanatomical staining

For morphological visualization of the olfactory pathway, we double-labeled PNs and ORNs using retrograde labeling. PN labeling followed a similar dye loading preparation as for the calcium imaging (see above) using the fluorescent tracer Alexa Fluor 568 conjugated with 10 kDa dextran. For receptor neuron tracing, the antennae were ablated close to the base, exposing the antennal nerve. The exposed antennal nerve was inserted into a glass capillary, loaded with 10 kDa dextran-conjugated Alexa Fluor 488 (both dyes by Thermo Fisher Scientific, Waltham, MA, USA). Animals were incubated for 24h at 15°C, after which brains were quickly dissected and fixed in 4% paraformaldehyde (PFA) in phosphate-buffered saline (PBS) for 3h at 4°C in the dark. Brains were further washed in PBS and dehydrated in ascending concentrations of ethanol (50, 70, 90, 98, 100%), cleared in xylene for 10 minutes, and mounted in DPX mounting medium (Sigma-Aldrich, St Louis, MO, USA). Successfully stained antennal lobes were scanned as z-stacks with a Zeiss laser scanning microscope 880 equipped with an Airyscan fast detector and a 25x water immersion objective (LD LCI Plan-Apochromat 25x/0,8 Imm Korr DIC, Carl Zeiss, Jena, Germany) in the BioImaging facility at the University of Konstanz.

Confocal laser scanning microscopy

Confocal microscopy of separate optical sections was acquired using an LSM 510 laser scanning confocal microscope (Carl Zeiss, Jena, Germany), equipped with a 20× water immersion objective (Zeiss W Plan-Apochromat 20×/1,0 DIC VIS-IR, Carl Zeiss, Jena, Germany). The calcium-sensitive dye was excited with a 488 nm wavelength laser, and emitted light was filtered through a 500-550 nm band-pass filter. Optical sections were acquired at 1 Hz in two different depths (approx. 35 µm, and 140 µm from the surface of the AL), with a resolution of 0.77 µm/px (*x*, *y*), and a full-width half maximum of 25 µm (*z*).

Odor preparation, olfactory stimulation, and chemical analysis

Odor stimulation was delivered via a custom-built olfactometer with a flow speed of 10 mL/s, and odors were injected for two seconds via a Teflon tube (inner diameter, 0.87 mm) to the ipsilateral antenna (Raiser et al., 2017). Stimuli were delivered by activating valves that redirected air towards a vial containing 200 µL of diluted odor. In the case of a single odor, the flow via the odor headspace (200 mL/min) was compensated by closing a balancer that reduces the airflow by the same amount. For mixtures, the headspaces of the two odors (100 mL/min each) were passed through a common Teflon tube, allowing them to mix before arriving at the locust antenna. A two-minute inter-stimulus interval of clean air was used to flush any residues of odors and to let the PNs return to their resting state. The flow of the individual odors and the mixtures was monitored by a photoionization detector (Mini-PID model 200A, Aurora Scientific Inc, Ontario, Canada), which was placed at the opening of the odor delivery tube.

All synthetic compounds (purchased from Sigma-Aldrich, Steinheim, Germany) were diluted in mineral oil. Locusts were tested with the following odorants: cis-3-Hexenyl-acetate diluted to 10^{-2} "*Laa*"), 3-Hexen-1-ol diluted to 10^{-2} "*Z3hl*", 3-Octanol diluted to 10^{-2} "*Oct*", and 1-Hexanol diluted to 10^{-3} "*Hex*". Odour dilutions were chosen after an initial screening for average PN response magnitude comparable to that of the blackberry leaves *Lvs* in gregarious animals.

Lacking clear dominant candidates for emitted volatiles in the desert locusts (see latest summary of odor composition in Torto et al. (Torto et al., 2021)), we used an extraction from our locust colonies as the social "*Lct*" odor. This was done by placing an evenly spread cotton wool layer in a gregarious colony cage with nymphs of the last larval instar and immature adults for two consecutive days. Odor vials were filled with either 0.5 g of colony cotton wool or 200 µL of odor dilution on 0.5 g of pure cotton wool. Mixtures were prepared by combining half the amount of the respective odor dilution, leaf extract, or colony cotton wool.

Volatile compounds for chemical analysis of the blackberry leaves were collected via 1h leaf extract exposure of solid phase microextraction (100 µm Polydimethylsiloxane Coating SPME Fiber Assembly, Supelco, Bellefonte, USA) and analyzed with a TRACE GC Ultra Multi-channel gas chromatograph, coupled to DSQ II single quadrupole MS (Thermo Fisher Scientific, Waltham, MA, USA). The leaf extract was produced by grinding 1 g blackberry leaves in 200 µL mineral oil.

Analysis of calcium imaging data

For our calcium imaging analysis, we obtained a three-dimensional stack (x-y-time) for each stimulus and processed the data in MATLAB (Fig. 2d). First, we filtered raw images spatially to account for shot (photon) noise, using a combination of a median filter (3-by-3 pixels window) and a 2-D Gaussian filter (s.d. = 1). Potential bleaching was accounted for by subtracting a trendline (linear polynomial curve fit to each stimulus' median pixel intensity time course). Next, we aligned frames belonging to one stimulus using a non-rigid motion correction algorithm (NoRMCorre, (Pnevmatikakis & Giovannucci, 2017)) and a 2-D alignment based on phase differences (Kughlin & Hines, 1975). Carefully aligning our data allowed us to apply a box-shaped kernel (3 frames) in the temporal domain before calculating relative fluorescence changes ($\Delta F/F_0 = (F-F_0)/F_0$) with the mean pre-stimulus activity five frames before stimulus onset as baseline activity F_0. In the case of two repetitions, preprocessed stimulus sets were registered based on phase differences between the sets and eventually averaged.

Interested in an unbiased evaluation of AL responses and detailed quantification of complex response patterns, we referred from manually applying circular regions of interest. Instead, we opted for segmentation into individual, activity-dependent regions (granules) based on the Voronoi topology of the standard-deviation-projection (s.d.-projection) across the whole stimulus set. For this, we identified regional maxima and minima (pixel neighborhood was defined as pixels adjacent in the horizontal, vertical, or diagonal direction) in the s.d.-projection across all stimulus sets. Since the Voronoi diagram and Delaunay triangulation are geometric duals of each other, we could compute Voronoi granules from the Delaunay triangulation of the obtained regional extrema. This resulted in a rough 2-dimensional segmentation into regions that showed substantial changes in activity for any of the stimuli (regional maxima), separated by granules that lacked strong changes (regional minima).

Next, to obtain a more refined segmentation, we evaluated the activity of pixels along the Voronoi vertices. Specifically, we calculated the root median squared error between the activity of the pixel in question and the average activity of the neighboring Voronoi granule or the pixel's 'home' Voronoi granule, respectively. If the pixel had a smaller error with the neighboring Voronoi granule, we assigned it to this area in the next iteration. Alternatively, we kept the original assignment. This evaluation was applied to all pixels along borders between two granules and over a maximum of 50 iterations. Granules smaller than a minimum size of 5 px were fused with their neighboring granules. Last, we removed regions outside the AL and

classified all valid ones as 'active' or 'non-active' given each stimulus. For this, we applied Otsu's method to the respective mean intensity projection.

Construction of odor response vectors

To investigate network-spanning combinatorial coding patterns across all projection neuron cell bodies, we created a response magnitude matrix including data from all gregarious and solitarious animals. In this matrix, each row represents a single PN, and each column corresponds to the respective mean response magnitude during the window of analysis to each of the stimuli (*Laa*, *Lct*, *LaaLct*, *Z3hl*, *Z3hlLct*, *Oct*, *OctLct*, *Z3hlLaa*, and *OctLaa*; Fig. 2c). To account for inter-animal variability, we normalized the data belonging to a single animal. For this, we initially subtracted the minimum value in order to root-transform the data. Next, we centered the animal's data to have a mean of zero and scaled them to have a standard deviation of one. As a last step, we rescaled the range of each PN's vector (each row) to [-1, 1] before we projected the normalized response matrix into principal component (PC) space, retaining PCs that cumulatively explained at least 99% of the variance.

Following the preprocessing steps, we applied *k*-means clustering to construct distinct odor response vectors. The optimal number of clusters, k ($1<k\leq20$), was ascertained by identifying the elbow point of the Variance Ratio Criterion (VRC, Eqn. [2] curve, which was exponentially decaying with an increasing number of clusters. The VRC is defined as

$$\mathrm{VRC(k)} = \frac{\mathrm{SSB(N-k)}}{\mathrm{SSW(k-1)}} \qquad [2]$$

Here, *SSB* denotes the between-cluster variance, *SSW* denotes the within-cluster variance, and *N* denotes the number of observations corresponding to the rows in the response matrix. We defined the elbow point as the point on the VRC curve that was farthest from the line segment connecting the first *VRC(k = 2)* and last *VRC(k = 20)* points on the curve. We performed the *k*-means clustering based on squared Euclidean distances, with a maximum number of 10^6 iterations, 500 replicates, and with an online update phase in addition to the batch update phase, resulting in six odor response vectors.

Analysis of response consistency

Consistency in spatial odor representation was estimated with three general odorants: *Laa*, *Hex*, and *Oct*. Responses were captured in the focal depths of the PN cell bodies and glomeruli with repeated stimulus blocks (each stimulus presented once in semi-random order and repeated five times) to estimate the similarity between response maps. For this analysis, the rescaled (range set to $[0, 1]$) mean intensity maps from each animal were projected into the principal component (PC) space, treating each map as an observation and considering all pixels as features. We retained all PCs that cumulatively accounted for at least 95% of the variance. To evaluate the similarity between maps in PC space, we calculated the Euclidean distance between maps of the same odor stimulus and across maps from different stimuli. Using the average linkage method, we created a hierarchical cluster tree for each animal. Further, we estimated the overall within- and between-stimulus Euclidean distances to pool results across all animals.

Analysis of dynamical odor response motifs for locust phenotype prediction

To gain deeper insight into the dynamics of odor-induced PN responses and their variation across different stimuli, we identified distinct temporal response motifs. For this, we adopted an approach comparable to the one used to analyze odor response vectors (see above). We used the PN cell body confocal microscopy dataset, encompassing data from all gregarious and solitarious animals, to construct a response profile matrix (Fig. 5a). Unlike the response vectors matrix, we treated all frames as features, each cell body appeared as three observations – one for each stimulus (*Laa*, *Lct*, and *LaaLct*) – and we z-scored each row. However, the principal component analysis-based preprocessing and *k*-means clustering remained consistent, identifying six odor response motifs based on the distinct patterns observed.

Next, we tracked how PN response motif assignments changed with odors. For this, we estimated the transition probabilities between response motifs (e.g., motif 2 → motif 4) from one stimulus to another (e.g., *Lct* → Laa) for each individual animal. We used this information to fit a discriminant analysis classifier to differentiate between gregarious and solitarious animals based on the dynamics of motif transitions(same diagonal covariance matrix for both phenotypes). The classifier was trained using a leave-one-out approach, with each iteration including all but one animal for training (the model's weights were adjusted to compensate for unequal sample sizes across classes) and employing the model to predict the phenotype of the excluded animal. This procedure was repeated for each animal in the dataset, providing a robust

evaluation of the classification accuracy. Further, given the high feature dimensionality, we initially reduced the feature set (transition probabilities) using PCA, retaining all PCs that cumulatively accounted for at least 83% (based on screening different values) of the variance.

Analysis of synergistic stimulus interaction

To dissect odor response interactions, we analyzed motif triplets using the Bliss score (Eqn. [3), a standardized measure to categorize pairwise interactions ((Bliss, 1939).

$$f_{expected} = \left(\frac{f_1}{2} + \frac{f_2}{2}\right) - \left(\frac{f_1}{2} \cdot \frac{f_2}{2}\right)$$

$$f_{observed} = f_3 \qquad [3]$$

$$\text{Bliss score} = 100\left(f_{observed} - f_{expected}\right)$$

Here, f_1 and f_2 denote the individual response strengths ($\Delta F/F_0$ as decimal rather than percentage) to *Laa* and *Lct*, respectively, while f_3 represents the observed response strength to the mixture (*LaaLct*). Positive Bliss scores, which arise when the observed response strength (*LaaLct* response) exceeds the expected response strength, indicate synergistic interaction effects between *Laa* and *Lct*. Conversely, negative values represent antagonistic effects, and values approximating zero indicate additive effects. Note that we divided f_1 and f_2 by two in Eqn. [3 to account for using only half of each component (*Laa* and *Lct*) when creating the mixture.

Statistical analysis

All statistical analysis steps were conducted in MATLAB. Unless stated otherwise, we report averages as grand means, which represent the mean of animal means, together with bootstrapped 95% confidence intervals (with a bootstrap sample size of 5000) as shaded areas or error bars, respectively. Further, we used bootstrap randomization tests with $B = 10^7$ samples cf. (Mackinnon, 2009) for statistical inference. We employed the following test statistic (Eqn. [4) for a paired, two-tailed comparison of observations *z* and *y* with the resulting pairwise difference *x* (mean $\bar{x}$, standard deviation σ_x, sample size *n*).

$$T_{\text{paired two-sample}} = \frac{|\bar{x}|}{\sigma_x/\sqrt{n}} \quad [4]$$

For an unpaired, two-sample, two-tailed test, comparing observations *z* (mean $\bar{z}$, standard deviation σ_z, sample size *n*) and y (mean $\bar{y}$, standard deviation σ_y, sample size *m*), we used the following test statistic (Eqn. [5].

$$T_{\text{two-sample}} = \frac{|\bar{z} - \bar{y}|}{\sqrt{\frac{\sigma_z^2}{n} + \frac{\sigma_y^2}{m}}} \quad [5]$$

For both tests, we applied the same statistical summary to the permutated test statistic and to the test statistic of the original sample to determine the probability p of observing the permutated test statistic being the same or more extreme than the test statistic of the original sample. Note that this approach yields the lowest achievable *p*-value of $1/B = 1/10^{-7}$. In the case of a multiple comparison, the *p*-value was adjusted using the Bonferroni method.

RESULTS

Social plasticity and the sensory basis of foraging decisions

We start our investigation of how population density is linked with sensory processing and decision-making by analyzing the contribution of different sensory modalities to foraging decisions, focusing on social and food olfactory cues. For this, we employed simple patch selection assays that presented locusts with four options: food (blackberry leaves, denoted as *Lvs*), a social setting (eight gregarious locusts, *Lct*), a combination of leaves and locusts (*LvsLct*), and an empty control patch (*Ctr*). We controlled the availability of olfactory and visual cues by using different stimulus containers that either provided both visual and olfactory cues or limited one of them (see Fig. 1a and Methods for details). We observed that gregarious desert locusts, *Schistocerca gregaria*, exhibited a strong attraction to the patch containing both leaves and locusts, as shown in Fig. 1b (*Vis*(+)*Olf*(+)). This attraction diminished in the absence of either visual (*Vis*(-)*Olf*(+)) or olfactory cues (*Vis*(+)*Olf*(-), see also suppl. Fig. S1 for animal trajectories). In contrast, solitarious locusts typically disregarded social stimuli and predominantly approached patches where food was presented alone (Fig. 1d). Notably, just as

with gregarious animals, the choices of solitarious locusts were most pronounced when both visual and olfactory cues were available.

We dissected the contributions of different sensory cues to the decision process via a Bayesian decision-making model (Arganda et al., 2012; Günzel et al., 2023), extended to encompass the four types of cues available in the current assay: vision, olfaction, social, and food. Specifically, we estimated the reliability of each information class – socio-visual, food-visual, socio-olfactory, and food-olfactory – to elucidate how these factors influence locusts' choices (Fig. 1c&e, light gray bars; reliability parameter C_i in Eqn.

[1). The close alignment between our model's predictions and the observed choices (light and dark gray bars respectively in Fig. 1b&d) suggests that the integration of available sensory cues can effectively describe locust decisions. This model enabled us to dissect further and quantify the parameters that contributed to these decisions. Notably, we found that gregarious animals were highly responsive to social cues, with the highest information reliability scores associated with the presence of conspecific odors at a patch (Fig. 1c). In contrast, solitarious-reared animals appeared deterred by the sight of conspecifics, as indicated by their negative scores in this context (Fig. 1e).

Functional imaging revealed differences in olfactory processing between gregarious and solitarious locusts

Building on the importance of olfaction in patch discrimination, we mapped how respective odor cues are represented in the locust antennal lobe (AL). An anatomical reconstruction of the AL, using back-fill labeling of olfactory receptor neurons (ORNs) and projection neurons (PNs), shows the arrangement of PN cell bodies on the anterior surface of the AL, with their dendrites situated beneath, encircling a central fiber core. Here, they form functional units, microglomeruli, with ORN axon terminals (Fig. 2a-c). To monitor local calcium signals as a proxy for neuronal activity, we established a protocol for functional imaging via mass retrograde labeling of PNs with the fluorescent calcium indicator Cal-520 (Lock et al., 2015). This technique was optimized to label the vast majority of PNs, facilitating subsequent optical recordings (see Methods for further details).

Furthermore, we developed a data-driven analysis pipeline (Fig. 2d) that segments the highly arborized structure of the locust AL into distinct activity granules and overcomes the limitations of biased manual selection of specific regions of interest. Calcium signals were captured at focal depths of 35±25 μm and 140±25 μm, chosen to maximize the number of

detectable cell bodies and glomeruli, respectively (see Fig. 2c for anatomical reference with examples of functional maps below).

Interested in the AL representation of the cues presented in our behavioral experiment, we conducted a chemical analysis to identify dominant volatiles in the headspace of the blackberry leaves. Gas chromatography-mass spectroscopic analysis featured two prominent appetitive plant volatiles (Anton & Hansson, 1996): leaf alcohol acetate (cis-3-Hexenyl-acetate, denoted as *Laa*) and the leaf alcohol 3-Hexel-1-ol (denoted as *Z3hl*), Fig. 2e. We then used the identified volatiles and an extraction of the locust odor (*Lct*) as stimuli to measure PN responses in gregarious and solitarious animals.

Each stimulus elicited a response apparent as calcium signals in a large set of PNs distributed across the AL (functional maps at the focal depth of the cell bodies show odor-induced responses in regions matching in size, shape, and number to individual cell bodies; examples in Fig. 2f&h). In both gregarious and solitarious locusts, response magnitudes to the leaf odor (the prevalent leaf component *Laa*) were higher than those to the locust odor *Lct* (green and orange curves in Fig. 2f&h show population response averages for *Laa* and *Lct*, with respective responses to the solvent as control in gray). Notably, however, was the respective change in response magnitude when both odors were simultaneously delivered as a mixture (*LaaLct*; containing half the amount of each single component; see Methods for mixture preparation). PN responses of gregarious animals significantly increased when adding the social component to the food-related one ($p<0.0001$; paired two-tailed bootstrap randomization test), while in solitarious animals, adding the social component resulted even in a significant decrease in response magnitude ($p = 0.0316$; see average time courses in Fig. 2f&h with the respective comparisons for individual data points in the left panels of Fig. 2g&i for gregarious and solitarious animals, respectively). This difference is also reflected by the population response trajectories (suppl. Fig. S4), illustrating distinct response patterns for the different stimuli that are generally consistent across the two phenotypes, albeit with noticeable differences (especially in the first principal component).

We observed similar findings when testing PN responses to crushed blackberry leaves (*Lvs*) in combination with the locust odor (see suppl. Methods and suppl. Fig. S2a-e). Here, the response magnitude to *LvsLct* mixture was significantly higher compared to the individual components *Lvs* and *Lct* in gregarious ($p = 0.02$; paired two-tailed bootstrap randomization test) but not in solitarious ($p>0.99$) locusts. Since this experiment was conducted with a widefield microscope, which – despite being faster – lacks the capacity for thin optical slices,

we replicated the experiments with leaf alcohol acetate *Laa* for a direct comparison (suppl. Fig. S2g-j). With similar response magnitudes and comparable differences between the phenotypes, these results align with the confocal data. Additional tests of antennal responsiveness to the odors via electroantennograms (EAG), reflecting summed receptor potentials along the antenna (Schneider, 1957), show almost identical response patterns in gregarious and solitarious antennae (suppl. Fig. S3c&d). This observation suggests the differences between the social phenotypes are not present presynaptically to the AL. Altogether, we propose that neural processing of odor mixtures in locusts may be subjected to a density-dependent modulation in the AL, highlighting a potential neural mechanism underlying differences in social behavior.

Generality and specificity of synergistic mixture response

Next, we tested whether the increased response to the mixture could be generalized to other food-related components. For that, a subset of animals was tested with additional odor combinations, beginning with the second appetitive plant volatile in the blackberry leaf headspace, *Z3hl* (P. Wang et al., 2019). As for *Laa* and crushed leaves, PN responses to *Z3hl* in gregarious locusts significantly increased when the social component was added ($p = 0.0237$ for *Z3hl* vs *Z3hlLct*; paired two-tailed bootstrap randomization test). At the same time, in solitarious locusts, the response to the same mixture was not higher than to the individual components ($p = 0.3539$).

Considering the consistent phenotypic differences across all mixtures tested so far, we explored the possibility that mixture processing is broadly different in the two social phenotypes. We addressed this by evaluating whether the observed increase in gregarious response magnitude is specific to a mixture of a social with a food-related stimulus or whether it can also be observed for other mixtures. For this, we tested additional odor combinations containing a non-social and/or non-food component, combining equal amounts of a neutral (non-food and non-social) component 1-Octanol with *Laa* (*OctLaa*, other+food), *Laa* with the second leaf component Z3hl (*LaaZ3hl*, food+food) and the mixture of 1-Octanol with *Lct* (*OctLct*, other+social). For gregarious locusts (Fig. 2g), neither of the combinations – other+food, food+food, other+social – induced a change in PN responses magnitude ($p = 0.2781$, $p = 0.8534$, and $p = 0.1411$, respectively; paired two-tailed bootstrap randomization tests). Similarly, but as expected, no increase was observed for solitarious animals either ($p = 0.6247$, $p = 0.9531$, and $p = 0.0601$). Taken together, these findings suggest that the consistently

increased response observed in gregarious locusts when combining a social with a food-related odor – *LaaLct*, *Z3hlLct*, and *LvsLct* (suppl. Fig. S2 for the later) – represents a phenotype-specific difference in which the salience of food odors is heightened when accompanied by the presence of conspecifics.

Combinatorial odor processing with mixture-specific PNs in the locust antennal lobe

We further analyzed the odor-induced response maps to understand better how the mixtures are processed and what may mediate the increase in gregarious animals' response magnitude. At first, we noted that responses to the different stimuli were highly overlapping. Most PNs responded to multiple tested odors, with only a few responding to a narrower subset (Fig. 3a). Interestingly, out of these narrower ones, we could detect mixture-specific PNs which were activated by a mixture but not by its components, showing a clear phenotypic difference in the prevalence of *LaaLct*-specific cells (red and blue bars in Fig. 3b show the proportion of mixture-specific PNs in gregarious and solitarious locusts; $p_{(\text{LaaLct only})} = 0.0220$, $p_{(\text{OctLaa only})} = 0.9284$, $p_{(\text{LaaZ3hl only})} = 0.1161$, $p_{(\text{OctLct only})} = 0.5295$; two-sample two-tailed bootstrap randomization tests).

To investigate these PN response patterns, we employed a unified analysis approach. For this, we projected the response maps from all PNs and all tested odors across all animals into a unified odor response space, as illustrated in Fig. 3c. Despite the considerable overlap described above, we discerned distinct odor response vector classes. These classes aided in delineating PN response types, which we used to explore potential differences between the social phenotypes (Fig. 3d, and Fig. 3c for the linear discriminant analysis 2-D projection). Upon evaluating these response vectors, we found that the population response to a specific odor primarily drives certain vectors. For instance, vector 1 is predominantly influenced by *Lct*, and similarly, vector 2 by *Z3hl*, vector 4 by *Laa*, and vector 5 by *Oct*. Conversely, the other vectors encapsulate a more combinatorial response profile. For example, vector 3 demonstrates a combinatorial pattern with responses to a broad set of stimuli. The distribution of PN types according to the odor space clustering was largely similar in both phenotypes, with a difference in prevalence mainly for *Lct*-positive and *Lct*-negative types (pie charts in Fig. 3d show the proportion of each PN type in red and blue for gregarious and solitarious locusts, respectively).

Combinatorial odor maps stay consistent across multiple repetitions

Previous studies on locust odor mapping have shown that, although the population-level responses reliably determine odor identity, there can be substantial variability at the level of individual PNs (Mazor & Laurent, 2005). Thus, we continued our investigation by examining how consistent odor responses are across repetitions. Response consistency was determined for three general odors in the PN cell bodies (similar optical slice as before) and their dendritic terminals (concentrically arranged glomeruli captured at the focal depth that maximizes the number of visible glomeruli, 140 μm). As expected from a combinatorial coding system, odor-induced responses had considerable overlap (displayed as a color-coded overlay in Fig. 4a). However, these responses were distinct across different odors and remained consistent for the same odor over multiple trials (see Fig. 4b and suppl. Fig. S5 for individual trials in the example animal, and Fig. 4c for the population response).

Phase-dependent differences are consistent across cell compartments

By recording responses to social and food-related odors in the PN dendrites of gregarious (Fig. 4d-f) and solitarious (Fig. 4g-i) animals, we noted a trend further corroborating what we observed in the cell bodies and widefield imaging above. In gregarious animals, the response magnitude to the mixture (*LaaLct*) was again significantly higher than to *Laa* alone ($p = 0.0118$; two-tailed bootstrap randomization test). In contrast, we observed a strong trend for a decreased mixture response in solitarious animals ($p = 0.0761$). This is in line with a larger proportion of *LaaLct*-specific glomeruli in gregarious (0.12 [0.08, 0.18], mean [95% confidence interval]; suppl. Tbl. S1) than in solitarious animals (0.05 [0.02, 0.08]), and more *Laa*-specific glomeruli in solitarious (0.23 [0.11, 0.48]) than in gregarious (0.06 [0.04, 0.11]) animals.

Response motif dynamics in the locust antennal lobe reliably predict social phenotypes

Our results repeatedly suggest that social cues synergize with appetitive olfactory signals in antennal lobe projection neurons of gregarious locusts. Moreover, we observed sustained somatic activity patterns (Fig. 2f&h), which hint at complex response profiles following a network-spanning integration. Unlike transient glomerular responses (Fig. 4e&h), which could be more critical for stimulus detection, the sustained somatic patterns may provide a continuous assessment of the olfactory landscape for adaptive behavioral output. In view of that, we

continued to characterize individual PN response profiles on the level of the cell bodies to uncover what distinguishes gregarious and solitarious phenotypes.

We applied an unsupervised analysis to all PN cell body response profiles resulting from the three stimuli (*Lct*, *Laa*, *LaaLct*), identifying six distinct odor-induced response motifs (Fig. 5a&b). Ordered by peak magnitude and timing, these motifs categorize PN responses as inhibitory (below baseline motifs 1 and 2), delayed response (motif 3), excitatory phasic (motifs 4), strong excitatory phasic (motifs 5), and excitatory sustained (motif 6). Examining the proportion of PNs in each response category, which were averaged across animals for each stimulus (Fig. 5c), revealed key differences between gregarious and solitarious locusts (Fig. 5d). Notably, solitarious animals exhibited a higher prevalence of the inhibitory (motif 2) and delayed (motif 3) responses for the locust colony odor, and a higher prevalence of the strong phasic (motif 5) and sustained (motif 6) response for the food-related stimulus. In contrast, gregarious animals exhibited a higher prevalence of the excitatory phasic response (motif 4) for the mixture.

Particularly interested in what underlies the difference in mixture processing between gregarious and solitarious animals, we conducted a deeper analysis of the synergistic responses to the mixture. We tracked how PN response motif assignments change with odors and hence assigned each PN a response motif triplet. For instance, [2|4|5] (Fig. 5e left) corresponds to the neuron's response to the three presented stimuli (*Lct*, *Laa*, and *LaaLct*). Based on this information, we calculated an individual mixture-interaction score (Bliss score, Fig. 5e right) using Eqn. [3 (Bliss, 1939). Specifically, we estimated the mixture response as expected if there was no interaction between the individual components (*Laa* and *Lct*; Eqn. [3, $f_{expected}$) and compared it for each point in time with the observed response motif to the mixture (*LaaLct*). Consequently, the resulting score distinguishes synergistic interactions (score > zero) from antagonistic ones (score < zero) between *Laa* and *Lct*. We observed that certain motif triplets, and thus certain Bliss interaction scores, were more prevalent in either gregarious or solitarious animals. We identified the 12 triplets that most substantially differentiated the two phenotypes (Fig. 5f; color-coded according to the predominant phase) to further understand the crowding-induced synergy in processing food and social mixtures. Seven of these combinations involved PNs whose mixture responses were determined by either the stronger (e.g., 2|5|5) or the weaker component (e.g., 3|6|3). The remaining triplets display substantial mutual synergistic (e.g., 1|1|4 and 1|1|6) and antagonistic (e.g., 6|6|3) interactions, which are predominantly found in gregarious (red bliss score profiles) and solitarious (blue) locusts (see also table SI for triplet

prevalence). These types of gregarious synergistic triplets could account for the mixture-specific PNs labeled in Fig. 3b. Further, the proportion of strongly synergistic PNs (Bliss score larger than one standard deviation of the whole distribution) was significantly larger in gregarious (0.25 [0.21, 0.30], grand mean [95% confidence interval]) than in solitarious (0.13 [0.10, 0.20]) animals ($p = 0.0005$; two-sample two-tailed bootstrap randomization test). Pooling all PN Bliss interaction scores, except those with identical response motifs for all three stimuli, highlights the differences in mixture interactions between the two phenotypes in the context of their response motifs (Fig. 5g).

The increased level of synergy in gregarious processing, together with phenotype-specific motif triplets, suggests that the dynamics of motif transitions between odors carry information about odor processing that may classify the phenotypes. Our comprehensive dataset allowed us to estimate the probabilities of motifs changing, given a change in stimulus (see suppl. Fig. S6 for heatmaps summarizing the occurrence of all motif transitions). Based on this, we examined the predictive strength of a linear discriminant analysis (LDA) classification model trained on gregarious and solitarious motif transition maps (see Methods for details). This analysis revealed that antennal lobe response dynamics can reliably distinguish gregarious and solitarious phenotypes with 84.4% correct predictions (Fig. 5h). Taken together, our analysis suggests that network interaction variations are manifested in shifts of single PN response profiles, which conjointly give rise to a crowding-induced synergy in the olfactory processing of food and social odors.

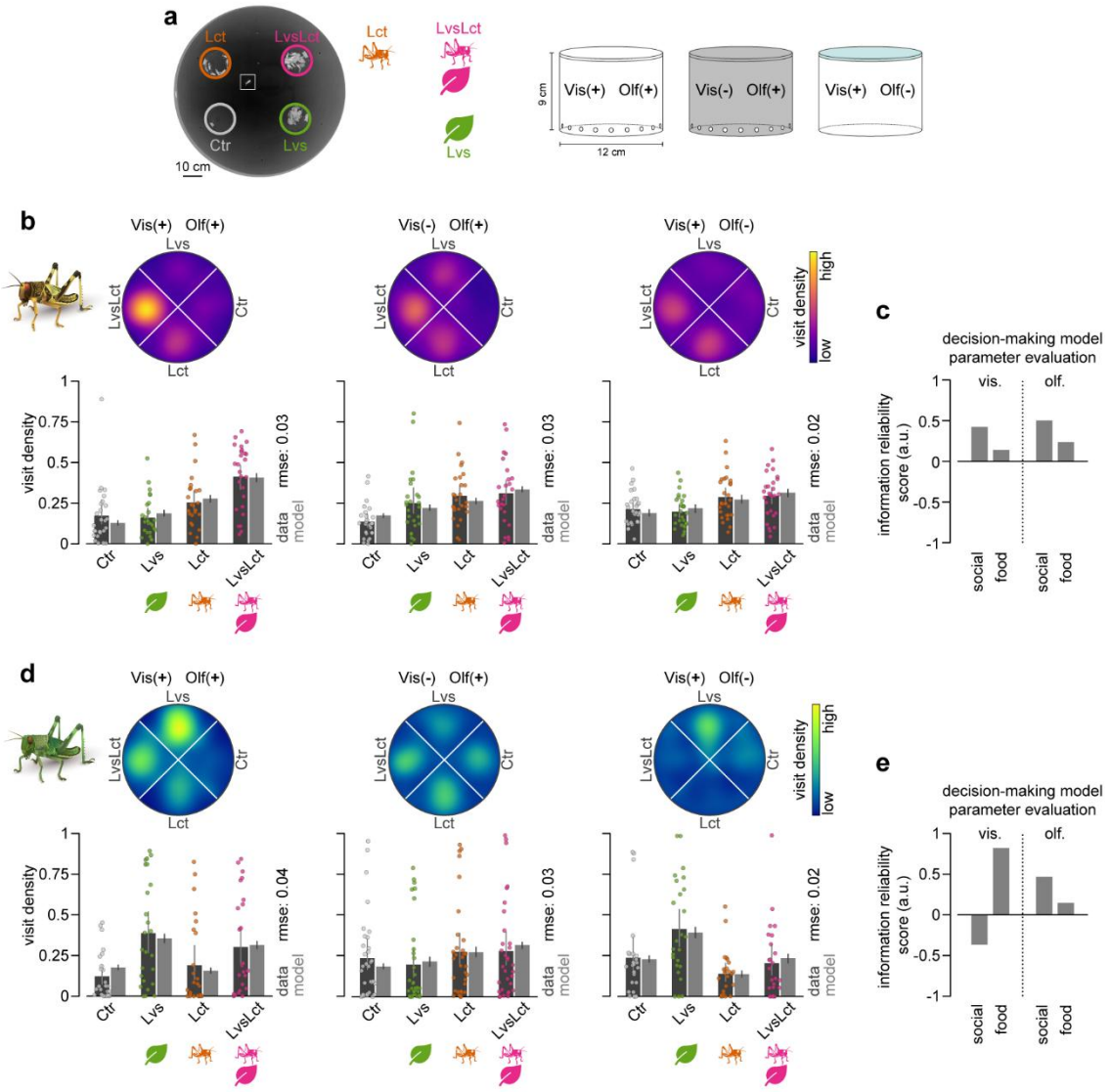

Fig. 1 – Interactions between social and food cues in patch selection. (a) Animals were tested in a circular arena with four patch options (blackberry leaves *Lvs*, locusts *Lct*, leaves and locusts *LvsLct*, and control *Ctr*) under one out of three sensory conditions (visual and olfactory cues available: *Vis*(+)*Olf*(+); olfactory but no visual cues: *Vis*(-)*Olf*(+); visual but no olfactory cues: *Vis*(+)*Olf*(-)) to isolate the effects of visual and olfactory cues during patch selection. On the left, we show a color-inverted, example frame from a gregarious animal trial. Here, the superimposed circles indicate the four patches, and the square shows the location of the locust. We used different stimulus containers for the different sensory conditions (schematics on the right) that were either transparent and odor-permeable with surrounding holes to provide both visual and olfactory cues (*Vis*(+)*Olf*(+)), opaque with holes to restrict visual cues (*Vis*(-)*Olf*(+)), or transparent but sealed with Parafilm (blue-shaded top) to restrict olfactory cues (*Vis*(+)*Olf*(-)). (b) We tested gregarious locusts under the three sensory conditions. Heatmaps depict average locust density in each stimulus quarter (blackberry leaves *Lvs*, locusts *Lct*, leaves and locusts *LvsLct*, and control *Ctr*) for different sensory conditions (visual and olfactory cues available: *Vis*(+)*Olf*(+), left (n = 26); olfactory but no visual cues: *Vis*(-)*Olf*(+), center (n = 26); visual but no olfactory cues: *Vis*(+)*Olf*(-), right (n = 28)). Swarm plots represent individual locusts' mean density in each stimulus quarter, dark gray bar plots with error bars indicate corresponding grand means with 95% confidence intervals, and light gray bar plots with error bars indicate means and 95% credible intervals from a decision-making model (5000 simulations; see Methods). (c) Information reliability scores for each information class (social, food) and sensory modality (visual, olfactory), were obtained by fitting a decision-making model to the patch selection data in (b). (d-e) Similar experiments and analysis as in b-c, but for solitarious animals (*Vis*(+)*Olf*(+): n = 25; *Vis*(-)*Olf*(+): n = 32; *Vis*(+)*Olf*(-): n = 25). Source data are provided as a Source Data file.

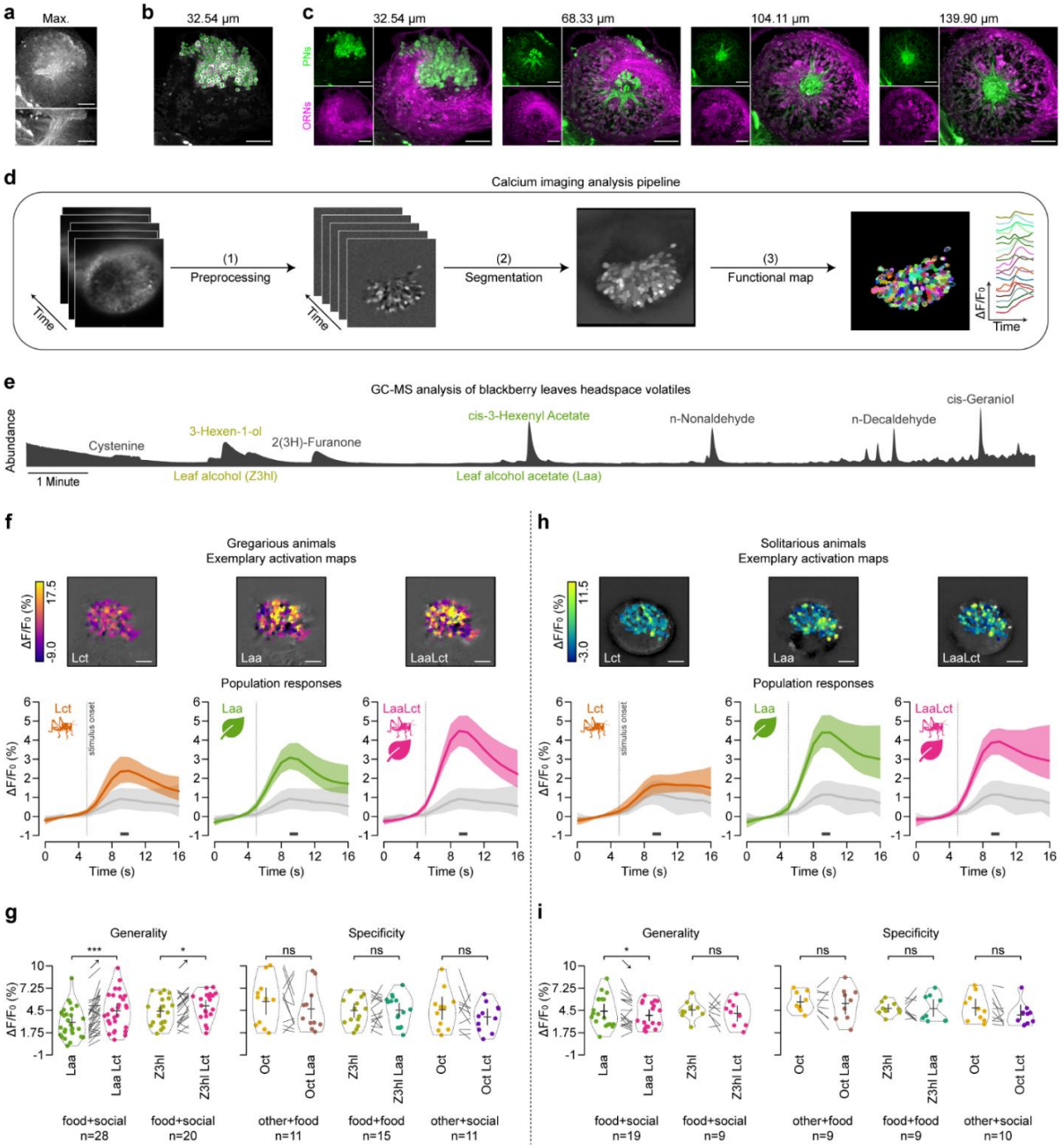
a
Max.
b
32.54 µm
c
32.54 µm
68.33 µm
104.11 µm
139.90 µm
PNs
ORNs
d
Calcium imaging analysis pipeline
(1)
Preprocessing
(2)
Segmentation
(3)
Functional map
Time
ΔF/F0
e
GC-MS analysis of blackberry leaves headspace volatiles
Abundance
Cystenine
3-Hexen-1-ol
2(3H)-Furanone
cis-3-Hexenyl Acetate
n-Nonaldehyde
n-Decaldehyde
cis-Geraniol
1 Minute
Leaf alcohol (Z3hl)
Leaf alcohol acetate (Laa)
f
Gregarious animals
Exemplary activation maps
ΔF/F0 (%)
17.5
-9.0
Lct
Laa
LaaLct
Population responses
stimulus onset
Time (s)
h
Solitarious animals
Exemplary activation maps
11.5
-3.0
g
Generality
Specificity
***
*
ns
food+social n=28
food+social n=20
other+food n=11
food+food n=15
other+social n=11
i
food+social n=19
food+social n=9
other+food n=9
food+food n=9
other+social n=10

Fig. 2 – Functional imaging of the antennal lobe representation of the odor cues used in patch choice experiments. (a) Maximum projection of a confocal stack of a projection neuron (PN) backfill staining along the z-axis (top) or the y-axis (bottom). (b) Identification of 181 individually stained PN somata (superimposed green dots) in one section of the scanned locust antennal lobe. (c) Confocal scans with a double backfill staining of PNs (green) and olfactory receptor neurons (ORNs, magenta) at various imaging depths (indicated above, Z = 0 corresponds to the anterior surface of the AL). (d) Schematic diagram detailing the staining protocol for PNs in locust antennal lobes for in-vivo functional calcium imaging and the subsequent analysis pipeline (see Methods for specifics). (e) Gas chromatography analysis identifies leaf alcohol acetate (*Laa*, cis-3-Hexenyl Acetate) and leaf alcohol (*Z3hl*, 3-Hexen-1-ol) as prominent food-related volatiles in blackberry leaves. (f) Confocal microscopy data of odor-induced responses to the locust odor *Lct* (left), leaf alcohol acetate *Laa* (center), and their combination *LaaLct* (right). Average activity time courses (grand means with 95% confidence intervals as shaded areas) show the responses of all gregarious animals (n = 28), while the false color-coded images show the mean intensity projections of an exemplary animal during the window for analysis (dark gray bars below the time courses; stimulus onset is indicated by vertical dotted lines). Responses to the solvent are shown as light gray time courses. (g) Evaluation of gregarious animals' mixture responses to test for generality (increase in response magnitude for other food-related stimuli upon addition of the social component) and specificity (the increase in mixture response occurs only for the combination of a food-related with a social stimulus). Swarm plots show individual animal means during the window for analysis, violin plots indicate probability density estimates, while crosses depict grand means and 95% confidence intervals for all stimuli (*Laa*, *Z3hl*, and 1-Octanol *Oct*) and respective combinations (generality: $n_{(food1+social)}$ = 28, $n_{(food2+social)}$ = 20; specificity: $n_{(other+food)}$ = 11, $n_{(food+food)}$ = 25, $n_{(other+social)}$ = 11). (h-i) Correspond to f-g, but for solitarious animals (generality: $n_{(food1+social)}$ = 19, $n_{(food2+social)}$ = 9; specificity: $n_{(other+food)}$ = 9, $n_{(food+food)}$ = 9, $n_{(other+social)}$ = 10). Statistical inferences in g and i were based on paired two-tailed bootstrap randomization tests (ns: not significant; p<0.05: *; p<0.01: **; p<0.001: *** with gregarious $p_{(food1+social)} = 3.58*10^{-5}$, $p_{(food2+social)}$ = 0.0237, $p_{(other+food)}$ = 0.2781, $p_{(food+food)}$ = 0.8534, $p_{(other+social)}$ = 0.1411; solitarious $p_{(food1+social)}$ = 0.0316, $p_{(food2+social)}$ = 0.3539, $p_{(other+food)}$ = 0.6247, $p_{(food+food)}$ = 0.9531, $p_{(other+social)}$ = 0.0601). Scale bars: 100 µm. Source data are provided as a Source Data file.

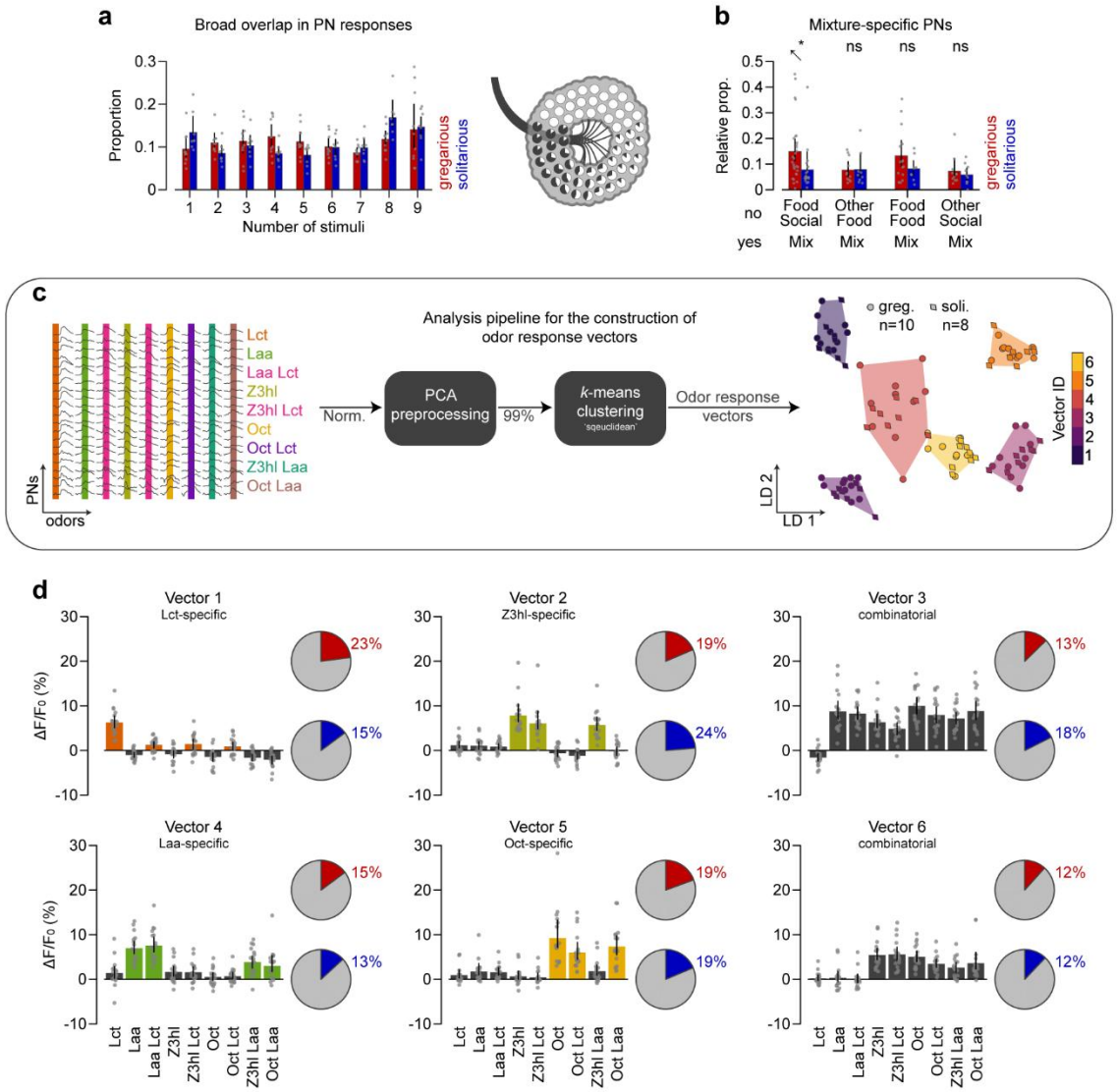

Fig. 3 – Combinatorial coding of odor responses in antennal lobe projection neurons of gregarious and solitarious animals. (a) The proportion of gregarious (red) and solitarious (blue) PNs that respond to a given number of stimuli, as symbolized on the right by the pie charts with the proportion of responses for each PN, overlaid onto the antennal lobe illustration. All animals ($n_{(greg.)}$ = 10; $n_{(soli.)}$ = 8) were tested with nine stimuli (locust odor *Lct*, leaf alcohol acetate *Laa*, leaf alcohol *Z3hl*, 1-Octanol *Oct*, as well as their mixtures *LaaLct*, *Z3hlLct*, *OctLaa*, *Z3hlLaa*, and *OctLct*). (b) The relative proportion of mixture-specific PNs – regions that are responsive to a two-component mixture ('yes') but not to its two components ('no'). The proportion of mixture-specific PNs was calculated out of all PNs responding to that mixture (specific+non-specific) for gregarious (red; $n_{(LaaLct\ only)}$ = 28, $n_{(OctLaa\ only)}$ = 11, $n_{(Z3hlLaa\ only)}$ = 15, $n_{(OctLct\ only)}$ = 11) and solitarious (blue; $n_{(LaaLct\ only)}$ = 19, $n_{(OctLaa\ only)}$ = 9, $n_{(Z3hlLaa\ only)}$ = 9, $n_{(OctLct\ only)}$ = 10) animals. (c) Diagram explaining the clustering of individual PNs' response magnitude sets into odor response vectors. The scatter plot displays the linear discriminant analysis 2-D projection after clustering to visualize the classification into activity vectors (circles: gregarious (n = 10); diamonds: soliatrious (n = 8) animals). (d) Representation of each odor response vector along with pie charts displaying the relative allocation of gregarious (red) and solitarious (blue) PNs to the respective vector. Bars, color-coded to signify response vector type (color: odor-specific; gray: combinatorial), indicate grand means with 95% confidence interval error bars $n_{(greg.)}$ = 10; $n_{(soli.)}$ = 8). Statistical inference in b was based on two-sided two-tailed bootstrap randomization tests (ns: not significant; p<0.05: *; p<0.01: **; p<0.001: *** with $p_{(LaaLct\ only)}$ = 0.022, $p_{(OctLaa\ only)}$ = 0.9284, $n_{(Z3hlLaa\ only)}$ = 0.1161, $n_{(OctLct\ only)}$ = 0.5295). Source data are provided as a Source Data file.

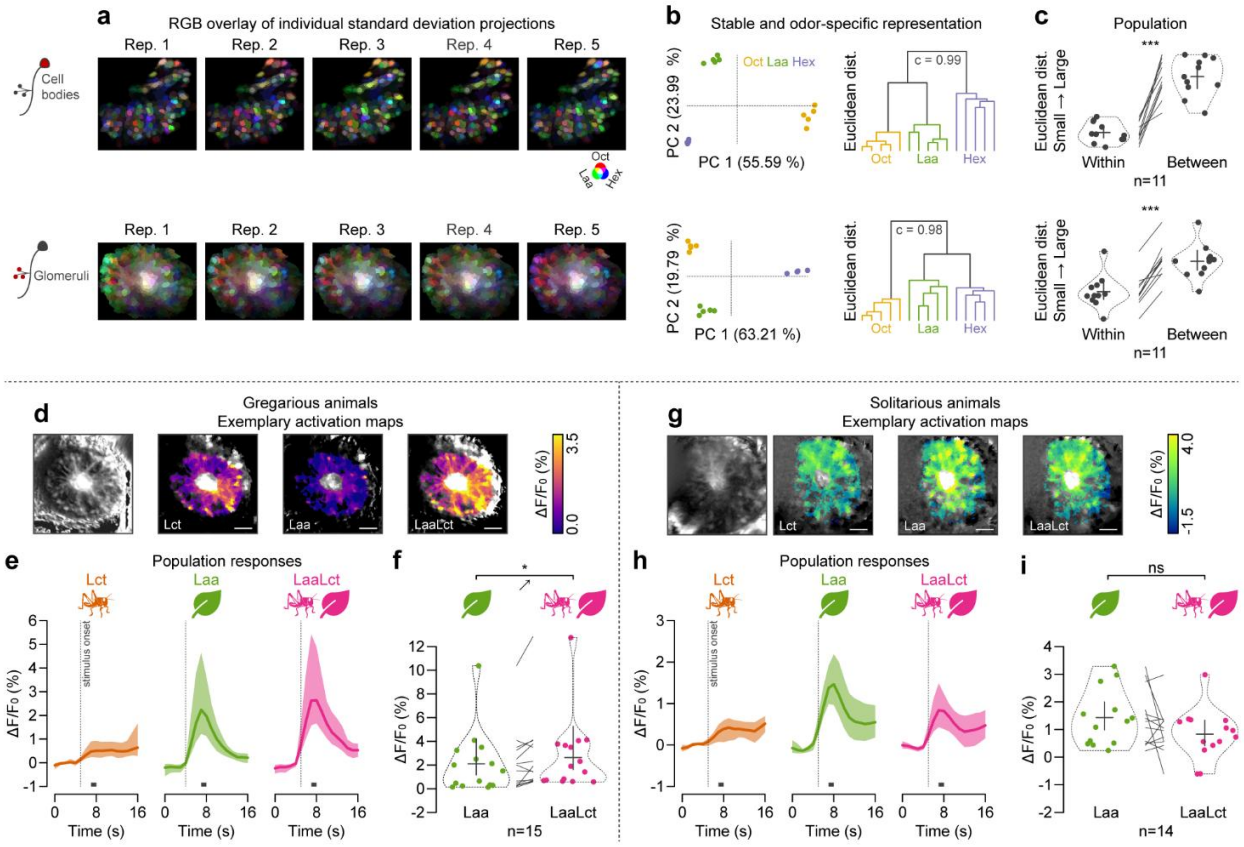

Fig. 4 – Consistency of odor response patterns in projection neuron cell bodies and glomeruli. (a) Examination of projection neuron (PN) response maps in cell bodies (top row) and glomeruli (bottom row) following repeated presentations of three single-molecule odorants (1-Octanol *Oct*, leaf alcohol acetate *Laa*, 1-Hexanol *Hex*) in an exemplary animal. Individual standard deviation projections of the repeated presentation of three stimuli were overlayed in RGB color space (red: *Oct*, green: *Laa*, blue: *Hex*) to visualize regions responding to one stimulus alone or to several stimuli (see suppl. Fig. S5 for all standard deviation projections). (b) Principal component analysis (PCA) of PN responses to five trials of each odor with an accompanying hierarchical binary cluster tree dendrogram (cophenetic correlation coefficient as *c*). Data correspond to a. (c) Euclidean distance in PC space between responses of trials with the same odor (within) and different odors (between) in $n = 11$ gregarious animals. Swarm plots show individual animal means, violin plots for probability density estimates, and crosses for grand means and 95% confidence intervals (with $p = 4.46*10^{-6}$ for cell bodies and $p = 6*10^{-8}$ for glomeruli). (d) Functional confocal microscopy data of odor-induced responses to the locust odor *Lct*, leaf alcohol acetate *Laa*, and their combination *LaaLct* in the glomerulus layer of an exemplary gregarious animal. The heatmaps show the standard deviation projections across all stimuli (grayscale), alongside the mean intensity projections (color) during the window of analysis (see gray bars in e). (e) Average activity time courses of all glomerular regions (medial tract excluded; stimulus onset is indicated by vertical dotted lines) across all $n = 15$ gregarious animals (grand means with shaded 95% confidence intervals). (f) Swarm plots of individual animal means during the window of analysis. Violin plots indicate probability density estimates, and crosses show grand means and 95% confidence intervals ($p = 0.0177$, same animals as in e). (g-i) Correspond to d-f, but for $n = 14$ solitarious animals with $p = 0.1141$. Statistical inference in c, f, and i was based on paired two-tailed bootstrap randomization tests (ns: not significant; $p<0.05$: *; $p<0.01$: **; $p<0.001$: ***). Scale bars: 100 µm. Source data are provided as a Source Data file.

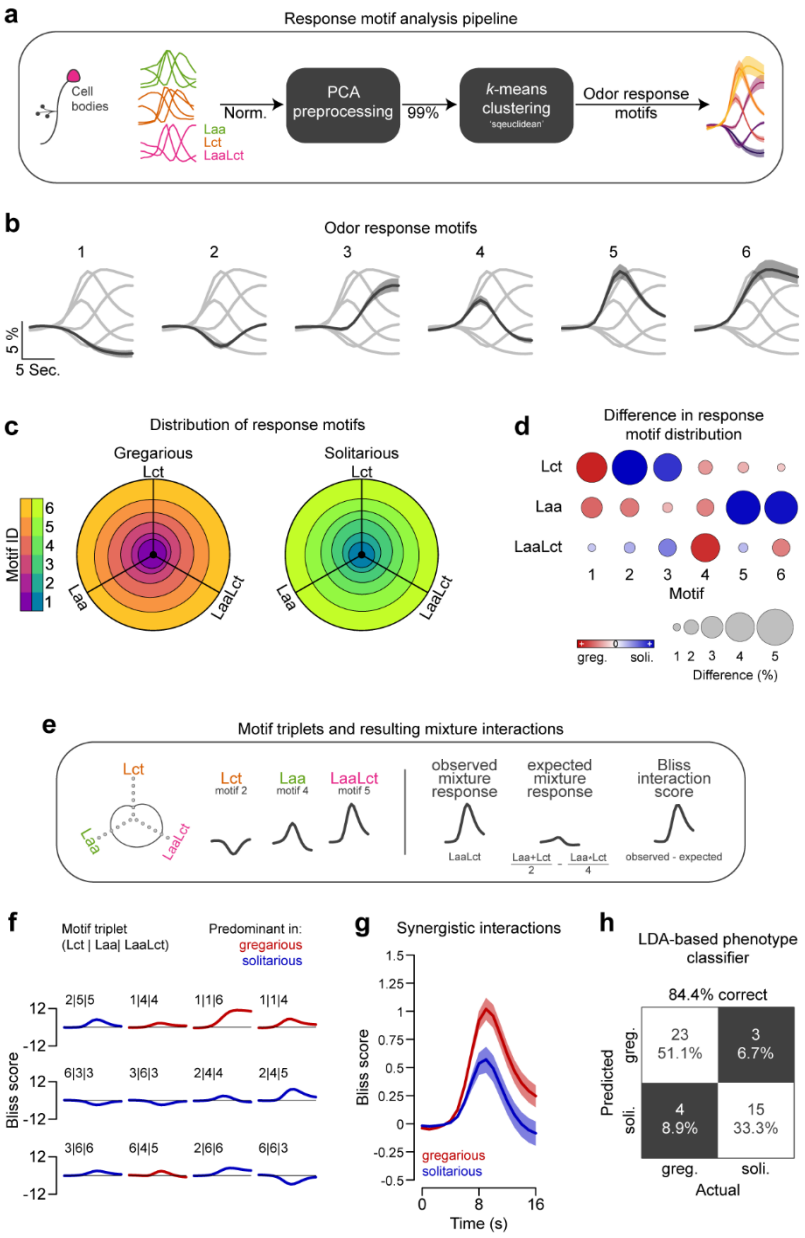

Fig. 5 – Analysis of dynamical odor response motifs. (a) Schematic illustration of the clustering process used to categorize the activity profiles of individual cell bodies into six distinct odor-induced response motifs. (b) Temporal profiles of the response motifs, arranged according to peak magnitude and timing. Shown are grand means for each motif across both gregarious and solitarious animals with shaded 95% confidence intervals ($n_{(greg.)}$ = 28; $n_{(soli.)}$ = 19). (c) Circular stacked bar plots represent the proportion of each response motif for each of the three stimuli (the locust odor *Lct*, leaf alcohol acetate *Laa*, and their combination *LaaLct*). Gregarious animals are shown on the left (n = 28), and solitarious animals on the right (n = 19). (d) Distinct differences in response motif allocation between gregarious and solitarious animals. Variations in circle color and size denote the degree of disparity (absolute difference in proportion for each motif and odor). (e) Diagram demonstrating the dynamics of motif transitions with odors, which lead to a unique motif triplet for every cell body. We used this to calculate a mixture interaction (Bliss) score for each cell, by comparing the observed *LaaLct* response motif to the ones expected from the *Lct* and *Laa* components if there was no interaction between them. (f) Analysis of motif interactions using Bliss interaction score time courses to distinguish between synergistic (scores>zero) and antagonistic (scores<zero) interactions between *Laa* and *Lct*. Shown are bliss profiles of the 12 triplet combinations that exhibited the largest differences in prevalence between gregarious and solitarious locusts (cf. suppl. Tbl. S1). (g) The average (mean with shaded 95% confidence intervals) Bliss interaction score time courses based on all (but those with identical response motifs across all three stimuli) gregarious (red; n = 28) and solitarious (blue; n = 19) motif triplets. (h) A confusion matrix showing correct (white) and incorrect (dark gray) phenotype classifications using a linear discriminant analysis model. The model was trained on the dynamics of motif transitions (the proportion of PNs that switch motifs between for a given change between stimuli; see suppl. Fig. S6) for predicting each animal's phenotype (see Methods for details). Source data are provided as a Source Data file.

DISCUSSION

In this study, we investigated the neural processing of olfactory information in changing social environments, allowing locusts to make decisions appropriately in a context-dependent manner. We established an *in vivo* functional calcium imaging protocol to reliably monitor the activity of a large subset of antennal lobe (AL) projection neurons (PN). Our results indicate a crowding-induced synergy in the processing of food and social odors that originates from phenotype-specific transition dynamics between distinct response motifs. As a direct consequence, this allowed us to use the AL network dynamics to reliably predict whether a locust was gregarious (group-living) or solitarious. Moreover, our study draws connections between the physiological observations and behaviorally tested patch preferences, providing further insight into the locust decision-making system during foraging.

During foraging, the presence of others can indicate both resource quality and location, offering graded and discrete information, respectively (Dall et al., 2005). In gregarious locusts, this social information serves as an attractive cue for individuals to join a food patch (Günzel et al., 2023; Lihoreau et al., 2017), potentially even more than the sight/smell of the food itself (Fig. 1b). We used a Bayesian decision-making rule (Arganda et al., 2012; Günzel et al., 2023), a powerful approach for disentangling multiple contributing factors in behavioral data (Meyniel et al., 2015; Pérez-Escudero & de Polavieja, 2011; Wystrach et al., 2015), to estimate the relative contribution of the different cue types. Our analysis indicates that both visual and olfactory cues influenced patch selection, and it revealed phenotype-specific differences: while in solitarious locusts visual cues qualitatively predict patch choices on their own (similar preference in *Vis*(+)*Olf*(-) and *Vis*(+)*Olf*(+), Fig. 1d), it is only when both modalities are simultaneously present that a clear preference is demonstrated in gregarious locusts. Taken together, this revealed the nuanced roles different sensory modalities play in affecting locust foraging decisions, allowing for an investigation of the underlying neural mechanisms.

Given the importance of olfaction for patch selection, we monitored odor-induced neuronal activity across the primary olfactory center. The results showed that PN responses to appetitive odors are modulated by phenotype (i.e., with phase change) when mixed with the social odor. Previous work on gregarious and solitarious locusts described that the two phenotypes have a generally similar AL anatomy (except for a higher number of sensilla in solitarious individuals, potentially relating to their longer developmental period (Ochieng et al., 1998), similar PN spiking properties (Ignell et al., 1998), and response probabilities to single tested compounds (Anton et al., 2002). The ability to map odor responses across a large set of PNs in a single

animal verified that the phenotypic differences are indeed subtle (i.e., same response motifs in Fig. 5b; largely overlapping response vectors in Fig. 3d; similar response trajectories in an unifying principal component space shown in suppl. Fig. S4), but clearly distinguish the evaluation of the food+social mixture. Given additionally that electroantennography recordings do not reflect the same phenotypic difference observed in the AL (see suppl. Fig. S3), we suggest that locust phase change is less likely to impact presynaptic receptor sensitivity, but that the observed crowding-dependent modulation is probably mediated by lateral network interactions. All other tested mixture combinations (lacking either the colony compound or appetitive food odor) were not different from the response to their components, reflecting a hypo-additive, or elemental, mixture response (Clifford & Riffell, 2013; Mohamed et al., 2019; Shen et al., 2013). The comparison of PN response profiles to the food+social mixture revealed higher mixture synergism in gregarious locusts, which is reflected by both a larger proportion of mixture-specific PNs (Fig. 3b) and synergistic response triplets (i.e., [1 | 1 | 4] and [1 | 1 | 6] in Fig. 5f). The resulting odor profile – constructed from all PNs' response statistics – reliably separates gregarious and solitarious phenotypes (LDA analysis, Fig. 5h) and gives rise to specific differences in mixture processing. These predominantly rely on a higher proportion of PNs subjected to antagonistic mixture interactions in solitarious animals and synergistic in gregarious (Fig. 5f). Mechanistically, given the lack of observed excitatory local interneurons (LNs) (Ernst et al., 1977), these changes in network processing are likely mediated by disinhibition of lateral inhibitory LNs, innervated by *Laa*- or *Lct*-sensitive PNs. Local disinhibition will enable motif switches via the temporally and structurally diverse nature of LN populations (Barth-Maron et al., 2023; Nagel & Wilson, 2016; Vogt et al., 2021) and thus give rise to differential response profiles with increasing population density.

State-dependent regulation of odor processing in the insect antennal lobe has been predominantly investigated in the context of hunger, which incites animals to approach odor cues they would typically avoid (reviewed by Lin et al. (Lin et al., 2019) and Sayin et al. (Sayin et al., 2018)). This reconfiguration involves both modulation of presynaptic receptor sensitivity (Root et al., 2011) and recruitment of local interneuronal input by neuromodulatory pathways (Albin et al., 2015; Vogt et al., 2021) . Another relevant type of context-dependent modulation in olfactory circuits is enhanced courtship receptivity in flies after detecting a food source nearby (S. Das et al., 2017; Grosjean et al., 2011) . This enhancement is mediated by lateral excitatory input to the pheromone-sensitive glomerulus in the presence of vinegar smell (S. Das et al., 2017). In that context, differential lateral processing can be locally modulated by

state-dependent (e.g., sex-specific, or virgin vs. mated) modifications to LN innervation patterns (S. Das et al., 2017). In locusts, similar network-spanning adjustments could occur with changes in population density to enhance food detection in swarms. This can be mediated via adaptive regulation of various components of the interweaved AL network – from local gain control by presynaptic interglomerular inhibition that attenuates ORN-PN signal transfer (Barth-Maron et al., 2023; Olsen & Wilson, 2008; Warren & Kloppenburg, 2014) to lateral interactions between LN pairs that sharpen odor discrimination and tune transient PN synchronization patterns (MacLeod et al., 1998; MacLeod & Laurent, 1996; Patel et al., 2009). Similarly, local inhibitory circuits within the mouse olfactory bulb – mediated by dendro-dendritic synaptic connections between mitral cells and granule cells (Abraham et al., 2010; Shepherd et al., 2004), analogous to antennal lobe PNs and LNs, respectively – facilitate the discrimination of closely related stimuli (Schoppa & Urban, 2003). Taken together, nonlinear processing steps are essential for a context-dependent regulation of the olfactory system (Badel et al., 2016). However, future research is needed to address how the locust AL network can be fine-tuned for swarming.

Our functional imaging approach complements previous work on locust olfaction characterizing odor mapping as a dynamic code of temporally evolving PN response trajectories that code odor identity (Laurent & Davidowitz, 1994; MacLeod & Laurent, 1996; Mazor & Laurent, 2005; Stopfer et al., 2003) in a history- and context-dependent manner (Broome et al., 2006; Ling et al., 2023; Saha et al., 2015; Stopfer et al., 2003). Now, our study expands on this by mapping the spatial arrangement of odor responses across PNs in a single preparation. We demonstrate that individual odors activate broad, overlapping sets of multiglomerular PNs across the AL. Similar to other insects, these subsets are odor-specific and stable across repetitions (Fig. 4a-c, in agreement with Mazor and Laurent (Mazor & Laurent, 2005)). Recent observations from clonal raider ants – another insect species with largely arborized ALs, similar to locusts – revealed a highly stereotyped odor encoding logic in the ORN population (Hart et al., 2023). The many-to-many wiring map of single sensory neurons innervating multiple glomeruli in locusts predicts a broad combinatorial PN response (as seen here), even for narrowly tuned receptors (Chang et al., 2023) . The implications of such a wiring scheme on coding capacity, which is generally enhanced in the postsynaptic PN layer (Bhandawat et al., 2007; Lüdke et al., 2018; Raman et al., 2010), need further investigation.

Furthermore, we recorded from different cellular compartments – PN cell bodies (Fig. 2) and glomeruli (Fig. 4d-h) – revealing synergistic interactions for both. Previous studies suggest that locust cell bodies match the overall PN activity profiles generated via local field potential recordings (Laurent et al., 1996). This is in line with PN cell bodies in *Drosophila* clearly exhibiting the odor tuning observed in the respective glomeruli (Root et al., 2007). Yet, our recordings also show differences between somatic and glomerular response properties that potentially reconcile disparities between the literature on locust olfaction and other insects. On the one hand, prolonged and temporally-varying somatic odor responses (Fig. 2f&h) align with electrophysiological recordings from PN cell bodies in locusts (Anton et al., 2002; Mazor & Laurent, 2005; Saha et al., 2015). On the other hand, fast rise and decay times in the glomerular calcium signals (Fig. 4e&h) are consistent with more transient combinatorial maps described in other insects with functional imaging at the dendritic terminals (e.g., Sachse and Galizia or Vosshall et al. (Sachse & Galizia, 2003; Vosshall et al., 2000)). Taken together, these points advocate for stable glomerular odor separation across species and AL structures, which is reformatted via network processing into temporally dynamic odor maps for behaviorally relevant representations.

Swarms of desert locusts can span several hundred square kilometers and threaten the food security of millions. The density-dependent phase change from one phenotype to another is accompanied by substantial changes in the quantity, quality, and type of information animals can gather. Our results suggest that crowding already operates in early sensory processing centers, modulating – in our case – the antennal lobe output to influence animals' foraging decisions. The higher proportion of mixture-specific PNs to both food+social but also food+food mixtures in gregarious animals (Fig. 3b) may indicate a more general adaptation of gregarious locusts to handle multiple simultaneous odor signals in complex environments, such as swarms or varying ecological settings. Yet, to fully understand locust phase change and swarm formation, future research is needed to address the multimodal nature of this phenomenon. Our Bayesian decision-making model suggests that the integration of olfactory with visual information is essential for reliable decision-making, offering new research venues in the fields of vision and multimodal cue integration.

Furthermore, our robust and data-driven calcium imaging analysis provides a comprehensive way to measure odor representation across the locust AL. Given the natural gradient of sociality in locusts, this can be further extended to investigate the cellular mechanisms of adaptive social behavior in changing sensory environments. Altogether, considering their behavioral and social

plasticity, locusts provide an excellent opportunity for investigating olfactory processing in complex environments and offer a trackable system for linking sensory adaptations to behaviorally relevant tasks.

ACKNOWLEDGEMENTS

The authors thank Yvonne Hertenberger and Hannes Kübler for help with data collection; Nina Schwarz for providing locust illustrations; the team of the Bioimaging Centre at the University of Konstanz for help with obtaining confocal microscopy scans of antennal lobe double stainings; Marco Paoli for valuable insight on calcium imaging and corresponding analyses; Giovanni Galizia for providing feedback and facilities; Dieter Spiteller for GC advice and Hanna Schnell for odor preparation and support with the GC operation and analysis. James Foster, Ahmed El Hadi and Katrin Vogt for insightful comments on the manuscript. This work was completed with the support of the Deutsche Forschungsgemeinschaft (DFG, German Research Foundation) under Germany's Excellence Strategy—EXC 2117—422037984 (supporting Y.G., S.S., S.K. and E.C.F.) and DFG project grant CO 1758/3-1 (E.C.F.).

FUNDING

Open Access funding enabled and organized by Projekt DEAL.

COMPETING INTERESTS

The authors declare no competing interests.

DATA AND CODE AVAILABILITY

Source data is provided as a source data file under accession code:
https://doi.org/10.5281/zenodo.10931394.
Source data for each figure are provided with this paper and can be accessed online: *https://www.nature.com/articles/s41467-024-49719-7#Sec27*

CODE AVAILABILITY

All analysis code used for this paper is publicly available under accession code: *https://doi.org/10.5281/zenodo.11190013.*

PEER REVIEW INFORMATION

Nature Communications thanks Brian Smith and the other, anonymous, reviewer(s) for their contribution to the peer review of this work. A peer review file is available: *https://static-content.springer.com/esm/art%3A10.1038%2Fs41467-024-49719 7/MediaObjects/41467_2024_49719_MOESM2_ESM.pdf*

SUPPLEMENTARY INFORMATION

Supporting methods

Widefield calcium imaging

We conducted calcium imaging analysis at a widefield fluorescence microscope (BX51WI, Olympus, Tokyo, Japan), equipped with a 20x water immersion objective (Olympus, UM Plan Fl 20x/0.50W), using an Omicron LED system, equipped with a 470 nm LED (Omicron-Laserage Laserprodukte GmbH, Rodgau-Dudenhofen, Germany) for light excitation with a 410 nm short-pass filter and a 410 nm dichroic mirror. In the emission pathway, the light was filtered through a 440 nm long-pass filter. Images with a spatial resolution of approx. 1.59 px/µm were captured at 10 fps with a sCMOS camera (1024x1024 pixel with 2x2 on-chip binning; Prime BSI Express; Teledyne Photometrics, Tuscon AZ, USA).
Odors were delivered via an automatic multi-sampler for gas chromatography (Combi PAL, CTC Analytics AG, Zwingen, Switzerland), which injected the odor pulse into a continuous flow of 1 mL/s of purified air with a matching injection speed. The stimulus odor was directed via a Teflon tube (inner diameter, 0.87 mm) to the antenna ipsilateral to the imaging site. Leaf extract (*Lvs*) was produced by grinding blackberry leaves in mineral oil. Odor vials were filled with either 0.5 g of colony cotton wool, 0.3 g leaf extract, or 200 µL of cis-3-Hexenyl-acetate (diluted to 10^{-2}, *Laa*) on 0.5 g of pure cotton wool. Mixtures were prepared by combining half the amount of the respective odor dilution, leaf extract, or colony cotton wool.
Data preprocessing followed the same steps as described in the main Methods section, with the only differences in the median filter size (11-by-11 pixels) for spatial filtering, resizing the images to 256-by-256 pixels, the box-shaped kernel size (11 frames) for temporal filtering, and baseline length (20 frames) for calculating relative fluorescence changes ($\Delta F/F_0 = (F-F_0)/F_0$).

Electroantennography (EAG) recordings

We conducted EAG recordings to measure the voltage fluctuations between the tip and the base of antennae from gregarious and solitarious animals, elicited in response to a social olfactory stimulus (the smell of the colony, *Lct*), a food-related stimulus (leaf alcohol acetate, *Laa*), and their mixture (*LaaLct*; same stimuli and their preparation as described in the main text for functional confocal microscopy). In preparation for the EAG experiments, we inserted the base and the tip of a freshly dissected antenna into glass capillaries (1.2 mm OD x 0.69 mm

ID, Harvard Apparatus, Holliston, MA, United States) filled with locust saline (9.82 g/L NaCl; 0.48 g/L KCl; 0.73 g/L $MgCl_2$*6H_20; 0.47 g/L $CaCl_2$*$6H_2O$; 0.95 g/L NaH_2P0_4*$2H_2O$; 0.18 g/L *$NaHCO_3$*; pH of 7.2 with *NaOH*; after: Mordue and Goldsworthy (1969)), connected to electrode holders. The tip electrode and base electrode were connected to an Axon Instruments CV-7B headstage, and voltage deflections were amplified using a MultiClamp 700B Microelectrode Amplifier (Molecular Devices, Sunnyvale, CA, United States) with respective MultiClamp 700B Commander software. We recorded the data at 25 KHz with a Micro1401 A/D converter and Spike2 data acquisition software (v7.01, Cambridge Electronic Design, Cambridge, UK), as illustrated in suppl. Fig. 3a. Baseline drift was accounted for by online or offline high-pass filtering (cutoff frequency of 3 Hz) followed by offline low-pass filtering (100 Hz) of the signal (suppl. Fig. S3b).

Using the same custom-built olfactometer as for the functional confocal microscopy experiments (see main text for details; Raiser *et al.* (2017) (Raiser et al., 2017)), we delivered each stimulus as three consecutive, 2-second-long odor pulses with an inter-pulse interval of 10 s. Stimuli were presented in a pseudo-random.

For each of the three repetitions, we used two-second long pre- and post-stimulus intervals and normalized the data to the minimum (i.e., most extreme) value in the respective response to *Laa* (e.g., first repetition to *Lct* was normalized with the first repetition to *Laa*). Next, we averaged the repetitions to the same stimulus before normalizing to *Laa* again to account for subtle differences between repetitions. Consequently, the relative response magnitude was measured as the minimum value during stimulus presentation, with values less negative than -1 indicating weaker responses and values more negative than -1 indicating stronger responses compared to *Laa*.

For statistical inference, we used bootstrap randomization tests with $B = 10^7$ samples and a one-sample, two-tailed test statistic (suppl. Eqn. S1). To test a sample with mean $\bar{z}$, standard deviation σ_z, and sample size *n* against a pre-determined value μ_o (-1 in our case) we drew samples from the empirical distribution $\bar{z}_i = z_i - \bar{z} + \mu_0$ with $i = 1,...,n$ (see main text for details on bootstrap randomization tests). We used the same test statistic as denoted in the main text for unpaired, two-sample, two-tailed tests, comparing gregarious with solitarious data (Eqn. [5).

$$\boldsymbol{T_{one-sample}} = \frac{|\bar{\boldsymbol{z}} - \boldsymbol{\mu_0}|}{\boldsymbol{\sigma_z/n}} \qquad \text{(S1)}$$

Temporal evolution of odor responses in principal component space

Projecting response patterns of neuronal ensembles into a common space can offer more insight into the evolution of temporal patterns. To this end, we concatenated the data of all cell bodies from all gregarious and solitarious animals to project them into principal component (PC) space (based on singular value decomposition), obtaining a single coefficient and a single score matrix for our dataset. Using the matching columns of the coefficient matrix, we then projected each animal's data into PC-space. This allowed us to calculate the grand mean (mean of animal means) trajectories for gregarious and solitarious animals, respectively. Moreover, we used the score matrix to estimate the effect of the first PC. For this, we projected the data back: once using the full coefficient and score matrices, and once excluding the first principal component.

Supporting figures

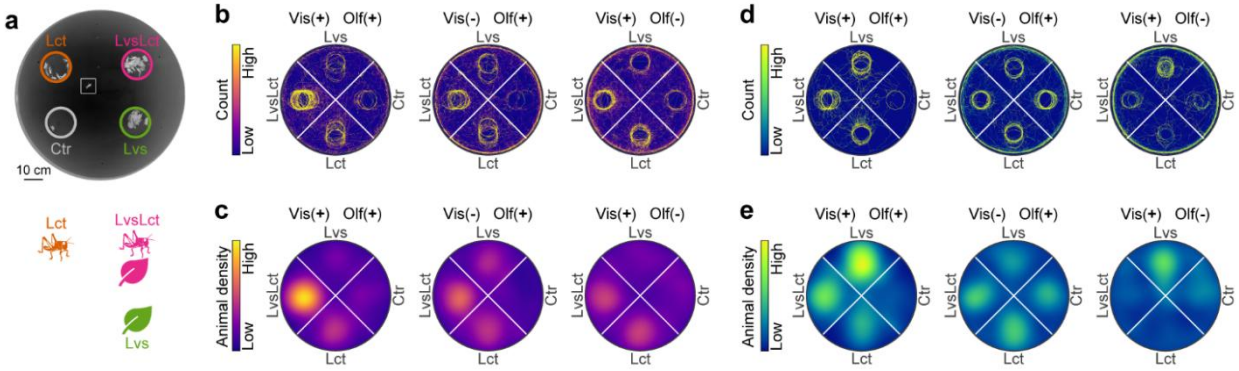

suppl. Fig. S1 – Details on patch selection experiments. (a) Animals were tested in a circular arena with four patch options (blackberry leaves *Lvs*, locusts *Lct*, leaves and locusts *LvsLct*, and control *Ctr*) under one out of three conditions (visual and olfactory cues available: *Vis*(+)*Olf*(+); olfactory but no visual cues: *Vis*(-)*Olf*(+); visual but no olfactory cues: *Vis*(+)*Olf*(-)). Shown is a color-inverted, exemplary frame from testing a gregarious animal. The superimposed circles indicate the four patches, and the square shows the location of the locust. The animal was tested with both visual and olfactory cues available. (b) Bivariate histograms with 1000-by-1000 equally spaced bins were used to pool the 2-D trajectories of all tested gregarious animals (*Vis*(+)*Olf*(+): $n = 26$; *Vis*(-)*Olf*(+): $n = 26$; *Vis*(+)*Olf*(-): $n = 28$). (c) Bivariate histograms from b were used for estimating animal density in each stimulus quarter (same as in Fig. 1). (d-e) As in b-c, but for solitarious animals (*Vis*(+)*Olf*(+): $n = 25$; *Vis*(-)*Olf*(+): $n = 32$; *Vis*(+)*Olf*(-): $n = 25$).

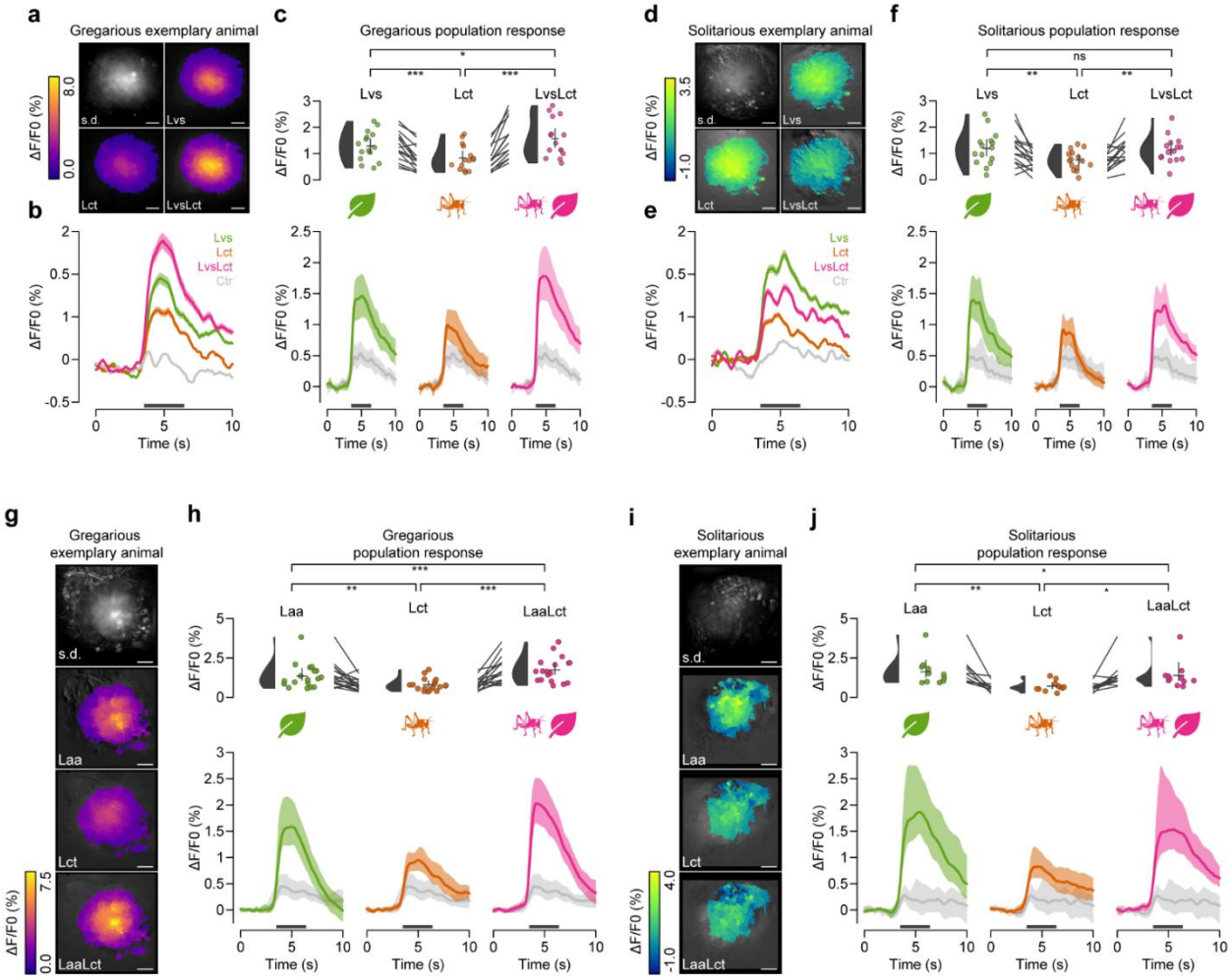

suppl. Fig. S2 – Functional widefield imaging of the antennal lobe representation of the odor cues used in patch choice experiments. (a) Widefield calcium imaging data following the presentation of the olfactory stimuli used in the patch selection assay (blackberry leave extract: *Lvs*, locust odor *Lct*, and their combination *LvsLct*). The grayscale heatmap shows the standard deviation projection across all stimuli of an exemplary gregarious animal, alongside the mean intensity projection after olfactory stimulation during the window of activity (see b). (b) Average activity time courses (mean across all active regions with shaded 95% confidence intervals) of the exemplary animal shown in a for each stimulus (air control in light gray). (c) Average activity time courses of all $n = 15$ gregarious animals (grand means with shaded 95% confidence intervals, bottom panels) and respective swarm plots of the individual animal means during the window of activity (dark gray bars) above, with half-violin plots for probability density estimates, and crosses for grand means and 95% confidence intervals ($p_{(Lvs/LvsLct)} = 0.0217$, $p_{(Lvs/Lct)} = 1.7022*10^{-4}$, $p_{(Lct/LvsLct)} = 8.28*10^{-6}$). (d-f) Same as a-c, but for $n = 15$ solitarious animals with $p_{(Lvs/LvsLct)}>0.99$, $p_{(Lvs/Lct)} = 0.0067$, and $p_{(Lct/LvsLct)} = 0.0093$. (g) Same as in a, but for leaf alcohol acetate (*Laa*, cis-3-Hexenyl Acetate) instead of *Lvs*, as *Laa* could be identified as a dominant volatile in blackberry leaves (cf. Fig. 2e). (h) Same as in c, but for leaf alcohol acetate and $n = 18$ gregarious animals ($p_{(Laa/LaaLct)} = 5.481*10^{-4}$, $p_{(Laa/Lct)} = 0.0094$, $p_{(Lct/LaaLct)} = 3.774*10^{-5}$). (i-j) Same as g-h, but for $n = 11$ solitarious animals ($p_{(Laa/LaaLct)} = 0.0284$, $p_{(Laa/Lct)} = 0.0027$, $p_{(Lct/LaaLct)} = 0.0431$). Statistical inference in c, f, h, and j was based on paired two-sample two-tailed bootstrap randomization tests with Bonferroni correction accounting for multiple comparisons (ns: not significant; $p<0.05$: *; $p<0.01$: **; $p<0.001$: ***). Source data are provided as a Source Data file.

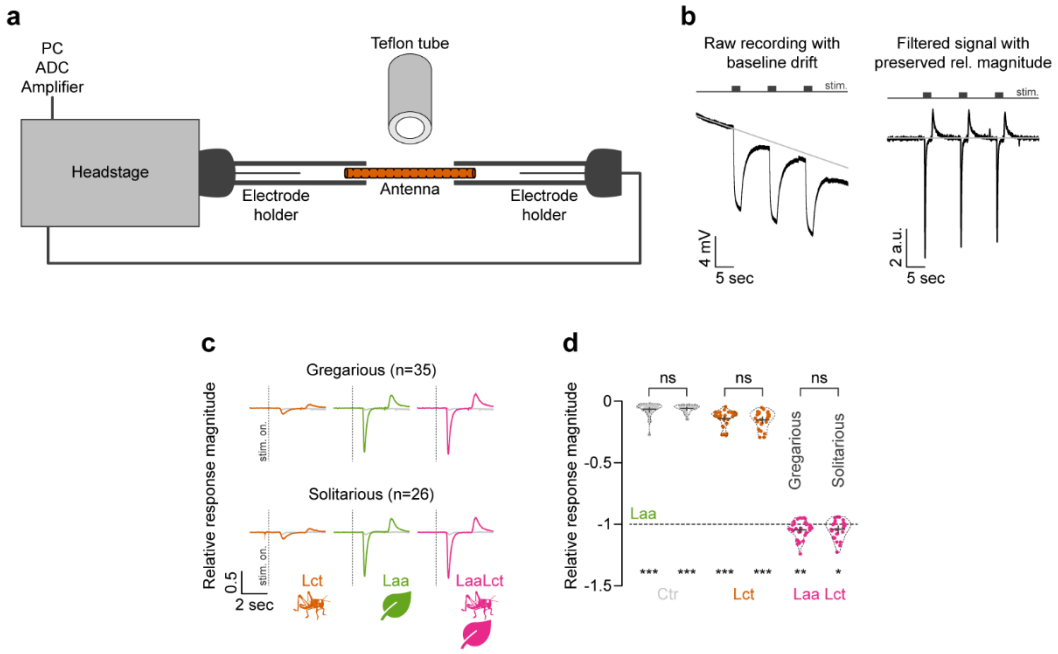

suppl. Fig. S3 – Electroantennogram (EAG) analysis of the odor cues used in patch choice experiments. (a) Schematic illustration of the EAG setup used to record voltage fluctuations along a locust antenna. (b) EAG recordings can be affected by drifting baselines that may complicate an exact calculation of response magnitudes. For this reason, we filtered the signal (3 Hz and 100 Hz cutoff frequencies for high-pass and low-pass filtering, respectively), preserving the relative differences between responses while accounting for the drift. This is exemplified by a raw recording from a gregarious antenna. (c) Average activity time courses of all gregarious (top row; $n = 35$) and solitarious (bottom row; $n = 26$) antennae in response to stimulation with leaf alcohol acetate *Laa*, the locust odor *Lct*, and their combination *LaaLct*. Responses to the solvent are shown as light gray time courses. Stimulus onset is indicated by vertical dotted lines. (d) Response magnitudes for all antennae are shown as swarm plots (pairwise for each stimulus, with gregarious on the left and solitarious on the right; same color code as in c). Responses were normalized to *Laa* (dotted horizontal line). Statistical inference in d was based on one-sample two-tailed bootstrap randomization tests to test whether values are different from *Laa*, and unpaired two-sample two-tailed bootstrap randomization tests to compare gregarious with solitarious responses (ns: not significant; $p<0.05$: *; $p<0.01$: **; $p<0.001$: *** with $p_{(Ctr)} = 0.5399$, $p_{(Lct)} = 0.5219$, and $p_{(LaaLct)} = 0.7656$). Source data are provided as a Source Data file.

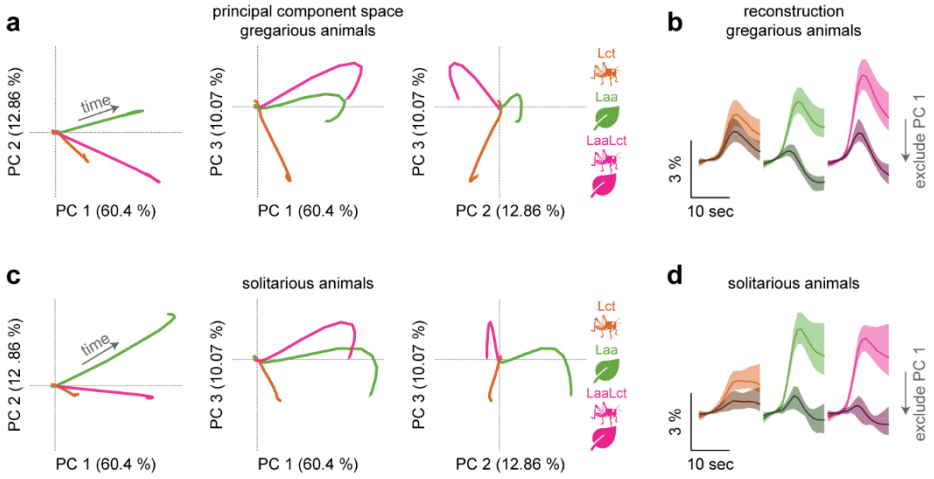

suppl. Fig. S4 – Principal component trajectories of temporally evolving odor response patterns differ between stimuli. (a) Trajectories of gregarious (top row; $n = 28$) and solitarious (bottom row; $n = 19$) animals, projected into principal component space, of odor-induced responses in projection neuron cell bodies to the locust odor *Lct* (orange), leaf alcohol acetate *Laa* (green), and their combination *LaaLct* (magenta). (b) Reconstruction of the original signals, either based on all principal components (light shades) or all but the first (dark shades). (c-d) Same as a-b, but for solitarious animals. Source data are provided as a Source Data file.

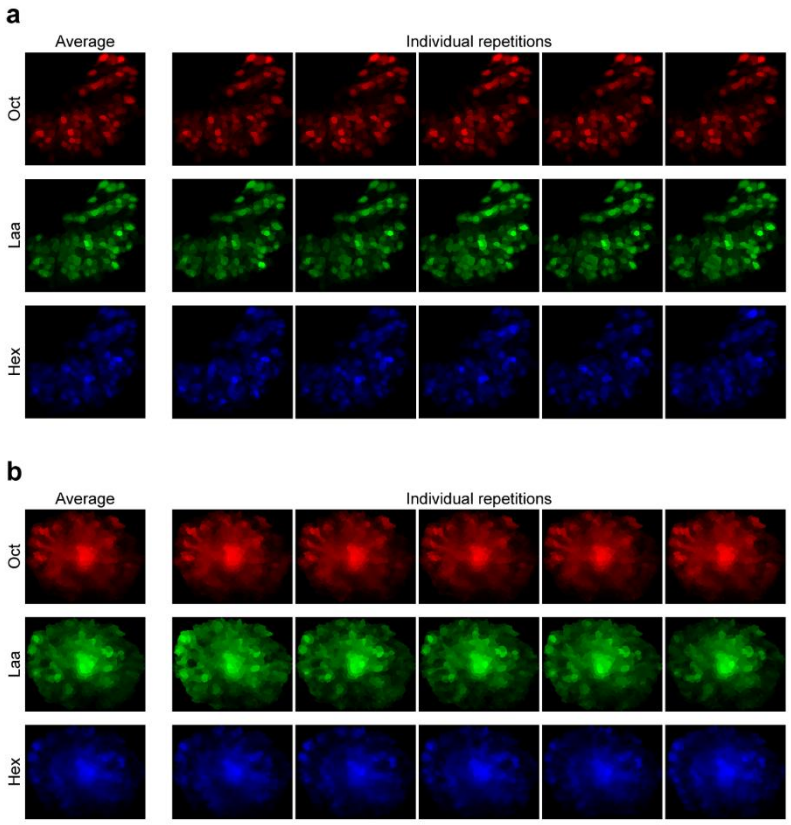

suppl. Fig. S5 – Details on response consistencies. Individual trials of the example animals in Fig. 4a-b. Shown are odor-based color-coded standard deviation intensity projections of projection neuron cell bodies (a) and glomeruli (b) to repeated presentations of the odorants 1-Octanol *Oct*, leaf alcohol acetate *Laa*, and 1-Hexanol *Hex*. The left panels show average responses (as in Fig. 4) with the individual repetitions beside them.

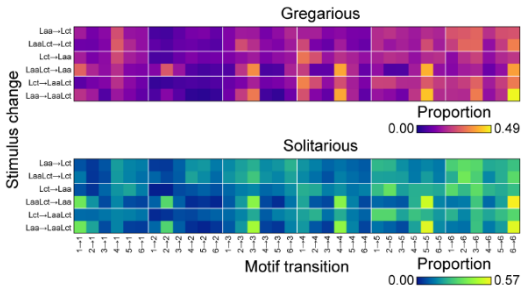

suppl. Fig. S6 – Response motif transition probabilities. Visualization of the transition probabilities between response motifs used for phenotype classifications in Fig. 5. Color codes for the proportion of cell bodies undergoing transitions between motifs (columns) across two stimulations (rows). Data for gregarious animals are in the top panel, with solitarious response transition probabilities below.

Supporting tables

suppl. Tbl. S1 – Average proportion (grand mean [95% confidence interval]) of PNs responding in functional confocal laser scanning microscopy for the logical relationship between stimuli.

Sets	cell bodies (greg.)	cell bodies (soli.)	glomeruli (greg.)	glomeruli (soli.)
Laa only	0.07 [0.05,0.11]	0.09 [0.07,0.13]	0.06 [0.04,0.11]	0.23 [0.11,0.48]
Lct only	0.13 [0.11,0.15]	0.15 [0.12,0.19]	0.08 [0.04,0.15]	0.14 [0.08,0.23]
LaaLct only	0.11 [0.08,0.15]	0.06 [0.04,0.12]	0.12 [0.08,0.18]	0.05 [0.02,0.08]
Laa & Lct	0.06 [0.05,0.09]	0.06 [0.05,0.08]	0.03 [0.02,0.06]	0.04 [0.02,0.05]
Laa & LaaLct	0.19 [0.16,0.23]	0.26 [0.22,0.31]	0.31 [0.20,0.42]	0.19 [0.13,0.26]
Lct & LaaLct	0.13 [0.11,0.15]	0.07 [0.05,0.09]	0.11 [0.06,0.22]	0.05 [0.02,0.10]
all	0.32 [0.27,0.40]	0.31 [0.26,0.35]	0.29 [0.22,0.38]	0.31 [0.21,0.39]

suppl. Tbl. S2 – Details on the prevalence of triplet combinations. We calculated how many times more a given motif triplet occurred than chance level (gregarious: 34.33; solitarious: 23.61) for both locust phenotypes. We report the 12 triplet combinations with the largest absolute difference between gregarious and solitarious animals, matching the Bliss interaction score time courses in Fig. 5f. A value of 1 indicates that the triplet occurred as many times as expected by chance.

motif triplet	greg.	soli.	abs. diff.
2|5|5	1.49	6.23	4.74
1|4|4	6.17	2.67	3.51
1|1|6	3	0.38	2.62
1|1|4	3.23	0.8	2.43
6|3|3	3.12	5.34	2.22
3|6|3	1.31	3.47	2.16
2|4|4	2.1	4.07	1.97
2|4|5	0.96	2.92	1.96
3|6|6	5.01	6.86	1.85
6|4|5	2.97	1.23	1.74
2|6|6	1.49	3.22	1.73
6|6|3	1.51	3.18	1.66

CHAPTER 3

THE BEHAVIORAL MECHANISMS GOVERNING COLLECTIVE MOTION IN SWARMING LOCUSTS

Sercan Sayin, Einat Couzin-Fuchs, Inga Petelski, Yannick Günzel, Mohammad Salahshour, Chi-Yu Lee, Jacob M. Graving, Liang Li, Oliver Deussen, Gregory A. Sword, Iain D. Couzin

Science 2025

CHAPTER SUMMARY

Chapter 3 shifts focus from socially modulated olfactory coding of solitarious versus gregarious locusts and its behavioral implications amidst small, uncoordinated groups of conspecifics to the collective dynamics of individuals within immense swarms to examine the cognitive mechanisms and sensory basis underlying the synchronized large-scale motion of gregarious animals. Once more, the initial flash of inspiration for this work came from field studies in Kenya during the major locust outbreak in 2020, where we witnessed the perfect coordination of migrating juvenile gregarious locusts, with vision occurring as the decisive sensory modality. Between 2019 and 2020, Kenya suffered from the worst locust infestations in over 70 years, affecting at least 70000 ha land. We recorded that hopper marching direction could not be linked to topography, sun position or prevailing weather conditions. However, we observed that juvenile hoppers flexibly responded to their social and asocial environment, split up into small, well-aligned, marching subgroups or shifted between tight coordination and dispersed motion.

Collective, ordered motion of animal groups of all kinds had thus far been described by optomotor response, an escape-pursuit system or other rigid, rule-based self-propelled particle models. The latter assumes that animals, just like particles in liquids, ram each other and, through this tactile interaction, finally face the same direction. However, classical models are based on a critical minimum density, enabling uncorrelated fluctuations to be cancelled out for 'flow' to emerge.

To uncover the sensory mechanisms involved in group organization, we deprived marching locusts in the field of olfaction, vision and polarized vision, respectively. As a result, we clearly

identified vision as the pivotal sensory modality, which is necessary and sufficient to maintain collective movement. In a next step, our lab colleagues took over the research and extended our field work using an immersive virtual reality (VR) setup. VR enables the precise manipulation and control of virtual conspecifics, a feature perfectly suited to test these long-hold beliefs about collective motion. Freely moving focal individuals emerged into virtual swarms of varying size and alignment levels. VR experiments and the careful re-evaluation of a marching experiment in another study, which corroborated the classical model, inferred that group order does not depend on the number of conspecifics, but their conformity, hence, the degree or quality of coherent alignment of fellow locusts. Moreover, while gregarious animals in the VR setup exhibited optomotor responses to moving dot stimuli simulating optic flow, these reflexes could not explain collective order, as they were also displayed by solitarious animals, which failed to engage in coordinated marching along with their virtual conspecifics. Those findings were complemented with additional VR and arena-based experiments, revealing a pulling effect on focal gregarious animals during marching, which was exerted by conspecifics in the front. Also, contrary to classic models' predictions, animals in the VR decided to join one swarm when placed directly between two identical ones and, in another experiment, turned towards one virtual conspecific when two were presented at a specific lateral distance ahead.

With none of the results aligning with the predictions made by the classical models, those investigations clearly contradict the prevailing theories about the emergence and maintenance of collective group motion and thereby challenge the foundational assumptions about collective locust behavior. It follows from those findings, that locusts might actively evaluate social information and make context-dependent decisions using a neuronal ring-attractor network. Such a visual network lets the individual under focus dynamically encode its own orientation and bearing relative to neighboring, external objects, which are projected as excitatory or inhibitory neural bumps that compete against each other, ultimately leading to a consensus. Also, this study calls for follow-up experiments to find out how these mechanisms scale across different species, ecological contexts, or developmental stages, and how the suggested underlying neuronal wiring scheme supports this visually guided group coordination.

Science. 2025 Feb 28;387(6737):995-1000. doi: 10.1126/science.adq7832. Epub 2025 Feb 27.

The behavioral mechanisms governing collective motion in swarming locusts

Sercan Sayin [1 2 3], Einat Couzin-Fuchs [1 2 3], Inga Petelski [1 2 3], Yannick Günzel [1 2 3], Mohammad Salahshour [1 2 3], Chi-Yu Lee [1 3], Jacob M Graving [1 2 3 4], Liang Li [1 2 3], Oliver Deussen [1 5], Gregory A Sword [6], Iain D Couzin [1 2 3]

Affiliations + expand

PMID: 40014712 DOI: 10.1126/science.adq7832

ABSTRACT

Collective motion, which is ubiquitous in nature, has traditionally been explained by "self-propelled particle" models from theoretical physics. Here we show, through field, lab, and virtual reality experimentation, that classical models of collective behavior cannot account for how collective motion emerges in marching desert locusts, whose swarms affect the livelihood of millions. In contrast to assumptions made by these models, locusts do not explicitly align with neighbors. While individuals respond to moving-dot stimuli through the optomotor response, this innate behavior does not mediate social response to neighbors. Instead, locust marching behavior, across scales, can be explained by a minimal cognitive framework, which incorporates individuals' neural representation of bearings to neighbors and internal consensus dynamics for making directional choices. Our findings challenge long-held beliefs about how order can emerge from disorder in animal collectives.

INTRODUCTION

Theoretical models from physics, such as the highly influential Vicsek model (Vicsek et al., 1995), describe how simple local interactions, where individuals align their movement with nearby individuals, can generate large-scale, coordinated (meaning aligned or ordered) motion in groups. This model makes the prediction that groups should exhibit a spontaneous transition between two collective states – from a disordered state (akin to a gas) to an ordered state (akin to a driven fluid) – as density increases. This concept has implications for understanding collective behavior across biological systems, from cellular aggregates to human crowds.

The results of empirical studies, including experiments with juvenile desert locusts (*Schistocerca gregaria*), have lent support to this theory. Locust swarms, which can cover vast areas and greatly impact food security (Steedman, 1988), serve as a prominent example of collective motion. Laboratory findings have suggested that increasing locust density in a ring-shaped arena leads to a shift from disordered to ordered motion, appearing to validate the predicted density-dependent phase transition (Buhl et al., 2006) . Thus, despite inherent errors in individual alignment, a sufficient density of individuals is argued to enable an averaging out of noise and the emergence of coherent group movement. In general, comparison of model predictions and empirically observed collective motion has provided evidence supporting these "classical" models of collective behavior (Becco et al., 2006; Buhl et al., 2006, 2012; Lukeman et al., 2010; Mann et al., 2013; Sumpter et al., 2012).

There exists an inherent problem with this approach, however. Given that density and order are positively correlated, it is challenging to establish cause and effect. This raises the question of whether alignment results from the averaging out of uncorrelated errors at high densities, as classical theory suggests, or whether the coherence of motion itself triggers alignment, independent of density. That is, is it the density (corresponding to the "amount" of information) or the order (the "quality" of information) that is predominantly important or rather how the two interact? Furthermore, do individuals explicitly align their direction of travel with near neighbors, as is assumed in these classic models? Addressing these questions is crucial not only for understanding the fundamentals of biological collective motion but also for gaining insights into the formation and maintenance of locust swarms, which affect human wellbeing (Steedman, 1988). Using a combination of field experiments with naturally occurring locust swarms and analysis of how visual interactions are mediated using immersive virtual reality (VR) (Sridhar et al., 2021; Stowers et al., 2017), we reveal that classical models of collective behavior [such as the Vicsek model and Couzin model (Couzin et al., 2002, 2005;

Katz et al., 2011; Vicsek et al., 1995)] cannot account for collective motion exhibited by locusts and that the mechanism proposed for the emergence of their collective motion needs to be corrected. We demonstrate that locusts do not explicitly align with neighbors and that their behavior is consistent with a minimal cognitive model of spatiotemporal decision-making. We argue for an approach to the study of collective behavior that moves from descriptive to generative models, with the latter taking into account that organisms are not self-propelled particles but rather probabilistic decision-making entities that base their decisions explicitly on the representation and integration of sensory information.

RESULTS

Field experiments

The largest East African outbreak of the desert locust in recent years began in late 2019. In February 2020, we conducted experiments on large "marching bands" of flightless juvenile locusts in the Samburu and Isiolo counties of Kenya to establish the predominant sensory modalities used in coordinating motion. Swarms of locust nymphs were encountered at a large number of locations, ranging from first to sixth instar (juvenile) stages (Fig. 1, A and B). In 56 cases where we recorded marching band directions, a prominence along the north/northeast axis was noted (Fig. 1B and suppl. Tbl. S1). Consistent with previous studies (Ellis & Ashall, 1957), marching direction did not clearly relate to immediate weather conditions, elevation, or sun position (suppl. Fig. S1).

To assess the role of different modalities used by focal locusts in maintaining coordinated group movement, we independently manipulated olfaction (by clipping antennae), polarized vision (by painting ocelli and the dorsal rim area of the compound eyes), and vision (by painting ocelli and the entirety of the compound eyes). Control insects were similarly handled but left with their senses intact. All insects were painted with an identifiable color marking on their pronotum before being returned to an undisturbed section of the marching band.

Reintroduced control locusts, anosmic locusts, and locusts deprived of polarized vision exhibited a strong, and rapid, tendency to march with, and in the direction of, conspecifics in the band (Fig. 1C, i, ii, and iii, respectively). Completely blinded insects, by contrast, moved in random directions with respect to the band direction (Fig. 1C, iv, and E). Although these blinded individuals remained mobile – likely owing to tactile cues that increase movement probability to avoid cannibalistic interactions (Bazazi et al., 2008; Chang et al., 2023; Simpson et al., 2006) – in many cases, contact alone did not provide directional guidance, even in

densely packed, highly directional swarms. Thus, we conclude that vision is both necessary and sufficient for individuals to coordinate motion with neighbors.

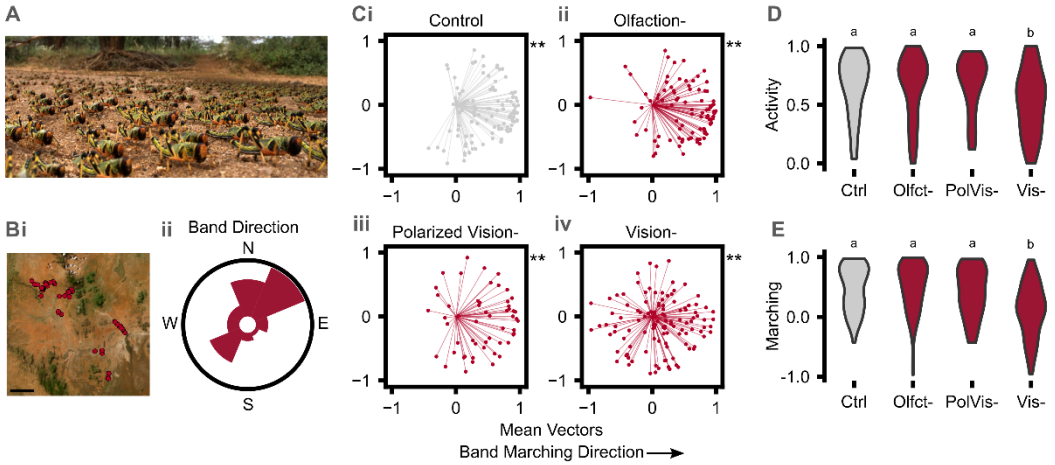

Fig. 1 – Sensory deprivation experiments in the field. (A) A marching band of *S. gregaria* photographed in Kenya in 2020. (B) (i) Locust bands in a total of 112 locales between 27 February and 12 March of 2020 in the Samburu and Isiolo districts of Kenya. Scale bar: 15 km. (ii) Observed marching band directions. n = 56 bands. Histogram counts: min = 2, max = 23. (C) Single tagged locusts were reintroduced to a marching band after antennectomy (Olfaction−, n = 89) or visual occlusion (Polarized Vision−: dorsal eyes and ocelli, n = 54; Vision−: complete eyes and ocelli, n = 114). Control n = 110. Locust movements were reported as mean vectors. Statistical annotations on each upper right corner stand for the results of Rayleigh test for nonuniformity. (D and E) Mean binarized Euclidean distance (Activity) and mean vector magnitude in congruence with marching band (Marching) by control and treated animals. Olfct, olfaction; PolVis, polarized vision; Vis, vision. See suppl. Tbl. S2 for statistical summaries.

Virtual Reality (VR) experiments

As noted above, there has been a confound in previous approaches to establish the mechanism by which locusts regulate their behavior in swarms because of the inherent (theoretical) positive correlation between density and order. To decouple these two factors, we enabled real locusts to interact with virtual conspecifics. Notably, our system was fully panoramic, allowing untethered, freely moving locusts to interact with visual stimuli from fully volumetric three dimensional ("holographic") marching conspecifics with no constraints resulting from boundaries (Fig. 2, A and B).

In order to conduct a full parametric scan of density-order space, we considered independent combinations of density, from 1 to 64 locusts per m2, and order (from 0, equivalent to randomly moving individuals, to 1, where virtual conspecifics are in perfect alignment with one another) (Fig. 2, C and D). We note that our upper and lower insect densities exceed the range tested (2 to 62 moving locusts per m2) by Buhl *et al.* (2006).

Locusts' alignment with the virtual swarm was found to strongly depend on the order parameter, that is, the "quality" of information presented, with no significant dependency on density (Fig. 2, E to G, and suppl. Fig. S4A). With higher order, focal locusts marched longer distances in more-directed trajectories (max: 46.1 m; suppl. Figs. S3 and S4A, i and ii).We note that the cumulative distances covered by focal insects were comparable between different order and density conditions (suppl. Fig. S4A, iii). Clearly, if no directional cues are present, locusts have no social context on which to base their movements, but we find that even with very sparse but high-quality (i.e., ordered) information, they exhibit a strong tendency to align with the motion of others. Notably, while these results are apparently in contradiction to the data of Buhl *et al.* (2006) (Buhl et al., 2006), a reevaluation of their data, taking into account statistical effects associated with different group sizes, reveals that collective alignment (order) is also independent of locust density in these experiments (suppl. Fig. S6).

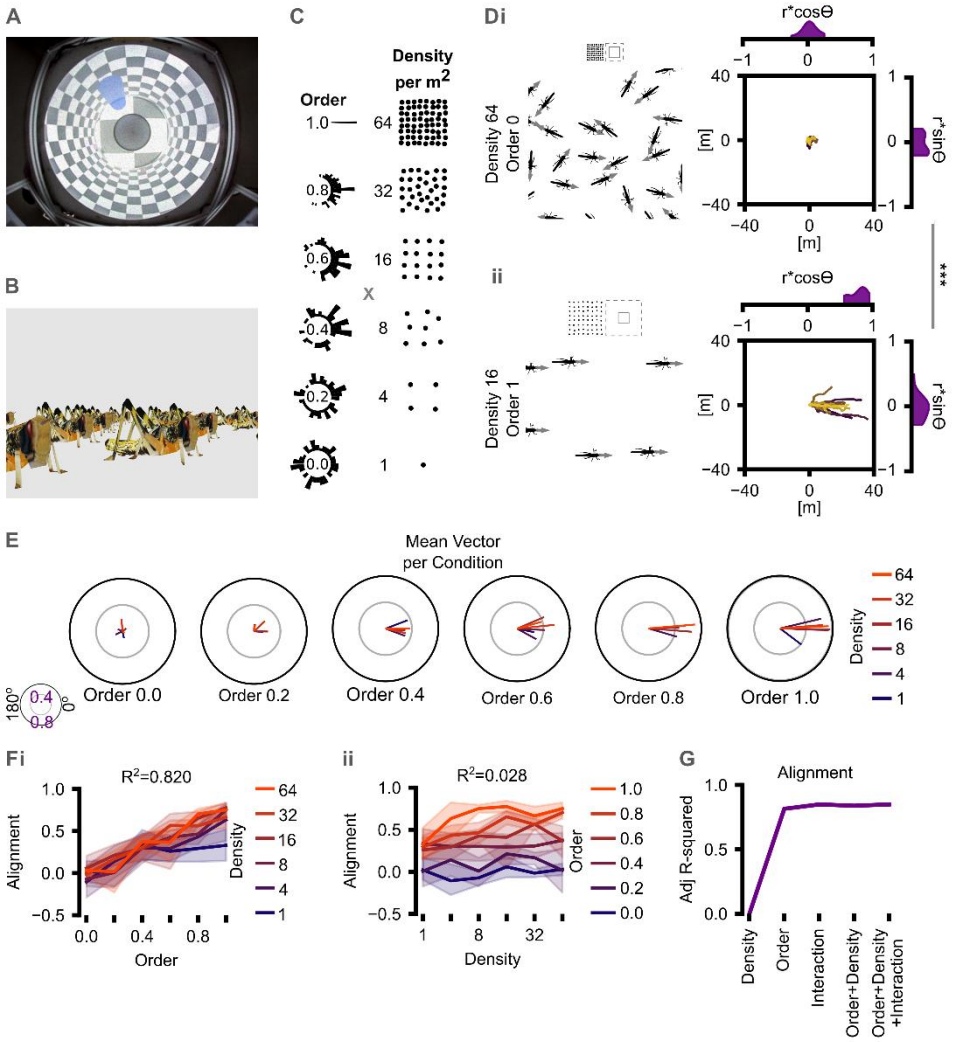

Fig. 2 – Reconstructing marching in an immersive virtual reality. (A) Top-down view of the virtual reality system. A motion compensation system stabilizes an untethered fifth instar desert locust in position, and from this perspective, a panoramic virtual world is projected in 100-Hz high refresh rate. (B) Virtual marching band. The virtual reality engine draws animated juvenile desert locust visual stimuli with real-world kinematics data (suppl. Fig. S2) and constant velocity. Throughout an experiment, periodic boundaries set for virtual band guarantee that the experimental focal juvenile locust is located at the virtual band's center. (C) Experimental design. Virtual bands were generated to vary by two parameters, order and marching band density per square meter. For a given order value, von Mises distributions constituted a marching band's coherence de novo. Focal locusts were tested once for one condition per 20 min. Completed trials equaled 421 once outliers were removed. See the Methods section of the supplementary materials for details of the experimental design and the analysis pipeline. (D) Exemplary order and density combinations. Schematics depict virtual locust positions and directions at a given time. Above each schematic, periodic boundaries and zoomed areas are drawn with dashed and solid lines, respectively. All bands consist of 64 virtual locusts. Individual trajectories per condition are shown on the right. n = 13 for both groups. Mean vector (r) projections onto axes congruent with (r*cosq) and perpendicular to (r*sinq) marching band directions were used for multivariate analyses. To see all trajectories, refer to suppl. Fig. S3. (E) Means per each condition of 64 order and density combinations. (F) Alignment (calculated as r*cosq) versus order (i) and density (ii) as primary parameters for reporting. Color codes designate secondary parameter. Coefficient of determination (R2) scores showcase explanatory power of respective primary parameters alone. See comparison of directedness, marching, and Euclidean distances with respect to either density or order "alone" in suppl. Fig. S4. See suppl. Fig. S5 for clustering of all data groups. (G) Adjusted R2 from ordinary least squares regression models on alignment group means for different explanatory variables used. See suppl. Tbl. S2 for statistical summaries.

Behavioral response to optical flow

It has long been considered that coherent motion in animal groups may be mediated by the optomotor response. If animals, such as insects or fish, are presented with coherently moving dots or stripes, they will tend to move in the direction of the resulting optical flow stimulus. Being an innate and robust behavior, optical flow is often intuitively considered an important if not essential mechanistic basis of collective motion in large mobile groups [see Harpaz et al. and Shaw and Sachs (Harpaz et al., 2021; Shaw & Sachs, 1967) for fish, and Bleichman et al. and Krongauz et al. (Bleichman et al., 2023; Krongauz et al., 2024) for locusts]. Yet, direct evidence in support of this hypothesis is lacking. Recently, Bleichman et al. (Bleichman et al., 2023) presented coherent moving dots on either side of a rigidly tethered locust and demonstrated that the motion could alter the probability of the locust moving. However, the focal locusts in this study were constrained to only be fully aligned with the stimuli and could not alter their direction in response to stimuli.

We assessed whether locusts are sensitive to optical flow under conditions where they could freely move with respect to the presented cue. In evaluating this, we took advantage of the fact that locusts exhibit extreme phenotypic plasticity, including in social behavior. If reared in isolation, locusts are sedentary insects that avoid conspecifics, a phenotype that is referred to as “solitarious” (Pener & Simpson, 2009; Pflüger & Bräunig, 2021; Rogers et al., 2014). It is only when they are reared together that they become “gregarious” and exhibit increased activity and attraction to other locusts (Pener & Simpson, 2009; Pflüger & Bräunig, 2021; Rogers et al., 2014). Should optomotor response to optical flow cues underlie the alignment among individuals in swarms, we may expect that gregarious locusts would be more responsive to such cues than are solitarious insects.

We find that this is not the case. Both solitarious and gregarious locusts exhibit a similar propensity to turn in the direction of the widefield moving-dot stimulus, with solitarious insects exhibiting a slightly stronger response (Fig. 3A). However, when placed in a coherently moving virtual swarm, solitarious insects do not align their direction of travel with the virtual conspecifics (Fig. 3B), whereas gregarious individuals strongly do so (Figs. 2 and 3B). These results are inconsistent with the view that the optomotor response is involved in regulating social interactions in marching locusts.

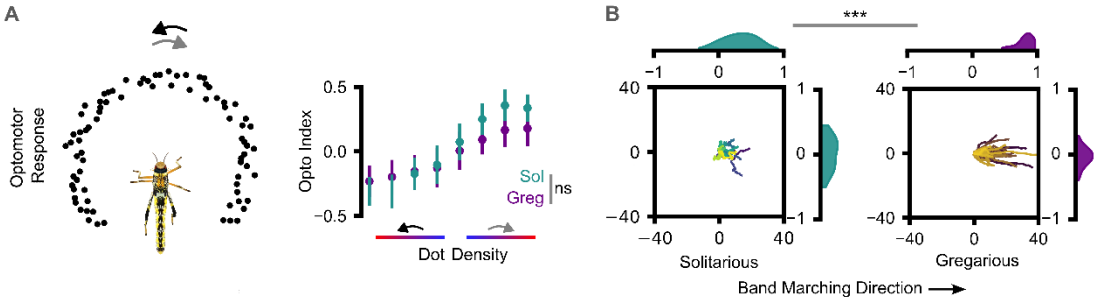

Fig. 3 – Optical flow does not drive marching. (A) (Left) The moving-dot paradigm schematic used in the study. (Right) Optomotor responses of solitarious (Sol) and gregarious (Greg) desert locusts to moving-dot stimuli of different densities, color coded blue to red for low to high density. All stimuli have 100% coherence, meaning that the moving dots in an experiment move either counterclockwise or clockwise. The optomotor response, or opto-index, is a preference index calculated as the difference between summed absolute counterclockwise and clockwise velocities, then dividing that difference by the sum of these velocities for a given trial. n = 32 locusts tested. Number of dots in the density paradigm was 64, 256, 1024, and 4096. (B) Trajectories for solitarious locusts (n = 34) and gregarious control locusts (n = 32) within a virtual gregarious marching band (order: 1; density: 16). See suppl. Tbl. S2 for statistical summaries.

The role of 'pull' in swarms

Another aspect that classical collective movement models and the optical flow hypothesis do not consider is the frame of reference of focal individuals with respect to the direction of collective movement (Krongauz et al., 2024; Vicsek et al., 1995) . Addressing this, later models, again relying on theoretical physics, speculated whether collective motion can be generated by collisions and escape and pursuit mechanisms (Grossman et al., 2008; Romanczuk et al., 2009). We devised a scenario to test how visual stimuli from receding swarms of virtual insects affect the behavior of focal locusts. In this condition, highly ordered marching bands at a 5-cm offset from focal positions were generated (Fig. 4A). Virtual locusts presented as moving away were sufficient to recapitulate focal locust alignment behavior with comparable distances covered as in the full virtual marching band conditions (Fig. 4B, compare with Fig. 2D, ii). Furthermore, our analysis of neighbor positions for locusts surrounded by conspecifics in a full marching band and in experiments when only one receding virtual locust was present showed that focal individuals closely follow neighbors (Fig. 4, C and D). As a validation of our VR experiments, quantification of locust interactions in an arena experiment with 2000 locusts revealed a similar proximal pursuit mechanism in real-world interactions as well (suppl. Fig. S11). These results show that moving-away conspecifics play a strong "pulling" role in the regulation of marching behavior, consistent with a mechanism involving pursuit.

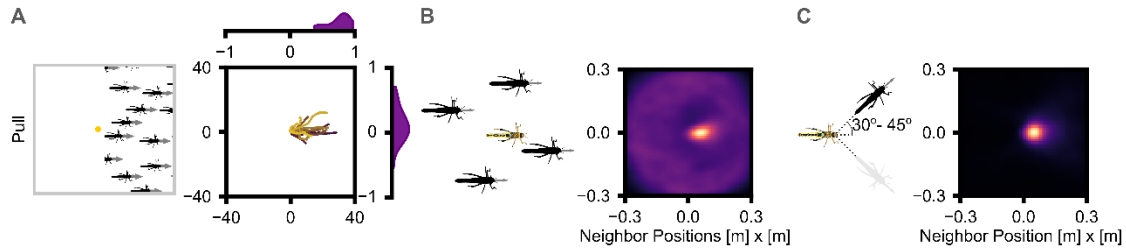

Fig. 4 – Attraction to conspecifics for locust virtual bands. (A) Pull experimental design. A focal locust is positioned immediately behind a highly ordered marching band. n = 21. Periodic boundaries ensured constant distance between focal locust and marching band edge. See suppl. Fig. S7 for "Push" condition. Suppl. Fig. S9 explores roles of order and distance in pull conditions. (B) Density map for egocentric neighbor positions in a highly ordered marching as in Fig. 2D. Focal heading is along +x axis. Focal n = 22. See suppl. Fig. S10 for neighbor-follow duration. (C) Density map for neighbor positions in single virtual locust assay. A single virtual locust, with constant velocity, was positioned in front of focal locust, at 30° to 45° offset. A single trial lasted as long as the distance between follower focal locust and virtual target was maintained within a threshold distance (50 cm). Focal heading is along +x axis. Focal n = 12. Normalized densities are displayed with a color gradient from dark purple for the minimum to bright yellow for the maximum. See suppl. Fig. S10 for neighbor-follow durations.

A vectorial representation of conspecifics

Our above findings show that locusts may not base decisions on simple fixed "rules." An alternative framework considers the generative process by which decisions are made; for example, Sridhar et al. (Sridhar et al., 2021) developed a model of spatial decision-making based on neural principles. Consistent with neurobiological studies of insects (Lyu et al., 2021; Seelig & Jayaraman, 2015) and vertebrates (Sarel et al., 2017), neighbors are considered to induce neural activity bumps on a "ring attractor" network, with their position on the ring reflecting their bearing with respect to the focal animal. Given that neural activity encodes both directional information (bearings) and the "strength" of influence (encoded by the magnitude of neural activity), this is a "vectorial representation" of conspecifics. Ongoing internal dynamics on the ring attractor network, defined predominantly by local excitation and long-range and/or global inhibition, facilitate the integration of these sensory inputs, generating a self-organized bump of activity on the ring (a collective neural consensus mechanism) that represents the animal's subsequent directional preference [for details, see Gorbonos et al., Oscar et al., and Sridhar et al. (Gorbonos et al., 2024; Oscar et al., 2023; Sridhar et al., 2021)]. This type of cognitive model, which we refer to as the vectorial hypothesis, makes directly testable predictions with respect to behavior, and these predictions are in stark contrast to those of the optical flow hypothesis. For example, if presented with two conspecifics moving in the same direction and speed at a fixed lateral distance (L) (Fig. 5A), our model predicts that a follower should occupy, on average, a position directly between them, up to a critical distance

above which there should exist a dynamical bifurcation in the neural dynamics, resulting in a decision to choose to follow one or the other. That is, the brain should suddenly transition between an "averaging" and a "winner takes all" dynamic (Sridhar et al., 2021). The optomotor (optical flow) hypothesis, by contrast, predicts that a focal locust should align with conspecifics irrespective of their lateral distance. In both models, there exists a further, maximal distance at which interactions become impossible owing to insufficient sensory information.

Presenting a pair of marching virtual conspecifics with different lateral distances, we see, as predicted by the vectorial hypothesis (Fig. 5B, i), a clear bifurcation in the relative position adopted by the real locust (Fig. 5B, ii). We note that in conventional laboratory experiments with real interacting insects, it is not possible to conduct such a test of the underlying cognitive mechanism, thus highlighting an advantage of the VR approach for establishing the nature of visual social interactions. A further, complementary experiment to test the mechanistic basis of social interactions is how a focal locust will behave if positioned directly between two coherently marching swarms. In classic models of collective behavior that include attraction, the symmetry of attractive "forces" in one direction and the other would result in them tending to cancel out, and an explicit alignment term, if present, would dominate, resulting in alignment with directional cues (see Supplementary text in the Supplementary materials). Similarly, the optical flow hypothesis would predict motion in alignment with swarm direction. The cognitive model, by contrast, which only considers attraction but captures the competition between conflicting directional information (owing to the presence of long-range inhibition), predicts that in this scenario, locusts should move in a direction perpendicular to the swarm motion. To evaluate these hypotheses, locusts were placed at a fixed equal distance (either 8 or 50 cm) in between two parallel virtual marching bands, both moving in the same direction (Fig. 5C). Here, optical flow is parallel to marching direction (+x axis, as indicated by the blue circle), while vectors representing conspecifics are (approximately) perpendicular (±y axis, as indicated by the orange circles) to the collective movement. For model agents (Fig. 5D) and focal locusts (Fig. 5E and suppl. Fig. S14), movement direction was predominantly directly toward one marching band or the other and not in congruence with optical flow (or with classic self-propelled particle models; see Supplementary text).

Our results suggest that locust marching behavior is mediated by a vectorial encoding strategy and not a strategy that uses explicit alignment. To establish whether individuals utilizing this same mechanism can account for the emergence of long-range coordinated motion in locusts, we also considered the scenario of conspecific representation as (competing) bumps on a neural

ring attractor network (see Supplementary materials for details), revealing that it can account for the emergence of highly ordered collective motion (suppl. Fig. S15).

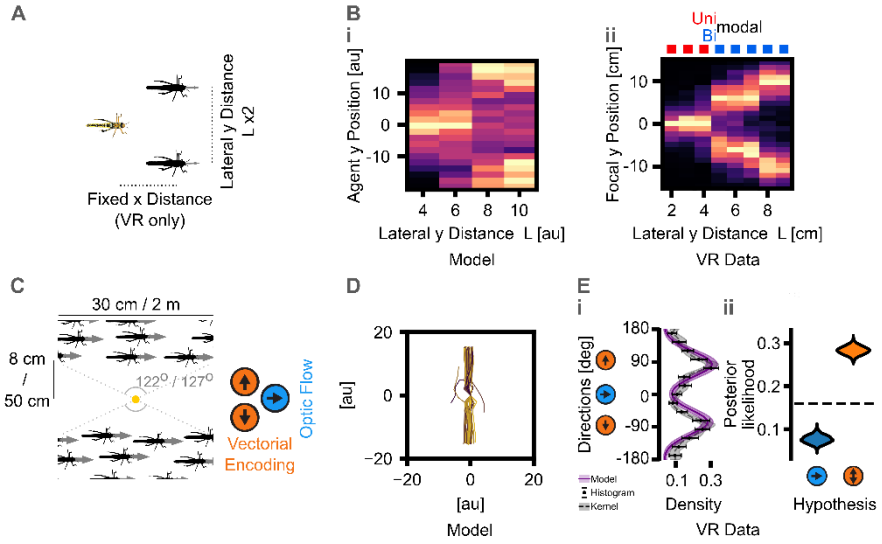

Fig. 5 – Vector computations can explain individuals' response to conspecifics. (A) Schematic of the two conspecific "targets" scenario used in our simulation model and VR experiments. Lateral distance (along y axis) between two targets was set to constant at 2× L. In all VR trials, horizontal distance (along x axis) between focal locust and two targets was fixed. (B) (i) Model agent y positions when a focal agent is presented with two moving targets. au, arbitrary units. See suppl. Fig. S12 for two-dimensional position histograms. n = 200 for all conditions. (ii) Instances in VR where focal locust followed targets depicted as a heatmap as in focal individual's y position versus lateral distance L. Dip test of unimodality is used to assess y position distribution (red: $P > 0.05$; blue: $P < 0.05$). Focal locust n = 11. Histogram range is displayed with a color gradient from dark purple for the minimum to bright yellow for the maximum. (C) Experimental design to evaluate the possible roles of optical flow versus vectorial representation in coordinating marching for VR experiments. At a given fixed lateral distance (8 or 50 cm) to the focal locust, two highly ordered bands move in same direction. Each virtual locust has a 100-ms life span, to preserve optical flow and positional cues but to prevent the focal locust from persistently "locking onto" a single target. (D) Trajectories of simulated agents. Similar to (C), an agent is placed in between two sets of targets moving in the same direction. The initial lateral distance of the agent to targets was 20 au. Trajectories plotted for the first 20 au covered by each agent. n = 100. (E) Hierarchical Bayesian model used to infer predominant movement directions in VR scenarios tested as in (C). (i) The posterior model density compared with nonparametric bootstrapped histogram density and kernel density estimates (see materials and methods for details). Lines and points show the median of the posterior or bootstrap distribution, whereas the bars and bands show the 95% interval (2.5 to 97.5%; n = 4000 samples per density type). (ii) Distributions of posterior likelihood scores for hypothesis testing. n = 4000 samples per hypothesis. Dashed line represents a random walk hypothesis as a uniform likelihood. Suppl. Fig. S14 offers focal locust trajectories for both conditions tested in (C). Tested locusts n = 50. See suppl. Tbl. S2 for statistical summaries.

CONCLUSIONS

Our work suggests that, contrary to previous assertions, classical models of collective motion fail to account for the mechanism by which coherent motion is established and maintained in desert locust swarms. For example, we found no evidence that locusts explicitly align with one another nor that they use the optomotor response to mediate social interactions. Furthermore, both our data and a critical revaluation of those of Buhl et al. (Buhl et al., 2006) find no evidence for a density-dependent transition from disorder to ordered swarm motion, further questioning the dominant paradigm used to study animal collectives more broadly. By contrast, we find that individual and collective locust behavior is consistent with a minimal cognitive model (a ring attractor network) in which individuals (targets) are represented as competing neural bumps. This suggests that widefield optical flow cues (such as those used for self-motion estimation and/or wide-field landscape information) are separate from those cues used in neighbor tracking. Circuits responsible for pursuing neighbors are yet to be described for locusts. Beyond a simple detection of objects against a moving background, vectorial representation and wide-field motion necessitate competition under certain scenarios, and how global information is suppressed is yet to be explored. Revealing these circuits will enable the identification of afferent and modulatory inputs, which will be instrumental to infer causality regarding the forces that govern pursuit and collective motion. Furthermore, given the clear discrepancy between gregarious and solitarious behavior in locusts, we suggest future exploration of differential modulation or developmental regulation of visual attraction and decision-making networks. Our work argues for a refreshed perspective in the study of collective animal behavior that moves beyond the "self-propelled particle" paradigm and considers explicitly the sensory and cognitive mechanisms by which interactions are mediated.

ACKNOWLEDGMENTS

The authors thank student assistants M. C. Karakurt, J. Klein, and Z. Sener for VR data collection; E. Mamonova, H. Kübler, and N. Schwarz for tracking field data; L. Schröder and N. Schwarz for trackball data collection; F. Oberhauser for being an invaluable team member in Kenya; M. Mahmoud for contributing to VR development in its early phases; A. Bahl and K. Slangewal for implementing real-time orientation tracking in VR; and D. S. Calovi for experimental design discussions. J.M.G. thanks J. Bak-Coleman for help with model debugging and M. L. Smith for the use of his GPU. J.M.G. acknowledges support from

NVIDIA Corporation's Academic Hardware Grant Program. We thank C. Buhl and K. Yates for providing Buhl *et al.* (2006) data. We also thank C. Buhl for feedback on the manuscript. We acknowledge the use of ChatGPT, a language model developed by OpenAI, for minor suggestions with respect to the text, equations, software, and figures. Funding: Deutsche Forschungsgemeinschaft (DFG, German Research Foundation) under Germany's Excellence Strategy–EXC 2117-422037984. To E.C.-F.: DFG GZ: CO 1758/5-1. To I.D.C.: the Max Planck Society, the European Union's Horizon 2020 Research and Innovation Programme under Marie Skłodowska-Curie Grant 860949, the DFG Gottfried Wilhelm Leibniz Prize 2022 584/22, the Struktur- und Innovationsfonds für die Forschung of the State of Baden-Württemberg, the PathFinder European Innovation Council Work Programme 101098722, and the Office of Naval Research Grant N0001419-1-2556: To G.A.S.: NSF Biology Integration Institute Program Grant DBI-2021795.

COMPETING INTERESTS

The authors declare that they have no competing interests.

DATA AND MATERIALS AVAILABILITY

The source data and material and the analysis scripts are available in Zenodo.

SUPPLEMENTARY MATERIALS

Materials and methods

Field experiments

Locust encounters in the field were marked with a GPS tracker, Garmin GPS MAP64s. Marching band sizes in terms of area (m^2) were estimated by circumnavigating the invasion area and using the GPS tracker to obtain coordinates.

Elevation differences were calculated from the NASA Shuttle Radar Topography Mission dataset (Farr et al., 2007). Local weather information was retrieved from Historical Weather API (Zippenfenig, 2023) . Sun positions at time of logging were generated using ephemeris calculations based on geographic coordinates.

For sensory deprivation experiments, during their peak marching activity, fifth instar juvenile locusts were captured using a fishing net into a container. At once, focal locusts were treated

and marked on pronotum with acrylic paint to distinguish treatment groups. Treatments included one of the following: clipping antennae with fine dissection scissors to prevent detection of olfactory stimuli, covering the dorsal rim area of the compound eyes and ocelli to prevent detection of polarized light, fully covering both compound eyes and ocelli to remove all visual stimuli. Control locusts were marked and reintroduced to the marching band without further treatment. Locusts were gently and sequentially released into the band.

The scene was recorded from above with a GoPro camera mounted on a tripod. All videos were resampled at 25 fps, at 2704–by-1520 pixels. Marching band directions were extracted by optic flow detection using Farnebäck algorithm at 5 fps (Farnebäck, 2003). Focal trajectories were manually tracked (Günzel et al., 2024). Trajectories and flow maps were then corrected via 2-D projective geometric transformation to account for differences in perspective across videos. The average local optic flow was calculated within a 400-pixel radius around focal locusts, excluding an inner 50-pixel radius to eliminate contributions from the focal locusts' own movement. Frames lacking significant local optic flow, in which focal locusts exited the swarm and were no longer immersed within it, were excluded from further analysis. Focal trajectories were spatially discretized with a minimum step size of 40 pixels.

After normalizing to (the visible) swarm's marching direction at each step, mean vector r was

$$\boldsymbol{r} = \frac{\sqrt{(\sum_{i=1}^{n}\mathbf{cos}(\boldsymbol{\theta})^2 + \sum_{i=1}^{n}\mathbf{sin}(\boldsymbol{\theta})^2)}}{\boldsymbol{n}} \qquad \text{(S1)}$$

where θ represents the normalized focal heading direction per discretized step.

Marching behavior was assessed via the dot product between the mean vector r and the swarm direction. To quantify activity, non-discretized trajectories were binarized and averaged using a 5-pixel Euclidean distance threshold.

Animal husbandry

All locusts tested in this study were reared in an animal facility of University of Konstanz, at 24°C and 65% humidity, 12/12 h light/dark cycle. Locusts were fed wheat grass ad libitum. 50-by-50-by-80 cm enclosures were used to raise gregarious locusts (200-300 insects per cage). First-generation solitarious locusts were reared in individual containers (9-by-9-by-14 cm) featuring opaque sides, situated in a different room with continuous air flow to minimize exchange of visual and olfactory stimuli among isolated locusts. Locusts were starved overnight prior to all laboratory experiments.

Locust virtual reality

The locust virtual reality setup was developed in collaboration with, and constructed by Loopbio GmbH (Stowers et al., 2017). A high-speed motion compensator system stabilized a freely walking 5th instar juvenile locust on a 600 mm sphere. From this frame of reference, a perspective-correct, fully immersive 3D virtual world is achieved by projecting the scene on a cylindrical surface at 100 Hz, 1280-by-720 pixel resolution, with the anamorphic illusion providing the appropriate volumetric cues.

The virtual fifth instar locust bounding-box dimensions and appendage kinematics were calculated from 103 fifth instar locusts tracked in an arena. Locust positions and pose estimations were generated by DeepPosekit (Graving et al., 2019) . After an initial assumption for an alternate tripod gate, each gait event was recognized through a composite Euclidean distance signal. Random sample consensus was used to calculate each appendage translocations, which were then fed to Blender 2.7.4 for creation of bone-animation at 120 Hz.

In marching band experiments, speed of virtual locusts was set to 4 cm/s based on previous arena experiments (except Fig. 4B: 2 cm/s) (Bazazi et al., 2011). In single target experiments in Fig. 4C, virtual locust speed was set to match focal locust speed within range of 1-5 cm/s.

Virtual marching band's direction was randomized in each experiment to prevent side bias. The band direction is determined by experimental order parameter. For n number of virtual agents, with constant heading of θ, the order is:

$$\boldsymbol{Order} = \frac{\sqrt{(\sum_{i=1}^{n}\mathbf{cos}(\boldsymbol{\theta})^2 + \sum_{i=1}^{n}\mathbf{sin}(\boldsymbol{\theta})^2)}}{\boldsymbol{n}} \qquad \text{(S2)}$$

Virtual marching band experiments in VR lasted for 20 minutes for a single condition. In an initial acclimatization period, lasting 8 minutes, a single black bar was presented to the focal locust.

The experimental duration was 60 minutes for experiments in Fig. 4C & Fig. 5B. For these experiments, no stimulus was present for 8 minutes of acclimatization for these experiments.

All VR experiments were conducted at 30°C and 20% humidity.

During analysis of virtual marching band experiments, we excluded cases where the focal locust did not complete at least 80% of the experiment or traveled a total distance of less than 1 meter. Mahalanobis distance, on mean vector cosine and sine values, per condition (threshold = 2.5) was used to further exclude outliers.

In one-target (virtual locust) experiments, focal angular deviation (to target, < = 20 degrees) and speed (>1 cm/s) were used as criteria in calculating time following and distance. In two-target experiments, trials commenced with one target presentation and two-target phase started only subsequent to the focal individual reaching the one target. Here, selection criteria for a particular trial was focal angular deviation (to +x axis, < = 10 degrees), speed (>1 cm/s) and follow time (> = 1 minute). Furthermore, due to observed side bias, absolute focal y positions for successful trials were shuffled and half of the samples were inverted back. This mirrored dataset then was resampled from its Gaussian kernel density estimation (sample size = 1000) and subjected to Dip's test of unimodality. This resampling has been replicated for 1000 rounds in suppl. Fig. S13.

For the collision experiments in suppl. Fig. S8, after acclimatization, each focal locust was tested in 8 trials in which a virtual locust was initiated 40 cm away, a specified angle with respect to the focal individual, and moved towards it at constant 4 cm/s speed until collusion. Trial duration was pseudorandomized (126-130 seconds). The angular position of the virtual locust per trial was determined with respect to the current focal locust heading at offsets ranging from 0 to 360 degrees in a randomized sequence. Trials with inactive locusts (Euclidean distance < 10 cm) were excluded from analysis.

In mean vector calculations, raw trajectories were discretized at 3 body lengths (BL) (Bovet & Benhamou, 1988). When analyzing trajectories, due to limitations of traditional circular statistics, we performed multivariate analysis of variance (MANOVA) tests, using sine and cosine values of mean vectors, to compare different experimental groups (Landler et al., 2022). Otherwise, group comparisons relied on non-parametric Kruskal-Wallis and post-hoc Dunn's tests.

After trajectory discretization, heading angle θ of each subdivision is calculated. Then, a mean vector of a trajectory, with n subdivisions, is calculated using Equation 1.

For Bayesian inference we performed in Fig. 5E: Movement trajectories are highly auto-correlated and are oversampled where movement speed is low. To reduce autocorrelation and to decouple sampling from movement speed, we spatially re-discretized trajectories into vectors with a step length of 6 BL. This step length was chosen primarily for practical reasons, to maximize the amount of data while sufficiently reducing auto-correlation. We find a range of step lengths from 2 to 10 BL produce similar results for our model fitting procedure described below, but below 2 BL the data exhibit high auto-correlation, which strongly violates assumptions for model fitting, while above 10 BL there are too few data to reasonably fit a

model. We then calculate the direction of the vector for each step in the trajectory relative to the previous step location producing a set of directional vectors for each individual.

The distribution of directional vectors is both cyclical (wrapped), can be bimodal given the possibility of bifurcation, and samples are repeatedly observed from the same individuals. To account for these effects, we model these data using a hierarchical bimodal von Mises-Mixture likelihood with two components (modes) to disentangle the average population-level effect across all individuals from individual-level variance, while also accounting for potential bimodality. We define our individual-level likelihood for the distribution of vector directions as:

$$\boldsymbol{p}(\boldsymbol{y}|\boldsymbol{i}) \;=\; \boldsymbol{p}(\boldsymbol{y}|\boldsymbol{\theta}_i) \;=\; \boldsymbol{p}(\boldsymbol{y}|\boldsymbol{\mu}_i, \boldsymbol{\kappa}_i, \boldsymbol{\omega}_i)$$

$$= \frac{\mathbf{1}}{\boldsymbol{Z}(\boldsymbol{\kappa}_i, \boldsymbol{\omega}_i)}\left[\boldsymbol{\omega}_i \exp\left(\boldsymbol{\kappa}_{i,1}\cos\left(\boldsymbol{\mu}_{i,1} - \boldsymbol{y}\right)\right) + (\mathbf{1} - \boldsymbol{\omega}_i)\exp\left(\boldsymbol{\kappa}_{i,2}\cos\left(\boldsymbol{\mu}_{i,2} - \boldsymbol{y}\right)\right)\right] \qquad \text{(S3)}$$

where $p(y|i)$ is the likelihood for observation y from individual i for $i = 1, \ldots, M$, where M is the number of individuals, $\Theta_i = \{\mu_i, \kappa_i, \omega_i\}$ is an array of parameters for individual i, ω_i is the mixture coefficient for individual i with the range $\omega_i \in [0,1]$, $\mu_i = \{\mu_{i,1}, \mu_{i,2}\}$ is a 2d vector of directional means for individual i with the range $\mu_i \in [-\pi, \pi]$, $\kappa_i = \{\kappa_{i,1}, \kappa_{i,2}\}$ is a 2d vector of positive concentration (inverse variance) parameters for individual i with $\kappa > 0$, and

$$\boldsymbol{Z}(\boldsymbol{\kappa}_i, \boldsymbol{\omega}_i) \;=\; \boldsymbol{\omega}_i / \left(\mathbf{2}\boldsymbol{\pi}\boldsymbol{I}_{\mathbf{0}}\left(\boldsymbol{\kappa}_{i,1}\right)\right) + (\mathbf{1} - \boldsymbol{\omega}_i) / \left(\mathbf{2}\boldsymbol{\pi}\boldsymbol{I}_{\mathbf{0}}\left(\boldsymbol{\kappa}_{i,2}\right)\right) \qquad \text{(S4)}$$

is a normalizing constant such that

$$\int \boldsymbol{p}(\boldsymbol{y}|\boldsymbol{i})\boldsymbol{d}\boldsymbol{y} \;=\; \mathbf{1}, \qquad \text{(S5)}$$

where I_0 is a zeroth-order Bessel function.

We parameterize our model hierarchically by using partially-pooled parameters where likelihood parameters for each individual are modeled as a population-level parameter plus an individual specific offset with a link function to constrain the parameters to the appropriate range of values for the likelihood function:

$$\boldsymbol{\mu}_i \;=\; \boldsymbol{\mu}_{\mathbf{0}} + \boldsymbol{\mu}_{i,\Delta} \qquad \text{(S6)}$$

$$\boldsymbol{\varphi}^{-\mathbf{1}}(\boldsymbol{\kappa}_i) \;=\; \boldsymbol{\varphi}^{-\mathbf{1}}(\boldsymbol{\kappa}_{\mathbf{0}}) + \boldsymbol{\varphi}^{-\mathbf{1}}(\boldsymbol{\kappa}_i)_{\Delta} \qquad \text{(S7)}$$

$$\boldsymbol{\sigma}^{-\mathbf{1}}(\boldsymbol{\omega}_i) \;=\; \boldsymbol{\sigma}^{-\mathbf{1}}(\boldsymbol{\omega}_{\mathbf{0}}) + \boldsymbol{\sigma}^{-\mathbf{1}}(\boldsymbol{\omega}_i)_{\Delta} \qquad \text{(S8)}$$

where μ_0, κ_0, ω_0 are population-level parameters for the means, concentrations, and mixture coefficient, $\mu_{i,\Delta}$, $\varphi^{-1}(\kappa_i)_\Delta$, and $\sigma^{-1}(\omega_i)_\Delta$ are individual-specific additive offsets. $\sigma(\cdot)$ is the logistic sigmoid link function

$$\boldsymbol{\sigma(x)} \;=\; \mathbf{1/1 + \exp(-x)} \qquad \text{(S9)}$$

which constrains the output to $[0,1]$, and $\varphi(\cdot)$ is the softplus link function

$$\boldsymbol{\varphi(x)} \;=\; \mathbf{\log(\exp(x) + 1)}, \qquad \text{(S10)}$$

which constrains the output to be strictly positive, with $\sigma^{-1}(\cdot)$ and $\varphi^{-1}(\cdot)$ being their inverse functions. We then select priors for our model parameters as:

$$\boldsymbol{\mu_0 \sim \mathbf{Uniform}(-\pi, \pi)}$$

$$\boldsymbol{\varphi^{-1}(\kappa_0) \sim \mathcal{N}(\varphi^{-1}(2), 0.5)}$$

$$\boldsymbol{\sigma^{-1}(\omega_0) \sim \mathcal{N}(0, 0.5)}$$

$$\boldsymbol{\mu_{i,\Delta} \sim \mathbf{VonMises}(0, 20)}$$

$$\boldsymbol{\varphi^{-1}(\kappa_i)_\Delta \sim \mathcal{N}(0, 0.5)}$$

$$\boldsymbol{\sigma^{-1}(\omega_i)_\Delta \sim \mathcal{N}(0, 1.0)}$$

In general, we chose priors to constrain the model likelihood to a reasonable space of observations without biasing the model toward a particular result. We recovered nearly identical results across a range of prior distributions likely due to the large number of observations in the dataset, which easily overwhelms the influence of the prior.

To estimate the posterior parameters

$$\boldsymbol{p(\theta|y)} \;=\; \boldsymbol{p(y|\theta)p(\theta)/p(y)}, \qquad \text{(S11)}$$

we implemented the model in PyMC v5.0.1 (Abril-Pla et al., 2023) and used the No-U-Turn Sampler (NUTS) (Hoffman & Gelman, 2014) , a self-tuning variant of Hamiltonian Monte Carlo, to draw MCMC samples $\theta \sim p(\theta|y)$. We sampled 1000 warm-up/tuning samples, which were discarded, followed by 1000 tuned samples across 4 independent chains for a total of 4000 posterior samples. The MCMC chains did not show any signs of degenerate behavior (divergences, exceeding max tree depth, etc.) and converged with good mixing across chains

(ranked R-hat = 1.00 for all parameters) and low correlation between samples (effective sample size (ESS) >100 for all parameters) indicating ideal sampling behavior.

After drawing posterior samples, we then make population-level inferences by evaluating two hypotheses using the population-level parameters setting the individual offsets to zero, thereby factoring out individual-level variance:

$$\boldsymbol{p(y) = p(y|\theta_0) = p(y|\mu_0, \kappa_0, \omega_0)}$$
$$= \frac{\mathbf{1}}{\boldsymbol{Z(\kappa_0, \omega_0)}}\left[\boldsymbol{\omega_0 \exp(\kappa_{0,1} \cos(\mu_{0,1} - y)) + (1 - \omega_0) \exp(\kappa_{0,2} \cos(\mu_{0,2} - y))}\right] \quad \text{(S12)}$$

To evaluate our two directional hypotheses, we use samples from the posterior distribution of parameters $\theta_0 \sim p(\theta_0|y)$ to calculate the posterior likelihood distribution for the forward direction $p(y = 0|\theta_0)$ and for bimodal perpendicular directions

$$\boldsymbol{[p(y = \pi/2|\theta_0) + p(y = -\pi/2|\theta_0)]/2} \quad \text{(S13)}$$

which gives us a posterior distribution of likelihood scores for evaluating the validity of the two hypotheses. We compare these hypotheses to a uniform distribution (random walk) which is calculated as simply:

$$\boldsymbol{U(y) = 1/2\,\pi}$$

We evaluate the model fit by comparing the posterior model density (population-level likelihood) to non-parametric estimates of the population-level data density across the range $[-\pi, \pi]$. We use two types of non-parametric estimates: (1) hierarchically bootstrapped (Saravanan et al., 2020) histogram bins and (2) hierarchically bootstrapped kernel density estimates (using a von Mises kernel with $\kappa = 30$). We find a large amount of overlap between the parametric model density and non-parametric data densities suggesting that the model is a good fit for the data (Fig. 5Ei).

Moving-dot paradigm

5th instar locusts are tethered at the protonum and placed on an air-suspended trackball (8 cm), which was surrounded by three high refresh rate (144 Hz) monitors. Monitors horizontally subtended 276 degrees for a panoramic view. By rendering a 360-degree panorama with BonVision library on Bonsai, black dots (2° in size) were created to move in clockwise and

counterclockwise direction along the dorsal-ventral axis of the animals at 64 °/s speed. Single trials lasted 25 seconds, with 5 seconds inter-stimulus interval. Locusts were acclimatized with pre-stimulus uniform grey screen for 60 seconds.

Locust movement, recorded at 144 Hz, was reconstructed using Fictrac (Moore et al., 2014). Trials with less than 5 cm Euclidian distance were not considered in analysis. Optomotor index was calculated as below, while ccw stands for counterclockwise movement and cw for clockwise movement:

$$\boldsymbol{Optomor\ Index} = \frac{\boldsymbol{\Sigma}\,|\boldsymbol{Velocity}_{ccw}| - \boldsymbol{\Sigma}\,|\boldsymbol{Velocity}_{cw}|}{\boldsymbol{\Sigma}\,|\boldsymbol{Velocity}_{ccw}| + \boldsymbol{\Sigma}\,|\boldsymbol{Velocity}_{cw}|} \tag{S14}$$

A mixed-effects model was later employed to compare solitarious and gregarious locust turning behavior to assess difference for optomotor response. The model evaluated relationship between an outcome variable optomotor index and predictors dot density, locust state (solitarious and gregarious), and their interaction, accounting for random intercepts across different locust subject identity.

Arena experiments

Experiments were conducted using 2000 locusts, on March 27, 2023, at 11:29 AM, and observed for approximately 300 seconds. The locusts' movements were captured using an infrared motion capture system (Qualisys AB, Gothenburg, Sweden) at a rate of 100 frames per second. We applied interpolation for each tracklet, in cases where one or two frames were missing. Tracklets with durations smaller than one second (100 frames) per locust were filtered out. Additionally, to eliminate instances where locusts were stationary, we incorporated a speed filter, discarding data for locusts moving at less than 2 cm/s in the x-y plane. We identified leader-follower patterns by finding the nearest neighbor to each leader, ensuring the follower was consistently behind the leader for at least 0.5 seconds and the angle between their moving was less than 45 degrees. Data were then aggregated based on the local coordinates of the leader, highlighting the most frequently occupied positions by followers relative to the leaders.

Modelling

The model of individual movement used here considers an agent equipped with a ring attractor neural network composed of N_s neurons. The neurons are modeled as spin variables (see

Sridhar *et al.* (2021) (Sridhar et al., 2021) for the formal analysis demonstrating mathematical equivalence to classic neural ring-attractor models), which govern the agent's movement. Each neuron can take two states, active, +1, and inactive, -1. The activity of each neuron, i, is determined by input from other neurons, and an external field. The external field is determined based on the sensory input on the neuron. Each neuron, i, has a receptive field centered around the angle $\alpha_i = 2\pi/N_S$. Neuron i responds to external stimuli at an angle θ_t according to a Gaussian,

$$\boldsymbol{h_i} = \left(\frac{\boldsymbol{h_0}}{\sqrt{\boldsymbol{2\pi\sigma^2}}}\right) \boldsymbol{e}^{\frac{\alpha_i-\theta_t}{2\sigma^2}}, \tag{S15}$$

and its dynamic is governed by a Hamiltonian,

$$\boldsymbol{H} = -\left(\frac{\boldsymbol{1}}{\boldsymbol{N_s}}\right)[\sum \boldsymbol{J_{ij}\sigma_i\sigma_j} + \sum \boldsymbol{h_i\sigma_i}], \tag{S16}$$

equations respectively. The Glauber dynamics (Amit, 1989) is used to simulate the network's dynamics. At each step, a neuron is chosen at random, and the energy difference resulting from updating the neuron's state is calculated. The neuron's state is flipped with certainty if the energy difference becomes negative, and it is flipped with probability $\exp(-\beta E)$ if the energy difference is positive. Here, ΔE is the energy difference resulting from flipping the focal spin. The agent's position is updated such that the agent's speed is

$$\vec{\boldsymbol{v}} = \frac{\boldsymbol{v_0}}{\boldsymbol{N_s}} \sum\nolimits_{\boldsymbol{active\ spins}} \boldsymbol{\alpha_i} \tag{S17}$$

according to the equilibrium state of the network. The network equilibrium state is determined after $50\ N_S$ spin updates. The synaptic connectivity is taken to be

$$\boldsymbol{J_{ij}} = \boldsymbol{\cos}\left[\boldsymbol{\pi}\left(\frac{\boldsymbol{\alpha_i - \alpha_j}}{\boldsymbol{\pi}}\right)^{\boldsymbol{\nu}}\right], \tag{S18}$$

where $\nu = 0.5$. The parameter values are as follows: $N_s = 400$, $v_0 = 10$, $\sigma = 2\pi/N_s$, $h_0 = 0.01$, and $\beta = 64$. For the computational experiment with moving bars we have considered a space with linear dimension $L = 100$. Two moving bars are composed of 40 targets each moving with speed $v_t = 1$ to the right. For the two moving targets experiment $L = 400$ and the two targets move with speed $v_t = 2$.

The model of collective movement (suppl. Fig. S15) considers $N = 320$ such agents with $N_s = 100$, $v_0 = 10$, $\sigma = 2\pi/N_s$ and $\beta = 1600$, moving in a space with periodic boundaries and linear size $L = 1000$. Each agent 'sees' other agents and aims to move toward them with a strength of external field $h_0 = 0.02$.

Supplementary text

Classic self-propelled particle models fail to account for locust behavior

In our experiment shown in Fig. 5C, we positioned focal locusts between two coherently moving swarms. Since we conducted experiments with two distances to the swarms, 8 cm and 50 cm, and we saw strong attraction towards the swarms in both conditions, we can be assured that the stimuli individuals are not outside the perception range. Our experiments demonstrated that locusts do not move in alignment with the motion of these swarms, as would be the prediction of both the optical flow hypothesis and the Vicsek model (Vicsek et al., 1995) (since it only incorporates explicit alignment among individuals).

Other self-propelled particle (SPP) models, such as the 'zonal' Couzin model (Couzin et al., 2002), include additional terms; local repulsion, intermediate alignment, and long-range attraction. A smaller subset of SPP models do not employ explicit alignment, and include only local repulsion and long-range attraction, such as by assuming a Lennard-Jones type 'social force' potential among individuals (D'Orsogna et al., 2006). Such SPP models also fail to explain the data from real locusts.

To explain why, we can consider the two main variants of the Couzin model, the original 3-zone formulation explained above (Couzin et al., 2002), and a simplified version with only 2 zones, local repulsion and a larger zone with both alignment with, and attraction towards, neighbors (Couzin et al., 2005, 2011) .

Let's consider the attraction term first. Since, in this experiment, we have a symmetrical scenario, with an approximately equal number of individuals on each side of the focal individual (irrespective of its initial heading), the attraction vectors pointing to one side tend to cancel the effect of those pointing in the opposite direction (if you add each vector and calculate the length of the resultant vector, it is close to zero), thus there exists no consistent attraction to one side, or the other.

The resulting attraction vector with length near zero has effectively no influence on the future direction. Even if normalized (to be a unit vector, for example), it will point in near-uniform

random directions in each timestep (since the direction of a vector with length near zero is dominated by stochastic fluctuations). This would mean the agent is either stationary, or exhibits a random walk, and thus would exhibit no coherent motion to one swarm or the other (remaining between the stimuli with a very, very slow stochastic drift).

If the individuals in the swarms were close enough to be in the alignment zone, then the focal individual would align with the direction of motion of the swarms, as predicted by the optical flow hypothesis (and the Vicsek model (Vicsek et al., 1995)).

If there are overlapping zones, such as where alignment and attraction co-occur over the same range (Couzin et al., 2005, 2011), since the attraction vectors nullify each other (see above), the alignment term dominates motion and, again, the agent will align with the stimulus swarms.

One possible way to break the deadlock in attraction terms would be to considerably limit the field of perception to the front. In this way, stochastic directional changes could result in only one side, or the other, being seen, and thus responded to. This is, however, not consistent with our data (locusts are responsive to those behind them), and also fails to account for locust (and fruit fly) spatial decision-making in non-social contexts, such as the bifurcations observed during spatial decision-making with respect to multiple static targets, whereas the neural ring attractor model does (Sridhar et al., 2021) .

In summary, in classical SPP models, movement decisions are based on simple 'rules', such as the averaging of positions and/or orientations of neighbors. This cannot account for the behavior we see in our experiments. By contrast, the neural ring attractor network framework introduces a simple, but essential, aspect of cognition: that movement decisions arise from neurobiologically-informed feedback processes within the brain. This allows the individual to integrate sensory inputs, and – via an ongoing neural consensus dynamic – to generate a self-organized dynamical bump of activity on the ring, which represents the animals' directional preference (which is then translated into motor output; see below for model details). It is this dynamical feedback process (in the form of local excitation and long-range/global inhibition) that is essential to explain the observed movement decisions. We hope this parsimonious, biologically-motivated framework (and future extensions of it), will allow deeper insights into a broad range of individual and collective-level behaviors.

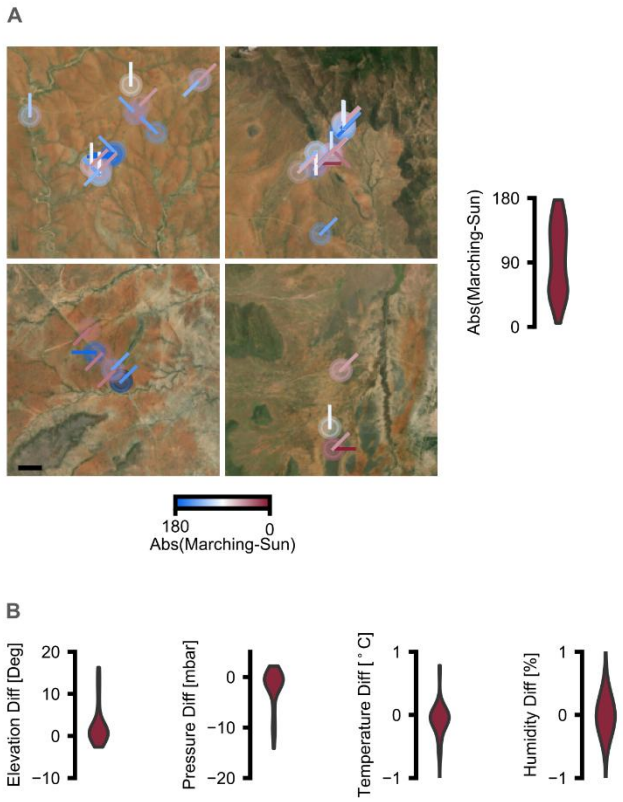

suppl. Fig. S1 – Environmental factors in field experiments. (A) Direction of marching bands from Fig. 1B depicted here in relation to sun azimuth position. (B) Change in estimated environmental conditions from Fig. 1B.

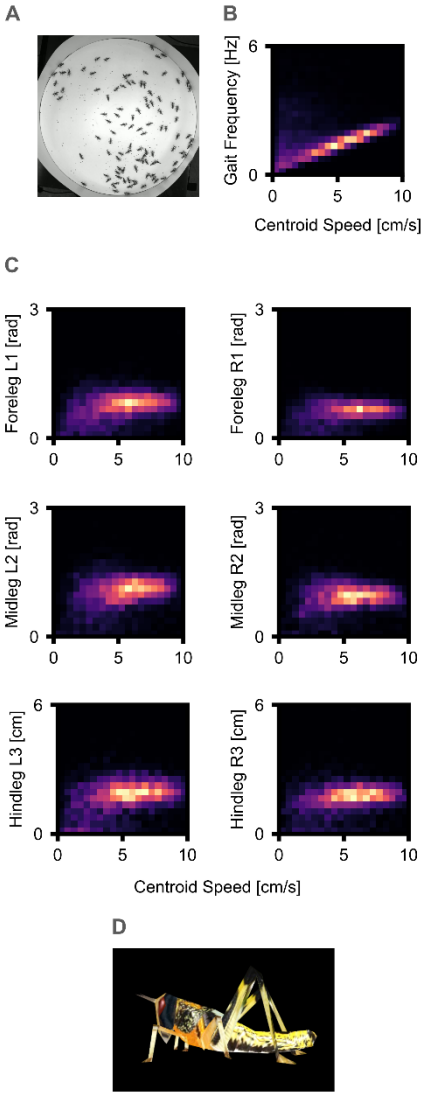

suppl. Fig. S2 – Real-world data curation for virtual locust model bone-animation kinematics. (A) Arena used in the study for pose estimation. Locusts were tracked at 30 frames-per-second. n = 103. (B) Alternate tripod gait cycle versus centroid speed. (C) Calculation of appendage kinematics. For fore- and mid-legs, each appendage was reconstituted as a single axis from base of femur to distal tarsus end and angular change in these axes was reported a swing per gait. Hindleg displacements were measured in Euclidean distance from a distal tarsus end positions over time. Histogram range is displayed with a color gradient from dark purple for the minimum to bright yellow for the maximum. (D) Snapshot of a virtual locust.

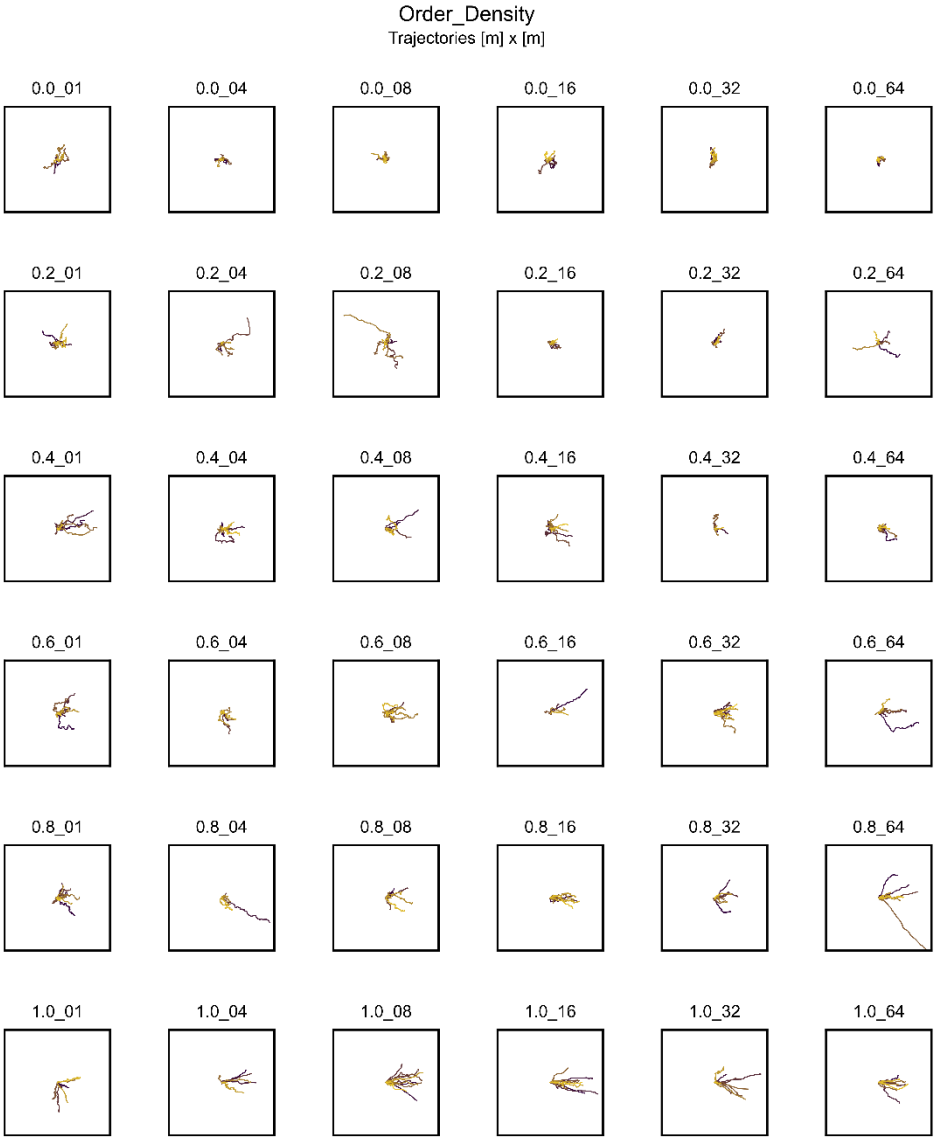

suppl. Fig. S3 – Focal trajectories under different order & density parameters. Trajectories that satisfied filtering conditions and used in the analyses in Fig. 2 are depicted here. Each trajectory describes a focal locust movement under a certain parameter combination for 20 minutes. Locusts were tested only once.

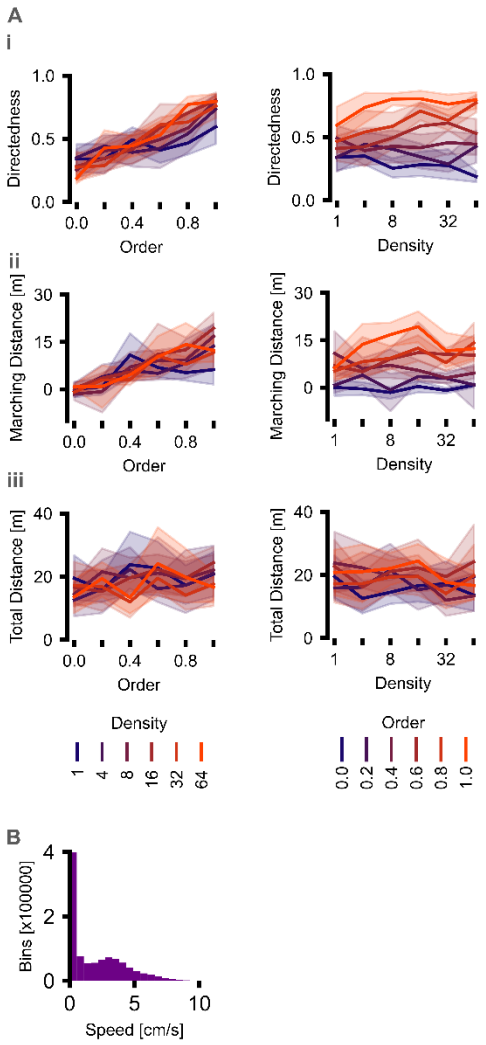

suppl. Fig. S4 – Impact of order and density on locust activity. (i) Directedness (mean vector magnitude), (ii) marching distance (distance covered in congruence with marching band), (iii) total (Euclidean) distance traveled for conditions in Fig. 2, grouped by density (left) and order (right). No statistical difference was observed with a non-parametric comparison for total distance covered. Please see suppl. Tbl. S2 for statistical summaries. (B) Speed histograms for all data presented in Fig. 2.

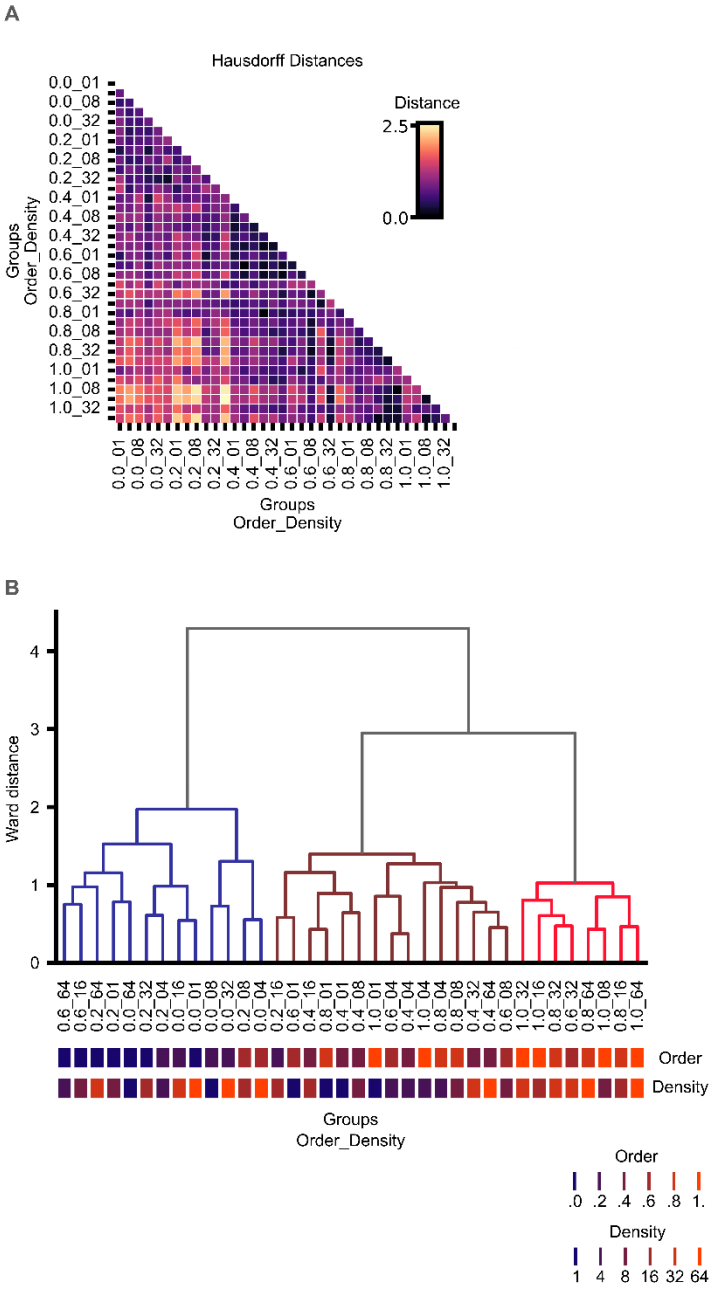

suppl. Fig. S5 – Clustering of trajectories based on mean vector projections. (A) Hausdorff distances to measure and cluster multivariate inter-group distances. Hausdorff distances were calculated with cosine and sine values for individual mean vectors presented in Fig. 2. (B) Dendrogram for Hausdorff distances. Group clustering reflects order parameter, rather than density.

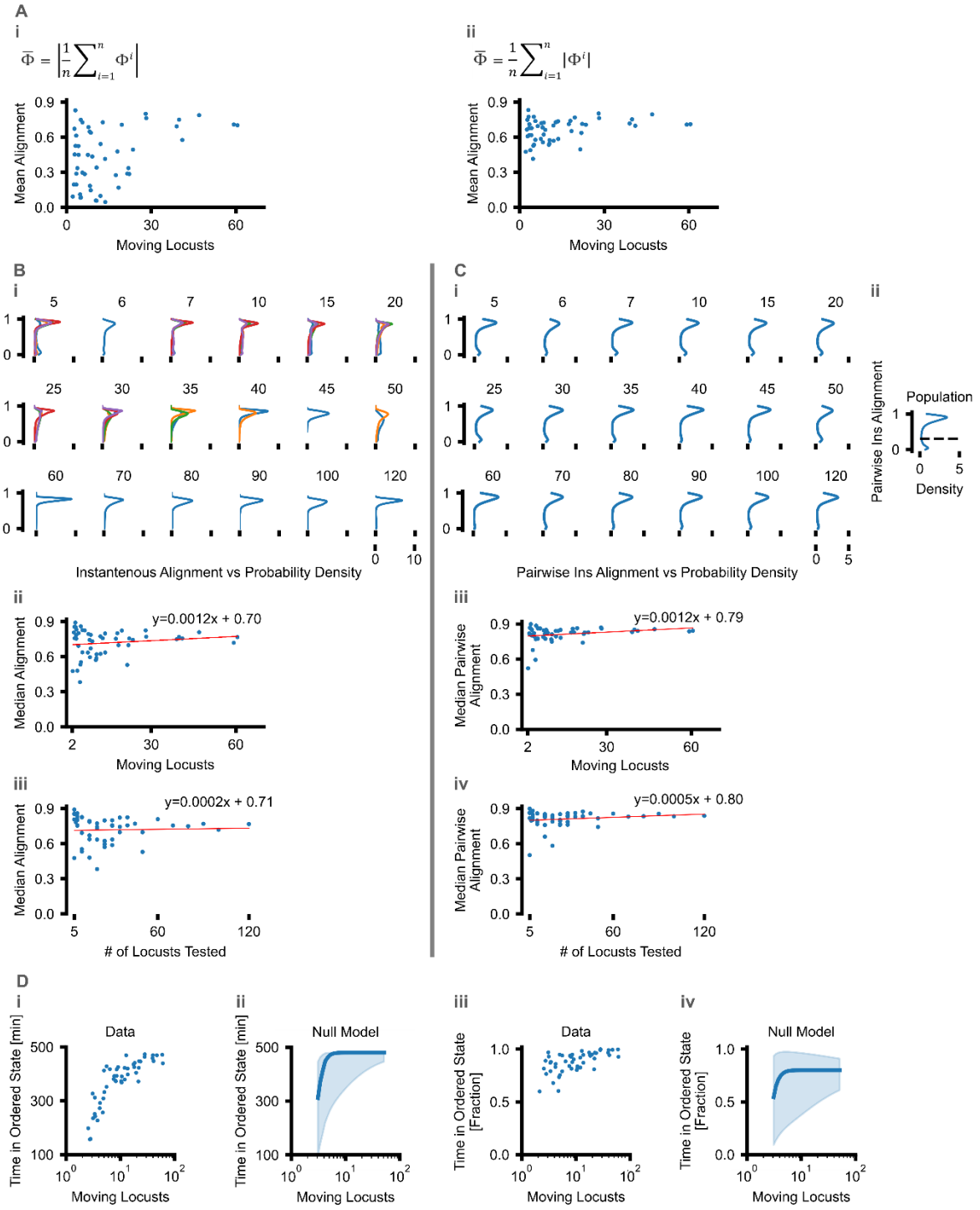

suppl. Fig. S6 – Our consideration of Buhl *et al.* (2006) results. (A) i: Absolute mean alignment for moving locusts. Buhl *et al.* (2006) explored impact of density on locust collective motion via calculating instantaneous alignment, with a range of ~-1 (clockwise) and ~1 (counterclockwise), in a circular arena. ii: Mean absolute alignment for moving locusts. Locusts exhibited direction changes according to Buhl *et al.* (2006) (Buhl et al., 2006). Under certain cases, such intermittency would result in near-zero mean alignment even though underlying locust collective movements could be highly coordinated (see Buhl *et al.* (2006) Fig. 2B). This is because summing ~-1 (clockwise) and ~1 (counterclockwise) results in a value close to zero. Accounting for this problem reveals high mean absolute alignments across all ranges tested (although median is a more appropriate statistic—see below). (B) i: Probability density distributions plotted against tested locust numbers in the circular arena. As per Buhl *et al.* (2006), only frames with at least two locusts moving are considered for analysis.ii: Median absolute alignment for mean number of moving locusts per trial. As an aggregate statistic, median is less influenced by outliers and thus more suitable to summarize heavy-tailed distributions. The slope of the linear regression fit shows there is no evidence that median alignment increases as a function of density. iii: Median absolute alignments (as in ii) versus group

size. (C) i: Pairwise instantaneous alignment plotted against tested locust numbers in the circular arena. Calculating instantaneous alignment for all moving locusts within a given frame introduces statistical group size effects, potentially obscuring behavioral variability in larger groups. To mitigate this, we also calculated pairwise alignment between a randomly-selected two moving locusts per frame; these distributions (probability density functions) are heavily weighted towards high alignment and are very similar across the full range of group sizes tested. ii: Population probability of pairwise instantaneous alignment. Dashed line represents 'ordered state' cut-off threshold introduced by Buhl *et al.* (2006). Alignment instances higher than 0.3 were defined as the group being in the 'ordered state'. Probability of two locusts being in the 'ordered state' was ~0.80 (~80%). iii & iv: Median absolute pairwise alignment versus mean number of moving locusts (iii) and versus group size (iv) for each trial. Alignment can be seen to be consistently high for all group sizes. (D) Time in 'ordered state'. i & iii: Time in 'ordered state' versus moving locusts per trial in minutes (i) and fraction of frames where at least two locusts were moving (ii). ii & iv: Null model predictions of time spent in 'ordered state' based on probabilistic pairwise alignment and group size in minutes (ii) and fraction of frames where at least two locusts were moving (iv). Buhl *et al.* (2006) did not ask what the null (random) expectation is for the relationship between total time spent in the ordered state and mean number of moving locusts. Since locusts only move approximately half of the time (~51%), and that 2 or more must be active to calculate the collective order parameter, one can conceptually think about it as a binomial problem: what is the probability of getting at least 2 moving locusts per frame as a function of number of group size? Since this probability increases steeply and asymptotes, a steeply increasing relationship is an inevitability, as a statistical artifact of how collective order is calculated. To demonstrate this, we created a binomial null model that calculates the probability of locusts being in an 'ordered state' by considering the likelihood of locusts moving (51% as defined by Buhl *et al.* (2006)) and aligning (with 0.3 threshold: ~80%) for a given group size. In these null model plots (Dii, iv), solid lines represent expected time spent in the 'ordered state' as predicted by the binomial null model. Shaded regions correspond to 95% confidence interval derived using the Wilson score interval method (E. B. Wilson, 1927). The null model serves as a baseline to assess whether observed 'increase' in 'ordered state' can emerge via a statistical artifact. The large overlap between the data and the null expectation demonstrates that these data do not support the hypothesis of a density-dependent phase transition between collectively disordered and ordered motion, as was asserted in Buhl *et al.* (2006).

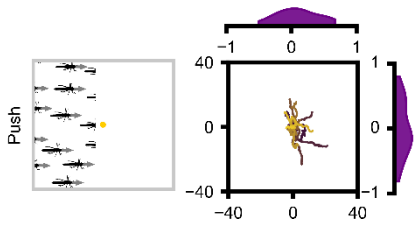

suppl. Fig. S7 – Congruent focal movement was not observed with pushing bands. A focal agent is positioned at front (Push) of a high-ordered marching band. n = 24. Periodic boundaries ensured constant distance between agent and band edge. Focal locust trajectories predominantly indicate perpendicular motion with respect to the marching band. The movement can be either explained via escape behavior or as an 'intent' to rejoin the group in the absence of stimuli in front. Here, the offset between the pushing marching band and focal locust prevents collisions. See suppl. Fig. S8 for impact of collisions on focal behavior.

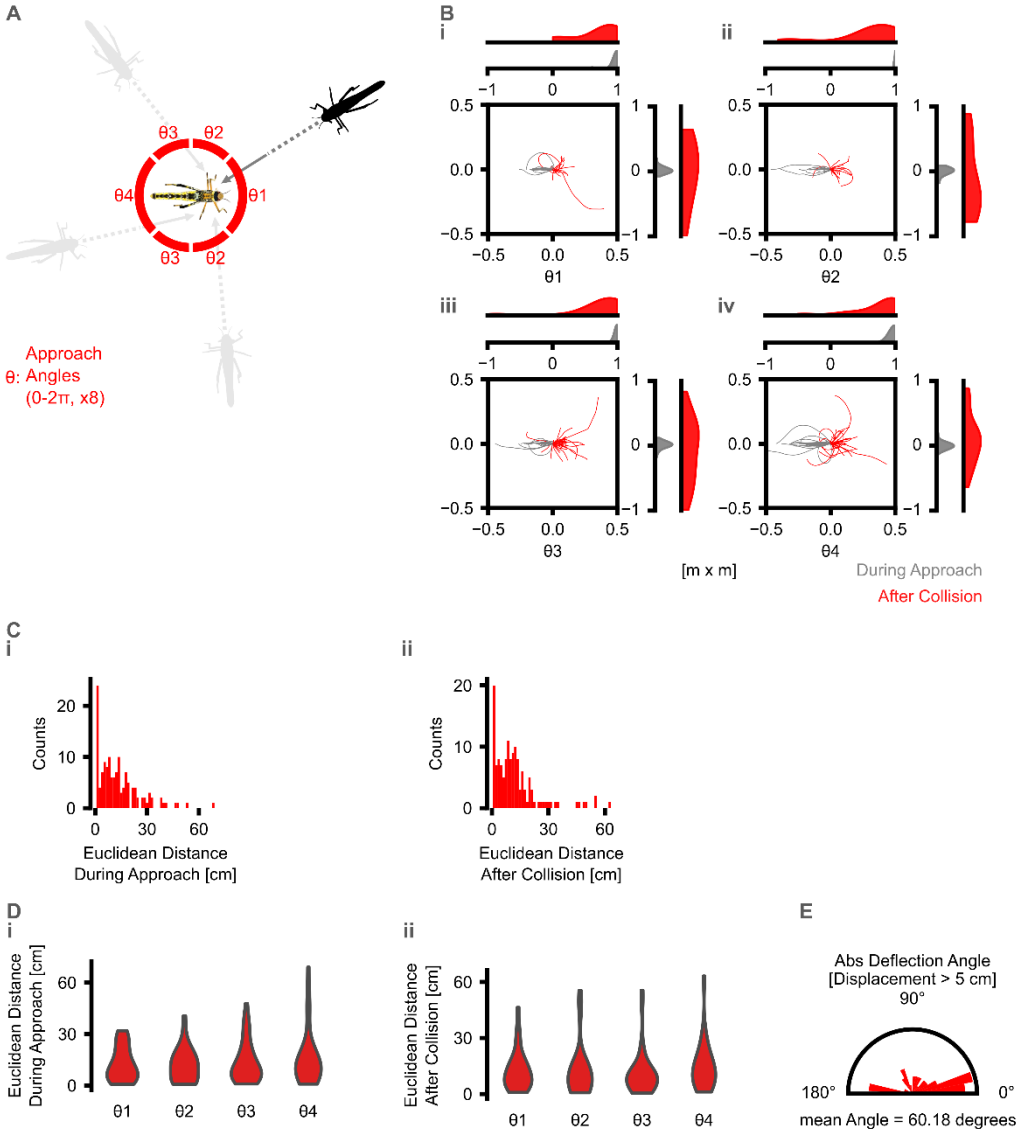

suppl. Fig. S8 – Collision avoidance in VR. (A) Experimental design. A single virtual locust placed at a distance moves toward focal locust with constant speed for 10 seconds until collision. Depending on approach angle, trials are pooled into four groups. (B) Focal trajectories. Trajectories are color coded as: grey for virtual locust approach until collision and red for after collision. Analysis of cosine and sine values of mean vectors did not yield statistical significance with MANOVA. n = 24, 24, 40, 50. Tested locust n = 56. (C) Histograms for before (i) and after collision (ii). (D) Euclidean distance covered before (i) and after (ii) collision per approach angle. No significance observed with Kruskal-Wallis test. (E) Angular deflection after collision. Please see suppl. Tbl. S2 for statistical summaries.

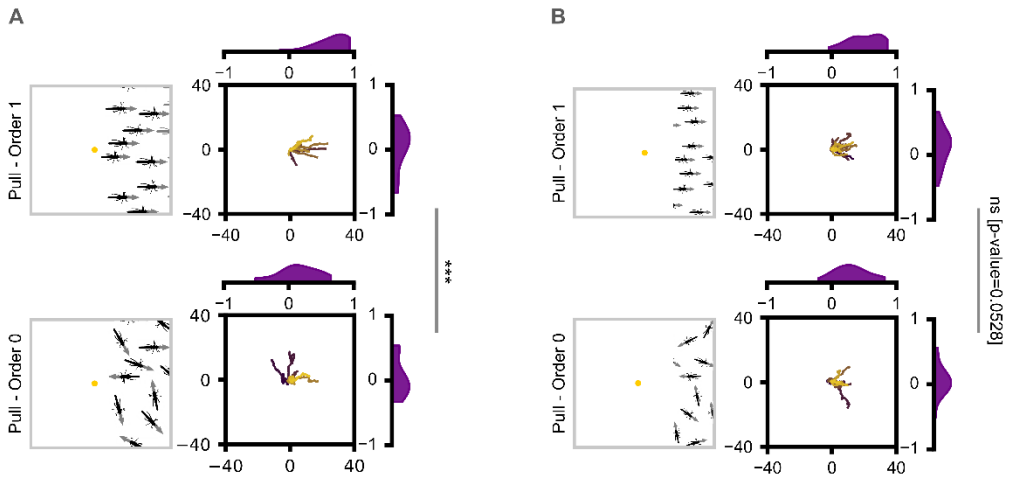

suppl. Fig. S9 – Testing pulling marching bands on different conditions. (A) Focal trajectories when faced with a pulling marching band with order 1 (Up) and a disordered band (Down). (B) Comparison as in A, however, periodic boundaries are set at 50 cm. Please see suppl. Tbl. S2 for statistical summaries.

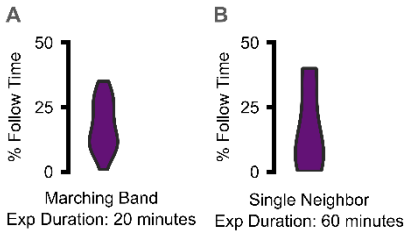

suppl. Fig. S10 – Virtual locust following durations. (A, B) Follow time in percentage for experiments in Fig. 4C and Fig. 4D.

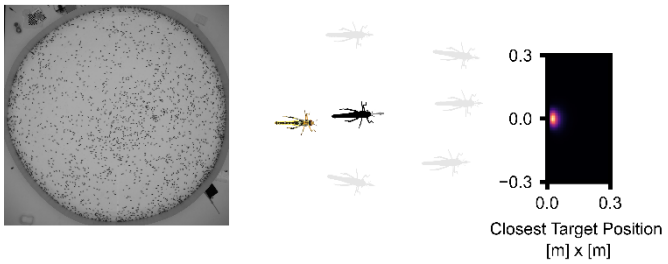

suppl. Fig. S11 – Pulling attraction in arena experiments. (Left) A snapshot of 2000 locust arena experiment. (Middle) Schematic for analysis pipeline. Follower – target interactions were identified via analysis of continuous congruent tracklets. (Right) Density of nearest target position. n = 342016 tracklets. Normalized densities are displayed with a color gradient from dark purple for the minimum to bright yellow for the maximum.

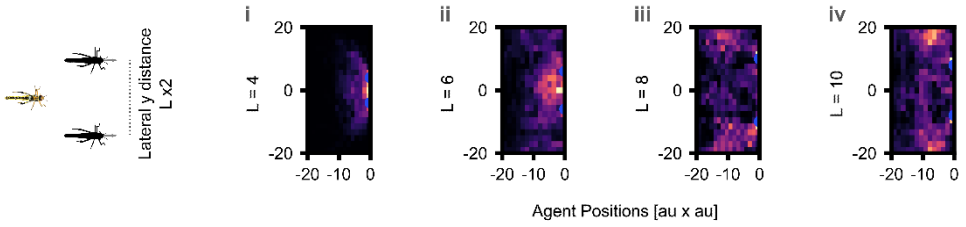

suppl. Fig. S12 – Model agent positions in two-target pursuit. (Left) Experiment design. (i – iv) Agent position densities at different lateral distances between targets for 100 frames. Only agents behind the two targets are considered as actively following. Agents with a larger distance than 30 au from two target's center of gravity are excluded. Target positions are designated in blue. n = 100 per condition. Histogram range is displayed with a color gradient from dark purple for the minimum to bright yellow for the maximum.

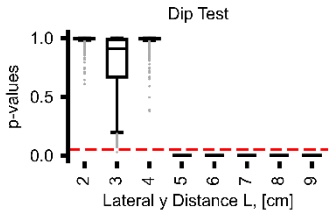

suppl. Fig. S13 – **p-values for the repeated Dip Tests of Unimodality**. Data analysis pipeline in Fig. 5B VR data here is repeated for 1000 times. Red dashed line represents statistical threshold (0.05). See Methods for the details.

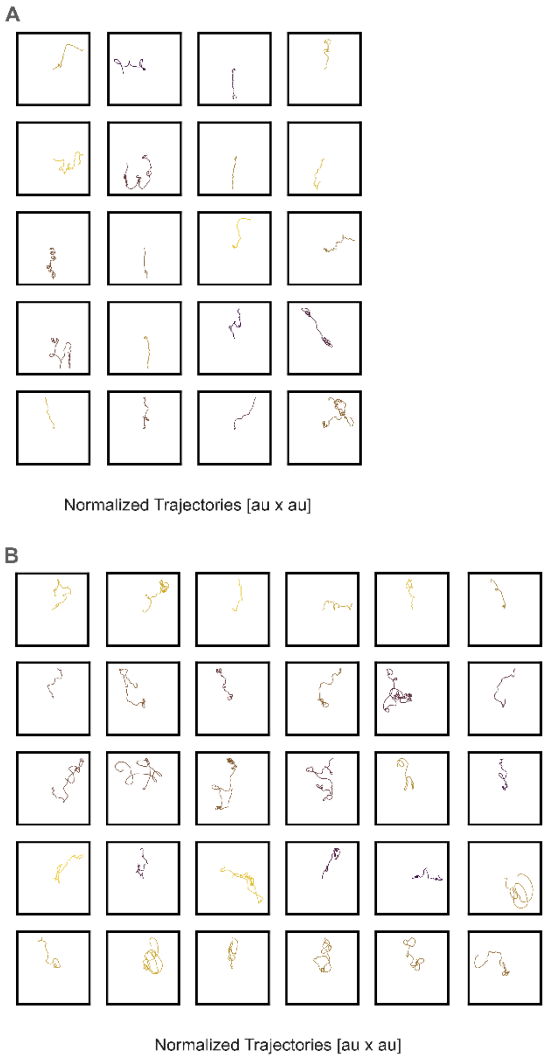

suppl. Fig. S14 – Normalized trajectories from Figure 5C, E. (A) Trajectories generated in proximal condition (fixed lateral distance = 8 cm). (B) Trajectories generated in distal condition (fixed lateral distance = 50 cm).

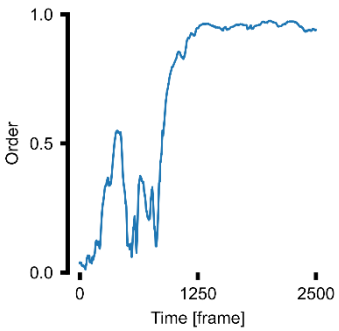

suppl. Fig. S15 – Collective motion of neural ring attractor networks. Order of agents over 2500 frames. Simulated neural ring attractor agents were placed in a space with periodic boundaries. Over time, these agents formed and sustained high-degree collective motion. Trajectories are spatially discretized at 3 au. n = 320.

suppl. Tbl. S1 – Extended data for marching bands logged in Kenya, 2020.

Latitude	Longitude	Timestamp (Local)	Direction	Low Cloud Cover %	Molt stage	Band size [m^2]
0.894424	37.368537	2020-02-27 10:05:20+03:00	east	18.0	3/4	na
0.897966	37.373476	2020-02-28 10:11:34+03:00	north/north-east	19.0	3/4	na
0.899008	37.374553	2020-03-01 07:44:13+03:00	south-east	0.0	4/5	na
0.6813	37.635757	2020-03-02 06:08:15+03:00	east/north-east	0.0	4/5	na
0.905147	37.376172	2020-03-02 13:01:31+03:00	north-east	0.0	5	na
0.908041	37.377609	2020-03-02 13:17:08+03:00	north-east	0.0	5	na
0.907843	37.377729	2020-03-02 13:55:25+03:00	north-east	0.0	5	na
0.892979	37.367124	2020-03-07 15:35:33+03:00	north-east	14.0	5	na
0.909998	37.377923	2020-03-03 09:20:43+03:00	north/north-east	0.0	5	na
0.909648	37.378408	2020-03-03 10:01:46+03:00	north/north-east	28.0	5	na
0.434429	37.565447	2020-03-04 08:44:20+03:00	north-east	2.0	1/2	na
0.434093	37.565232	2020-03-04 09:27:48+03:00	north-east	0.0	1/2	na
0.680893	37.635667	2020-03-04 14:15:28+03:00	north-east	0.0	5	na
0.685719	37.632503	2020-03-02 16:56:16+03:00	north-east	0.0	5	na
0.701032	37.623702	2020-03-04 16:01:35+03:00	south-west	0.0	5	na
0.691474	37.628315	2020-03-04 17:16:58+03:00	south-west	0.0	5	na
0.684992	37.633007	2020-03-04 17:19:30+03:00	south-west	0.0	5	na
0.89785	37.372833	2020-03-05 07:29:56+03:00	south-west/north-east	0.0	5	9210
0.768734	37.329245	2020-03-05 12:25:43+03:00	south/south-west	0.0	6	na
0.907815	37.378407	2020-03-05 15:23:59+03:00	north/north-east	0.0	5	na
0.898654	37.367585	2020-03-06 07:19:27+03:00	south/south-west	0.0	5	na
0.412322	37.561074	2020-03-07 06:56:24+03:00	north	0.0	1/2	na
0.404162	37.5623	2020-03-07 07:04:13+03:00	east/north-east	0.0	1/2	na
0.692148	37.625643	2020-03-07 08:40:17+03:00	west	0.0	4/5	na
0.547951	37.532046	2020-03-07 10:36:20+03:00	north-east	0.0	1/2	na
0.560591	37.496804	2020-03-07 11:33:19+03:00	south-west	0.0	1/2	na
0.560334	37.496757	2020-03-07 11:36:07+03:00	south-west	0.0	1/2	na
0.894296	37.368761	2020-03-09 07:26:05+03:00	north-east	17.0	5	na
0.891208	37.361105	2020-03-09 11:20:00+03:00	north-east	77.0	5	na
0.935827	37.212109	2020-03-08 13:19:42+03:00	north	32.0	4/5	na
0.867486	37.369428	2020-03-09 15:56:07+03:00	north-east	5.0	5	na
0.949572	37.276905	2020-03-10 08:37:15+03:00	south-west/north-east	47.0	5	2818
0.940079	37.254376	2020-03-10 09:02:48+03:00	north-east	28.0	5	693
0.936762	37.252342	2020-03-10 09:10:32+03:00	north-west/south-east	28.0	5	644
0.921881	37.244654	2020-03-10 09:20:05+03:00	north-west	28.0	5	na
0.921246	37.243897	2020-03-10 09:21:50+03:00	west	28.0	5	na
0.920203	37.242566	2020-03-10 09:23:51+03:00	west	28.0	5	na
0.913406	37.238613	2020-03-10 09:29:45+03:00	north/north-west	10.0	5	1368
0.929442	37.260341	2020-03-10 10:33:34+03:00	north-west	28.0	5	227
0.947674	37.250596	2020-03-10 16:07:18+03:00	north	0.0	5	971
0.915465	37.239108	2020-03-11 07:24:56+03:00	south-west/north-east	46.0	5/6	2881
0.91686	37.235641	2020-03-12 08:01:27+03:00	north/north-east	11.0	5/6	na

suppl. Tbl. S2 – Statistical summaries.

Figure 1C

Rayleigh's Test

	p-value
i	6.9693e-25
ii	3.2281e-19
iii	2.1766e-07
iv	3.8526e-04

Figure 1D

Kruskal-Wallis H-test

H-statistic	p-value
21.395812026417115	8.711605681795934e-05

Dunn's Test

	Control	Olfaction-	Polarized Vision-	Vision-
Control	1.0	1.0	1.0	0.001033
Olfaction-	1.0	1.0	1.0	0.001520
Polarized Vision-	1.0	1.0	1.0	0.002479
Vision-	0.001033	0.001520	0.002479	1.0

Figure 1E

Kruskal-Wallis H-test

H-statistic	p-value
49.4551020656495	1.0436050570931105e-10

Dunn's Test

	Control	Olfaction-	Polarized Vision-	Vision-
Control	1.0	8.164723e-01	8.164723e-01	4.303666e-08
Olfaction-	8.164723e-01	1.0	4.770080e-01	3.728776e-09
Polarized Vision-	8.164723e-01	4.770080e-01	1.0	5.228693e-04
Vision-	4.303666e-08	3.728776e-09	5.228693e-04	1.0

Figure 2D

MANOVA

Intercept

Statistic	Value	Num DF	Den DF	F Value	Pr > F
Wilks' lambda	0.9957	2.0000	384.0000	0.8295	0.4370
Pillai's trace	0.0043	2.0000	384.0000	0.8295	0.4370
Hotelling-Lawley trace	0.0043	2.0000	384.0000	0.8295	0.4370
Roy's greatest root	0.0043	2.0000	384.0000	0.8295	0.4370

Groups

Statistic	Value	Num DF	Den DF	F Value	Pr > F
Wilks' lambda	0.3836	70.0000	768.0000	6.7440	0.0000
Pillai's trace	0.6707	70.0000	770.0000	5.5503	0.0000
Hotelling-Lawley trace	1.4657	70.0000	722.3219	8.0208	0.0000
Roy's greatest root	1.3618	35.0000	385.0000	14.9799	0.0000

Figure 2Fi

OLS Regression Results

Model	OLS	F-statistic	154.9
Method	Least Squares	Prob (F-statistic)	3.27e-14
No. Observations	36	Log-Likelihood	29.464
Df Residuals	34	AIC	-54.93
Df Model	1	BIC	-51.76
R-squared	0.82	Covariance Type	nonrobust
Adj. R-squared	0.815		

Coefficients

	Intercept	order
coef	-0.008	0.6669
std err	0.032	0.054
t	-0.247	12.444
P>|t|	0.806	0.0
[0.025	-0.074	0.558
0.975]	0.058	0.776

Other Statistics

Omnibus	7.447	Durbin-Watson	2.102
Prob(Omnibus)	0.024	Jarque-Bera (JB)	5.988
Skew	-0.877	Prob(JB)	0.0501
Kurtosis	3.958	Cond. No.	3.73

continued suppl. Tbl. S2 – Statistical summaries.

Figure 2Fii

OLS Regression Results

Model	OLS	F-statistic	0.9773
Method	Least Squares	Prob (F-statistic)	0.33
No. Observations	36	Log-Likelihood	-0.88956
Df Residuals	34	AIC	5.779
Df Model	1	BIC	8.946
R-squared	0.028	Covariance Type	nonrobust
Adj. R-squared	-0.001		

Coefficients

	Intercept	density
coef	0.2853	0.0019
std err	0.059	0.002
t	4.849	0.989
P>|t|	0.0	0.33
[0.025	0.166	-0.002
0.975]	0.405	0.006

Other Statistics

Omnibus	2.645	Durbin-Watson	0.329
Prob(Omnibus)	0.266	Jarque-Bera (JB)	1.363
Skew	0.041	Prob(JB)	0.506
Kurtosis	2.051	Cond. No.	41.7

Figure 3A

Mixed Linear Model Regression Results

Model:	MixedLM	Dependent Variable:	opto_index
No. Observations:	379	Method:	REML
No. Groups:	31	Scale:	0.0904
Min. group size:	4	Log-Likelihood:	-122.1071
Max. group size:	16	Converged:	Yes
Mean group size:	12.2		

	Coef.	Std.Err.	z	P>|z|	[0.025	0.975]
Intercept	-0.041	0.046	-0.908	0.364	-0.131	0.048
growth_environment[T.s]	0.060	0.035	1.680	0.093	-0.010	0.129
stim_type	0.000	0.000	5.012	0.000	0.000	0.000
stim_type:growth_environment[T.s]	0.000	0.000	2.448	0.014	0.000	0.000
1 | Subject	-0.000	0.003	-0.081	0.935	-0.005	0.005
Group Var	0.008	0.014				

Figure 3B

MANOVA

Intercept

Statistic	Value	Num DF	Den DF	F Value	Pr > F
Wilks' lambda	0.1175	2.0000	57.0000	214.1464	0.0000
Pillai's trace	0.8825	2.0000	57.0000	214.1464	0.0000
Hotelling-Lawley trace	7.5139	2.0000	57.0000	214.1464	0.0000
Roy's greatest root	7.5139	2.0000	57.0000	214.1464	0.0000

Groups

Statistic	Value	Num DF	Den DF	F Value	Pr > F
Wilks' lambda	0.4469	2.0000	57.0000	35.2780	0.0000
Pillai's trace	0.5531	2.0000	57.0000	35.2780	0.0000
Hotelling-Lawley trace	1.2378	2.0000	57.0000	35.2780	0.0000
Roy's greatest root	1.2378	2.0000	57.0000	35.2780	0.0000

Figure 5Bii

Hartigan's Dip Test

Group = 0.02	Dip: 0.009486760618999735, p-value: 0.8508515610979599
Group = 0.03	Dip: 0.009459508382413 83, p-value: 0.8542947209214838
Group = 0.04	Dip: 0.007245477193895223, p-value: 0.9916346911182579
Group = 0.05	Dip: 0.04902727113400673, p-value: 0.0
Group = 0.06	Dip: 0.06340660293635085 , p-value: 0.0
Group = 0.07	Dip: 0.07763692009768237, p-value: 0.0
Group = 0.08	Dip: 0.10368876232850613, p-value: 0.0
Group = 0.09	Dip: 0.10790718316624762, p-value: 0.0

continued suppl. Tbl. S2 – Statistical summaries.

Fig. S8B During Approach

MANOVA

Intercept

Statistic	Value	Num DF	Den DF	F Value	Pr > F
Wilks' lambda	0.0450	2.0000	72.0000	763.7361	0.0000
Pillai's trace	0.9550	2.0000	72.0000	763.7361	0.0000
Hotelling-Lawley trace	21.2149	2.0000	72.0000	763.7361	0.0000
Roy's greatest root	21.2149	2.0000	72.0000	763.7361	0.0000

Groups

Statistic	Value	Num DF	Den DF	F Value	Pr > F
Wilks' lambda	0.9807	2.0000	72.0000	0.7087	0.4957
Pillai's trace	0.0193	2.0000	72.0000	0.7087	0.4957
Hotelling-Lawley trace	0.0197	2.0000	72.0000	0.7087	0.4957
Roy's greatest root	0.0197	2.0000	72.0000	0.7087	0.4957

Fig. S8B After Collision

MANOVA

Intercept

Statistic	Value	Num DF	Den DF	F Value	Pr > F
Wilks' lambda	0.7068	2.0000	73.0000	15.1427	0.0000
Pillai's trace	0.2932	2.0000	73.0000	15.1427	0.0000
Hotelling-Lawley trace	0.4149	2.0000	73.0000	15.1427	0.0000
Roy's greatest root	0.4149	2.0000	73.0000	15.1427	0.0000

Groups

Statistic	Value	Num DF	Den DF	F Value	Pr > F
Wilks' lambda	0.9825	2.0000	73.0000	0.6493	0.5254
Pillai's trace	0.0175	2.0000	73.0000	0.6493	0.5254
Hotelling-Lawley trace	0.0178	2.0000	73.0000	0.6493	0.5254
Roy's greatest root	0.0178	2.0000	73.0000	0.6493	0.5254

Fig. S9A

MANOVA

Intercept

Statistic	Value	Num DF	Den DF	F Value	Pr > F
Wilks' lambda	0.9035	2.0000	31.0000	1.6558	0.2074
Pillai's trace	0.0965	2.0000	31.0000	1.6558	0.2074
Hotelling-Lawley trace	0.1068	2.0000	31.0000	1.6558	0.2074
Roy's greatest root	0.1068	2.0000	31.0000	1.6558	0.2074

Groups

Statistic	Value	Num DF	Den DF	F Value	Pr > F
Wilks' lambda	0.5580	2.0000	31.0000	12.2789	0.0001
Pillai's trace	0.4420	2.0000	31.0000	12.2789	0.0001
Hotelling-Lawley trace	0.7922	2.0000	31.0000	12.2789	0.0001
Roy's greatest root	0.7922	2.0000	31.0000	12.2789	0.0001

Fig. S9B

MANOVA

Intercept

Statistic	Value	Num DF	Den DF	F Value	Pr > F
Wilks' lambda	0.5820	2.0000	35.0000	12.5666	0.0001
Pillai's trace	0.4180	2.0000	35.0000	12.5666	0.0001
Hotelling-Lawley trace	0.7181	2.0000	35.0000	12.5666	0.0001
Roy's greatest root	0.7181	2.0000	35.0000	12.5666	0.0001

Groups

Statistic	Value	Num DF	Den DF	F Value	Pr > F
Wilks' lambda	0.8453	2.0000	35.0000	3.2025	0.0528
Pillai's trace	0.1547	2.0000	35.0000	3.2025	0.0528
Hotelling-Lawley trace	0.1830	2.0000	35.0000	3.2025	0.0528
Roy's greatest root	0.1830	2.0000	35.0000	3.2025	0.0528

GENERAL DISCUSSION

GENERAL RELEVANCE OF THE THESIS

Throughout the duration of my PhD research, me and my colleagues elucidated how personal performances and preferences, as well as sensory processing of individual insects is context dependent and can be reshaped, even overwritten, by naturalistic social conditions. Those conditions range from total isolation, through the cues of a small group of conspecifics, to the cohesive movement within gigantic swarms. By using electrophysiology and by establishing calcium imaging of projection neurons (PNs) in the antennal lobes (ALs) of both species, we managed to monitor spatio-temporal neural activity in olfactory pathways in relation to different stimulations, which insects experience during isolation and while navigating in groups. The physiological observations were complemented with behavioral experiments carried out in the field, in an open environmental arena, or in a well-controllable virtual reality setup.

We discovered that the behavioral and neuronal modulation is especially prominent in highly social, group living individuals, in which sensory perception is both a component of the display of social behavior, and a target of modification by interactions with conspecifics. Furthermore, we found that, through synergistic and inhibitory interactions, social olfactory cues in both species were capable of modulating neuronal response motifs to food odors across the AL. Our results highlight that American cockroaches and gregarious desert locusts are strongly influenced by public sensory cues, with olfaction playing a crucial role during food perception in both species and vision being the pivotal modality for collective alignment and motion in locusts.

This suggests that individuals actively weigh up multimodal sensory input in a context-dependent manner, dynamically prioritizing the most relevant and best suited sensory input for a particular behavior. This gives cockroaches and locusts the flexibility to adapt to varying degrees of social context and personal experiences, as well as to a wide, unpredictable array of environmental conditions.

HEMIMETABOLOUS INSECTS

In contrast to holometabolous insects, which significantly differ in their sensory systems, morphologies, and ecological niches before and after metamorphosis, hemimetabolous locusts

and cockroaches mature through a series of wingless nymphal stages that resemble the adult stage. This is accompanied by a well-developed and perfectly functioning olfactory system in the hatchlings of both cockroaches (Prillinger, 1981) and locusts (Sun et al., 2024). While the number of neurons remains constant in cockroaches (Chambille & Rospars, 1985), the development in locusts is accompanied by a slight increase in the number of glomeruli and olfactory receptor neurons (ORNs) that converge on the constant number of neurons in the growing AL (Anton et al., 2002). For comparison, holometabolous sphinx moth *Manduca sexta* or honeybee *Apis mellifera* only feature a small, rudimentary larval antennal center that gradually develops into the fully functioning, adult AL during pupation (Masson & Arnold, 1984; Oland & Tolbert, 1996).

In the experiments described in *Chapter 1* and *2*, we conducted calcium imaging on adult cockroaches and locusts. However, due to the strong tendency of adult locusts to fly, and their reluctancy to walk, we had to perform all behavioral locust experiments of *Chapter 2* and *3* with individuals in the final nymphal stage, assuming that the functional architecture, including odor coding and neural dynamics in nymphs, closely resemble those of adults. Encouragingly, recent research on the odor coding across locusts' developmental stages corroborates our assumption that the organization, the neuronal morphology and tuning, the response dynamics, as well as the odor-evoked activation patterns in ORNs, local interneurons (LNs) and PNs, remain consistent and stable throughout the ageing process in locusts (Jiang et al., 2024; Sun et al., 2024). Although there are minor differences in hatchlings, such as fewer spike generation in PNs during spontaneous activity and odor exposure - possibly resulting from increased activity of inhibitory gamma-aminobutyric acid (GABA)-ergic interneurons – both hatchling and adult PNs exhibit similar odor-induced excitatory and inhibitory responses and oscillatory synchrony. Furthermore, LNs in both stages of maturity show similar physiological odor response patterns (Sun et al., 2024).

SPECIES-SPECIFIC ADAPTATIONS

To our surprise, the cockroaches and the gregarious locusts described in *Chapter 1* and *2*, respectively exhibited opposing responses to a combination of conspecifics and appetitive cues, which, at first glance, seemed counterintuitive. Why would social cockroaches, even in the absence of alternative food sources, prefer an empty shelter over one signaling both conspecific presence and food, whereas social, gregarious locusts are most attracted to this specific combination? And why would gregarious locusts ignore a promising, untouched food

source in favor of one which is surrounded by - possibly cannibalistic - competitors? Upon closer examination, however, these contrasting behaviors align well with the distinct ecological demands, environmental pressures, and social strategies of the two species.

Cockroaches form elaborate social structures, even facing ‘isolation syndromes’ when kept alone (Lihoreau et al., 2009). This behavior should make us assume that there was a strong attraction towards a shelter that indicates the simultaneous presence of food and conspecifics. Indeed, cockroaches do utilize conspecifics’ cues to locate food sources and benefit from socially transmitted information about resource availability. However, residing in groups comes along with costs, such as the risk of reduced individual growth rate (Wharton et al., 1968), overexploitation, food depletion or disease transmission (Mond & Pietri, 2023). The findings presented in *Chapter 1*, namely, that cockroaches avoid food associated cues when combined with sufficiently high concentrations of social odor, are consistent with these costs. Hence, when alternative food sources might be accessible, or when cockroaches are sufficiently satiated, solitary foraging may be more advantageous. This reflects the trade-off between maximizing the exchange of social information with conspecifics and the maximization of the efficiency of individual foraging and suggests that the olfactory system of cockroaches is well adapted to mediate and balance their food-searching strategies to achieve optimal results.

On another note, all our experiments were conducted during daytime, which coincides with the resting phase of cockroaches. It might be an interesting idea to conduct experiments at night, when individuals are naturally more active and might be strongly motivated to forage. This could shift their behavioral priority towards food acquisition and might influence the attraction towards the shelter that is scented with a mixture of vanillin and conspecifics cues.

Comparing the ecological needs and lifestyles of cockroaches and gregarious locusts reveals pronounced differences in their group strategies. Gregarious locusts live in highly mobile, synchronized groups, where individuals profit from the protective and ecological benefits of swarm membership. Losing connection to their alliances can leave an individual isolated, making it an easy target for predators and increasing its likelihood of mortality in harsh or resource-scarce environments. For such locusts, maintaining proximity to the swarm and tuning their senses to it is, therefore, far more essential to survival than engaging in solitary foraging adventures. The olfactory tuning, together with the visual adaptations to large groups, described in *Chapter 3*, supports successful food detection capabilities and marching behavior, while the locust remains immersed in the complex, olfactory noisy and visually complex swarm environment.

Comparative behavioral and neuronal experiments in solitary locusts support these findings. Solitary individuals can rely on their camouflage abilities and solitary behavior, and the sudden appearance of cannibalistic conspecifics would disrupt their strategies, which are fine-tuned for predator avoidance and independent foraging. Hence, for solitary locusts, the sensory and behavioral adaptations, which cause them to avoid the combination of social and food cues, are indeed ecologically sensible, and are accompanied by increased sensitivity and less developed higher sensory integration centers (Ott & Rogers, 2010).

SENSORY PROCESSING IN NATURAL ENVIRONMENTS

Animals did not evolve to perceive isolated, quantified odorants in sterile laboratory conditions. Instead, they are immersed in chemically rich environments, where a multitude of volatile compounds, such as the scent of food, conspecifics, predators, or the surrounding habitat are constantly released, diluted, dispersed, and intermingled. These olfactory signals fluctuate across space and time and often coincide with additional sensory stimuli, including visual, auditory, mechanosensory, or thermal cues. The ability to detect, process, filter, and prioritize relevant information within this noisy sensory background can be critical for survival. Throughout this thesis, we highlight that insects, such as cockroaches and locusts, integrate multimodal signals and rely heavily on their sense of smell during some ecologically relevant decisions. To master the challenge of decoding and extracting relevant olfactory information, insects exhibit exceptionally efficient and flexible olfactory systems.

ORNs, located in the sensilla of the antennae, express odorant receptors (ORs) that differ in their odor affinity and specificity. They range from narrowly tuned receptors with a high degree of selectivity for odors of exceptional - often sexual - importance, to broadly tuned receptors, which detect a large range of chemical odorants (Hansson & Stensmyr, 2011; Wicher & Miazzi, 2021).

For example, certain ORs in the mosquito *Aedes aegypti* are narrowly tuned to just a few components of the human scent, with signals being relatively insensitive to inhibitory cross-interactions. However, the majority of the around 300 human-emitted volatiles are detected, by the mosquito, via combinatorial coding, whereby an odorant activates specific ORN, and thus glomerular subset. Importantly, some mosquito ORNs express several ORs, thereby breaking the canonical one-receptor-per-neuron rule (Carey et al., 2010). It is noteworthy that mosquitoes display a sophisticated, multimodal sensory integration along hierarchically valued sensory channels, which rely not only on body odors during host tracking (Gibson & Torr,

1999; McMeniman et al., 2014). Rather, long-range host tracking starts with the detection of intermittently released carbon dioxide (CO2) from exhaled breath, which initiates upwind flight behavior and enhances sensitivity to visual and additional olfactory stimuli (Turner et al., 2011; Vinauger et al., 2019). At intermediate distances, mosquitoes orient themselves towards high-contrast visual objects (Van Breugel et al., 2015), which are subsequently integrated with proximal cues that include moisture, body temperature, and infrared radiation for final host identification and landing (Chandel et al., 2024).

In fact, with a few exceptions of labeled line coding, the olfactory system of all insects mainly relies on combinatorial ORN ensemble activation, which terminate in the AL glomeruli. This combinatorial activation is achieved in that the ORNs synapse onto PNs and LNs, such that odorant detection creates a spatial, mosaic-like activation pattern that reflects odor identity (Galizia & Menzel, 2001). Increasing odor concentration recruits additional ORNs and glomeruli, while intensity is encoded in the oscillatory firing (Ito et al., 2009; Raccuglia et al., 2016).

At this point, it is critical to emphasize the temporal coding capabilities of the olfactory system, which will be done with special focus on locusts. While locust PNs exhibit high spontaneous activity (Moreaux & Laurent, 2007), their odor-evoked firing becomes transiently synchronized into oscillatory bursts, which are driven by coordinated input from ORNs and shaped by inhibitory GABAergic LNs (MacLeod & Laurent, 1996; Stopfer et al., 2003). Those LNs synapse onto PNs, other LNs, and sometimes directly onto ORNs (Wilson, 2013). Oscillatory PN synchrony in locusts and other insects enables gain control by sharpening the contrast, allows a better discrimination through enhanced signal-to-noise ratios and a better decorrelation of overlapping odor representations (Assisi & Bazhenov, 2012; MacLeod & Laurent, 1996; Olsen & Wilson, 2008; Stopfer et al., 2003; Wilson & Laurent, 2005). Together with odor identity and intensity (Stopfer et al., 2003), those dynamic signals also encode the rate of change of odor concentrations (Kim et al., 2015).

Such combination of spatial and temporal olfactory coding is an essential feature, which allows locusts and other insects to distinguish overlapping odor plumes and fast-changing olfactory stimuli in their natural environment. As the olfactory signals propagate to higher-order brain centers such as mushroom body (MB) and lateral horn (LH), the PN input is transformed into a sparse, high-content code, which enables selective filtering, memory formation, or context-dependent immediate behavioral responses (Christensen & Hildebrand, 1997; Laurent & Naraghi, 1994; Perez-Orive et al., 2002).

In cockroaches, the rhythmic oscillatory dynamics have been described, but are less well-characterized than in locusts. What we know, however, is that the odorant discrimination starts already at their exceptionally long antennae and also relies on spatiotemporal mechanisms. The ORNs from different antennal segments terminate in distinct glomerular regions within the cockroach AL, with stimuli applied to proximal antennal regions evoking earlier and stronger neural responses compared to distal stimuli. Furthermore, it is known that responses are concentration-dependent and odorants with similar chemical properties activate overlapping glomerular regions, which indicates that the chemical identity is also encoded spatially (Paoli et al., 2020).

Besides the spatial arrangement, information about odor concentration changes is formed by a dynamic, concentration-sensitive code, where 'ON' ORNs preferentially respond to rising concentrations, while 'OFF' ORNs respond during decreasing concentrations (Tichy et al., 2023). ORN input in cockroaches is relayed to a macroglomerular sex-pheromone complex or ordinary glomeruli and transformed into a complex temporal firing of a smaller population of PNs, with specific PNs exhibiting consistent increases or decreases in spike frequency during odor stimulation. This results in the encoding of odor identity and, possibly, temporal odor dynamics (Lemon & Getz, 2000). Additionally, mixture separation and temporal resolution is improved through two functionally different types of uniglomerular PNs, which originate from different glomerular groups and target spatially segregated areas in the MB and LH (Watanabe et al., 2017).

While those studies in locusts and cockroaches reveal the complexity of extracting olfactory signals and emphasize the temporal dynamics of odor coding, our own calcium imaging experiments presented in *Chapter 1* and *2*, are inherently constrained by the temporal resolution of this method and calcium signals can only serve as a proxy for neuronal activity. Calcium indicators visualize the intracellular calcium transients and thus only indirectly reflect the electrical spiking activity (Stringer & Pachitariu, 2019). The accurate estimation of the fast, complex firing dynamics of a neuron across the whole AL would require high-resolution 3D microscopy with minimal light-scattering, and computational techniques, such as temporal deconvolution, to reconstruct firing rates from calcium traces (Moreaux & Laurent, 2007; Yaksi & Friedrich, 2006).

Despite this, our analysis pipeline of *Chapter 2* enabled us to explore and analyse the spatial combinatorial coding together with the temporal dynamics of calcium transients in single planes of the AL, with prolonged but temporally varying odor responses of different

magnitudes in PN somata and various temporal response motifs and strengths, including fast rise and decay times at PN dendritic terminals. This suggests that cross-glomerular interactions and inhibitory shaping by LNs contribute to PN output and support the idea of a temporally refined, dynamic AL odor processing. In a next step, those inhibitory interactions could be assessed through the application of different GABA antagonists, which can block the activity of either fast inhibitory chloride channels ($GABA_A$) or slow, prolonged inhibition via G protein and second messenger ($GABA_B$) (Terunuma, 2018).

OLFACTORY NEUROMODULATION

Long-term rearing of over several generations in solitude or in gregarious conditions can greatly modify the plastic olfactory system of locusts in adaptive ways that perfectly fit the ecological demands. For example, long-term solitarious locusts house more sensilla on their antennae and have an improved food discrimination ability (Greenwood & Chapman, 1984; Ochieng et al., 1998). This is accompanied by a larger AL size relative to the brain volume and the midbrain in comparison to their gregarious counterparts (Ott & Rogers, 2010). Nevertheless, the total brain size, including higher-order brain centers such as LH and MBs, in gregarious animals exceeds the one of solitary locusts (Burrows et al., 2011; Ott & Rogers, 2010). Notably, apart from slight functional tuning differences, the gross AL PN anatomy barely differs between the gregarious and solitarious phase (Anton et al., 2002).

Excitingly, our experiments described in *Chapter 2* demonstrate striking differences in odor-evoked responses between the two phases, and highlight the plasticity of the locust's nervous system. This was observed despite the fact that our animals did not undergo several generations of long-term social exposure or deprivation. Instead, all individuals derived from a common F0 generation and differed only in whether they had experienced egg separation and solitary development or constant crowding. It is well known that behavioral modifications in solitarious locusts, such as increased tendency to approach conspecifics, can be induced after as little as four hours of crowding (Rogers et al., 2014). Such rapid shifts are important for a fast adaptation and swarm formation when the environmental conditions are favorable; however, the immediate mechanisms involved in olfactory odor processing remain speculative.

In our setup, the nonlinear, synergistic interactions between food-related odors and social signals in the brain of gregarious locusts must arise in the AL, because antennograms lacked signal distortions upon odor exposure between the two phases. In locusts, ORN terminals release excitatory acetylcholine (Ach), with acts on dendrites of cholinergic PNs and

predominantly GABA-ergic, modulatory LNs. These LNs span the whole AL, allowing global inhibition and spatially targeted lateral interactions (Bergmann & Bicker, 2021; Warren & Kloppenburg, 2014). In the insect brain, LNs form synapses primarily with PNs, but also with other LNs, and occasionally ORNs, in order to enhance contrast and control timing and oscillatory synchronization (Assisi & Bazhenov, 2012; Christensen et al., 1998; Sachse & Galizia, 2002). Furthermore, LNs are capable of synthesizing neurotransmitters and modulators (Berg et al., 2007; A. Das et al., 2011; Fusca & Kloppenburg, 2021).

In the social context, the adjustment of olfactory responses to appetitive odors in PNs likely involves a highly complex interplay between multiple neuronal mechanisms that are triggered by hormones, neurotransmitters, or neuropeptides. Using high performance liquid chromatography, Rogers et al. identified several neurotransmitters and neuromodulators, which differ in their quantity between the solitarious and gregarious locust phase (Rogers et al., 2004). Among them, serotonin exhibited a particularly strong increase - in the thoracic ganglia of *Schistocerca gregaria* - after only four hours of crowding, followed by elevated levels of serotonin in the brain and optic lobes after twenty-four hours. The titer decreased again upon long-term gregariousness. In addition to the rise in serotonin, octopamine began to rise in the optic lobes and thorax, together with tyramine, after a minimum of twenty-four-hours of crowding. In contrast, long-term solitary desert locusts showed elevated levels of glutamate and dopamine. However, the latter (dopamine) also rose during crowding, and, at the same time, initiated solitarious-like behavior upon injection, which indicates a multifaceted, context dependent role (Alessi et al., 2014; Rogers et al., 2004).

Although research about the mechanistic processes of synergistic olfactory neuromodulation in the locusts' brain is limited, comparative insights from locusts and other species provide a basis for informed speculations. As serotonin in the thoracic ganglia plays a central role in crowding-induced gregarization in desert locusts, it is one of the candidates which might be involved in the modulation of olfactory processing in the AL, which we observed in *Chapter 2*. Serotonergic input to the AL arises from extrinsic neurons, with cell bodies located in the protocerebrum that arborize across most or all glomeruli (Homberg & Müller, 1999; Ignell et al., 2001). This architecture supports broad modulatory functions and aligns with recent findings regarding the fine-tuning in the peripheral nervous system of locusts. There, serotonergic input potentially regulates GABAergic mechanisms, providing negative feedback to ORN activity at high odor concentrations (Lv et al., 2023). Importantly, it has recently been shown that serotonin increases the overall PN responses and shapes behavioral output in a

valence-dependent manner, in that it increases the responses to innate appetitive odors, while suppressing responses to aversive or neutral odors (Bessonova & Raman, 2023).

In the particular example of the moth *Manduca sexta*, it is known that the application of serotonin enhances glomerular responses by increasing firing rates and response durations. This leads to an increased sensitivity to some odorants, which, accordingly, can be better discriminated (Dacks et al., 2008). Importantly, in the same species of moth, low serotonin concentrations can suppress PN odor responses and enhance the activity of inhibitory LNs, indirectly resulting in reduced ORN terminal neurotransmitter release (Kloppenburg & Hildebrand, 1995). It has also been shown that with *Drosophila*, serotonin enhances flexible AL PN sensitivity and response intensity in some glomeruli. Further, serotonin is involved in the odorant-specific response modulation and suppression via enhanced inhibitory LN responses (Dacks et al., 2009; Lv et al., 2023). On the other hand, another study on *Drosophila* found a global PN odor response suppression though endogenous serotonin (Zhang & Gaudry, 2016). On a behavioral level, the injection of serotonin enhances arousal behavior such as aggression and courtship in invertebrates, and, for example, can renew fighting motivation in decapod crustaceans (Huber et al., 1997).

Those findings support the assumption that elevated serotonin levels may contribute to the valence-based amplification of olfactory responses, particularly by enhancing neural sensitivity to innately attractive food odors in the presence of social olfactory cues. This amplification of olfactory responses may occur through modulation of the AL circuitry, such as disinhibition, or through increased PN excitability, while suppressing non-relevant or aversive odor responses.

Besides serotonin, there are other possible and prominent neuromodulators, which are involved in physiological and behavioral processes of the phase transition, and which might contribute to a context-dependent neuromodulation; such as octopamine and dopamine. What is known is that octopamine, which is unique to invertebrates, fulfils neuromodulatory, neurotransmitting, and neurohormonal functions. It is involved in modulatory olfactory processes through inhibitory LNs in the AL (Sinakevitch et al., 2013), plays a critical role in associative olfactory learning (Hammer & Menzel, 1998; Sinakevitch et al., 2013), and enhances olfactory processing in an odor- and glomerulus-specific manner (Roeder, 2005). For example, in the silkworm *Bombyx mori*, octopamine increases sensitivity specifically to pheromone components (Pophof, 2002). In the locust nervous system, octopaminergic dorsal unpaired median neurons project, among others, from the suboesophageal ganglion to the AL (Duch et

al., 1999). It is further known that octopamine, together with tyramine, enhances dynamic action (Goosey & Candy, 1980), and modulates and controls mechanisms such as the activity of flight muscles, the sensory input, or learning and memory (Verlinden et al., 2010).

Dopaminergic neurons mediate aversive learning (Aso et al., 2010) and arborize in the AL (Dacks et al., 2012), which suggests potential input to the olfactory processing mechanisms. In the moth *Manduca sexta*, dopamine amplifies odor-evoked responses in most AL output neurons, while it decreases responses in a small subpopulation of neurons (Dacks et al., 2012). In *Drosophila*, dopamine modulates responses to pheromones (Keleman et al., 2012). In the migratory locust, on the other hand, dopamine modulates olfactory-driven social behavior through the dopaminergic receptor Dop1, which is expressed in higher-order processing centers such as the MBs and is involved in the regulation of conspecific olfactory attraction (Guo et al., 2018).

Besides a vast variety of neuropeptides, which are implicated in the neurobiology of the phase-transition in locusts (Hou et al., 2015; Schoofs et al., 1997), nitric oxide (NO) has also emerged as an important neuronal signaling molecule in the MB and AL. In the AL, NO is regulated by neuropeptides, synthesized by LNs (Elphick et al., 1995), and functions as a co-transmitter in GABAergic circuits, contributing to the interglomerular integration and modulation of olfactory input (Seidel & Bicker, 1997).

Unlike locusts, cockroaches do not exhibit any kind of phase polyphenism. Hence, the olfactory neuromodulation, which we discovered in the calcium imaging experiments of *Chapter 1*, was context-dependent, rather than both context- and phase-specific. Instead of long-term genetic or epigenetic neurochemical shifts that are driven by the density of the population, olfactory modulation in cockroaches appears to operate through transient mechanisms that are depending on the internal state and immediate environment of an individual. The altered odor-driven response profiles and weakened activity to food odors in the presence of the smell of conspecifics suggest fast neuromodulatory adjustments in the AL circuitry. Here, classical neurotransmitters likely shape the core excitatory and inhibitory odor coding, most probably via LN-mediated glomerular crosstalk between pheromone-sensitive and food-responsive PN dendrites within the glomeruli. In addition, biogenic amines such as serotonin (Salecker & Distler, 1990), octopamine, and tachykinin (Jung et al., 2013), could further integrate the internal state of the animal to mediate the context-dependent changes in olfactory responsiveness and allow animals to integrate social and motivational contexts.

ADVANCING FUNCTIONAL IMAGING

Before calcium imaging in the locust brain was available, recordings from the highly complex, arborized and interconnected olfactory system of locusts (Ignell et al., 2001) were largely limited to electrophysiological approaches (Cui et al., 2011; Wegener et al., 1993). Nevertheless, those methods provided crucial information about dynamic population coding within targeted neuronal ensembles in locusts, revealing, for instance, the oscillatory synchrony between AL neurons and downstream MB regions (Laurent & Davidowitz, 1994), or the precise timing, coordination and signal propagation of olfactory signals across the circuit (Broome et al., 2006; Perez-Orive et al., 2002; Stopfer et al., 1997). More recently, researchers began to correlate population-level neuronal activity with behavioral outcomes in locusts (Ling et al., 2023). Calcium imaging in locusts at that time, though restricted to single neurons, was pioneered by Moreaux and Laurent, who combined intracellular recordings with dye-filling, in order to study the temporal *in vivo* dynamics of single PNs and to link spike output to calcium transients (Moreaux & Laurent, 2007). Their work allowed subsequent *in vivo* and *in vitro* functional imaging studies, including the one of Bergmann and Bicker, who characterized locust AL neurons and their neurotransmitters in cell cultures by measuring calcium responses (Bergmann & Bicker, 2021).

Enabled through the transgenic insertion of genetically encoded calcium indicators, by the time of starting my PhD, *in vivo* calcium imaging of olfactory circuits had long been elaborated and was routinely employed as standard approach for the investigation of olfactory processing in *Drosophila melanogaster* or *Apis mellifera* (Galizia & Vetter, 2004; Mahabir & Sandquist, 2024; Sandoz, 2011; Wang et al., 2003), and a few non-model organisms as, for instance, ants (Hart et al., 2023) and mosquitos (Bui et al., 2019).

With the goal of dissecting and comparing the network-wide olfactory activation patterns and temporal dynamics of the entire locust AL across individuals over extended time periods, we had to expand the calcium imaging methodology in locusts to a level which we had already reached in cockroaches of *Chapter 1* (Günzel et al., 2021; Paoli et al., 2020, 2017). Accordingly, a tremendously frustrating and tedious, yet ultimately rewarding challenge during my time as PhD student was the development of an *in vivo* calcium imaging protocol to target large proportion of PNs in the locust AL.

After numerous trials which involved various locust maturation stages, injection sites, calcium indicators, incubation times and ambient conditions, we were the first group who established a robust and reproducible protocol for *in vivo* AL PN calcium imaging in the AL of *Schistocerca gregaria*. The methodological advancement, in which we retrogradely backfilled PNs with calcium indicator Cal-520 from the calyces of the MBs represents a cost-effective and technically accessible alternative to the use of genetically encoded calcium sensors. While genetic encoding of calcium indicators offers the elegant advantage of cell-specific targeting without the physical disturbance of neuronal structures or even direct or indirect feedback pathways from higher order brain centers, their application in non-model organisms such as locusts and cockroaches is extremely costly, time-consuming, and technically demanding. In contrast, our approach enabled stable, population-wide recordings of PN activity over extended time periods without the need for genetic manipulation in two species, which, at that time, lacked advanced genetic toolkits.

Our calcium imaging recordings were complemented by the development of the segmentation algorithm CalciSeg. CalciSeg is an unsupervised analysis pipeline for the automated – and thus unbiased - segmentation and quantification of calcium imaging data, which was created by my colleague and co-author Yannick Günzel. It is broadly applicable for the mapping of neuronal dynamics in heterogenous biological tissues of various species (Günzel et al., 2024).

While our study focused on the AL PN dynamics and innervation patterns in *Schistocerca gregaria*, recent research by Jiang et al. introduced a powerful, novel tool to gain insights into the spatial organization of odor-evoked AL activity in *Locusta migratoria* across developmental stages *in-vivo*. By employing the CRISPR/Cas9 mediated genome editing technology, their research team successfully generated the first transgenic locusts, which express the genetically encoded calcium-sensitive indicator protein GCaMP6s in the majority of ORNs under the control of the endogenous Orco promoter (Jiang et al., 2024). In this breakthrough work, they managed to combine high-resolution two-photon calcium imaging with precise genetic manipulation. They revealed chemotopic, ring-shaped olfactory activity patterns in the locust AL. Those contain information about the chemical identity and the ecological meaning, with responses to aromatic, social odors located in the outer layers and responses to aliphatic, food-related cues clustering around the central PN fiber.

GLOMERULAR ORGANIZATION IN LOCUSTS

The AL of locusts exhibits a unique, multiglomerular organization that significantly deviates from the arrangement found in many other insect taxa. That intricate architecture more closely resembles the one of the vertebrate olfactory bulb (Boeckh et al., 1990). It allows overlapping, distributed olfactory input, which might enable robust, combinatorial coding and better odor discrimination in complex swarms.

The recent study of Jian et al. (Jiang et al., 2024) and our findings in *Chapter 2* (Petelski et al., 2024) offer complementary insights from different angles into this system and enrich our understanding of olfactory processing in locusts. Jiang et al. demonstrated that ORNs in the locust AL encode chemical odor identity via conserved, ring-shaped spatial activation patterns, which are maintained across developmental stages. Those patterns reflect a stable topography and suggest early-stage odor categorization by AL ORNs.

Our study builds on those findings by imaging downstream PN activity at both dendritic and somatic levels. We confirmed that odors reliably evoke robust, reproducible combinatorial activation across individuals and glomeruli. Importantly, we further revealed that the odor-evoked responses can be dynamically modulated by the social context and differ between the two phases. Moreover, our automated analysis pipeline showed temporal dynamics and underscored the flexible, contextual modulation of odor signals. Together, these studies offer novel tools and insights for future exploration of sensory processing in the mysterious locust AL.

THE INFLUENCE OF INTERNAL STATE

It is clear that external ecological demands do influence sensory-guided behavior in locusts and cockroaches. However, it remains an open question whether and how their internal physiological state (i.e. circadian rhythm, mating status, age, or feeding state), which has been studied in many insect species (Gadenne et al., 2016), contributes to shaping the olfactory processing in dependence on the social context. Beyond the informational awareness of an animal, the internal parameters such as metabolic rate are often positively correlated with sociability. However, this link starts to weaken at a certain degree of food deprivation, as individuals must shift their behavioral priority and senses towards foraging (Killen et al., 2016). This change in preference is intuitively understandable from our own experience: after a long,

stressful day in the lab without a lunch break, we may head straight for a buffet when arriving at a birthday party, while momentarily ignoring our friends in favor of the food.

In insects, hunger and satiation are well-known modulators of behavior and neuronal activity. For example, starved *Drosophila* exhibit increased olfactory responsiveness of ORNs to attractive odors via insulin cues (Root et al., 2011) and short neuropeptide F (sNPF), which also promote food searching behavior in locusts and cockroaches through elevated expression levels in the brain (Tan et al., 2019) and midgut (Fadda et al., 2019). Furthermore, starvation in fruit flies sensitizes glomeruli that are wired for attraction through sNPF, and suppresses glomeruli attributed to aversion via tachykinin (Ko et al., 2015). Those processes, and the integration of hunger signals in the MB, which are relayed from Kenyon cells (KCs) to MB output neurons (Tsao et al., 2018), significantly promote food-search behavior in fruit flies. Food limitations in schooling fish lead to a larger value of nearest neighbor distance (Wilson et al., 2019) and to an increased food load size in worker ants (Josens & Roces, 2000). Locusts, which can regulate the intake of proteins, carbohydrates, salt, and water though modulated taste receptor responsiveness (Simpson & Raubenheimer, 2000), interrupt their collective movement with rising hunger levels (Dkhili et al., 2019). Instead of marching, individuals migrate toward the periphery of the group, causing dispersal, decreased density, and with that a negative feedback loop which counteracts gregarization (Georgiou et al., 2025) and enhances solitary food acquisition.

In our experimental procedures, cockroaches and locusts were starved overnight, prior to all calcium imaging and behavioral trials, to provide sufficient time for the dye to retrogradely label the PNs of the AL, and to increase the animal's activity levels. Performing calcium imaging in cockroaches and locusts under different degrees of starvation and satiation in future experiments might reveal direct, dynamic modification of the neuronal olfactory pathways. It would be highly interesting to record how hunger enhances the sensitivity or gain of olfactory circuits in the AL or how it alters the tuning of glomeruli responsive to appetitive odors through, for example, sNPF (Fadda et al., 2019), or hormones. AL LNs and PNs could shift their excitability or synaptic strength under neuropeptide regulation. On a behavioral level, starvation might cause a change in the salience of food-related cues and motivate individuals to look for food sources, even when those are accompanied by potentially aversive, conflicting social information. Great hunger might therefore drive cockroaches away from the empty shelter towards the one containing social and food cues and dissolve the preference of

gregarious and solitarious locusts for combined conspecific and food odor cues, and for pure food odor, respectively.

By comparing glomerular activity and stimulus discrimination with behavioral output under different starvation levels, the methods we developed, and which were described in *Chapters 1* and *2*, should make it possible to assess whether hunger reshapes the olfactory representation at an early processing level and, if so, whether those changes predict behavioral performance. The findings of such studies could be complemented with the study of higher-order brain centers, and combined with the visual, virtual reality experiments used in our study described in *Chapter 3*. If the above hypothesis were true, such studies could show that increased hunger interferes with the locust's willingness to align, thereby forcing them to switch from visually guided marching behavior towards olfactory led foraging.

A further study could directly test the attractivity of food odors under varying olfactory social context levels using the proboscis extension reflex (PER) paradigm. The PER assay is well established for appetitive olfactory conditioning, learning and responsiveness in insects, such as honeybees (Bitterman et al., 1983; Giurfa & Sandoz, 2012; Takeda, 1961), and was recently adapted for the maxillary palps of, for example, locusts (Simões et al., 2011) and cockroaches (Arican et al., 2020).

Other promising studies could be directed at further investigating the visual signal integration in cockroaches. The study described in *Chapter 1* was inspired by reports in the existing literature that cockroaches exhibited excellent olfactory learning capabilities, and primarily relied on olfaction for foraging-related decision making (Lihoreau & Rivault, 2011; Sakura & Mizunami, 2001). Our experiments could confirm that the presence of social odors suffices to evoke the same behavioral response as the real presence of conspecifics. However, cockroaches were found to associate visual cues with food (Durier & Rivault, 2002) and extract tactile cues gathered with their antennae (Okada & Toh, 2004). Hence follow-up studies could be directed at untangling the involvement of the multimodal information used in cockroaches, similar to what we did in locusts (see *Chapters 2* and *3*). For example, by repeating experiments under olfactory deprivation, while providing visual information in a manner comparable to our locust setup.

ECOLOGICAL IMPORTANCE OF STUDYING PEST SPECIES

Nearly every publication about locusts, including ours and the current thesis, emphasizes the immense, devastating impact of locust plagues. The hope being that advancing our

understanding might contribute to the creation of better targeted control measures. Unfortunately, despite all the ongoing research and progress regarding physiology, behavior, or swarm dynamics of locusts, we still lack sufficient knowledge or tools to develop truly effective, sustainable, and affordable strategies to fight them. Until now, there has been a strong sense of urgency surrounding the successful fight against locust swarms and the inhibition of their emergence, all without causing collateral damage to humans and the environment. Between 2018 and 2021, the Food and Agriculture Organization (FAO) recorded a major locust plague spreading from the Middle East, to Africa, and towards India and Pakistan. The plague was triggered by climate change, which caused rising sea surface temperatures and warming anomalies in the Indian Ocean Dipole. This resulted in cyclones and heavy localized rainfall and vegetation growth in the recession areas of the locust, the Arabian desert and Ethiopia, followed by localized, temporally synchronized breeding and the emergence of gregarious nymphs (Cai et al., 2009). During the infestation, 1.6 million hectares of land were sprayed from air and ground with over one million liters of pyrethroid insecticides and highly neurotoxic, broad-spectrum organophosphates, most of which are banned in the EU (Mullié et al., 2023).

The use of these substances resulted in far-reaching ecological harm, affecting innumerable species, including critically endangered, endemic grasshoppers (Hodjat et al., 2019), reptiles, and honeybees. The substantial honeybee mortality entailed a reduction in annual honey production of 78% in Ethiopia (Mullié et al., 2023). This was coupled with drastic pollination losses and long-lasting effects on honeybee longevity (Worku et al., 2022), which is detrimental for the human population.

Birds, being a major natural predator of locusts, also strongly suffer under organophosphates. Counts in Senegal showed a drop in the number of birds by 60% upon spraying (Mullie & Keith, 1993). Furthermore, broad-range insecticides in grasshopper control were found to significantly attenuate the interference capability of natural parasitoids and predators such as tenebrionid beetle larvae, which leads to an augmentation of locust populations in the coming year (Van der Valk et al., 1999). Long term effects of the chemical applications on the partly indigenous human residents, their livestock, and the entire ecosystem are still unclear, due to the remoteness and inaccessibility of affected areas. As a much safer, non-hazardous alternative, the application of the bio-insecticide fungus *Metarhizium acridum* showed promising results in the lab (Hu & Xia, 2019). However, its use in the field in Somalia revealed some unintended consequences, such as the eradication of rare grasshopper species (Hochkirch

& Bhaskar, 2021), or the development of resistance in locusts (Li & Xia, 2022). The experimental application of the toxin produced by fungus *Metarhizium anisopliae* in Mauritania led to logistical challenges during distribution because of its gel-like consistency.

During our field trip to Kenya in 2019, we witnessed firsthand the devastating impact of locust plagues and encountered the complexities of predicting locust behavior under natural conditions. A major challenge was to translate our findings from isolated, laboratory reared animals into effective, ecologically relevant, and field applicable control experiments. For instance, while gregarious locusts in our controlled lab arena eagerly tracked food odor cues, marching hoppers within the huge bands in the field did not abandon their conspecifics for a remotely placed appetitive odor. On top of that, as elaborated in *Chapter 3*, the locusts' alignment did not depend on the density of individuals, which contradicted classical assumptions derived from laboratory experiments in behavioral arenas. These contrasts underscore the limitations of translating the results from sterile, small-scale laboratory conditions to dynamic, natural field settings, where animals at varying behavioral states are embedded in the dynamics of migratory mass movement.

This emphasizes the need for an integrative approach to improve control technologies: - one that bridges neurophysiological and ecological findings with naturalistic environmental variability, internal state, behavioral plasticity, and social dynamics. Such an approach is essential for advancing our understanding of swarm biology and, at the same time, for designing field-effective control strategies. Unfortunately, at the time of writing this thesis, unfavorable, cold and steady weather conditions will still represent the most sustainable and effective means of controlling locust plagues.

FINAL THOUGHTS

Insects have a huge impact on the world, which ranges from catastrophic agricultural plagues to playing an essential role in the functioning of ecosystems. Nevertheless, they are often underestimated and considered simple, because of their miniature brains. In this thesis, I have shown that those tiny animals do, in fact, exhibit a remarkable capacity for complex behavioral performances and finely tuned sensory integration within elaborate social structures. The fact that insects are immersed in - and transformed by - fluctuating social systems (whether solitary or immersed in a group), creates paradoxical situations, namely the need to incorporate collective signals without losing individual adaptability and fitness.

By applying novel, interdisciplinary approaches in the laboratory and field, we followed the path from the modulation of individual olfactory preferences in cockroaches (*Chapter 1*), to social olfactory plasticity in locusts (*Chapter 2*), and finally to the dynamics of collective visual behavior in gigantic swarms (*Chapter 3*). This revealed that the sensory systems of individual locusts and cockroaches can be modulated to process and integrate multimodal social and personal information in an elaborate, context-sensitive manner that cannot be predicted by static, fixed physical rules. This flexibility in their neuronal pathways and behavior enables these species to navigate and respond to a multitude of different environmental challenges and social scenarios, which can range from social isolation to the collective dynamics of massive swarms.

These insights deepen our understanding of the role of conspecifics in shaping sensory processes and behavior. They also open up new avenues for exciting, interdisciplinary research that can expand upon our findings regarding olfactory coding, decision-making, communication, and adaptation across species.

AUTHOR CONTRIBUTIONS

CHAPTER 1

Jaclyn McCollum, Marco Paoli, and Einat Couzin-Fuchs designed the study; Jaclyn McCollum and Inga Petelski carried out behavioral and calcium imaging experiments; Marco Paoli and Giovanni Galizia guided calcium imaging; Yannick Günzel and Marco Paoli performed data analysis, curated data availability and reproducibility; Einat Couzin-Fuchs supervised overall data collection and analysis; All authors contributed to the final writing.

CHAPTER 2

Inga Petelski and Einat Couzin-Fuchs established the calcium imaging technique, deployed behavioral setups, and performed preliminary data evaluation; Inga Petelski set up odor protocols and extraction, carried out chemical analysis and neuroanatomical stainings, and acquired anatomical brain scans; Inga Petelski and Susanne Kraus conducted behavior experiments and bright field and confocal functional imaging with Sercan Sayin and Yannick Günzel providing technical advice; Yannick Günzel recorded EAG data, developed analysis models, analyzed data, created figures and wrote the first draft with Einat Couzin-Fuchs; All authors contributed to the final writing.

CHAPTER 3

Sercan Sayin and Iain D. Couzin wrote the original draft and conceptualized the project with Einat Couzin-Fuchs and Gregory A. Sword; Sercan Sayin, Chi-Yu Lee, and Iain D. Couzin conducted investigations and performed analysis together with Mohammad Salahshour, Jacob M. Graving, and Liang Li; Einat Couzin-Fuchs and Inga Petelski planned and carried out field trials; Inga Petelski visualized GPS locations and assessed field recordings; Sercan Sayin, Einat Couzin-Fuchs, Jacob M. Graving, and Iain D. Couzin developed methodology; Einat Couzin-Fuchs and Iain D. Couzin administered and supervised the project and acquired funding; Yannick Günzel, Jacob M. Graving, Liang Li, and Iain D. Couzin provided resources; Sercan Sayin and Jacob M. Graving visualized results and validated them with Yannick Günzel and Iain D. Couzin; All authors contributed to the final editing or review.

REFERENCES

Abraham, N. M., Egger, V., Shimshek, D. R., Renden, R., Fukunaga, I., Sprengel, R., Seeburg, P. H., Klugmann, M., Margrie, T. W., Schaefer, A. T., & Kuner, T. (2010). Synaptic Inhibition in the Olfactory Bulb Accelerates Odor Discrimination in Mice. Neuron, 65(3), 399–411. https://doi.org/10.1016/J.NEURON.2010.01.009/ATTACHMENT/FD8F0393-85A1-4DCD-81B6-2EFCB9F23FD1/MMC1.PDF

Abril-Pla, O., Andreani, V., Carroll, C., Dong, L., Fonnesbeck, C. J., Kochurov, M., Kumar, R., Lao, J., Luhmann, C. C., Martin, O. A., Osthege, M., Vieira, R., Wiecki, T., & Zinkov, R. (2023). PyMC: a modern, and comprehensive probabilistic programming framework in Python. PeerJ Computer Science, 9, e1516. https://doi.org/10.7717/PEERJ-CS.1516/FIG-10

Ache, B. W., & Young, J. M. (2005). Olfaction: diverse species, conserved principles. Neuron, 48(3), 417–430. https://doi.org/10.1016/j.neuron.2005.10.022

Aimon, S., Katsuki, T., Jia, T., Grosenick, L., Broxton, M., Deisseroth, K., Sejnowski, T. J., & Greenspan, R. J. (2019). Fast near-whole–brain imaging in adult Drosophila during responses to stimuli and behavior. PLOS Biology, 17(2), e2006732. https://doi.org/10.1371/JOURNAL.PBIO.2006732

Akerboom, J., Chen, T.-W., Wardill, T. J., Tian, L., Marvin, J. S., Mutlu, S., Calderón, N. C., Esposti, F., Borghuis, B. G., Sun, X. R., Gordus, A., Orger, M. B., Portugues, R., Engert, F., Macklin, J. J., Filosa, A., Aggarwal, A., Kerr, R. A., Takagi, R., … Looger, L. L. (2012). Optimization of a GCaMP calcium indicator for neural activity imaging. The Journal of Neuroscience : The Official Journal of the Society for Neuroscience, 32(40), 13819–13840. https://doi.org/10.1523/JNEUROSCI.2601-12.2012

Albin, S. D., Kaun, K. R., Knapp, J. M., Chung, P., Heberlein, U., & Simpson, J. H. (2015). A Subset of Serotonergic Neurons Evokes Hunger in Adult Drosophila. Current Biology, 25(18), 2435–2440. https://doi.org/10.1016/j.cub.2015.08.005

Alessi, A. M., O'Connor, V., Aonuma, H., & Newland, P. L. (2014). Dopaminergic modulation of phase reversal in desert locusts. Frontiers in Behavioral Neuroscience, 8(November), 371. https://doi.org/10.3389/FNBEH.2014.00371/ABSTRACT

Amé, J. M., Halloy, J., Rivault, C., Detrain, C., & Deneubourg, J. L. (2006). Collegial decision making based on social amplification leads to optimal group formation. Proceedings of the National Academy of Sciences of the United States of America, 103(15), 5835–5840. https://doi.org/10.1073/PNAS.0507877103

Ame, J. M., Rivault, C., & Deneubourg, J. L. (2004). Cockroach aggregation based on strain odour recognition. Animal Behaviour, 68(4), 793–801. https://doi.org/10.1016/J.ANBEHAV.2004.01.009

Amit, D. J. (1989). Modeling Brain Function: The World of Attractor Neural Networks. Modeling Brain Function. https://doi.org/10.1017/CBO9780511623257

Andersson, M. N., Löfstedt, C., & Newcomb, R. D. (2015). Insect olfaction and the evolution of receptor tuning. Frontiers in Ecology and Evolution, 3(MAY), 145054. https://doi.org/10.3389/FEVO.2015.00053/PDF

Anstey, M. L., Rogers, S. M., Ott, S. R., Burrows, M., & Simpson, S. J. (2009). Serotonin mediates behavioral gregarization underlying swarm formation in desert locusts. Science (New York, N.Y.), 323(5914), 627–630. https://doi.org/10.1126/SCIENCE.1165939

Anton, S., & Hansson, B. (1996). Antennal lobe interneurons in the desert locust Schistocerca gregaria (Forskal): Processing of aggregation pheromones in adult males and females.

Journal of Comparative Neurology. https://doi.org/10.1002/(SICI)1096-9861(19960617)370:1

Anton, S., Ignell, R., & Hansson, B. S. (2002). Developmental changes in the structure and function of the central olfactory system in gregarious and solitary desert locusts. Microscopy Research and Technique, 56(4), 281–291. https://doi.org/10.1002/JEMT.10032

Arganda, S., Pérez-Escudero, A., & De Polavieja, G. G. (2012). A common rule for decision making in animal collectives across species. Proceedings of the National Academy of Sciences of the United States of America, 109(50), 20508–20513. https://doi.org/10.1073/PNAS.1210664109

Arican, C., Bulk, J., Deisig, N., & Nawrot, M. P. (2020). Cockroaches Show Individuality in Learning and Memory During Classical and Operant Conditioning. Frontiers in Physiology, 10, 1539. https://doi.org/10.3389/FPHYS.2019.01539/FULL

Ariel, G., & Ayali, A. (2015). Locust Collective Motion and Its Modeling. In PLoS Computational Biology (Vol. 11, Issue 12). Public Library of Science. https://doi.org/10.1371/journal.pcbi.1004522

Aso, Y., Siwanowicz, I., Bräcker, L., Ito, K., Kitamoto, T., & Tanimoto, H. (2010). Specific dopaminergic neurons for the formation of labile aversive memory. Current Biology, 20(16), 1445–1451. https://doi.org/10.1016/j.cub.2010.06.048

Assisi, C., & Bazhenov, M. (2012). Synaptic inhibition controls transient oscillatory synchronization in a model of the insect olfactory system. Frontiers in Neuroengineering, 5(APRIL). https://doi.org/10.3389/FNENG.2012.00007,

Badel, L., Ohta, K., Tsuchimoto, Y., & Kazama, H. (2016). Decoding of Context-Dependent Olfactory Behavior in Drosophila. Neuron, 91(1), 155–167. https://doi.org/10.1016/J.NEURON.2016.05.022/ATTACHMENT/C02EF5D2-A534-4FFD-BC2F-224CA455C68C/MMC5.PDF

Barth-Maron, A., D'Alessandro, I., & Wilson, R. I. (2023). Interactions between specialized gain control mechanisms in olfactory processing. Current Biology, 33(23), 5109-5120.e7. https://doi.org/10.1016/J.CUB.2023.10.041/ATTACHMENT/171E82B0-FA5D-4423-A811-DF6B5D56FBB2/MMC3.PDF

Bazazi, S., Buhl, C., Hale, J. J., Anstey, M. L., Sword, G. A., Simpson, S. J., & Couzin, I. D. (2008). Collective motion and cannibalism in locust migratory bands. Current Biology : CB, 18(10), 735–739. https://doi.org/10.1016/J.CUB.2008.04.035

Beauchamp, G. (2011). Long-distance migrating species of birds travel in larger groups. Biology Letters, 7(5), 692. https://doi.org/10.1098/RSBL.2011.0243

Becco, C., Vandewalle, N., Delcourt, J., & Poncin, P. (2006). Experimental evidences of a structural and dynamical transition in fish school. Physica A: Statistical Mechanics and Its Applications, 367, 487–493. https://doi.org/10.1016/J.PHYSA.2005.11.041

Bell, W. J., Louis M. Roth, & Christine A. Nalepa. (2007). Cockroaches : ecology, behavior, and natural history.

Benton, R., Vannice, K. S., Gomez-Diaz, C., & Vosshall, L. B. (2009). Variant ionotropic glutamate receptors as chemosensory receptors in Drosophila. Cell, 136(1), 149–162. https://doi.org/10.1016/J.CELL.2008.12.001

Berg, B. G., Schachtner, J., Utz, S., & Homberg, U. (2007). Distribution of neuropeptides in the primary olfactory center of the heliothine moth Heliothis virescens. Cell and Tissue Research, 327(2), 385–398. https://doi.org/10.1007/S00441-006-0318-X,

Berg, L., Gerdey, J., & Masseck, O. A. (2020). Optogenetic Manipulation of Neuronal Activity to Modulate Behavior in Freely Moving Mice. Journal of Visualized Experiments : JoVE, 2020(164). https://doi.org/10.3791/61023

Bergmann, G. A., & Bicker, G. (2021). Cholinergic calcium responses in cultured antennal lobe neurons of the migratory locust. Scientific Reports, 11(1). https://doi.org/10.1038/s41598-021-89374-2

Berry, S. L., Beatty, W. W., & Klesges, R. C. (1985). Sensory and social influences on ice cream consumption by males and females in a laboratory setting. Appetite, 6(1), 41–45. https://doi.org/10.1016/S0195-6663(85)80049-0

Bessonova, Y., & Raman, B. (2023). Serotonergic amplification of odor-evoked neural responses maps onto flexible behavioral outcomes. ELife, 12. https://doi.org/10.7554/ELIFE.91890

Bhandawat, V., Olsen, S. R., Gouwens, N. W., Schlief, M. L., & Wilson, R. I. (2007). Sensory Processing in the Drosophila Antennal Lobe Increases the Reliability and Separability of Ensemble Odor Representations. Nature Neuroscience, 10(11), 1474. https://doi.org/10.1038/NN1976

Bisch-Knaden, S., Dahake, A., Sachse, S., Knaden, M., & Hansson, B. S. (2018). Spatial Representation of Feeding and Oviposition Odors in the Brain of a Hawkmoth. Cell Reports, 22(9), 2482–2492. https://doi.org/10.1016/J.CELREP.2018.01.082/ATTACHMENT/44373B66-AA25-4EC1-B184-22BDD106F969/MMC3.PDF

Bitterman, M. E., Menzel, R., Fietz, A., & Schäfer, S. (1983). Classical conditioning of proboscis extension in honeybees (Apis mellifera). Journal of Comparative Psychology (Washington, D.C. : 1983), 97(2), 107–119. https://doi.org/10.1037/0735-7036.97.2.107

Bleichman, I., Yadav, P., & Ayali, A. (2023). Visual processing and collective motion-related decision-making in desert locusts. Proceedings of the Royal Society B: Biological Sciences, 290(1991). https://doi.org/10.1098/rspb.2022.1862

Bliss, C. I. (1939). THE TOXICITY OF POISONS APPLIED JOINTLY1. Annals of Applied Biology, 26(3), 585–615. https://doi.org/10.1111/J.1744-7348.1939.TB06990.X

Boeckh, J., Distler, P., Ernst, K. D., Hösl, M., & Malun, D. (1990). Olfactory Bulb and Antennal Lobe. Chemosensory Information Processing, 201–227. https://doi.org/10.1007/978-3-642-75127-1_13

Bortolotti, L., & Costa, C. (2014). Chemical Communication in the Honey Bee Society. Neurobiology of Chemical Communication, 147–210. https://doi.org/10.1201/b16511

Bovet, P., & Benhamou, S. (1988). Spatial analysis of animals' movements using a correlated random walk model. Journal of Theoretical Biology, 131(4), 419–433. https://doi.org/10.1016/S0022-5193(88)80038-9

Bräcker, L. B., Siju, K. P., Arela, N., So, Y., Hang, M., Hein, I., Vasconcelos, M. L., & Grunwald Kadow, I. C. (2013). Essential role of the mushroom body in context-dependent CO2 avoidance in drosophila. Current Biology, 23(13), 1228–1234. https://doi.org/10.1016/j.cub.2013.05.029

Broome, B. M., Jayaraman, V., & Laurent, G. (2006). Encoding and Decoding of Overlapping Odor Sequences. Neuron, 51(4), 467–482. https://doi.org/10.1016/j.neuron.2006.07.018

Brown, S. L., Joseph, J., & Stopfer, M. (2005). Encoding a temporally structured stimulus with a temporally structured neural representation. Nature Neuroscience 2005 8:11, 8(11), 1568–1576. https://doi.org/10.1038/nn1559

Buhl, J., Sumpter, D. J. T., Couzin, I. D., Hale, J. J., Despland, E., Miller, E. R., & Simpson, S. J. (2006). From disorder to order in marching locusts. Science, 312(5778), 1402–1406. https://doi.org/10.1126/SCIENCE.1125142/SUPPL_FILE/BUHL.SOM.PDF

Buhl, J., Sword, G. A., & Simpson, S. J. (2012). Using field data to test locust migratory band collective movement models. Interface Focus, 2(6), 757–763. https://doi.org/10.1098/RSFS.2012.0024

Bui, M., Shyong, J., Lutz, E. K., Yang, T., Li, M., Truong, K., Arvidson, R., Buchman, A., Riffell, J. A., & Akbari, O. S. (2019). Live calcium imaging of Aedes aegypti neuronal tissues reveals differential importance of chemosensory systems for life-history-specific foraging strategies. BMC Neuroscience, 20(1), 1–17. https://doi.org/10.1186/S12868-019-0511-Y/FIGURES/4

Burrows, M., Rogers, S. M., & Ott, S. R. (2011). Epigenetic remodelling of brain, body and behaviour during phase change in locusts. Neural Systems & Circuits, 1(1). https://doi.org/10.1186/2042-1001-1-11

Burtt, E. T., & Uvarov, B. (1967). Grasshoppers and Locusts: A Handbook of General Acridology. Vol. 1. Anatomy, Physiology, Phase Polymorphism, Introduction to Taxonomy. Journal of Applied Ecology, 4(1), 261. https://doi.org/10.2307/2401426

Cai, W., Sullivan, A., & Cowan, T. (2009). Climate change contributes to more frequent consecutive positive Indian Ocean Dipole events. Geophysical Research Letters, 36(23). https://doi.org/10.1029/2009GL040163

Calvo Martín, M., Eeckhout, M., Deneubourg, J. L., & Nicolis, S. C. (2021). Consensus driven by a minority in heterogenous groups of the cockroach Periplaneta american a. Iscience, 24(7), 102723–102723. https://doi.org/10.1016/J.ISCI.2021.102723

Calvo Martín, M., Nicolis, S. C., Planas-Sitjà, I., & Deneubourg, J. L. (2019). Conflictual influence of humidity during shelter selection of the American cockroach (Periplaneta americana). Scientific Reports, 9(1). https://doi.org/10.1038/S41598-019-56504-W

Camazine, S., DENEUBOURG, J.-L., FRANKS, N. R., SNEYD, J., THERAULAZ, G., & BONABEAU, E. (2020). Self-Organization in Biological Systems. https://doi.org/10.2307/J.CTVZXX9TX

Canonge, S., Deneubourg, J. L., & Sempo, G. (2011). Group living enhances individual resources discrimination: the use of public information by cockroaches to assess shelter quality. PloS One, 6(6). https://doi.org/10.1371/JOURNAL.PONE.0019748

Canonge, S., Sempo, G., Jeanson, R., Detrain, C., & Deneubourg, J. L. (2009). Self-amplification as a source of interindividual variability: shelter selection in cockroaches. Journal of Insect Physiology, 55(11), 976–982. https://doi.org/10.1016/J.JINSPHYS.2009.06.011

Carey, A. F., Wang, G., Su, C. Y., Zwiebel, L. J., & Carlson, J. R. (2010). Odourant reception in the malaria mosquito Anopheles gambiae. Nature, 464(7285), 66. https://doi.org/10.1038/NATURE08834

Caron, S. J. C., Ruta, V., Abbott, L. F., & Axel, R. (2013). Random Convergence of Olfactory Inputs in the Drosophila Mushroom Body. Nature, 497(7447), 113. https://doi.org/10.1038/NATURE12063

Castro, D., Ruffier, F., & Eloy, C. (2024). Modeling collective behaviors from optic flow and retinal cues. Physical Review Research, 6(2). https://doi.org/10.1103/PHYSREVRESEARCH.6.023016

Catterall, W. A. (2011). Voltage-Gated Calcium Channels. Cold Spring Harbor Perspectives in Biology, 3(8), a003947. https://doi.org/10.1101/CSHPERSPECT.A003947

Chambille, I., & Pierre Rospars, J. (1985). Neurons and identified glomeruli of antennal lobes during postembryonic development in the cockroach Blaberus craniifer burm. (dictyoptera : blaberidae). International Journal of Insect Morphology and Embryology, 14(4), 203–226. https://doi.org/10.1016/0020-7322(85)90055-8

Chandel, A., DeBeaubien, N. A., Ganguly, A., Meyerhof, G. T., Krumholz, A. A., Liu, J., Salgado, V. L., & Montell, C. (2024). Thermal infrared directs host-seeking behaviour in Aedes aegypti mosquitoes. Nature 2024 633:8030, 633(8030), 615–623. https://doi.org/10.1038/s41586-024-07848-5

Chang, H., Cassau, S., Krieger, J., Guo, X., Knaden, M., Kang, L., & Hansson, B. S. (2023). A chemical defense deters cannibalism in migratory locusts. Science, 380(6644). https://doi.org/10.1126/SCIENCE.ADE6155/SUPPL_FILE/SCIENCE.ADE6155_DATA_S1_TO_S7.ZIP

Chang, H., Unni, A. P., Tom, M. T., Cao, Q., Liu, Y., Wang, G., Llorca, L. C., Brase, S., Bucks, S., Weniger, K., Bisch-Knaden, S., Hansson, B. S., & Knaden, M. (2023). Odorant detection in a locust exhibits unusually low redundancy. Current Biology, 33(24), 5427-5438.e5. https://doi.org/10.1016/J.CUB.2023.11.017/ATTACHMENT/6E579D67-E04F-48DA-B82C-AF6C6E16EDA6/MMC8.PDF

Charpak, S. (2001). Odor-evoked calcium signals in dendrites of rat mitral cells. Proceedings of the National Academy of Sciences, 98(3), 1230–1234. https://doi.org/10.1073/PNAS.021422798

Chen, T.-W., Wardill, T. J., Sun, Y., Pulver, S. R., Renninger, S. L., Baohan, A., Schreiter, E. R., Kerr, R. A., Orger, M. B., Jayaraman, V., Looger, L. L., Svoboda, K., & Kim, D. S. (2013). Ultrasensitive fluorescent proteins for imaging neuronal activity. Nature, 499(7458), 295–300. https://doi.org/10.1038/nature12354

Christensen, T. A., & Hildebrand, J. G. (1997). Coincident stimulation with pheromone components improves temporal pattern resolution in central olfactory neurons. Journal of Neurophysiology, 77(2), 775–781. https://doi.org/10.1152/JN.1997.77.2.775,

Christensen, T. A., Pawlowski, V. M., Lei, H., & Hildebrand, J. G. (2000). Multi-unit recordings reveal context-dependent modulation of synchrony in odor-specific neural ensembles. Nature Neuroscience, 3(9), 927–931. https://doi.org/10.1038/78840

Christensen, T. A., Waldrop, B. R., & Hildebrand, J. G. (1998). GABAergic mechanisms that shape the temporal response to odors in moth olfactory projection neurons. Annals of the New York Academy of Sciences, 855, 475–481. https://doi.org/10.1111/J.1749-6632.1998.TB10608.X,

Cisse, S., Ghaout, S., Mazih, A., Babah Ebbe, M. A. O., Benahi, A. S., & Piou, C. (2013). Effect of vegetation on density thresholds of adult desert locust gregarization from survey data in Mauritania. Entomologia Experimentalis et Applicata, 149(2), 159–165. https://doi.org/10.1111/eea.12121

Clifford, M. R., & Riffell, J. A. (2013). Mixture and odorant processing in the olfactory systems of insects: A comparative perspective. Journal of Comparative Physiology A: Neuroethology, Sensory, Neural, and Behavioral Physiology, 199(11), 911–928. https://doi.org/10.1007/S00359-013-0818-6/METRICS

Collett, M., Despland, E., Simpson, S. J., & Krakauer, D. C. (1998). Spatial scales of desert locust gregarization. Proceedings of the National Academy of Sciences of the United States of America, 95(22), 13052–13055. https://doi.org/10.1073/PNAS.95.22.13052/ASSET/4211262A-6C0E-4003-8D3C-549A9FCC8119/ASSETS/GRAPHIC/PQ2283077003.JPEG

Conradt, L., & Roper, T. J. (2005). Consensus decision making in animals. Trends in Ecology & Evolution, 20(8), 449–456. https://doi.org/10.1016/J.TREE.2005.05.008

Couto, A., Alenius, M., & Dickson, B. J. (2005). Molecular, anatomical, and functional organization of the Drosophila olfactory system. Current Biology, 15(17), 1535–1547. https://doi.org/10.1016/j.cub.2005.07.034

Couzin, I. D., & Couzin-Fuchs, E. (2023). The chemical ecology of locust cannibalism. Science (New York, N.Y.), 380(6644), 454–455. https://doi.org/10.1126/SCIENCE.ADH5264

Couzin, I. D., Ioannou, C. C., Demirel, G., Gross, T., Torney, C. J., Hartnett, A., Conradt, L., Levin, S. A., & Leonard, N. E. (2011). Uninformed individuals promote democratic

consensus in animal groups. Science, 334(6062), 1578–1580. https://doi.org/10.1126/SCIENCE.1210280/SUPPL_FILE/1210280.COUZIN.SOM.PDF

Couzin, I. D., Krause, J., Franks, N. R., & Levin, S. A. (2005). Effective leadership and decision-making in animal groups on the move. Nature, 433(7025), 513–516. https://doi.org/10.1038/nature03236

Couzin, I. D., Krause, J., James, R., Ruxton, G. D., & Franks, N. R. (2002). Collective memory and spatial sorting in animal groups. Journal of Theoretical Biology, 218(1), 1–11. https://doi.org/10.1006/jtbi.2002.3065

Cui, X., Wu, C., & Zhang, L. (2011). Electrophysiological response patterns of 16 olfactory neurons from the trichoid sensilla to odorant from fecal volatiles in the locust, Locusta migratoria manilensis. Archives of Insect Biochemistry and Physiology, 77(2), 45–57. https://doi.org/10.1002/ARCH.20420,

Cullen, D. A., Cease, A. J., Latchininsky, A. V., Ayali, A., Berry, K., Buhl, C., De Keyser, R., Foquet, B., Hadrich, J. C., Matheson, T., Ott, S. R., Poot-Pech, M. A., Robinson, B. E., Smith, J. M., Song, H., Sword, G. A., Vanden Broeck, J., Verdonck, R., Verlinden, H., & Rogers, S. M. (2017). From Molecules to Management: Mechanisms and Consequences of Locust Phase Polyphenism. Advances in Insect Physiology, 53, 167–285. https://doi.org/10.1016/BS.AIIP.2017.06.002

Dacks, A. M., Christensen, T. A., & Hildebrand, J. G. (2008). Modulation of olfactory information processing in the antennal lobe of Manduca sexta by serotonin. Journal of Neurophysiology, 99(5), 2077–2085. https://doi.org/10.1152/JN.01372.2007,

Dacks, A. M., Green, D. S., Root, C. M., Nighorn, A. J., & Wang, J. W. (2009). Serotonin modulates olfactory processing in the antennal lobe of drosophila. Journal of Neurogenetics, 23(4), 366–377. https://doi.org/10.3109/01677060903085722

Dacks, A. M., Riffell, J. A., Martin, J. P., Gage, S. L., & Nighorn, A. J. (2012). Olfactory modulation by dopamine in the context of aversive learning. Journal of Neurophysiology, 108(2), 539. https://doi.org/10.1152/JN.00159.2012

Dall, S. R. X., Giraldeau, L. A., Olsson, O., McNamara, J. M., & Stephens, D. W. (2005). Information and its use by animals in evolutionary ecology. Trends in Ecology and Evolution, 20(4), 187–193. https://doi.org/10.1016/

Dambach, M., & Goehlen, B. (1999). Aggregation density and longevity correlate with humidity in first-instar nymphs of the cockroach (Blattella germanica L., Dictyoptera). Journal of Insect Physiology, 45(5), 423–429. https://doi.org/10.1016/S0022-1910(98)00141-3

Das, A., Chiang, A., Davla, S., Priya, R., Reichert, H., VijayRaghavan, K., & Rodrigues, V. (2011). Identification and analysis of a glutamatergic local interneuron lineage in the adult Drosophila olfactory system. Neural Systems & Circuits, 1(1). https://doi.org/10.1186/2042-1001-1-4

Das Chakraborty, S., & Sachse, S. (2021). Olfactory processing in the lateral horn of Drosophila. Cell and Tissue Research, 383(1), 113. https://doi.org/10.1007/S00441-020-03392-6

Das, S., Sadanandappa, M. K., Dervan, A., Larkin, A., Lee, J. A., Sudhakaran, I. P., Priya, R., Heidari, R., Holohan, E. E., Pimentel, A., Gandhi, A., Ito, K., Sanyal, S., Wang, J. W., Rodrigues, V., & Ramaswami, M. (2011). Plasticity of local GABAergic interneurons drives olfactory habituation. Proceedings of the National Academy of Sciences of the United States of America, 108(36), E646-54. https://doi.org/10.1073/pnas.1106411108

Das, S., Trona, F., Khallaf, M. A., Schuh, E., Knaden, M., Hansson, B. S., & Sachse, S. (2017). Electrical synapses mediate synergism between pheromone and food odors in Drosophila melanogaster. Proceedings of the National Academy of Sciences of the

United States of America, 114(46), E9962–E9971. https://doi.org/10.1073/PNAS.1712706114

Datta, S. R., Vasconcelos, M. L., Ruta, V., Luo, S., Wong, A., Demir, E., Flores, J., Balonze, K., Dickson, B. J., & Axel, R. (2008). The Drosophila pheromone cVA activates a sexually dimorphic neural circuit. Nature, 452(7186), 473–477. https://doi.org/10.1038/NATURE06808,

Dawson, E. H., Bailly, T. P. M., Dos Santos, J., Moreno, C., Devilliers, M., Maroni, B., Sueur, C., Casali, A., Ujvari, B., Thomas, F., Montagne, J., & Mery, F. (2018). Social environment mediates cancer progression in Drosophila. Nature Communications 2018 9:1, 9(1), 1–7. https://doi.org/10.1038/s41467-018-05737-w

De Bruyne, M., Foster, K., & Carlson, J. R. (2001). Odor coding in the Drosophila antenna. Neuron, 30(2), 537–552. https://doi.org/10.1016/S0896-6273(01)00289-6

Despland, E., & Simpson, S. J. (2000). Small-scale vegetation patterns in the parental environment influence the phase state of hatchlings of the desert locust. Physiological Entomology, 25(1), 74–81. https://doi.org/10.1046/J.1365-3032.2000.00166.X

Despland, E., & Simpson, S. J. (2005). Food choices of solitarious and gregarious locusts reflect cryptic and aposematic antipredator strategies. Animal Behaviour, 69(2), 471–479. https://doi.org/10.1016/J.ANBEHAV.2004.04.018

Dillon, R. J., Vennard, C. T., & Charnley, A. K. (2001). A Note: Gut bacteria produce components of a locust cohesion pheromone.

Distler, P. (1989). Histochemical demonstration of GABA-like immunoreactivity in cobalt labeled neuron individuals in the insect olfactory pathway. Histochemistry, 91(3), 245–249. https://doi.org/10.1007/BF00490139

Distler, P. G., & Boeckh, J. (1997). Synaptic connections between identified neuron types in the antennal lobe glomeruli of the cockroach, Periplaneta americana: II. Local multiglomerular interneurons. Journal of Comparative Neurology, 383(4), 529–540. https://doi.org/10.1002/(SICI)1096-9861(19970714)383

Dkhili, J., Maeno, K. O., Idrissi Hassani, L. M., Ghaout, S., & Piou, C. (2019). Effects of starvation and Vegetation Distribution on Locust Collective Motion. Journal of Insect Behavior, 32(3), 207–217. https://doi.org/10.1007/S10905-019-09727-8/FIGURES/6

Doi, N., & Toh, Y. (1992). Modification of Cockroach Behavior to Environmental Humidity Change by Dehydration (Dictyoptera: Blattidae). In Journal of Insect Behavior (Vol. 5, Issue 4).

Donlea, J. M., & Shaw, P. J. (2009). Sleeping together using social interactions to understand the role of sleep in plasticity. Advances in Genetics, 68, 57–81. https://doi.org/10.1016/S0065-2660(09)68003-2

D'Orsogna, M. R., Chuang, Y. L., Bertozzi, A. L., & Chayes, L. S. (2006). Self-propelled particles with soft-core interactions: Patterns, stability, and collapse. Physical Review Letters, 96(10), 104302. https://doi.org/10.1103/PHYSREVLETT.96.104302/FIGURES/5/THUMBNAIL

Duch, C., Mentel, T., & Pflüger, H. J. (1999). Distribution and activation of different types of octopaminergic DUM neurons in the locust. Journal of Comparative Neurology, 403(1), 119–134. https://doi.org/10.1002/(SICI)1096-9861(19990105)403:1<119::AID-CNE9>3.0.CO;2-F,

Dunlap, A. S., Nielsen, M. E., Dornhaus, A., & Papaj, D. R. (2016). Foraging Bumble Bees Weigh the Reliability of Personal and Social Information. Current Biology : CB, 26(9), 1195–1199. https://doi.org/10.1016/J.CUB.2016.03.009

Durier, V., & Rivault, C. (2000). Learning and foraging efficiency in German cockroaches, Blattella germanica (L.) (Insecta: Dictyoptera). Animal Cognition, 3(3), 139–145. https://doi.org/10.1007/S100710000065/METRICS

Durier, V., & Rivault, C. (2002). Importance of spatial and olfactory learning on bait consumption in the German cockroach. https://doi.org/10.34894/VQ1DJA

Dussutour, A., Deneubourg, J. L., & Fourcassié, V. (2005). Amplification of individual preferences in a social context: The case of wall-following in ants. Proceedings of the Royal Society B: Biological Sciences, 272(1564), 705–714. https://doi.org/10.1098/rspb.2004.2990

Dyer, J. R. G., Ioannou, C. C., Morrell, L. J., Croft, D. P., Couzin, I. D., Waters, D. A., & Krause, J. (2008). Consensus decision making in human crowds. Animal Behaviour, 75(2), 461–470. https://doi.org/10.1016/J.ANBEHAV.2007.05.010

Edwards, T. N., & Meinertzhagen, I. A. (2010). The functional organisation of glia in the adult brain of Drosophila and other insects. Progress in Neurobiology, 90(4), 471–497. https://doi.org/10.1016/J.PNEUROBIO.2010.01.001

Ellis, P., & Ashall, C. (1957). Field Studies on diurnal Behaviour, Movement and Aggregation in the Desert Locust (Schistocerca gregaria Forskål).

Elphick, M. R., Rayne, R. C., Riveros-Moreno, V., Moncada, S., & O'Shea, M. (1995). Nitric oxide synthesis in locust olfactory interneurones. Journal of Experimental Biology, 198(3), 821–829. https://doi.org/10.1242/JEB.198.3.821,

Engel, M. S., & Grimaldi, D. A. (2004). New light shed on the oldest insect. Nature 2004 427:6975, 427(6975), 627–630. https://doi.org/10.1038/nature02291

Ernst, K. D., Boeckh, J., & Boeckh, V. (1977). A neuroanatomical study on the organization of the central antennal pathways in insects - II. Deutocerebral connections in Locusta migratoria and Periplaneta americana. Cell and Tissue Research, 176(3), 285–308. https://doi.org/10.1007/BF00221789/METRICS

Ernst, U. R., Van Hiel, M. B., Depuydt, G., Boerjan, B., De Loof, A., & Schoofs, L. (2015). Epigenetics and locust life phase transitions. In Journal of Experimental Biology (Vol. 218, Issue 1, pp. 88–99). Company of Biologists Ltd. https://doi.org/10.1242/jeb.107078

Estevez, I., Andersen, I. L., & Nævdal, E. (2007). Group size, density and social dynamics in farm animals. Applied Animal Behaviour Science, 103(3–4), 185–204. https://doi.org/10.1016/J.APPLANIM.2006.05.025

Fadda, M., Hasakiogullari, I., Temmerman, L., Beets, I., Zels, S., & Schoofs, L. (2019). Regulation of feeding and metabolism by neuropeptide F and short neuropeptide F in invertebrates. Frontiers in Endocrinology, 10(FEB), 64. https://doi.org/10.3389/FENDO.2019.00064/FULL

FAQs | FAO | Food and Agriculture Organization of the United Nations. (n.d.). Retrieved 15 February 2025, from https://www.fao.org/locusts/faqs/en/

Farnebäck, G. (2003). Two-Frame Motion Estimation Based on Polynomial Expansion. Lecture Notes in Computer Science (Including Subseries Lecture Notes in Artificial Intelligence and Lecture Notes in Bioinformatics), 2749, 363–370. https://doi.org/10.1007/3-540-45103-X_50

Farr, T. G., Rosen, P. A., Caro, E., Crippen, R., Duren, R., Hensley, S., Kobrick, M., Paller, M., Rodriguez, E., Roth, L., Seal, D., Shaffer, S., Shimada, J., Umland, J., Werner, M., Oskin, M., Burbank, D., & Alsdorf, D. E. (2007). The Shuttle Radar Topography Mission. Reviews of Geophysics, 45(2), 2004. https://doi.org/10.1029/2005RG000183

Fişek, M., & Wilson, R. I. (2013). Stereotyped connectivity and computations in higher-order olfactory neurons. Nature Neuroscience 2013 17:2, 17(2), 280–288. https://doi.org/10.1038/nn.3613

Fishilevich, E., & Vosshall, L. B. (2005). Genetic and functional subdivision of the Drosophila antennal lobe. Current Biology : CB, 15(17), 1548–1553. https://doi.org/10.1016/J.CUB.2005.07.066

Foster, W. A., & Treherne, J. E. (1981). Evidence for the dilution effect in the selfish herd from fish predation on a marine insect. Nature, 293(5832), 466. https://doi.org/10.1038/293466A0

Frechter, S., Bates, A. S., Tootoonian, S., Dolan, M. J., Manton, J., Jamasb, A. R., Kohl, J., Bock, D., & Jefferis, G. (2019). Functional and anatomical specificity in a higher olfactory centre. ELife, 8. https://doi.org/10.7554/ELIFE.44590

Fuchs, E., Kutsch, W., & Ayali, A. (2003). Neural correlates to flight-related density-dependent phase characteristics in locusts. Journal of Neurobiology, 57(2), 152–162. https://doi.org/10.1002/NEU.10261

Fusca, D., Husch, A., Baumann, A., & Kloppenburg, P. (2013). Choline acetyltransferase-like immunoreactivity in a physiologically distinct subtype of olfactory nonspiking local interneurons in the cockroach (periplaneta americana). The Journal of Comparative Neurology, 521(15), 3556–3569. https://doi.org/10.1002/CNE.23371

Fuscà, D., & Kloppenburg, P. (2021). Odor processing in the cockroach antennal lobe-the network components. Cell and Tissue Research, 383(1), 59–73. https://doi.org/10.1007/S00441-020-03387-3

Fusca, D., & Kloppenburg, P. (2021). Task-specific roles of local interneurons for inter- and intraglomerular signaling in the insect antennal lobe. ELife, 10. https://doi.org/10.7554/ELIFE.65217

Gadenne, C., Barrozo, R. B., & Anton, S. (2016). Plasticity in Insect Olfaction: To Smell or Not to Smell? Annual Review of Entomology, 61, 317–333. https://doi.org/10.1146/ANNUREV-ENTO-010715-023523,

Galizia, C. G. (2014). Olfactory coding in the insect brain: data and conjectures. European Journal of Neuroscience, 39(11), 1784–1795. https://doi.org/10.1111/EJN.12558

Galizia, C. G. (2020). 3.21 - Insect Olfaction. The Senses: A Comprehensive Reference: Volume 1-7, Second Edition, 3, 423–452. https://doi.org/10.1016/B978-0-12-809324-5.23892-3

Galizia, C. G., McIlwrath, S. L., & Menzel, R. (1999). A digital three-dimensional atlas of the honeybee antennal lobe based on optical sections acquired by confocal microscopy. Cell and Tissue Research, 295(3), 383–394. https://doi.org/10.1007/S004410051245

Galizia, C. G., & Menzel, R. (2001). The role of glomeruli in the neural representation of odours: results from optical recording studies. Journal of Insect Physiology, 47(2), 115–130. https://doi.org/10.1016/S0022-1910(00)00106-2

Galizia, C. G., & Rössler, W. (2010). Parallel olfactory systems in insects: anatomy and function. Annual Review of Entomology, 55, 399–420. https://doi.org/10.1146/ANNUREV-ENTO-112408-085442

Galizia, C. G., & Sachse, S. (2010). Odor Coding in Insects. The Neurobiology of Olfaction, 35–70. https://doi.org/10.1201/9781420071993-c2

Galizia, C. G., Sachse, S., Rappert, A., & Menzel, R. (1999). The glomerular code for odor representation is species specific in the honeybee Apis mellifera. Nature Neuroscience 1999 2:5, 2(5), 473–478. https://doi.org/10.1038/8144

Galizia, C. G., & Szyszka, P. (2008). Olfactory coding in the insect brain: molecular receptive ranges, spatial and temporal coding. Entomologia Experimentalis et Applicata, 128(1), 81–92. https://doi.org/10.1111/j.1570-7458.2007.00661.x

Galizia, C. G., & Vetter, R. S. (2004). Optical methods for analyzing Odor-Evoked activity in the insect brain. Methods in Insect Sensory Neuroscience, 349–392. https://doi.org/10.1201/9781420039429.CH13

Galizia, G., & Lledo, P.-M. (2014). Neurosciences - From Molecule to Behavior: a university textbook.

http://www.springer.com/springer+spektrum/biowissenschaften/neurowissenschaft/book/978-3-642-10768-9

Gao, Q., Yuan, B., & Chess, A. (2000). Convergent projections of Drosophila olfactory neurons to specific glomeruli in the antennal lobe. Nature Neuroscience 2000 3:8, 3(8), 780–785. https://doi.org/10.1038/77680

Georgiou, F., Buhl, C., Green, J. E. F., Lamichhane, B., & Thamwattana, N. (2025). Including population and environmental dynamic heterogeneities in continuum models of collective behaviour with applications to locust foraging and group structure. PLOS Computational Biology, 21(4), e1011469. https://doi.org/10.1371/JOURNAL.PCBI.1011469

Gholami Pourbadie, H., & Sayyah, M. (2018). Optogenetics: Control of Brain Using Light. Iranian Biomedical Journal, 22(1), 4. https://pmc.ncbi.nlm.nih.gov/articles/PMC5712383/

Gibson, G., & Torr, S. J. (1999). Visual and olfactory responses of haematophagous Diptera to host stimuli. Medical and Veterinary Entomology, 13(1), 2–23. https://doi.org/10.1046/J.1365-2915.1999.00163.X

Giurfa, M., & Sandoz, J. C. (2012). Invertebrate learning and memory: Fifty years of olfactory conditioning of the proboscis extension response in honeybees. Learning and Memory, 19(2), 54–66. https://doi.org/10.1101/LM.024711.111

Godziiiska, E. J., & A.Lenoir, ’. (2006). Social Isolation in Ants : Evidence of its Impact on Survivorship and Behavior in Camponotus fe//ah (Hymenoptera, Formicidae).

Goosey, M. W., & Candy, D. J. (1980). The d-octopamine content of the haemolymph of the locust, Schistocerca Americana gregaria and its elevation during flight. Insect Biochemistry, 10(4), 393–397. https://doi.org/10.1016/0020-1790(80)90009-8

Gorbonos, D., Gov, N. S., & Couzin, I. D. (2024). Geometrical Structure of Bifurcations during Spatial Decision-Making. PRX Life, 2(1), 013008. https://doi.org/10.1103/PRXLIFE.2.013008/FIGURES/10/MEDIUM

Graving, J. M., Chae, D., Naik, H., Li, L., Koger, B., Costelloe, B. R., & Couzin, I. D. (2019). Deepposekit, a software toolkit for fast and robust animal pose estimation using deep learning. ELife, 8. https://doi.org/10.7554/ELIFE.47994

Greenwood, M., & Chapman, R. F. (1984). Differences in numbers of sensilla on the antennae of solitarious and gregarious Locusta migratoria L. (Orthoptera: Acrididae). International Journal of Insect Morphology and Embryology, 13(4), 295–301. https://doi.org/10.1016/0020-7322(84)90004-7

Grider, M. H., Jessu, R., & Kabir, R. (2023). Physiology, Action Potential. StatPearls. https://www.ncbi.nlm.nih.gov/books/NBK538143/

Grienberger, C., & Konnerth, A. (2012). Imaging calcium in neurons. Neuron, 73(5), 862–885. https://doi.org/10.1016/j.neuron.2012.02.011

Grosjean, Y., Rytz, R., Farine, J. P., Abuin, L., Cortot, J., Jefferis, G. S. X. E., & Benton, R. (2011). An olfactory receptor for food-derived odours promotes male courtship in Drosophila. Nature 2011 478:7368, 478(7368), 236–240. https://doi.org/10.1038/nature10428

Grossman, D., Aranson, I. S., & Ben Jacob, E. (2008). Emergence of agent swarm migration and vortex formation through inelastic collisions. New Journal of Physics, 10(2), 023036. https://doi.org/10.1088/1367-2630/10/2/023036

Gruber, L., Cantera, R., Pleijzier, M. W., Steinert, M., Pertsch, T., Hansson, B. S., & Rybak, J. (2023). The unique synaptic circuitry of specialized olfactory glomeruli in Drosophila melanogaster. ELife, 12. https://doi.org/10.7554/ELIFE.88824.1

Grüter, C., Schürch, R., Czaczkes, T. J., Taylor, K., Durance, T., Jones, S. M., & Ratnieks, F. L. W. (2012). Negative Feedback Enables Fast and Flexible Collective Decision-Making in Ants. PLOS ONE, 7(9), e44501. https://doi.org/10.1371/JOURNAL.PONE.0044501

Grynkiewicz, G., Poenie, M., & Tsien, R. Y. (1985). A new generation of Ca2+ indicators with greatly improved fluorescence properties. Journal of Biological Chemistry, 260(6), 3440–3450. https://doi.org/10.1016/S0021-9258(19)83641-4

Guerrieri, F., Schubert, M., Sandoz, J. C., & Giurfa, M. (2005). Perceptual and neural olfactory similarity in honeybees. PLoS Biology, 3(4), 0718–0732. https://doi.org/10.1371/JOURNAL.PBIO.0030060

Günzel, Y., Couzin-Fuchs, E., & Paoli, M. (2024). CalciSeg: A versatile approach for unsupervised segmentation of calcium imaging data. NeuroImage, 298, 120758. https://doi.org/10.1016/J.NEUROIMAGE.2024.120758

Günzel, Y., McCollum, J., Paoli, M., Galizia, C. G., Petelski, I., & Couzin-Fuchs, E. (2021). Social modulation of individual preferences in cockroaches. IScience, 24(1), 101964. https://doi.org/10.1016/J.ISCI.2020.101964

Günzel, Y., Oberhauser, F. B., & Couzin-Fuchs, E. (2023). Information integration for decision-making in desert locusts. IScience, 26(4). https://doi.org/10.1016/J.ISCI.2023.106388/ATTACHMENT/65615E7B-2D8E-4573-9928-AB358E7763F9/MMC1.PDF

Guo, X., Ma, Z., Du, B., Li, T., Li, W., Xu, L., He, J., & Kang, L. (2018). Dop1 enhances conspecific olfactory attraction by inhibiting miR-9a maturation in locusts. Nature Communications 2018 9:1, 9(1), 1–16. https://doi.org/10.1038/s41467-018-03437-z

Guo, X., Ma, Z., & Kang, L. (2013). Serotonin enhances solitariness in phase transition of the migratory locust. Frontiers in Behavioral Neuroscience, 7(OCT), 60390. https://doi.org/10.3389/FNBEH.2013.00129/BIBTEX

Guo, X., Yu, Q., Chen, D., Wei, J., Yang, P., Yu, J., Wang, X., & Kang, L. (2020). 4-Vinylanisole is an aggregation pheromone in locusts. Nature, 584(7822), 584–588. https://doi.org/10.1038/S41586-020-2610-4

Guttal, V., Romanczuk, P., Simpson, S. J., Sword, G. A., & Couzin, I. D. (2012). Cannibalism can drive the evolution of behavioural phase polyphenism in locusts. Ecology Letters, 15(10), 1158–1166. https://doi.org/10.1111/J.1461-0248.2012.01840.X

Hall, C. L., & Kramer, D. L. (2008). The economics of tracking a changing environment: competition and social information. Animal Behaviour, 76(5), 1609–1619. https://doi.org/10.1016/J.ANBEHAV.2008.05.031

Hallem, E. A., & Carlson, J. R. (2004). The odor coding system of Drosophila. Trends in Genetics, 20(9), 453–459. https://doi.org/10.1016/J.TIG.2004.06.015/ASSET/3C5289BB-3B60-43EB-AFF5-AFD57464EC20/MAIN.ASSETS/GR3.SML

Hammer, M., & Menzel, R. (1998). Multiple Sites of Associative Odor Learning as Revealed by Local Brain Microinjections of Octopamine in Honeybees. Learning & Memory, 5(1), 146. https://doi.org/10.1101/lm.5.1.146

Hansson, B. S., & Anton, S. (2000). Function and morphology of the antennal lobe: new developments. Annual Review of Entomology, 45, 203–231. https://doi.org/10.1146/annurev.ento.45.1.203

Hansson, B. S., Ochieng, S. A., Grosmaitre S Anton, X., & Njagi, P. G. N. (1996). Physiological responses and central nervous projections of antennal olfactory receptor neurons in the adult desert locust, Schistocerca gregaria (Orthoptera: Acrididae). Journal of Comparative Physiology - A Sensory, Neural, and Behavioral Physiology, 179(2), 157–167. https://doi.org/10.1007/BF00222783/METRICS

Hansson, B. S., & Stensmyr, M. C. (2011). Evolution of insect olfaction. Neuron, 72(5), 698–711. https://doi.org/10.1016/J.NEURON.2011.11.003/ASSET/BC72B008-A0C2-4589-93C4-835726A48A3A/MAIN.ASSETS/GR6.JPG

Harpaz, R., Aspiras, A. C., Chambule, S., Tseng, S., Bind, M. A., Engert, F., Fishman, M. C., & Bahl, A. (2021). Collective behavior emerges from genetically controlled simple behavioral motifs in zebrafish. Science Advances, 7(41). https://doi.org/10.1126/SCIADV.ABI7460/SUPPL_FILE/SCIADV.ABI7460_MOVIES_S1_TO_S3.ZIP

Harrison, L. M., Churchill, E. R., Fairweather, M., Smithson, C. H., Chapman, T., & Bretman, A. (2024). Ageing effects of social environments in 'non-social' insects. Philosophical Transactions B, 379(1916). https://doi.org/10.1098/RSTB.2022.0463

Harshey, R. M. (2003). Bacterial Motility on a Surface: Many Ways to a Common Goal. Annual Review of Microbiology, 57(Volume 57, 2003), 249–273. https://doi.org/10.1146/ANNUREV.MICRO.57.030502.091014/CITE/REFWORKS

Hart, T., Frank, D. D., Lopes, L. E., Olivos-Cisneros, L., Lacy, K. D., Trible, W., Ritger, A., Valdés-Rodríguez, S., & Kronauer, D. J. C. (2023). Sparse and stereotyped encoding implicates a core glomerulus for ant alarm behavior. Cell, 186(14), 3079-3094.e17. https://doi.org/10.1016/J.CELL.2023.05.025

Hart, T., Lopes, L. E., Frank, D. D., & Kronauer, D. J. C. (2024). Pheromone representation in the ant antennal lobe changes with age. Current Biology, 34(14), 3233-3240.e4. https://doi.org/10.1016/J.CUB.2024.05.031/ASSET/B5BFBDD5-561D-430A-942E-7A2E9538008B/MAIN.ASSETS/GR4.JPG

Heisenberg, M. (1998). What Do the Mushroom Bodies Do for the Insect Brain? An Introduction. Learning & Memory, 5(1), 1. https://doi.org/10.1101/lm.5.1.1

Herre, M., Goldman, O. V., Lu, T. C., Caballero-Vidal, G., Qi, Y., Gilbert, Z. N., Gong, Z., Morita, T., Rahiel, S., Ghaninia, M., Ignell, R., Matthews, B. J., Li, H., Vosshall, L. B., & Younger, M. A. (2022). Non-canonical odor coding in the mosquito. Cell, 185(17), 3104-3123.e28. https://doi.org/10.1016/j.cell.2022.07.024

Hildebrand, J. G., & Shepherd, G. M. (1997). Mechanisms of olfactory discrimination: converging evidence for common principles across phyla. Annual Review of Neuroscience, 20, 595–631. https://doi.org/10.1146/annurev.neuro.20.1.595

Hochkirch, A., & Bhaskar, D. (2021). Minimize collateral damage in locust control. Science, 371(6535), 1214–1215. https://doi.org/10.1126/SCIENCE.ABH3128

Hodjat, S. H., Saboori, A., & Husemann, M. (2019). A view on the historic and contemporary acridid fauna (Orthoptera: Caelifera: Acrididae) of Iran-A call for conservation efforts. Journal of Crop Protection, 8(2), 135–142. http://jcp.modares.ac.ir/article-3-25563-en.html

Hoffman, M. D., & Gelman, A. (2014). The No-U-turn sampler. The Journal of Machine Learning Research, 15, 1593–1623. https://doi.org/10.5555/2627435.2638586

Homberg, U., & Müller, U. (1999). Neuroactive Substances in the Antennal Lobe. Insect Olfaction, 181–206. https://doi.org/10.1007/978-3-662-07911-9_8

Hou, L., Jiang, F., Yang, P., Wang, X., & Kang, L. (2015). Molecular characterization and expression profiles of neuropeptide precursors in the migratory locust. Insect Biochemistry and Molecular Biology, 63, 63–71. https://doi.org/10.1016/J.IBMB.2015.05.014

Hu, J., & Xia, Y. (2019). Increased virulence in the locust-specific fungal pathogen Metarhizium acridum expressing dsRNAs targeting the host F1F0-ATPase subunit genes. Pest Management Science, 75(1), 180–186. https://doi.org/10.1002/PS.5085

Huber, R., Smith, K., Delago, A., Isaksson, K., & Kravitz, E. A. (1997). Serotonin and aggressive motivation in crustaceans: Altering the decision to retreat. Proceedings of the

National Academy of Sciences of the United States of America, 94(11), 5939–5942. https://doi.org/10.1073/PNAS.94.11.5939/ASSET/1371B872-F3F6-4AD3-BE28-6D11DFD23239/ASSETS/GRAPHIC/PQ1070847003.JPEG

Husch, A., Paehler, M., Fusca, D., Paeger, L., & Kloppenburg, P. (2009). Calcium current diversity in physiologically different local interneuron types of the antennal lobe. The Journal of Neuroscience : The Official Journal of the Society for Neuroscience, 29(3), 716–726. https://doi.org/10.1523/JNEUROSCI.3677-08.2009

Ignell, R., Anton, S., & Hansson, B. S. (1998). Central nervous processing of behaviourally relevant odours in solitary and gregarious fifth instar locusts, Schistocerca gregaria. Journal of Comparative Physiology - A Sensory, Neural, and Behavioral Physiology, 183(4), 453–465. https://doi.org/10.1007/S003590050271/METRICS

Ignell, R., Anton, S., & Hansson, B. S. (2001). The Antennal Lobe of Orthoptera – Anatomy and Evolution. Brain Behavior and Evolution, 57(1), 1–17. https://doi.org/10.1159/000047222

Ignell, R., Couillaud, F., & Anton, S. (2001). Juvenile-hormone-mediated plasticity of aggregation behaviour and olfactory processing in adult desert locusts. Journal of Experimental Biology, 204(2), 249–259. https://doi.org/10.1242/JEB.204.2.249,

Imen, S., Christian, M., Virginie, D., & Colette, R. (2015). Intraspecific Signals Inducing Aggregation in Periplaneta americana (Insecta: Dictyoptera). Https://Doi.Org/10.1093/Ee/Nvv035, 44(3), 713–723. https://doi.org/10.1093/EE/NVV035

Ingram, S., Chisholm, K. I., Wang, F., De Koninck, Y., Denk, F., & Goodwin, G. L. (2024). Assessing spontaneous sensory neuron activity using in vivo calcium imaging. Pain, 165(5), 1131–1141. https://doi.org/10.1097/J.PAIN.0000000000003116

Ito, I., Bazhenov, M., Ong, R. C. ying, Raman, B., & Stopfer, M. (2009). Frequency Transitions in Odor-Evoked Neural Oscillations. Neuron, 64(5), 692–706. https://doi.org/10.1016/J.NEURON.2009.10.004

Jeanne, J. M., Fişek, M., & Wilson, R. I. (2018). The organization of projections from olfactory glomeruli onto higher-order neurons. Neuron, 98(6), 1198. https://doi.org/10.1016/J.NEURON.2018.05.011

Jeanson, R., Rivault, C., Deneubourg, J. L., Blanco, S., Fournier, R., Jost, C., & Theraulaz, G. (2005). Self-organized aggregation in cockroaches. Animal Behaviour, 69(1), 169–180. https://doi.org/10.1016/J.ANBEHAV.2004.02.009

Jiang, X., Dimitriou, E., Grabe, V., Sun, R., Chang, H., Zhang, Y., Gershenzon, J., Rybak, J., Hansson, B. S., & Sachse, S. (2024). Ring-shaped odor coding in the antennal lobe of migratory locusts. Cell, 187(15), 3973-3991.e24. https://doi.org/10.1016/J.CELL.2024.05.036

Jortner, R. A. (2013). Network architecture underlying maximal separation of neuronal representations. Frontiers in Neuroengineering, 5(AUGUST), 19. https://doi.org/10.3389/FNENG.2012.00019

Jortner, R. A., Farivar, S. S., & Laurent, G. (2007). A Simple Connectivity Scheme for Sparse Coding in an Olfactory System. Journal of Neuroscience, 27(7), 1659–1669. https://doi.org/10.1523/JNEUROSCI.4171-06.2007

Josens, R. B., & Roces, F. (2000). Foraging in the ant Camponotus mus: nectar-intake rate and crop filling depend on colony starvation. Journal of Insect Physiology, 46(7), 1103–1110. https://doi.org/10.1016/S0022-1910(99)00220-6

Jung, J. W., Kim, J. H., Pfeiffer, R., Ahn, Y. J., Page, T. L., & Kwon, H. W. (2013). Neuromodulation of olfactory sensitivity in the peripheral olfactory organs of the American cockroach, Periplaneta americana. PLoS ONE, 8(11). https://doi.org/10.1371/JOURNAL.PONE.0081361,

Katz, Y., Tunstrøm, K., Ioannou, C. C., Huepe, C., & Couzin, I. D. (2011). Inferring the structure and dynamics of interactions in schooling fish. Proceedings of the National Academy of Sciences of the United States of America, 108(46), 18720–18725. https://doi.org/10.1073/PNAS.1107583108/-/DCSUPPLEMENTAL/PNAS.1107583108_SI.PDF

Keleman, K., Vrontou, E., Kruttner, S., Yu, J. Y., Kurtovic-Kozaric, A., & Dickson, B. J. (2012). Dopamine neurons modulate pheromone responses in Drosophila courtship learning. Nature, 489(7414), 145–149. https://doi.org/10.1038/NATURE11345;SUBJMETA=1595,1731,1804,340,378,631;KWRD=LEARNING+AND+MEMORY,MOLECULAR+NEUROSCIENCE,PHEROMONE

Kendal, R. L., Coolen, I., & Laland, K. N. (2004). The role of conformity in foraging when personal and social information conflict. Behavioral Ecology, 15(2), 269–277. https://doi.org/10.1093/BEHECO/ARH008

Kendal, R. L., Coolen, I., & Laland, K. N. (2009). Adaptive Trade-offs in the Use of Social and Personal Information. Cognitive Ecology II, 249–271. https://doi.org/10.7208/CHICAGO/9780226169378.003.0013

Killen, S. S., Fu, C., Wu, Q., Wang, Y. X., & Fu, S. J. (2016). The relationship between metabolic rate and sociability is altered by food deprivation. Functional Ecology, 30(8), 1358–1365. https://doi.org/10.1111/1365-2435.12634

Kim, A. J., Lazar, A. A., & Slutskiy, Y. B. (2015). Projection neurons in Drosophila antennal lobes signal the acceleration of odor concentrations. ELife, 4(MAY). https://doi.org/10.7554/ELIFE.06651

King, A. J., & Cowlishaw, G. (2007). When to use social information: the advantage of large group size in individual decision making. Biology Letters, 3(2), 137–139. https://doi.org/10.1098/RSBL.2007.0017

Kloppenburg, P., & Hildebrand, J. G. (1995). Neuromodulation by 5-Hydroxytryptamine in the Antennal Lobe of the Sphinx Moth Manduca Sexta. Journal of Experimental Biology, 198(3), 603–611. https://doi.org/10.1242/JEB.198.3.603

Knaden, M., & Hansson, B. S. (2014). Mapping odor valence in the brain of flies and mice. Current Opinion in Neurobiology, 24(1), 34–38. https://doi.org/10.1016/J.CONB.2013.08.010

Knaden, M., Strutz, A., Ahsan, J., Sachse, S., & Hansson, B. S. (2012). Spatial representation of odorant valence in an insect brain. Cell Reports, 1(4), 392–399. https://doi.org/10.1016/J.CELREP.2012.03.002

Ko, K. I., Root, C. M., Lindsay, S. A., Zaninovich, O. A., Shepherd, A. K., Wasserman, S. A., Kim, S. M., & Wang, J. W. (2015). Starvation promotes concerted modulation of appetitive olfactory behavior via parallel neuromodulatory circuits. ELife, 4. https://doi.org/10.7554/ELIFE.08298

Korsching, S. I., Rummrich, A., Friedrich, R. W., & Weth, F. (1999). Spatial Representation of Odors in the Zebrafish Olfactory Epithelium and Olfactory Bulb. Advances in Chemical Signals in Vertebrates, 525–533. https://doi.org/10.1007/978-1-4615-4733-4_47

Koto, A., Mersch, D., Hollis, B., & Keller, L. (2015). Social isolation causes mortality by disrupting energy homeostasis in ants. Behavioral Ecology and Sociobiology, 69(4), 583–591. https://doi.org/10.1007/S00265-014-1869-6/FIGURES/4

Krafft, B., Krafft, B., Horel, A., & Julita, J.-M. (1986). Influence of Food Supply on the Duration of the Gregarious Phase of a Maternal-Social Spider, Coelotes Terrestris (Araneae, Agelenidae). The Journal of Arachnology, 14(2), 219--226. https://www.biodiversitylibrary.org/part/226212

Krause, J., & Ruxton, G. D. (2002). Living in Groups. Living in Groups. https://doi.org/10.1093/OSO/9780198508175.001.0001

Krongauz, D. L., Ayali, A., & Kaminka, G. A. (2024). Vision-based collective motion: A locust-inspired reductionist model. PLOS Computational Biology, 20(1), e1011796. https://doi.org/10.1371/JOURNAL.PCBI.1011796

Krüger, J., & Bach, M. (1981). Simultaneous recording with 30 microelectrodes in monkey visual cortex. Experimental Brain Research, 41(2), 191–194. https://doi.org/10.1007/BF00236609/METRICS

Kughlin, C., & Hines, D. (1975). The phase correlation image alignment method – ScienceOpen. Proc. IEEE International Conference on Cybernetics and Society. https://www.scienceopen.com/document?vid=250786ec-dc88-4779-af17-887241e8aa0e

Kulahci, I. G., Dornhaus, A., & Papaj, D. R. (2008). Multimodal signals enhance decision making in foraging bumble-bees. Proceedings of the Royal Society B: Biological Sciences, 275(1636), 797–802. https://doi.org/10.1098/rspb.2007.1176

Laurent, G. (2002). Olfactory network dynamics and the coding of multidimensional signals. Nature Reviews Neuroscience 2002 3:11, 3(11), 884–895. https://doi.org/10.1038/nrn964

Laurent, G., & Davidowitz, H. (1994). Encoding of Olfactory Information with Oscillating Neural Assemblies. Science, 265(5180), 1872–1875. https://doi.org/10.1126/SCIENCE.265.5180.1872

Laurent, G., & Naraghi, M. (1994). Odorant-induced oscillations in the mushroom bodies of the locust. Journal of Neuroscience, 14(5), 2993–3004. https://doi.org/10.1523/JNEUROSCI.14-05-02993.1994

Laurent, G., Wehr, M., & Davidowitz, H. (1996). Temporal Representations of Odors in an Olfactory Network. Journal of Neuroscience, 16(12), 3837–3847. https://doi.org/10.1523/JNEUROSCI.16-12-03837.1996

Laurent Salazar, M. O., Nicolis, S. C., Calvo Martín, M., Sempo, G., Deneubourg, J. L., & Planas-Sitjà, I. (2017). Group choices seemingly at odds with individual preferences. Royal Society Open Science, 4(7). https://doi.org/10.1098/RSOS.170232

Leadbeater, E., & Dawson, E. H. (2017). A social insect perspective on the evolution of social learning mechanisms. Proceedings of the National Academy of Sciences of the United States of America, 114(30), 7838–7845. https://doi.org/10.1073/PNAS.1620744114/ASSET/3E70F432-4EF4-4944-8864-0F8B39351BF9/ASSETS/GRAPHIC/PNAS.1620744114FIG04.JPEG

Lehmann, J., Günzel, Y., Khosravian, M., Cassau, S., Kraus, S., Libnow, J. S., Chang, H., Hansson, B. S., Breer, H., Couzin-Fuchs, E., Fleischer, J., & Krieger, J. (2024). SNMP1 is critical for sensitive detection of the desert locust aromatic courtship inhibition pheromone phenylacetonitrile. BMC Biology, 22(1), 1–22. https://doi.org/10.1186/S12915-024-01941-X/FIGURES/8

Leitch, B., & Laurent, G. (1993). Distribution of GABAergic synaptic terminals on the dendrites of locust spiking local interneurones. Journal of Comparative Neurology, 337(3), 461–470. https://doi.org/10.1002/cne.903370309

Leitch, B., & Laurent, G. (1996). GABAergic synapses in the antennal lobe and mushroom body of the locust olfactory system. J Comp Neurol, 372(4), 487–514. https://doi.org/10.1002/(SICI)1096-9861(19960902)372:4

Lemon, W. C., & Getz, W. M. (2000). Rate code input produces temporal code output from cockroach antennal lobes. Biosystems, 58(1–3), 151–158. https://doi.org/10.1016/S0303-2647(00)00118-0

Li, J., & Xia, Y. (2022). Host–Pathogen Interactions between Metarhizium spp. and Locusts. Journal of Fungi, 8(6), 602. https://doi.org/10.3390/JOF8060602

Li, W., Wang, Z., Syed, S., Lyu, C., Lincoln, S., O'Neil, J., Nguyen, A. D., Feng, I., & Young, M. W. (2021). Chronic social isolation signals starvation and reduces sleep in Drosophila. Nature, 597(7875), 239–244. https://doi.org/10.1038/S41586-021-03837-0;TECHMETA=24,38,64,91;SUBJMETA=1385,1457,378,519,631;KWRD=EMOTION,SLEEP

Light, D. M., Flath, R. A., Buttery, R. G., Zalom, F. G., Rice, R. E., Dickens, J. C., & Jang, E. B. (1993). Host-plant green-leaf volatiles synergize the synthetic sex pheromones of the corn earworm and codling moth (Lepidoptera). Chemoecology, 4(3–4), 145–152. https://doi.org/10.1007/BF01256549/METRICS

Lihoreau, M., Brepson, L., & Rivault, C. (2009). The weight of the clan: Even in insects, social isolation can induce a behavioural syndrome. Behavioural Processes, 82(1), 81–84. https://doi.org/10.1016/j.beproc.2009.03.008

Lihoreau, M., Charleston, M. A., Senior, A. M., Clissold, F. J., Raubenheimer, D., Simpson, S. J., & Buhl, J. (2017). Collective foraging in spatially complex nutritional environments. Philosophical Transactions of the Royal Society B: Biological Sciences, 372(1727). https://doi.org/10.1098/RSTB.2016.0238

Lihoreau, M., Clarke, I. M., Buhl, J., Sumpter, D. J. T., & Simpson, S. J. (2016). 1ollective selection of food patches in Drosophila. Journal of Experimental Biology, 219(5), 668–675. https://doi.org/10.1242/jeb.127431

Lihoreau, M., Costa, J. T., & Rivault, C. (2012). The social biology of domiciliary cockroaches: Colony structure, kin recognition and collective decisions. Insectes Sociaux, 59(4), 445–452. https://doi.org/10.1007/S00040-012-0234-X/METRICS

Lihoreau, M., Deneubourg, J. L., & Rivault, C. (2010). Collective foraging decision in a gregarious insect. Behavioral Ecology and Sociobiology, 64(10), 1577–1587. https://doi.org/10.1007/S00265-010-0971-7

Lihoreau, M., & Rivault, C. (2008). Tactile stimuli trigger group effects in cockroach aggregations. Animal Behaviour, 75(6), 1965–1972. https://doi.org/10.1016/J.ANBEHAV.2007.12.006

Lihoreau, M., & Rivault, C. (2011). Local enhancement promotes cockroach feeding aggregations. PLoS ONE, 6(7). https://doi.org/10.1371/JOURNAL.PONE.0022048

Lin, S., Senapati, B., & Tsao, C. H. (2019). Neural basis of hunger-driven behaviour in Drosophila. Open Biology, 9(3). https://doi.org/10.1098/RSOB.180259

Lin, Y.-Y., Chiang, A.-S., Chu, S.-W., & Hsu, K.-J. (2019). Optical properties of adult Drosophila brains in one-, two-, and three-photon microscopy. Biomedical Optics Express, Vol. 10, Issue 4, Pp. 1627-1637, 10(4), 1627–1637. https://doi.org/10.1364/BOE.10.001627

Ling, D., Zhang, L., Saha, D., Chen, A. B., & Raman, B. (2023). Adaptation invariant concentration discrimination in an insect olfactory system. BioRxiv, 2023.05.10.540073. https://doi.org/10.1101/2023.05.10.540073

Linster, C., Masson, C., Kerszberg, M., Personnaz, L., & Dreyfus, G. (1993). Formal Model of the Insect Olfactory Macroglomerulus. Computation and Neural Systems, 255–259. https://doi.org/10.1007/978-1-4615-3254-5_39

Locatelli, F. F., Fernandez, P. C., Villareal, F., Muezzinoglu, K., Huerta, R., Galizia, C. G., & Smith, B. H. (2013). Nonassociative plasticity alters competitive interactions among mixture components in early olfactory processing. The European Journal of Neuroscience, 37(1), 63–79. https://doi.org/10.1111/EJN.12021

Lock, J. T., Parker, I., & Smith, I. F. (2015). A comparison of fluorescent Ca2+ indicators for imaging local Ca2+ signals in cultured cells. Cell Calcium, 58(6), 638–648. https://doi.org/10.1016/J.CECA.2015.10.003

Lüdke, A., Raiser, G., Nehrkorn, J., Herz, A. V. M., Galizia, C. G., & Szyszka, P. (2018). Calcium in kenyon cell somata as a substrate for an olfactory sensory memory in drosophila. Frontiers in Cellular Neuroscience, 12, 364240. https://doi.org/10.3389/FNCEL.2018.00128/BIBTEX

Lukeman, R., Li, Y. X., & Edelstein-Keshet, L. (2010). Inferring individual rules from collective behavior. Proceedings of the National Academy of Sciences of the United States of America, 107(28), 12576–12580. https://doi.org/10.1073/PNAS.1001763107/SUPPL_FILE/SM03.MOV

Lv, M., Xu, X., Zhang, X., Yuwen, B., & Zhang, L. (2023). Serotonin/GABA receptors modulate odor input to olfactory receptor neuron in locusts. Frontiers in Cellular Neuroscience, 17, 1156144. https://doi.org/10.3389/FNCEL.2023.1156144/BIBTEX

Lyu, C., Abbott, L. F., & Maimon, G. (2021). Building an allocentric travelling direction signal via vector computation. Nature 2021 601:7891, 601(7891), 92–97. https://doi.org/10.1038/s41586-021-04067-0

Ma, Z., Guo, W., Guo, X., Wang, X., & Kang, L. (2011). Modulation of behavioral phase changes of the migratory locust by the catecholamine metabolic pathway. Proceedings of the National Academy of Sciences of the United States of America, 108(10), 3882–3887. https://doi.org/10.1073/PNAS.1015098108/SUPPL_FILE/SAPP.PDF

Mackinnon, J. G. (2009). Bootstrap Hypothesis Testing. Handbook of Computational Econometrics, 183–213. https://doi.org/10.1002/9780470748916.CH6

MacLeod, K., Bäcker, A., & Laurent, G. (1998). Who reads temporal information contained across synchronized and oscillatory spike trains? Nature 1998 395:6703, 395(6703), 693–698. https://doi.org/10.1038/27201

MacLeod, K., & Laurent, G. (1996). Distinct Mechanisms for Synchronization and Temporal Patterning of Odor-Encoding Neural Assemblies. Science, 274(5289), 976–979. https://doi.org/10.1126/SCIENCE.274.5289.976

Mahabir, S., & Sandquist, M. (2024). [Olfactory perception and learning in the honey bee (Apis mellifera): calcium imaging in the antenna lobe]. Journal de La Société de Biologie. https://doi.org/10.20935/ACADONCO7293

Malun, D., Waldow, U., Kraus, D., & Boeckh, J. (1993). Connections between the deutocerebrum and the protocerebrum, and neuroanatomy of several classes of deutocerebral projection neurons in the brain of male Periplaneta americana. Journal of Comparative Neurology, 329(2), 143–162. https://doi.org/10.1002/CNE.903290202

Mann, R. P., Perna, A., Strömbom, D., Garnett, R., Herbert-Read, J. E., Sumpter, D. J. T., & Ward, A. J. W. (2013). Multi-scale Inference of Interaction Rules in Animal Groups Using Bayesian Model Selection. PLOS Computational Biology, 9(3), e1002961. https://doi.org/10.1371/JOURNAL.PCBI.1002961

Martin, J. P., Beyerlein, A., Dacks, A. M., Reisenman, C. E., Riffell, J. A., Lei, H., & Hildebrand, J. G. (2011). The neurobiology of insect olfaction: Sensory processing in a comparative context. In Progress in Neurobiology (Vol. 95, Issue 3, pp. 427–447). https://doi.org/10.1016/j.pneurobio.2011.09.007

Masson, C., & Arnold, G. (1984). Ontogeny, maturation and plasticity of the olfactory system in the workerbee. Journal of Insect Physiology, 30(1), 7–14. https://doi.org/10.1016/0022-1910(84)90104-5

Mazor, O., & Laurent, G. (2005). Transient dynamics versus fixed points in odor representations by locust antennal lobe projection neurons. Neuron, 48(4), 661–673. https://doi.org/10.1016/j.neuron.2005.09.032

McFerran, B., Dahl, D. W., Fitzsimons, G. J., & Morales, A. C. (2010). I'll have what she's having: Effects of social influence and body type on the food choices of others. Journal of Consumer Research, 36(6), 915–926. https://doi.org/10.1086/644611

McMeniman, C. J., Corfas, R. A., Matthews, B. J., Ritchie, S. A., & Vosshall, L. B. (2014). Multimodal Integration of Carbon Dioxide and Other Sensory Cues Drives Mosquito Attraction to Humans. Cell, 156(5), 1060. https://doi.org/10.1016/J.CELL.2013.12.044

Mertes, M., Carcaud, J., & Sandoz, J. C. (2021). Olfactory coding in the antennal lobe of the bumble bee Bombus terrestris. Scientific Reports, 11(1), 10947. https://doi.org/10.1038/S41598-021-90400-6

Meunier, J. (2015). Social immunity and the evolution of group living in insects. Philosophical Transactions of the Royal Society B: Biological Sciences, 370(1669), 20140102. https://doi.org/10.1098/RSTB.2014.0102

Meyer, A., Giovanni Galizia, C., & Nawrot, M. P. (2013). Local interneurons and projection neurons in the antennal lobe from a spiking point of view. Journal of Neurophysiology, 110(10), 2465–2474. https://doi.org/10.1152/JN.00260.2013/ASSET/IMAGES/LARGE/Z9K0221321950004.JPEG

Meyer, H. J., & Norris, D. M. (1967). Vanillin and Syringaldehyde as Attractants for Scolytus multistriatus (Coleoptera: Scolytidae). Annals of the Entomological Society of America, 60(4), 858–859. https://doi.org/10.1093/AESA/60.4.858

Meyniel, F., Sigman, M., & Mainen, Z. F. (2015). Confidence as Bayesian Probability: From Neural Origins to Behavior. Neuron, 88(1), 78–92. https://doi.org/10.1016/J.NEURON.2015.09.039/ASSET/A62F7C43-B78C-432E-824A-87F217DCB6C7/MAIN.ASSETS/GR2.JPG

Milinski, M. (1984). A predator's costs of overcoming the confusion-effect of swarming prey. Animal Behaviour, 32(4), 1157–1162. https://doi.org/10.1016/S0003-3472(84)80232-8

Miller, N., Garnier, S., Hartnett, A. T., & Couzin, I. D. (2013). Both information and social cohesion determine collective decisions in animal groups. Proceedings of the National Academy of Sciences of the United States of America, 110(13), 5263–5268. https://doi.org/10.1073/PNAS.1217513110

Missbach, C., Dweck, H. K. M., Vogel, H., Vilcinskas, A., Stensmyr, M. C., Hansson, B. S., & Grosse-Wilde, E. (2014). Evolution of insect olfactory receptors. ELife, 2014(3). https://doi.org/10.7554/ELIFE.02115

Mohamed, A. A. M., Retzke, T., Das Chakraborty, S., Fabian, B., Hansson, B. S., Knaden, M., & Sachse, S. (2019). Odor mixtures of opposing valence unveil inter-glomerular crosstalk in the Drosophila antennal lobe. Nature Communications 2019 10:1, 10(1), 1–17. https://doi.org/10.1038/s41467-019-09069-1

Mond, M., & Pietri, J. E. (2023). Horizontal transmission of Salmonella Typhimurium among German cockroaches and its possible mechanisms. Ecology and Evolution, 13(5), e10070. https://doi.org/10.1002/ECE3.10070

Moore, R. J. D., Taylor, G. J., Paulk, A. C., Pearson, T., van Swinderen, B., & Srinivasan, M. V. (2014). FicTrac: A visual method for tracking spherical motion and generating fictive animal paths. Journal of Neuroscience Methods, 225, 106–119. https://doi.org/10.1016/J.JNEUMETH.2014.01.010

Moreaux, L., & Laurent, G. (2007). Estimating firing rates from calcium signals in locust projection neurons in vivo. Frontiers in Neural Circuits, 1(NOV). https://doi.org/10.3389/neuro.04/002.2007

Mucignat-Caretta, C. (2014). Neurobiology of Chemical Communication. Neurobiology of Chemical Communication. https://www.ncbi.nlm.nih.gov/books/NBK200990/

Mullie, W. C., & Keith, J. O. (1993). The Effects of Aerially Applied Fenitrothion and Chlorpyrifos on Birds in the Savannah of Northern Senegal. The Journal of Applied Ecology, 30(3), 536. https://doi.org/10.2307/2404193

Mullié, W. C., Prakash, A., Müller, A., & Lazutkaite, E. (2023). Insecticide Use against Desert Locust in the Horn of Africa 2019–2021 Reveals a Pressing Need for Change. Agronomy 2023, Vol. 13, Page 819, 13(3), 819. https://doi.org/10.3390/AGRONOMY13030819

Munichor, N., & Cooke, A. D. J. (2022). Hate the wait? How social inferences can cause customers who wait longer to buy more. Frontiers in Psychology, 13, 990671. https://doi.org/10.3389/FPSYG.2022.990671/BIBTEX

Nagel, K. I., & Wilson, R. I. (2016). Mechanisms Underlying Population Response Dynamics in Inhibitory Interneurons of the Drosophila Antennal Lobe. Journal of Neuroscience, 36(15), 4325–4338. https://doi.org/10.1523/JNEUROSCI.3887-15.2016

Nakai, J., Ohkura, M., & Imoto, K. (2001). A high signal-to-noise Ca2+ probe composed of a single green fluorescent protein. Nature Biotechnology 2001 19:2, 19(2), 137–141. https://doi.org/10.1038/84397

Namiki, S., Iwabuchi, S., A, R. K.-J. of C. P., & 2008, undefined. (2008). Representation of a mixture of pheromone and host plant odor by antennal lobe projection neurons of the silkmoth Bombyx mori. SpringerS Namiki, S Iwabuchi, R KanzakiJournal of Comparative Physiology A, 2008•Springer. https://link.springer.com/article/10.1007/s00359-008-0325-3

Nawrot, M. P. (2012). Dynamics of sensory processing in the dual olfactory pathway of the honeybee. Apidologie, 43(3), 269–291. https://doi.org/10.1007/S13592-012-0131-3)

Niewalda, T., Völler, T., Eschbach, C., Ehmer, J., Chou, W. C., Timme, M., Fiala, A., & Gerber, B. (2011). A combined perceptual, physico-chemical, and imaging approach to 'odour-distances' suggests a categorizing function of the Drosophila antennal lobe. PloS One, 6(9). https://doi.org/10.1371/JOURNAL.PONE.0024300

Nishino, H., Yoritsune, A., & Mizunami, M. (2009). Different growth patterns of two adjacent glomeruli responsible for sex-pheromone processing during postembryonic development of the cockroach Periplaneta americana. Neuroscience Letters, 462(3), 219–224. https://doi.org/10.1016/j.neulet.2009.07.012

Nizampatnam, S., Saha, D., Chandak, R., & Raman, B. (2018). Dynamic contrast enhancement and flexible odor codes. Nature Communications 2018 9:1, 9(1), 1–14. https://doi.org/10.1038/s41467-018-05533-6

Nowak, M. A., Tarnita, C. E., & Wilson, E. O. (2010). THE EVOLUTION OF EUSOCIALITY. Nature, 466(7310), 1057. https://doi.org/10.1038/NATURE09205

Ochieng, S. A., Hallberg, E., & Hansson, B. S. (1998). Fine structure and distribution of antennal sensilla of the desert locust, Schistocerca gregaria (Orthoptera: Acrididae). Cell and Tissue Research, 291(3), 525–536. https://doi.org/10.1007/s004410051022

Okada, J., & Toh, Y. (2004). Antennal system in cockroaches: a biological model of active tactile sensing. International Congress Series, 1269(C), 57–60. https://doi.org/10.1016/J.ICS.2004.05.014

Oland, L. A., & Tolbert, L. P. (1996). Multiple factors shape development of olfactory glomeruli: Insights from an insect model system. Journal of Neurobiology, 30(1), 92–109. https://doi.org/10.1002/(SICI)1097-4695(199605)30:1

Olsen, S. R., & Wilson, R. I. (2008). Lateral presynaptic inhibition mediates gain control in an olfactory circuit. Nature, 452(7190), 956–960. https://doi.org/10.1038/NATURE06864

Oscar, L., Li, L., Gorbonos, D., Couzin, I. D., & Gov, N. S. (2023). A simple cognitive model explains movement decisions in zebrafish while following leaders. Physical Biology, 20(4), 045002. https://doi.org/10.1088/1478-3975/ACD298

Ott, S. R., & Rogers, S. M. (2010). Gregarious desert locusts have substantially larger brains with altered proportions compared with the solitarious phase. Proceedings of the Royal

Society B: Biological Sciences, 277(1697), 3087–3096. https://doi.org/10.1098/rspb.2010.0694

Uvarov, B. B., & Entomologist, A. (1921). A revision of the genus Locusta, L. (= Pachytylus, Fieb.), with a new theory as to the periodicity and migrations of locusts. Bulletin of Entomological Research, 12, 135–163.

Paoli, M., Andrione, M., & Haase, A. (2017). Imaging Techniques in Insects. Neuromethods, 122, 471–519. https://doi.org/10.1007/978-1-4939-6725-4_15

Paoli, M., Nishino, H., Couzin-Fuchs, E., & Galizia, C. G. (2020). Coding of odour and space in the hemimetabolous insect Periplaneta americana. Journal of Experimental Biology, 223(3). https://doi.org/10.1242/JEB.218032/VIDEO-3

Parrish, J. K. (1989). Re-examining the selfish herd: are central fish safer? Animal Behaviour, 38(6), 1048–1053. https://doi.org/10.1016/S0003-3472(89)80143-5

Patel, M., & Rangan, A. (2021). Olfactory encoding within the insect antennal lobe: The emergence and role of higher order temporal correlations in the dynamics of antennal lobe spiking activity. Journal of Theoretical Biology, 522, 110700. https://doi.org/10.1016/J.JTBI.2021.110700

Patel, M., Rangan, A. V., & Cai, D. (2009). A large-scale model of the locust antennal lobe. Journal of Computational Neuroscience, 27(3), 553–567. https://doi.org/10.1007/S10827-009-0169-Z/METRICS

Pener, M. P., & Simpson, S. J. (2009). Locust Phase Polyphenism: An Update. Advances in Insect Physiology, 36, 1–272. https://doi.org/10.1016/S0065-2806(08)36001-9

Pérez-Escudero, A., & de Polavieja, G. G. (2011). Collective Animal Behavior from Bayesian Estimation and Probability Matching. PLOS Computational Biology, 7(11), e1002282. https://doi.org/10.1371/JOURNAL.PCBI.1002282

Perez-Orive, J., Mazor, O., Turner, G. C., Cassenaer, S., Wilson, R. I., & Laurent, G. (2002). Oscillations and sparsening of odor representations in the mushroom body. Science, 297(5580), 359–365. https://doi.org/10.1126/SCIENCE.1070502/SUPPL_FILE/1070502S5_THUMB.GIF

Petelski, I., Günzel, Y., Sayin, S., Kraus, S., & Couzin-Fuchs, E. (2024). Synergistic olfactory processing for social plasticity in desert locusts. Nature Communications 2024 15:1, 15(1), 1–15. https://doi.org/10.1038/s41467-024-49719-7

Pflüger, H. J., & Bräunig, P. (2021). One hundred years of phase polymorphism research in locusts. In Journal of Comparative Physiology A: Neuroethology, Sensory, Neural, and Behavioral Physiology (Vol. 207, Issue 3, pp. 321–326). Springer Science and Business Media Deutschland GmbH. https://doi.org/10.1007/s00359-021-01485-3

Planas-Sitja, I., & Deneubourg, J. L. (2018). The role of personality variation, plasticity and social facilitation in cockroach aggregation. Biology Open, 7(12), bio036582. https://doi.org/10.1242/BIO.036582

Planas-Sitjà, I., Deneubourg, J.-L., Gibon, C., & Sempo, G. (2015). Group personality during collective decision-making: a multi-level approach. Proceedings of the Royal Society B: Biological Sciences, 282(1802), 20142515. https://doi.org/10.1098/rspb.2014.2515

Plenzich, C., & Despland, E. (2018). Host-plant mediated effects on group cohesion and mobility in a nomadic gregarious caterpillar. Behavioral Ecology and Sociobiology, 72(4). https://doi.org/10.1007/S00265-018-2482-X

Pnevmatikakis, E. A., & Giovannucci, A. (2017). NoRMCorre: An online algorithm for piecewise rigid motion correction of calcium imaging data. Journal of Neuroscience Methods, 291, 83–94. https://doi.org/10.1016/J.JNEUMETH.2017.07.031

Polyakov, A. Y., Quinn, T. P., Myers, K. W., & Berdahl, A. M. (2022). Group size affects predation risk and foraging success in Pacific salmon at sea. Science Advances, 8(26).

https://doi.org/10.1126/SCIADV.ABM7548/SUPPL_FILE/SCIADV.ABM7548_SM.PDF

Pophof, B. (2002). Octopamine enhances moth olfactory responses to pheromones, but not those to general odorants. Journal of Comparative Physiology A: Neuroethology, Sensory, Neural, and Behavioral Physiology, 188(8), 659–662. https://doi.org/10.1007/S00359-002-0343-5/METRICS

Pregitzer, P., Jiang, X., Grosse-Wilde, E., Breer, H., Krieger, J., & Fleischer, J. (2017). In Search for Pheromone Receptors: Certain Members of the Odorant Receptor Family in the Desert Locust Schistocerca gregaria (Orthoptera: Acrididae) Are Co-expressed with SNMP1. International Journal of Biological Sciences, 13(7), 911. https://doi.org/10.7150/IJBS.18402

Prillinger, L. (1981). Postembryonic development of the antennal lobes in Periplaneta americana L. Cell and Tissue Research, 215(3), 563–575. https://doi.org/10.1007/BF00233532/METRICS

Prokopy, R. J., & Roitberg, B. D. (2001). Joining and avoidance behavior in nonsocial insects. Annual Review of Entomology, 46, 631–665. https://doi.org/10.1146/ANNUREV.ENTO.46.1.631,

Queller, D. C., & Strassmann, J. E. (2003). Eusociality. Current Biology : CB, 13(22), R861–R863. https://doi.org/10.1016/j.cub.2003.10.043

Raccuglia, D., McCurdy, L. Y., Demir, M., Gorur-Shandilya, S., Kunst, M., Emonet, T., & Nitabach, M. N. (2016). Presynaptic GABA Receptors Mediate Temporal Contrast Enhancement in Drosophila Olfactory Sensory Neurons and Modulate Odor-Driven Behavioral Kinetics. ENeuro, 3(4), ENEURO.0080-16.2016. https://doi.org/10.1523/ENEURO.0080-16.2016

Raiser, G., Galizia, C. G., & Szyszka, P. (2017). A High-Bandwidth Dual-Channel Olfactory Stimulator for Studying Temporal Sensitivity of Olfactory Processing. Chemical Senses, 42(2), 141–151. https://doi.org/10.1093/CHEMSE/BJW114

Raman, B., Joseph, J., Tang, J., & Stopfer, M. (2010). Temporally Diverse Firing Patterns in Olfactory Receptor Neurons Underlie Spatiotemporal Neural Codes for Odors. Journal of Neuroscience, 30(6), 1994–2006. https://doi.org/10.1523/JNEUROSCI.5639-09.2010

Renou, M. (2014). Pheromones and General Odor Perception in Insects. Neurobiology of Chemical Communication, 23–55. https://doi.org/10.1201/b16511

Rieucau, G., & Giraldeau, L. A. (2011). Exploring the costs and benefits of social information use: an appraisal of current experimental evidence. Philosophical Transactions of the Royal Society of London. Series B, Biological Sciences, 366(1567), 949–957. https://doi.org/10.1098/RSTB.2010.0325

Riffell, J. A., Shlizerman, E., Sanders, E., Abrell, L., Medina, B., Hinterwirth, A. J., & Kutz, J. N. (2014). Sensory biology. Flower discrimination by pollinators in a dynamic chemical environment. Science (New York, N.Y.), 344(6191), 1515–1518. https://doi.org/10.1126/SCIENCE.1251041

Rivault, C., & Cloarec, A. (1998). Cockroach aggregation: Discrimination between strain odours in Blattella germanica. Animal Behaviour, 55(1), 177–184. https://doi.org/10.1006/anbe.1997.0628

Roeder, T. (2005). Tyramine and octopamine: Ruling behavior and metabolism. Annual Review of Entomology, 50, 447–477. https://doi.org/10.1146/ANNUREV.ENTO.50.071803.130404,

Roessingh, P., Bouaïchi, A., & Simpson, S. J. (1998). Effects of sensory stimuli on the behavioural phase state of the desert locust, Schistocerca gregaria. Journal of Insect Physiology, 44(10), 883–893. https://doi.org/10.1016/S0022-1910(98)00070-5

Roessingh, P., Simpson, S. J., & James, S. (1993). Analysis of phase-related changes in behaviour of desert locust nymphs.

Rogers, S. M., Cullen, D. A., Anstey, M. L., Burrows, M., Despland, E., Dodgson, T., Matheson, T., Ott, S. R., Stettin, K., Sword, G. A., & Simpson, S. J. (2014). Rapid behavioural gregarization in the desert locust, Schistocerca gregaria entails synchronous changes in both activity and attraction to conspecifics. Journal of Insect Physiology, 65, 9–26. https://doi.org/10.1016/j.jinsphys.2014.04.004

Rogers, S. M., Matheson, T., Sasaki, K., Kendrick, K., Simpson, S. J., & Burrows, M. (2004). Substantial changes in central nervous system neurotransmitters and neuromodulators accompany phase change in the locust. The Journal of Experimental Biology, 207(Pt 20), 3603–3617. https://doi.org/10.1242/JEB.01183

Romanczuk, P., Couzin, I. D., & Schimansky-Geier, L. (2009). Collective motion due to individual escape and pursuit response. Physical Review Letters, 102(1), 010602. https://doi.org/10.1103/PHYSREVLETT.102.010602/FIGURES/3/THUMBNAIL

Root, C. M., Ko, K. I., Jafari, A., & Wang, J. W. (2011). Presynaptic facilitation by neuropeptide signaling mediates odor-driven food search. Cell, 145(1), 133–144. https://doi.org/10.1016/J.CELL.2011.02.008/ATTACHMENT/787D59D7-C513-439E-939C-98113DBD60B5/MMC1.PDF

Root, C. M., Semmelhack, J. L., Wong, A. M., Flores, J., & Wang, J. W. (2007). Propagation of olfactory information in Drosophila. Proceedings of the National Academy of Sciences of the United States of America, 104(28), 11826–11831. https://doi.org/10.1073/PNAS.0704523104/SUPPL_FILE/04523FIG9.PDF

Roussel, E., Carcaud, J., Combe, M., Giurfa, M., & Sandoz, J. C. (2014). Olfactory coding in the honeybee lateral horn. Current Biology : CB, 24(5), 561–567. https://doi.org/10.1016/J.CUB.2014.01.063

Royet, J. P., Souchier, C., Jourdan, F., & Ploye, H. (1988). Morphometric study of the glomerular population in the mouse olfactory bulb: numerical density and size distribution along the rostrocaudal axis. The Journal of Comparative Neurology, 270(4), 559–568. https://doi.org/10.1002/CNE.902700409

Russell, J. T. (2011). Imaging calcium signals in vivo: a powerful tool in physiology and pharmacology. British Journal of Pharmacology, 163(8), 1605. https://doi.org/10.1111/J.1476-5381.2010.00988.X

Sachse, S., & Galizia, C. G. (2002). Role of inhibition for temporal and spatial odor representation in olfactory output neurons: a calcium imaging study. Journal of Neurophysiology, 87, 1106–1117. https://doi.org/11826074

Sachse, S., & Galizia, C. G. (2003). The coding of odour-intensity in the honeybee antennal lobe: local computation optimizes odour representation. European Journal of Neuroscience, 18(8), 2119–2132. https://doi.org/10.1046/j.1460-9568.2003.02931.x

Sachse, S., Rappert, A., & Galizia, C. G. (1999). The spatial representation of chemical structures in the antennal lobe of honeybees: steps towards the olfactory code. The European Journal of Neuroscience, 11(11), 3970–3982. https://doi.org/10.1046/J.1460-9568.1999.00826.X

Saha, D., Li, C., Peterson, S., Padovano, W., Katta, N., & Raman, B. (2015). Behavioural correlates of combinatorial versus temporal features of odour codes. Nature Communications 2015 6:1, 6(1), 1–13. https://doi.org/10.1038/ncomms7953

Saïd, I., Costagliola, G., Leoncini, I., & Rivault, C. (2005). Cuticular hydrocarbon profiles and aggregation in four Periplaneta species (Insecta: Dictyoptera). Journal of Insect Physiology, 51(9), 995–1003. https://doi.org/10.1016/j.jinsphys.2005.04.017

Sakura, M., & Mizunami, M. (2001). Olfactory Learning and Memory in the Cockroach Periplaneta americana. Https://Doi.Org/10.2108/Zsj.18.21, 18(1), 21–28. https://doi.org/10.2108/ZSJ.18.21

Salecker, I., & Distler, P. (1990). Serotonin-immunoreactive neurons in the antennal lobes of the American cockroach Periplaneta americana: light- and electron-microscopic observations. Histochemistry, 94(5), 463–473. https://doi.org/10.1007/BF00272608/METRICS

Sandoz, J. C. (2011). Behavioral and neurophysiological study of olfactory perception and learning in honeybees. Frontiers in Systems Neuroscience, 5(DECEMBER 2011), 14474. https://doi.org/10.3389/FNSYS.2011.00098/XML/NLM

Sarel, A., Finkelstein, A., Las, L., & Ulanovsky, N. (2017). Vectorial representation of spatial goals in the hippocampus of bats. Science, 355(6321). https://doi.org/10.1126/SCIENCE.AAK9589/SUPPL_FILE/AAK9589-SAREL-SM.PDF

Sass, H. (1983). Production, release and effectiveness of two female sex pheromone components of Periplaneta americana. Journal of Comparative Physiology □ A, 152(3), 309–317. https://doi.org/10.1007/BF00606237

Sato, K., Pellegrino, M., Nakagawa, T., Nakagawa, T., Vosshall, L. B., & Touhara, K. (2008). Insect olfactory receptors are heteromeric ligand-gated ion channels. Nature 2008 452:7190, 452(7190), 1002–1006. https://doi.org/10.1038/nature06850

Sato, T., Hirono, J., Tonoike, M., & Takebayashi, M. (1994). Tuning specificities to aliphatic odorants in mouse olfactory receptor neurons and their local distribution. Journal of Neurophysiology, 72(6), 2980–2989. https://doi.org/10.1152/JN.1994.72.6.2980

Sayin, S., Boehm, A. C., Kobler, J. M., de Backer, J. F., & Grunwald Kadow, I. C. (2018). Internal state dependent odor processing and perception—The role of neuromodulation in the fly olfactory system. Frontiers in Cellular Neuroscience, 12, 320085. https://doi.org/10.3389/FNCEL.2018.00011/BIBTEX

Sayin, S., Couzin-Fuchs, E., Petelski, I., Günzel, Y., Salahshour, M., Lee, C.-Y., Graving, J. M., Li, L., Deussen, O., Sword, G. A., & Couzin, I. D. (2025). The behavioral mechanisms governing collective motion in swarming locusts. Science, 387(6737), 995–1000. https://doi.org/10.1126/SCIENCE.ADQ7832

Schafer, R., & Sanchez, T. V. (1973). Antennal sensory system of the cockroach, Periplaneta americana: postembryonic development and morphology of the sense organs. The Journal of Comparative Neurology, 149(3), 335–353. https://doi.org/10.1002/CNE.901490304

Schneider, D. (1957). Elektrophysiologische Untersuchungen von Chemo- und Mechanorezeptoren der Antenne des Seidenspinners Bombyx mori L. Zeitschrift Für Vergleichende Physiologie, 40(1), 8–41. https://doi.org/10.1007/BF00298148/METRICS

Schoofs, L., Veelaert, D., Vanden Broeck, J., & De Loof, A. (1997). Peptides in the locusts, Locusta migratoria and Schistocerca gregaria. Peptides, 18(1), 145–156. https://doi.org/10.1016/S0196-9781(96)00236-7

Schoppa, N. E., & Urban, N. N. (2003). Dendritic processing within olfactory bulb circuits. Trends in Neurosciences, 26(9), 501–506. https://doi.org/10.1016/S0166-2236(03)00228-5

Schultzhaus, J. N., Saleem, S., Iftikhar, H., & Carney, G. E. (2017). The role of the Drosophila lateral horn in olfactory information processing and behavioral response. Journal of Insect Physiology, 98, 29–37. https://doi.org/10.1016/J.JINSPHYS.2016.11.007

Seeley, T., Passino, K., & Visscher, K. (2006). Group Decision Making in Honey Bee Swarms. American Scientist, 94(3), 220. https://doi.org/10.1511/2006.59.220

Seelig, J. D., & Jayaraman, V. (2015). Neural dynamics for landmark orientation and angular path integration. Nature 2015 521:7551, 521(7551), 186–191. https://doi.org/10.1038/nature14446

Séguret, A., Bernadou, A., & Paxton, R. J. (2016). Facultative social insects can provide insights into the reversal of the longevity/fecundity trade-off across the eusocial insects. Current Opinion in Insect Science, 16, 95–103. https://doi.org/10.1016/J.COIS.2016.06.001

Seidel, C., & Bicker, G. (1997). Colocalization of NADPH-diaphorase and GABA-immunoreactivity in the olfactory and visual system of the locust. Brain Research, 769(2), 273–280. https://doi.org/10.1016/S0006-8993(97)00716-6

Seki, Y., Dweck, H. K. M., Rybak, J., Wicher, D., Sachse, S., & Hansson, B. S. (2017). Olfactory coding from the periphery to higher brain centers in the Drosophila brain. BMC Biology, 15(1), 1–20. https://doi.org/10.1186/S12915-017-0389-Z/FIGURES/8

Shanbhag, S. R., Müller, B., & Steinbrecht, R. A. (1999). Atlas of olfactory organs of Drosophila melanogaster: 1. Types, external organization, innervation and distribution of olfactory sensilla. International Journal of Insect Morphology and Embryology, 28(4), 377–397. https://doi.org/10.1016/S0020-7322(99)00039-2

Shang, Y., Claridge-Chang, A., Sjulson, L., Pypaert, M., & Miesenböck, G. (2007). Excitatory local circuits and their implications for olfactory processing in the fly antennal lobe. Cell, 128(3), 601–612. https://doi.org/10.1016/J.CELL.2006.12.034

Shaw, E., & Sachs, B. D. (1967). DEVELOPMENT OF THE OPTOMOTOR RESPONSE IN THE SCHOOLING FISH, MENIDIA MENIDIA. Journal of Comparative and Physiological Psychology, 63(3), 385–388. https://doi.org/10.1037/H0024636

Shen, K., Tootoonian, S., & Laurent, G. (2013). Encoding of mixtures in a simple olfactory system. Neuron, 80(5), 10.1016/j.neuron.2013.08.026. https://doi.org/10.1016/J.NEURON.2013.08.026

Shepherd, G. M., Chen, W. R., & Greer, C. A. (2004). Olfactory Bulb. The Synaptic Organization of the Brain. https://doi.org/10.1093/ACPROF:OSO/9780195159561.003.0005

Shimomura, O. (2005). The discovery of aequorin and green fluorescent protein. Journal of Microscopy, 217(1), 3–15. https://doi.org/10.1111/J.0022-2720.2005.01441.X

Silbering, A. F., Bell, R., Galizia, C. G., & Benton, R. (2012). Calcium imaging of odor-evoked responses in the Drosophila antennal lobe. Journal of Visualized Experiments : JoVE, 61. https://doi.org/10.3791/2976

Silbering, A. F., & Galizia, C. G. (2007). Processing of odor mixtures in the Drosophila antennal lobe reveals both global inhibition and glomerulus-specific interactions. The Journal of Neuroscience : The Official Journal of the Society for Neuroscience, 27(44), 11966–11977. https://doi.org/10.1523/JNEUROSCI.3099-07.2007

Silbering, A. F., Okada, R., Ito, K., & Galizia, C. G. (2008). Olfactory information processing in the Drosophila antennal lobe: anything goes? The Journal of Neuroscience : The Official Journal of the Society for Neuroscience, 28(49), 13075–13087. https://doi.org/10.1523/JNEUROSCI.2973-08.2008

Simões, P. M. V., Niven, J. E., & Ott, S. R. (2013). Phenotypic transformation affects associative learning in the desert locust. Current Biology, 23(23), 2407–2412. https://doi.org/10.1016/j.cub.2013.10.016

Simões, P., Ott, S. R., & Niven, J. E. (2011). Associative olfactory learning in the desert locust, Schistocerca gregaria. Journal of Experimental Biology, 214(15), 2495–2503. https://doi.org/10.1242/jeb.055806

Simpson, S. J., Despland, E., Hägele, B. F., & Dodgson, T. (2001). Gregarious behavior in desert locusts is evoked by touching their back legs. In PNAS March (Vol. 27, Issue 7). www.pnas.orgcgidoi10.1073pnas.071527998

Simpson, S. J., McCaffery, A. R., & Hägele, B. F. (1999). A behavioural analysis of phase change in the desert locust. Biological Reviews, 74(4), 461–480. https://doi.org/10.1111/J.1469-185X.1999.TB00038.X

Simpson, S. J., & Raubenheimer, D. (2000). The Hungry Locust. Advances in the Study of Behavior, 29(C), 1–44. https://doi.org/10.1016/S0065-3454(08)60102-3

Simpson, S. J., Sword, G. A., Lorch, P. D., & Couzin, I. D. (2006). Cannibal crickets on a forced march for protein and salt. Proceedings of the National Academy of Sciences of the United States of America, 103(11), 4152–4156. https://doi.org/10.1073/PNAS.0508915103/SUPPL_FILE/08915MOVIE2.MPG

Simpson, S., Sword, G., Whitman, D. W., & Ananthakrishnan, T. (2009). Phenotypic Plasticity of Insects: Mechanisms and Consequences - 1st Ed. Science Publishers. https://www.routledge.com/Phenotypic-Plasticity-of-Insects-Mechanisms-and-Consequences/Whitman/p/book/9781578084234?srsltid=AfmBOoqogYk-RZlgMIJmxnaZCQwsqkuV9hvs5WXA4GQJDv4xr7-lzXG0

Sinakevitch, I. T., Smith, A. N., Locatelli, F., Huerta, R., Bazhenov, M., & Smith, B. H. (2013). Apis mellifera octopamine receptor 1 (AmOA1) expression in antennal lobe networks of the honey bee (Apis mellifera) and fruit fly (Drosophila melanogaster). Frontiers in Systems Neuroscience, 7(OCT), 49805. https://doi.org/10.3389/FNSYS.2013.00070/BIBTEX

Smolla, M., Alem, S., Chittka, L., & Shultz, S. (2016). Copy-when-uncertain: Bumblebees rely on social information when rewards are highly variable. Biology Letters, 12(6). https://doi.org/10.1098/RSBL.2016.0188;CTYPE:STRING:JOURNAL

Song, H. (2005). Phylogenetic perspectives on the evolution of locust phase polyphenism. In JOURNAL OF ORTHOPTERA RESEARCH (Vol. 14, Issue 2). www.pestinfo.org/Literature/locspec.htm

Sridhar, V. H., Li, L., Gorbonos, D., Nagy, M., Schell, B. R., Sorochkin, T., Gov, N. S., & Couzin, I. D. (2021). The geometry of decision-making in individuals and collectives. Proceedings of the National Academy of Sciences of the United States of America, 118(50),e2102157118.https://doi.org/10.1073/PNAS.2102157118/SUPPL_FILE/PNAS.2102157118.SAPP.PDF

Sridhar, V. H., Roche, D. G., & Gingins, S. (2019). Tracktor: Image-based automated tracking of animal movement and behaviour. Methods in Ecology and Evolution, 10(6), 815–820. https://doi.org/10.1111/2041-210X.13166

Steedman, Alison. (1988). Locust handbook. 180. https://search.worldcat.org/title/18791698

Stensmyr, M. C., Dweck, H. K. M., Farhan, A., Ibba, I., Strutz, A., Mukunda, L., Linz, J., Grabe, V., Steck, K., Lavista-Llanos, S., Wicher, D., Sachse, S., Knaden, M., Becher, P. G., Seki, Y., & Hansson, B. S. (2012). A conserved dedicated olfactory circuit for detecting harmful microbes in drosophila. Cell, 151(6), 1345–1357. https://doi.org/10.1016/j.cell.2012.09.046

Stewart, W. B., Kauer, J. S., & Shepherd, G. M. (1979). Functional organization of rat olfactory bulb analysed by the 2-deoxyglucose method. Journal of Comparative Neurology, 185(4), 715–734. https://doi.org/10.1002/CNE.901850407

Stopfer, M., Bhagavan, S., Smith, B. H., & Laurent, G. (1997). Impaired odour discrimination on desynchronization of odour-encoding neural assemblies. Nature, 390(6655), 70–74. https://doi.org/10.1038/36335

Stopfer, M., Jayaraman, V., & Laurent, G. (2003). Intensity versus Identity Coding in an Olfactory System be thought of as a high-dimensional vector of principal neuron states

(e.g., instantaneous firing rates) evolving over the duration of the stimulus in a stimulus-specific. In Neuron (Vol. 39).

Stowers, J. R., Hofbauer, M., Bastien, R., Griessner, J., Higgins, P., Farooqui, S., Fischer, R. M., Nowikovsky, K., Haubensak, W., Couzin, I. D., Tessmar-Raible, K., & Straw, A. D. (2017). Virtual reality for freely moving animals. Nature Methods 2017 14:10, 14(10), 995–1002. https://doi.org/10.1038/nmeth.4399

Stringer, C., & Pachitariu, M. (2019). Computational processing of neural recordings from calcium imaging data. Current Opinion in Neurobiology, 55, 22–31. https://doi.org/10.1016/j.conb.2018.11.005

Strohm, E., & Bordon-Hauser, A. (2003). Advantages and disadvantages of large colony size in a halictid bee: the queen's perspective. Behavioral Ecology, 14(4), 546–553. https://doi.org/10.1093/BEHECO/ARG039

Strube-Bloss, M. F., & Rössler, W. (2018). Multimodal integration and stimulus categorization in putative mushroom body output neurons of the honeybee. Royal Society Open Science, 5(2). https://doi.org/10.1098/RSOS.171785;JOURNAL:JOURNAL:RSOS;WGROUP:STRING:PUBLICATION

Sumpter, D. J. T. (2005). The principles of collective animal behaviour. Philosophical Transactions of the Royal Society B: Biological Sciences, 361(1465), 5–22. https://doi.org/10.1098/RSTB.2005.1733

Sumpter, D. J. T., Mann, R. P., & Perna, A. (2012). The modelling cycle for collective animal behaviour. Interface Focus, 2(6), 764–773. https://doi.org/10.1098/RSFS.2012.0031

Sun, K., Ray, S., Gupta, N., Aldworth, Z., & Stopfer, M. (2024). Olfactory system structure and function in newly hatched and adult locusts. Scientific Reports 2024 14:1, 14(1), 1–15. https://doi.org/10.1038/s41598-024-52879-7

Sword, G. A., Lecoq, M., & Simpson, S. J. (2010). Phase polyphenism and preventative locust management. Journal of Insect Physiology, 56(8), 949–957. https://doi.org/10.1016/J.JINSPHYS.2010.05.005

Sword, G. A., Simpson, S. J., El Hadi, O. T. M., & Wilps, H. (2000). Density–dependent aposematism in the desert locust. Proceedings of the Royal Society of London. Series B: Biological Sciences, 267(1438), 63–68. https://doi.org/10.1098/RSPB.2000.0967

Szyszka, P., & Giovanni Galizia, C. (2015). Olfaction in Insects. Handbook of Olfaction and Gustation: Third Edition, 531–546. https://doi.org/10.1002/9781118971758.CH22

Tada, M., Takeuchi, A., Hashizume, M., Kitamura, K., & Kano, M. (2014). A highly sensitive fluorescent indicator dye for calcium imaging of neural activity in vitro and in vivo. The European Journal of Neuroscience, 39(11), 1720–1728. https://doi.org/10.1111/EJN.12476

Takeda, K. (1961). Classical conditioned response in the honey bee. Journal of Insect Physiology, 6(3), 168–179. https://doi.org/10.1016/0022-1910(61)90060-9

Tan, S., Li, A., Wang, Y., & Shi, W. (2019). Role of the neuropeptide F 1 in regulating the appetite for food in Locusta migratoria. Pest Management Science, 75(5), 1304–1309. https://doi.org/10.1002/PS.5244

Tanaka, S., & Nishide, Y. (2013). Behavioral phase shift in nymphs of the desert locust, Schistocerca gregaria: Special attention to attraction/avoidance behaviors and the role of serotonin. Journal of Insect Physiology, 59(1), 101–112. https://doi.org/10.1016/J.JINSPHYS.2012.10.018

Task, D., Lin, C. C., Vulpe, A., Afify, A., Ballou, S., Brbic, M., Schlege, P., Raji, J., Jefferis, G., Li, H., Menuz, K., & Potter, C. J. (2022). Chemoreceptor co-expression in Drosophila melanogaster olfactory neurons. ELife, 11. https://doi.org/10.7554/ELIFE.72599,

Thoma, M., Hansson, B. S., & Knaden, M. (2014). Compound valence is conserved in binary odor mixtures in Drosophila melanogaster. The Journal of Experimental Biology, 217(Pt 20), 3645–3655. https://doi.org/10.1242/JEB.106591

Tian, L., Hires, S. A., Mao, T., Huber, D., Chiappe, M. E., Chalasani, S. H., Petreanu, L., Akerboom, J., McKinney, S. A., Schreiter, E. R., Bargmann, C. I., Jayaraman, V., Svoboda, K., & Looger, L. L. (2009). Imaging neural activity in worms, flies and mice with improved GCaMP calcium indicators. Nature Methods, 6(12), 875–881. https://doi.org/10.1038/nmeth.1398

Tichy, H., Martzok, A., Linhart, M., Zopf, L. M., & Hellwig, M. (2023). Multielectrode recordings of cockroach antennal lobe neurons in response to temporal dynamics of odor concentrations. Journal of Comparative Physiology A: Neuroethology, Sensory, Neural, and Behavioral Physiology, 209(3), 411–436. https://doi.org/10.1007/S00359-022-01605-7/METRICS

Torney, C., Neufeld, Z., & Couzin, I. D. (2009). Context-dependent interaction leads to emergent search behavior in social aggregates. Proceedings of the National Academy of Sciences of the United States of America, 106(52), 22055–22060. https://doi.org/10.1073/pnas.0907929106

Torto, B., Kirwa, H., Kihika, R., & Niassy, S. (2021). Odor composition of field versus laboratory desert locust populations. Journal of Insect Physiology, 134, 104296. https://doi.org/10.1016/J.JINSPHYS.2021.104296

Tsao, C. H., Chen, C. C., Lin, C. H., Yang, H. Y., & Lin, S. (2018). Drosophila mushroom bodies integrate hunger and satiety signals to control innate food-seeking behavior. ELife, 7. https://doi.org/10.7554/ELIFE.35264,

Tucker, C. J., Hielkema, J. U., & Roffey, J. (1985). The potential of satellite remote sensing of ecological conditions for survey and forecasting desert-locust activity. International Journal of Remote Sensing, 6(1), 127–138. https://doi.org/10.1080/01431168508948429

Turner, G. C., Bazhenov, M., & Laurent, G. (2008). Olfactory representations by Drosophila mushroom body neurons. Journal of Neurophysiology, 99(2), 734–746. https://doi.org/10.1152/JN.01283.2007,

Turner, S. L., Li, N., Guda, T., Githure, J., Cardé, R. T., & Ray, A. (2011). Ultra-prolonged activation of CO2-sensing neurons disorients mosquitoes. Nature 2011 474:7349, 474(7349), 87–91. https://doi.org/10.1038/nature10081

Uchida, N., Takahashi, Y. K., Tanifuji, M., & Mori, K. (2000). Odor maps in the mammalian olfactory bulb: domain organization and odorant structural features. Nature Neuroscience, 3(10), 1035–1043. https://doi.org/10.1038/79857

Uzsák, A., Dieffenderfer, J., Bozkurt, A., & Schal, C. (2014). Social facilitation of insect reproduction with motor-driven tactile stimuli. Proceedings of the Royal Society B: Biological Sciences, 281(1783), 20140325. https://doi.org/10.1098/RSPB.2014.0325

Van Bergen, Y., Coolen, I., & Laland, K. N. (2004). Nine-spined sticklebacks exploit the most reliable source when public and private information conflict. Proceedings of the Royal Society B: Biological Sciences, 271(1542), 957. https://doi.org/10.1098/RSPB.2004.2684

Van Breugel, F., Riffell, J., Fairhall, A., & Dickinson, M. H. (2015). Mosquitoes use vision to associate odor plumes with thermal targets. Current Biology, 25(16), 2123–2129. https://doi.org/10.1016/j.cub.2015.06.046

Van der Valk, H. C. H. G., Niassy, A., & Bèye, A. B. (1999). Does grasshopper control create grasshopper problems? -Monitoring side-effects of fenitrothion applications in the western Sahel. Crop Protection, 18(2), 139–149. https://doi.org/10.1016/S0261-2194(99)00012-5

Verkhratsky, A. (2005). Physiology and pathophysiology of the calcium store in the endoplasmic reticulum of neurons. Physiological Reviews, 85(1), 201–279. https://doi.org/10.1152/PHYSREV.00004.2004/ASSET/IMAGES/LARGE/Z9J0010503500023.JPEG

Verlinden, H., Vleugels, R., Marchal, E., Badisco, L., Pflüger, H. J., Blenau, W., & Broeck, J. Vanden. (2010). The role of octopamine in locusts and other arthropods. Journal of Insect Physiology, 56(8), 854–867. https://doi.org/10.1016/j.jinsphys.2010.05.018

Vicsek, T., Czirk, A., Ben-Jacob, E., Cohen, I., & Shochet, O. (1995). Novel type of phase transition in a system of self-driven particles. Physical Review Letters, 75(6), 1226–1229. https://doi.org/10.1103/PHYSREVLETT.75.1226

Vinauger, C., Van Breugel, F., Locke, L. T., Tobin, K. K. S., Dickinson, M. H., Fairhall, A. L., Akbari, O. S., & Riffell, J. A. (2019). Visual-Olfactory Integration in the Human Disease Vector Mosquito Aedes aegypti. Current Biology, 29(15), 2509-2516.e5. https://doi.org/10.1016/j.cub.2019.06.043

Visscher, P. K. (2007). Group decision making in nest-site selection among social insects. Annual Review of Entomology, 52, 255–275. https://doi.org/10.1146/ANNUREV.ENTO.51.110104.151025,

Vogt, K., Zimmerman, D. M., Schlichting, M., Hernandez-Nunez, L., Qin, S., Malacon, K., Rosbash, M., Pehlevan, C., Cardona, A., & Samuel, A. D. T. (2021). Internal state configures olfactory behavior and early sensory processing in drosophila larvae. Science Advances, 7(1). https://doi.org/10.1126/SCIADV.ABD6900/SUPPL_FILE/ABD6900_SM.PDF

Vosshall, L. B., & Laissue, P. P. (2008). The Olfactory Sensory Map in Drosophila. Advances in Experimental Medicine and Biology, 628, 102–114. https://doi.org/10.1007/978-0-387-78261-4_7

Vosshall, L. B., Wong, A. M., & Axel, R. (2000). An olfactory sensory map in the fly brain. Cell, 102(2), 147–159. https://doi.org/10.1016/S0092-8674(00)00021-0

Wada-Katsumata, A., Zurek, L., Nalyanya, G., Roelofs, W. L., Zhang, A., & Schal, C. (2015). Gut bacteria mediate aggregation in the German cockroach. Proceedings of the National Academy of Sciences of the United States of America, 112(51), 15678–15683. https://doi.org/10.1073/PNAS.1504031112

Wang, J. W., Wong, A. M., Flores, J., Vosshall, L. B., & Axel, R. (2003). Two-Photon Calcium Imaging Reveals an Odor-Evoked Map of Activity in the Fly Brain. Cell, 112(2), 271–282. https://doi.org/10.1016/S0092-8674(03)00004-7

Wang, P., Yin, X., & Zhang, L. (2019). Plant Approach-Avoidance Response in Locusts Driven by Plant Volatile Sensing at Different Ranges. Journal of Chemical Ecology, 45(4), 410–419. https://doi.org/10.1007/s10886-019-01053-9

Wang, Q., Smid, H. M., Dicke, M., & Haverkamp, A. (2024). The olfactory system of Pieris brassicae caterpillars: from receptors to glomeruli. Insect Science, 31(2), 469–488. https://doi.org/10.1111/1744-7917.13304

Wang, Z., Yang, P., Chen, D., Jiang, F., Li, Y., Wang, X., & Kang, L. (2015). Identification and functional analysis of olfactory receptor family reveal unusual characteristics of the olfactory system in the migratory locust. Cellular and Molecular Life Sciences: CMLS, 72(22), 4429. https://doi.org/10.1007/S00018-015-2009-9

Warren, B., & Kloppenburg, P. (2014). Rapid and Slow Chemical Synaptic Interactions of Cholinergic Projection Neurons and GABAergic Local Interneurons in the Insect Antennal Lobe. Journal of Neuroscience, 34(39), 13039–13046. https://doi.org/10.1523/JNEUROSCI.0765-14.2014

Watanabe, H., Nishino, H., Mizunami, M., & Yokohari, F. (2017). Two Parallel Olfactory Pathways for Processing General Odors in a Cockroach. Frontiers in Neural Circuits, 11. https://doi.org/10.3389/FNCIR.2017.00032

Watanabe, H., Nishino, H., Nishikawa, M., Mizunami, M., & Yokohari, F. (2010). Complete mapping of glomeruli based on sensory nerve branching pattern in the primary olfactory center of the cockroach Periplaneta americana. The Journal of Comparative Neurology, 518(19), 3907–3930. https://doi.org/10.1002/CNE.22452

Watanabe, H., & Tateishi, K. (2023). Parallel olfactory processing in a hemimetabolous insect. Current Opinion in Insect Science, 59, 101097. https://doi.org/10.1016/J.COIS.2023.101097

Wegener, J. W., Boekhoff, I., Tareilus, E., & Breer, H. (1993). Olfactory signalling in antennal receptor neurones of the locust (Locusta migratoria). Journal of Insect Physiology, 39(2), 153–163. https://doi.org/10.1016/0022-1910(93)90107-3

Wehr, M., & Laurent, G. (1996). Odour encoding by temporal sequences of firing in oscillating neural assemblies. Nature 1996 384:6605, 384(6605), 162–166. https://doi.org/10.1038/384162a0

Wei, J., Shao, W., Cao, M., Ge, J., Yang, P., Chen, L., Wang, X., & Kang, L. (2019). Phenylacetonitrile in locusts facilitates an antipredator defense by acting as an olfactory aposematic signal and cyanide precursor. Science Advances, 5(1), 5495. https://doi.org/10.1126/sciadv.aav5495

Wendler, G., & Vlatten, R. (1993). The influence of aggregation pheromone on walking behaviour of cockroach males (Blattella germanica L.). Journal of Insect Physiology, 39(12), 1041–1050. https://doi.org/10.1016/0022-1910(93)90128-E

Wey, T., Blumstein, D. T., Shen, W., & Jordán, F. (2008). Social network analysis of animal behaviour: a promising tool for the study of sociality. Animal Behaviour, 75(2), 333–344. https://doi.org/10.1016/J.ANBEHAV.2007.06.020

Wharton, D. R. A., Lola, J. E., & Wharton, M. L. (1968). Growth factors and population density in the American cockroach, Periplaneta americana. Journal of Insect Physiology, 14(5), 637–653. https://doi.org/10.1016/0022-1910(68)90224-2

Wicher, D., & Miazzi, F. (2021). Functional properties of insect olfactory receptors: ionotropic receptors and odorant receptors. Cell and Tissue Research, 383(1), 7. https://doi.org/10.1007/S00441-020-03363-X

Wicher, D., Schäfer, R., Bauernfeind, R., Stensmyr, M. C., Heller, R., Heinemann, S. H., & Hansson, B. S. (2008). Drosophila odorant receptors are both ligand-gated and cyclic-nucleotide-activated cation channels. Nature 2008 452:7190, 452(7190), 1007–1011. https://doi.org/10.1038/nature06861

Wilson, A., Burns, A. L. J., Crosato, E., Lizier, J., Prokopenko, M., Schaerf, T. M., & Ward, A. J. W. (2019). Conformity in the collective: differences in hunger affect individual and group behavior in a shoaling fish. Behavioral Ecology, 30(4), 968–974. https://doi.org/10.1093/BEHECO/ARZ036

Wilson, E. B. (1927). Probable Inference, the Law of Succession, and Statistical Inference. Journal of the American Statistical Association, 22(158), 209–212. https://doi.org/10.1080/01621459.1927.10502953/ASSET//CMS/ASSET/312910F1-C454-4233-9583-0DF8BEF560A7/01621459.1927.10502953.FP.PNG

Wilson, & Hölldobler, B. (2005). Eusociality: Origin and consequences. Proceedings of the National Academy of Sciences of the United States of America, 102(38), 13367–13371. https://doi.org/10.1073/PNAS.0505858102/ASSET/F1D053FC-F7D4-47B5-9B3E-8D25CAD1497A/ASSETS/GRAPHIC/ZPQ0340593020001.JPEG

Wilson, R. I. (2013). Early Olfactory Processing in Drosophila: Mechanisms and Principles. Annual Review of Neuroscience, 36, 217. https://doi.org/10.1146/ANNUREV-NEURO-062111-150533

Wilson, R. I., & Laurent, G. (2005). Role of GABAergic inhibition in shaping odor-evoked spatiotemporal patterns in the Drosophila antennal lobe. Journal of Neuroscience, 25(40), 9069–9079. https://doi.org/10.1523/JNEUROSCI.2070-05.2005

Wilson, R. I., & Mainen, Z. F. (2006). Early events in olfactory processing. Annual Review of Neuroscience, 29(Volume 29, 2006), 163–201. https://doi.org/10.1146/ANNUREV.NEURO.29.051605.112950/CITE/REFWORKS

Worku, Z., Bihonegn, A., Begna, D., Ababor, S., & Gebeyehu, A. (2022). The Indirect Threats of Desert Locust Infestation on Honeybees in Ethiopia. Advances in Agriculture, 2022(1), 4269565. https://doi.org/10.1155/2022/4269565

Wystrach, A., Mangan, M., & Webb, B. (2015). Optimal cue integration in ants. Proceedings of the Royal Society B: Biological Sciences, 282(1816). https://doi.org/10.1098/RSPB.2015.1484

Yaksi, E., & Friedrich, R. W. (2006). Reconstruction of firing rate changes across neuronal populations by temporally deconvolved Ca2+ imaging. Nature Methods, 3(5), 377–383. https://doi.org/10.1038/NMETH874;KWRD=LIFE+SCIENCES

Zhang, J., Bisch-Knaden, S., Fandino, R. A., Yan, S., Obiero, G. F., Grosse-Wilde, E., Hansson, B. S., & Knaden, M. (2019). The olfactory coreceptor IR8a governs larval feces-mediated competition avoidance in a hawkmoth. Proceedings of the National Academy of Sciences of the United States of America, 116(43), 21828–21833. https://doi.org/10.1073/PNAS.1913485116

Zhang, X., & Gaudry, Q. (2016). Functional integration of a serotonergic neuron in the drosophila antennal lobe. ELife, 5(AUGUST). https://doi.org/10.7554/ELIFE.16836

Zhao, B., Sun, J., Zhang, X., Mo, H., Niu, Y., Li, Q., Wang, L., & Zhong, Y. (2019). Long-term memory is formed immediately without the need for protein synthesis-dependent consolidation in Drosophila. Nature Communications, 10(1), 1–11. https://doi.org/10.1038/S41467-019-12436-7;TECHMETA=1,14,24,35,64,69;SUBJMETA=1595,2649,378,631;KWRD=COGNITIVE+NEUROSCIENCE,LEARNING+AND+MEMORY

Zhukovskaya, M. I. (1995). Circadian rhythm of sex pheromone perception in the male American cockroach, Periplaneta americana L. Journal of Insect Physiology, 41(11), 941–946. https://doi.org/10.1016/0022-1910(95)00060-8

Zippenfenig, P. (2023). Open-Meteo.com Weather API. https://doi.org/10.5281/ZENODO.8426816

Zube, C., & Rössler, W. (2008). Caste- and sex-specific adaptations within the olfactory pathway in the brain of the ant Camponotus floridanus. Arthropod Structure & Development, 37(6), 469–479. https://doi.org/10.1016/J.ASD.2008.05.004

ACKNOWLEDGEMENTS

Einat: Looking back on this PhD adventure brings up a flood of emotions. It took me on the most spectacular locust field trip to Isiolo, chasing hoppers under the African sun and brought along the amazing, unforgettable arrival of little Lenni, alongside bursts of neural fireworks in the locust head. However, it also coincided with countless hours of non-responsive locust brains in the imaging setup and the two worst COVID breakdown years in and around the hospital. Through all those ups and downs, you constantly encouraged me, supported both my research interests and personal needs, and somehow even managed to secure funding throughout. I couldn't have asked for a better supervisor, who gave me the freedom to grow in the directions that interested me the most, while always having my back.

Giovanni: The successful pioneering of locust brain recordings could only have happened with the king of insect calcium imaging on board. Thank you so much for your invaluable help throughout the entire imaging avenue - from experimental setup to data interpretation - and for your essential contributions during the PAC meetings. I truly appreciate your expertise, patience, and encouragement at every step along the bumpy road to the PhD.

Amir: A big thank you goes out to Tel Aviv. It's a shame that COVID disrupted our plans, but I'm truly grateful that you welcomed me to your research team at TAU and appreciate all our helpful discussions and your valuable feedback.

Marco: It has been an amazing calcium imaging journey with you; one that started with flies, continued through cockroaches, and reached new heights with stubborn locusts. Thanks for all the technical advice and for being a great PAC member.

Yannick: We chased maati maati in Kenya, checked out Mikes crazy experiments in St. Louis, and hung out countless hours in the lab together. It's been such a pleasure to go through this PhD journey with you. Thank you for helping make sense of all my data and for being the most amazing co-PhD.

Sercan: You are the true sugar postdoc of the lab ☺. Thanks a lot for going through the imaging trouble with me and for celebrating my field data in Science.

Angela: One day, we will submerge on a submarine mission to study critically endangered sharks.

The whole cluster, IMPRS team (especially Lena and Francisca), the HR, and all Uni and MPI secretaries: You guys are amazing! Thank you all so much for the opportunity to do my PhD within such an outstanding research framework and for all the support behind the scenes.

Thilo, Lenni, Jimbo und die Kokosnuss: Die ALL-IN Karte war ohne jeden Zweifel die beste Entscheidung während der ganzen Doktorarbeit. Ab jetzt wird jede Sekunde Urlaub nachgeholt mit meiner weltbesten Familienclownstruppe. 1000 Küsse an euch und den allergrößten Dank fürs Daumen drücken, mitleiden und unterstützen!

Edith, Egbert und Torsten: "Wird das denn irgendwann mal was mit dieser Doktorarbeit?" Ja Papa, es könnte irgendwann vielleicht mal klappen. Riesen Dank an euch für die jahrelange, unendliche Unterstützung und Torsten für die Blitzkorrektur!

Sigi und (manchmal) Uli: Der Endspurt wäre ohne euch super Babysitter ganz schön gescheitert. Vielen lieben Dank!

The cockroaches and locusts of the TFA: Thank you for your tireless cooperation and for selflessly sacrificing yourself for the sake of my studies.

…now I am running out of time and must submit so thanks to everyone I forgot!

AFFIRMATIONS IN LIEU OF OATH

The doctoral thesis on the topic:

‘Sensory processing and decision making in a social context: From odors to swarm motion in insects’

is entirely my own work.

☒ I have used only the sources and aids indicated, and have not received assistance from unauthorized third parties. In particular, texts or ideas that were obtained from other works have been identified as such.

☐ My work does not copy or paraphrase any text passages or other content generated by an AI tool.

☒ If I have used text-generating AI tools as **aids**, I understand that I am solely responsible for the accuracy of the content of the AI-generated text passages and other AI- generated content, as well as for referencing other people's wording and ideas in accordance with the principles of good scientific practice. I have used AI tools as described below:

Grammarly and ChatGPT were used during proofreading to provide vocabulary and phrasing suggestions, and to assist with punctuation, spelling, and error detection

☒ The work or parts of the work have never been submitted to an institute of higher education in Germany or abroad as part of an examination or qualification procedure.

☒ I hereby affirm that the above statements are true and correct.

☒ I am aware of the significance of the affirmation in lieu of oath and the consequences under the penal code of giving an incorrect or incomplete affirmation in lieu of oath.

I hereby affirm that I have stated the truth to the best of my knowledge and have concealed nothing.

Konstanz, 15.04.2025 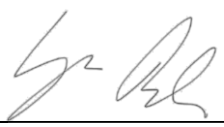

place and date (signature)

CURRICULUM VITAE

INGA PETELSKI
ingapetelski@yahoo.de
+49 178 1009014 (Germany)
Born: 08.08.1987
Nationality: German
Signature:

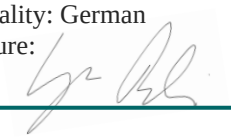

EDUCATION

since Jan. 2019	PhD on neuroethology at the international Max Planck Research School (IMPRS), University Konstanz, Germany From individual preference to collective motion – Neuroethology of decision making
Jun.2014-Dez.2014	Master thesis in neurobiology at the University Konstanz, Germany "The neuronal representation of the phytohormone ethylene in olfactory receptor neurons of the fruit fly *Drosophila melanogaster*" Final grade: very good (1.1)
Oct.2012-Dez.2014	Biological sciences Master's program (MSc), University Konstanz, Germany Stem cell/epigenetic research, chiropterology, parasitology/fish ecology
May.2012-Jul.2012	Bachelor thesis at the Max-Planck-Institute for Ornithology (MPIO), Radolfzell, Germany "The use of 3D tracking acceleration data for the assessment of behavioural classes in free-ranging mallards" Final grade: very good (1.0)
Sep.2010-Feb.2011	Semester abroad, University Lisbon, Portugal Marine biology, tropical ecology
Oct.2008-Jul.2012	Biological sciences Bachelor`s program (BSc), University Konstanz, Germany
Jun.2007	Matriculation (Abitur), Graf-Zeppelin-Gymnasium, Friedrichshafen, Germany Core disciplines: Biology, French, Sports

WORK EXPERIENCE

Sep.2023	Participation at the European Symposium for Insect Taste and Olfaction, Sardinia, Italy
May.2023	Poster presentation and talk at the NeuroDoWo conference in Konstanz
Jul.2022	Poster presentation at the International Congress of Neuroethology, Lisbon, Portugal
Nov.2021-Apr.22	Supervisor of a Bachelor thesis Differences in odor processing in the locust antennal lobe between solitarious and gregarious individuals
Jun.2020-Sep.2020	Supervisor of the advanced neurobiology courses at the University Konstanz Understanding the structure of the locust antennal lobe; The role of sensory modalities in gregarious and solitarious locusts; Effect of GABAergic interneurons on odor perception in the American cockroach *Periplaneta Americana*
Feb.2020-Mar.2020	Kenya field trip during a major locust plague outbreak, Isiolo, Africa Investigations and recordings on the role of sensory modalities in locusts during swarming behaviour
Aug.2019	Poster presentation at the Association for the Study of Animal Behavior summer conference in Konstanz Odor perception in a social context
	Research exchange at the Washington University in the lab of Prof. Barani Raman in St. Louis, USA Application of multielectrode arrays and patch clamp in the locust brain

Jun.2019	Poster presentation and participation at the Insect Chemical Ecology Workshop in Nairobi, Kenya
Oct 2018	PhD project outlining and organization in Tel Aviv, Israel
Mar.2018-Aug.2018	Project leader, Critical ecosystem partnership fund (CEPF), Mahé, Seychelles Leading the Environmental Impact Assessment in an area designated for construction, habitat mapping, organizing workshops and a management committee, preparation of nomination files together with the ministry of environment
May.2017-Mar.2018	Project leader, Prince Bernhard Nature Fund & Anse Forbans Community Conservation, Mahé, Seychelles Managing wetland renaturation/rehabilitation, GIS training, drone consultancy (3D modelling, mapping, NDVI, beach profiling etc.), invasive species control, 3D coral mapping, terrapin rehabilitation analysis for UNDP, supervising Master´s and Bachelor´s thesis
Nov.2015-May.2017	Project leader, Critical ecosystem partnership fund (CEPF), Mahé, Seychelles Wetland biodiversity assessment (Police Bay), drone picture-based GIS/Pix4D mapping, groundtruthing, georeferencing and classification, provision of developmental advice and guidelines, terrapin research, outreach work in local and national newspapers, universities and TV
Jan.2015-Oct.2015	Research assistant, Neurobiology/zoology lab, Prof. Galizia, University Konstanz Odour coding in *D. melanogaster*, Ca^{2+} imaging, supervisor animal physiology course
Jan.2014-Jul.2014	Scientific assistant, Neurobiology lab, Prof. Kleineidam, University Konstanz Cancer cell detection through olfactory receptor neuron activity in *D. melanogaster*
May.2013-Sep.2013	Research assistant, Max-Planck- Institute for Ornithology, Prof. Wikelski, Radolfzell, Germany
Aug.2013-Sep.2013	Student researcher, Evolutionary/parasitological fish ecology lab, Dr. Behrmann-Godel, University Konstanz Growth rate experiments, HPLC carotenoid analysis, perch susceptibility to *Ancyrocephalus paradoxus*
Mar.2011-Jul.2011 & Jan.2013-Mar.2013	Intern, Marine Conservation Society Seychelles (MCSS), Mahé, Seychelles Marine mammal and nesting turtle survey, beach profile monitoring, acoustic shark tracking and tagging, coastal development assessment
May.2010-Aug.2010	PhD assistant, Max-Planck-Institute for Ornithology (MPIO), Radolfzell, Germany *Corvus cornix* rearing and behavioural experiments
Sep.2009-Aug.2010	Student researcher, Aquatic botany group, Prof. Gross, University Konstanz Chemical ecology of submerged macrophytes; toad protection and assessment
Aug.2007-Jul.2008	Volunteer, ASVO (Asociation de Voluntarios para el Servicio en las Areas Protegidas), Costa Rica Hawksbill- & green-turtle protection

LANGUAGES

- German native language
- English fluent in speech and writing
- French fluent (Diplôme d'Etudes en langue française DELF B2)
- Spanish, Portuguese, Seychelles Creole basics

REFERENCES

Dr. Einat Couzin-Fuchs — Research group leader (PhD thesis supervisor) (+49) 1736338057
Insect neuroscience, Center for the advanced study of collective behavior, University Konstanz, Germany
einat.couzin@uni-konstanz.de; https://www.couzin-fuchs-lab.com

Prof. Dr. Giovanni Galizia — Chairman (supervisor during master thesis) (+49) 7541 882238
Zoology & Neurobiology, University Konstanz, Germany
giovanni.galizia@uni-konstanz.de; http://neuro.uni-konstanz.de

Dr. David Rowat — Chairman (boss during work for MCSS) (+248) 4345445
Marine Conservation Society, Seychelles (MCSS)
david@mcss.sc, www.mcss.sc

PUBLICATIONS/MEDIA OUTREACH

Publications:

- The behavioral mechanisms governing collective motion in swarming locusts
  Sayin, Couzin-Fuchs, Petelski, Günzel, Salahshour, Lee, Graving, Li, Deussen, Sword, Couzin
  (*Science, 2025*)
- Synergistic olfactory processing for social plasticity in desert locusts
  Petelski, Günzel, Sayin, Kraus, Couzin-Fuchs
  (*nature communications, 2024*)
- Social modulation of individual preferences in cockroaches
  Günzel, McCollum, Paoli, Petelski, Galizia, Couzin-Fuchs
  (*iScience, 2020*)

TV, Newspaper, Radio:

- Interview in the podcast “In the Swarm” of the Centre for the Advanced Study of Collective Behaviour
- Interview together with Yannick Günzel on SWR Wissen about our publication in Nature Communications “Heuschrecken passen in Schwärmen ihren Geruchssinn an”
- Article about our research field trip to Kenya in the Südkurier “Der Wettlauf mit den Heuschrecken” and in the Tagesblatt “Der Wettlauf mit den Heuschrecken – schlimmste Plage seit Jahrzehnten”
- Appearance on Arte Xenius: “Nützliche Heuschrecken - Und warum einige zur Plage werden”
- Interview about the impact of climate on locusts on Hr Fernsehen “Alle Wetter”
- Small blog about sharks in the local German newspaper Südkurier “Frag mal nach! Wie viele Haie schwimmen im Ozean?”
- Interview about a wetland conservation project in Seychelles on CNN “Inside Africa - The Seychelles are making a difference”